University of Alberta

Diffusion Tensor Imaging of Epilepsy

by

Min Liu

A thesis submitted to the Faculty of Graduate Studies and Research
in partial fulfillment of the requirements for the degree of

Doctor of Philosophy

Biomedical Engineering

©Min Liu
Fall 2013
Edmonton, Alberta

Abstract

Temporal lobe epilepsy (TLE) and idiopathic generalized epilepsy (IGE) are two common epilepsy syndromes. TLE is a type of focal epilepsy. It is frequently associated with mesial temporal sclerosis (MTS), a condition that is also medically intractable. Although TLE is characterized by a focal lesion, widespread gray matter (GM) and white matter (WM) abnormalities have been observed in patients. These reports suggest that TLE is a network disorder. IGE is characterized by bilateral epileptic discharges prominently in the frontal lobe. Magnetic resonance images (MRI) of patients suffering from IGE appear normal.

Diffusion tensor imaging (DTI) is sensitive to the WM microstructure in the brain. Tensor based tractography can reliably reconstruct large WM tracts in vivo. The integrity of WM tracts can be inferred through quantitative measurements performed on these reconstructed images. The research in this thesis attempts to track the acute stage of Wallerian degeneration after injury using DTI. The concomitant reduction of parallel and perpendicular diffusivities 1-2 days after injury may reflect beading and swelling of axolemma or other confounding physiological processes. DTI was used to probe WM abnormalities in subsyndromes of TLE. Patients with TLE and MTS were found to have more extensive WM abnormalities than TLE without MTS. The affected area extends beyond limbic WM to multiple extratemporal locations. Graph theoretical analysis provided further insight into the topological organization of the TLE brain network. Both global and local communication efficiency were impaired and the pivotal hubs were altered in TLE. It is unknown whether these white matter changes are progressive over time. A longitudinal study of TLE patients with and without surgery over a mean of six and a half years revealed Wallerian degeneration in the ipsilateral temporal WM but not

in the contralateral side in the surgical patients. No progressive change was found in the non-surgical patients other than normal aging. Finally, two clinically similar subsyndromes of IGE, i.e. juvenile myoclonic epilepsy and IGE with generalized tonic-clonic seizures only, were demonstrated to have distinct patterns of GM and WM abnormalities, indicating that those subsyndromes of IGE are the result of different underlying disease mechanisms. Overall, quantitative DTI has revealed structural brain differences in epilepsy that are not visible on standard MRI.

Acknowledgement

Table of Contents

List of Tables

List of Figures

List of Abbreviations

ADC	Apparent Diffusion Coefficient, 6
AED	Antiepileptic Drugs, 25
ALIC	Anterior Limb of the Internal Capsule, 142
ANOVA	Analysis of Variance, 145
ATL	Anterior Temporal Lobectomy, 53
bCC	body of the Corpus Callosum, 142
BOLD	Blood-Oxygen-Level-Dependent, 96
CSF	Cerebrospinal Fluid, 145
CST	Corticospinal Tracts, 142
CT	Cortical Thickness, 47
D	Diffusion Coefficient, 5
dCg	dorsal Cingulum, 142
EC	External Capsule, 142
EEG	Electroencephalography, 3
FA	Fractional Anisotropy, 1
FACT	Fiber Assignment by Continuous Tracking, 57
FDR	False Discovery Rate, 84
FLAIR	Fluid Attenuation Inversion Recovery, 13
fMRI	functional MRI, 3
Fx	Fornix, 142
G	The amplitude of the diffusion gradient pulse, 7
GABA	Gamma amino butyric acid, 25
gCC	genu of the Corpus Callosum, 142
GM	Gray Matter, 47
GMV	Gray Matter Volume, 145
IGE	Idiopathic Generalized Epilepsy, 137
IGE-GTC	Idiopathic Generalized Epilepsy with Tonic-Clonic seizures only, 137
ILAE	International League Against Epilepsy, 22
ILF	Inferior Longitudinal Fasciculus, 142
IPSP	Inhibitory Postsynaptic Potentials, 45
JME	Juvenile Myoclonic Epilepsy, 41

Chapter 1   Introduction

1.1   Objective and Hypothesis

Epilepsy is a spectrum of complex neurological disorders that cause dramatic mental and physical hardship. Among more than twenty types of syndromes, temporal lobe epilepsy and idiopathic generalized epilepsy are among the most prevalent. It was not until the advent of magnetic resonance imaging (MRI) techniques that physicians were able to see brain's inner structures in great detail. Hippocampal sclerosis, the underlying structural abnormality in a large number of temporal lobe epilepsy patients, can be identified and the resection of this lesion can greatly reduce seizures. However, visual examination of conventional MRI images in some temporal lobe epilepsy and idiopathic generalized epilepsy cases do not yield positive findings. In these patients, quantitative analysis is required to identify the subtle changes in brain structure that indicate disease. Such methods enhance our understanding of the structural changes caused by epilepsy and promise to become a routine tool in assisting diagnostic and treatment decisions.

Diffusion tensor imaging (DTI) is a MRI method sensitive to water diffusion in the brain. This technique can detect highly organized white matter tracts through the anisotropic diffusion pattern of water in white matter. Temporal lobe epilepsy patients have been shown to exhibit altered diffusion properties in some white matter structures, such as fornix, when compared to controls. The extent of the involvement of white matter in epilepsy remains unclear. The objective of the thesis is three-fold:

   1) to track the acute diffusion change of Wallerian degeneration in human brain in vivo using DTI for the first time,

   2) to identify the white matter changes associated with temporal lobe epilepsy and investigate its progression, and

   3) to identify the gray and white matter changes associated with idiopathic generalized epilepsy.

It has been shown that DTI has the capacity to track Wallerian degeneration. In animal models this degeneration has been characterized by axonal alterations, in the acute phase, and myelin loss, in the chronic phase (Song et al., 2003). The observed reduction of

fractional anisotropy (FA) is often the result of decreased parallel diffusivity in early stages and increased perpendicular diffusivity later on. Decreased parallel diffusivity can be related to axonal degeneration while an increase in perpendicular diffusivity is correlated to myelin breakdown. A previous study, of epilepsy patients with surgical transection of the corpus callosum, has confirmed this pattern and time course of water diffusion at 1 week and 2-4 months after injury consistent with the known stages of Wallerian degeneration (Concha et al., 2006); however, the DTI changes within the first week of injury have yet to be characterized and these findings may or may not hold true for a different tract injured by a different surgical procedure. To address this issue, an experiment was designed to assess the acute and chronic diffusion changes in the fimbria-fornix in six intractable temporal lobe epilepsy patients who underwent anterior temporal resection (including a portion of the fimbria-fornix) at several time points. We hypothesized that the acute diffusion changes of the injured fornix, within seven days after injury, would be similar to the observations from the animal study, i.e. decreased parallel diffusivity without change of the perpendicular diffusivity. We also hypothesized that the chronic diffusion changes would be consistent to the findings from previous animal and human studies, i.e. decreased parallel diffusivity and increased perpendicular diffusivity. The experiment design and results can be found in Chapter 2.

Previous literature had mainly focused on finding gray matter abnormalities associated with temporal lobe epilepsy since it is the most common focal epilepsy. About 70 – 90% of TLE patients are refractory to antiepileptic drugs (Semah et al., 1998). Only a limited number of groups, including this lab, have studied specific white matter tracts in temporal lobe epilepsy using DTI. However, there has been a growing realization that the extent of structural abnormality in different subsyndromes of temporal lobe epilepsy is not the same (Concha et al., 2009). Temporal lobe epilepsy with mesial temporal sclerosis (TLE+MTS) and temporal lobe epilepsy with negative MRI findings, dubbed nonlesional temporal lobe epilepsy (nlTLE), have very similar semiology; however, TLE+MTS showed more extensive gray matter change within and beyond the affected temporal lobe. This raised the question as to whether or not the two syndromes, similar by clinical criteria are based on distinct structural substrates. The experiment performed in Chapter 3 examined the diffusion properties of a large number of major white matter tracts (n = 13). The goal of this examination was to identify the extent of the involvement of white matter in these two cohorts. We hypothesized that TLE+MTS patients would present

2

more extensive white matter changes within and beyond the affected temporal lobe while nlTLE patients would show more limited diffusion change within the ipsilateral hemisphere.

The finding of widespread white matter changes in TLE+MTS suggests another question about how the topological organization of the epileptic brain network differs from a normal one. Graph theoretical analysis yields useful information about the global properties and key hub regions of the brain. This data is complementary to the analysis of local structural integrity. Network analysis based on EEG, functional MRI (fMRI) and PET (positron emission tomography) identified organizational shift at the onset of seizure. It is unknown whether the backbone of the structural network remains intact in these patients. We hypothesized that the architecture of the epileptic brain of TLE+MTS patients would deviate significantly from normal topological organization. This deviation should manifest as a lower global efficiency and a reduced regional efficiency within and beyond the ipsilateral temporal lobe. The results of this study can be found in Chapter 4.

Although structural abnormalities have been observed in TLE patients, the progressive nature of the gray and white matter remains unclear. Previous longitudinal neuroimaging studies were focused on gray matter changes over a short period of time, i.e. less than 3.5 years. Accelerating volume reduction was reported by some studies but not all. The longitudinal examination of the white matter was limited to patients who underwent surgery 4-6 months prior to the study. To explore the structural change of TLE patients over a longer period of time, we imaged subjects twice over a time span of 6.5 years. Subjects fell into one of three categories (1) TLE patietns who had undergone surgical intervention, (2) non-surgical TLE patients, and (3) healthy controls. In each imaging session we measured the diffusion properties of 14 white matter structures and the volume of the cortical gray matter, white matter, hippocampus and amygdala. We hypothesized that the surgical TLE patients would show Wallerian degeneration in the gray and white matter structures ipsilateral to the resection side. We also hypothesized that surgical TLE patients might also exhibit Wallerian degeneration on the contralateral side, but to a lesser extent. The non-surgical TLE patients were also expected to show significant gray and white matter changes between scans when compared with the changes shown by the aging normal controls. The preliminary results can be found in Chapter 5.

The widespread structural change found in subjects with TLE leads to the question as to whether or not subjects with idiopathic generalized epilepsy would show similar changes. Idiopathic generalized epilepsy by definition is not associated with abnormal conventional MRI. Given the generalized nature of its typical seizures, the structural substrates of the syndrome remain mysterious. Previous electroencephalography (EEG) studies have revealed bilateral epileptic discharge with a predominant distribution at the frontal lobe. This interesting observation led to a hypothesis that this group of patients may have abnormal frontal lobe. Some image analysis has been done to test the hypothesis using either region-of-interest or voxel-based methods. However, the findings differ from each other with some experiments resulting in reports of excessive volume, some reporting reduced volume in the frontal lobe and at least one well-designed study resulting in a report of no significant change. Furthermore, there have been a paucity of studies looking at white matter abnormality associated with the disorder. The experiment described in Chapter 6 has been designed to explore both gray and white matter alterations in two subsyndromes of idiopathic generalized epilepsy, i.e. juvenile myoclonic epilepsy and idiopathic generalized epilepsy with generalized tonic-clonic seizures, using MRI and diffusion tensor imaging. We hypothesized that these two clinically similar subsyndromes would show different structural changes with JME showing more motor pathway involvement due to the frequent myoclonic seizures they experience which is not a feature of idiopathic generalized epilepsy with generalized tonic-clonic seizures only.

The appendix shows the result of a comparison of six- and thirty- diffusion-encoding directions in analyzing the fornix. While there are absolute differences of the diffusion parameters, the six-direction scheme shows the same robustness as the 30-direction scheme and can provide consistent tractography results.

1.2   Diffusion MRI

1.2.1 Diffusion

1.2.1.1 Diffusion random walk

Diffusion is an important physical process where particles suspended in fluid or gas move randomly. Diffusion is distinct from bulk motion where stirring or other external forces are utilized to move the particles from one place to another. The random motion of diffusion was first described by Robert Brown, a Scottish botanist. He observed this motion through a microscope in 1827. He reported that some pollen grains suspended in water move around constantly, without external disturbance. This odd finding inspired him to examine other sources of particles including coal dust immersed in water (Brown, 1828). He observed the same random movement but was unable to discern the cause of the motion. Brown later realized that the source of motion was the water molecules that the particles were suspended in, rather than the particles themselves. He described the phenomenon as self-diffusion of water molecules. We now understand that water molecules experience constant random thermal motion at temperatures above zero degrees Kelvin and it is impossible to predict one molecule's position at a certain time. It is the behavior of an ensemble of water molecules that we are truly interested in. This was described by Alberta Einstein in 1905. The typical resolution of MRI images is 2 x 2 x 2 mm^3. Within this volume there are approximately 10^{20} water molecules. Given the large quantity of particles with no surrounding barrier, Einstein demonstrated that the fraction of particles travelling in n-dimensional space over a certain time t follows a Gaussian function whose width is determined by the diffusion coefficient D. The "Einstein's equation" summarized this relationship (Einstein, 1905):

$$\langle r^2 \rangle = 2nDt \qquad\qquad (1.1)$$

In 3D space, the isoprobability surface of the distribution of squared displacements from the origin is a sphere, of radius $\sqrt{6Dt}$ (Figure 1.1). For example, the diffusion coefficient of a cube of water is 3×10^{-3} mm^2/s at 37°C and the water molecules will move, on average, 25 μm on average in 30 ms.
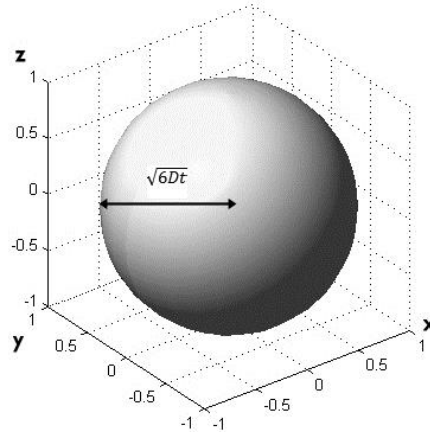
Figure 1.1 The isoprobability surface of the distribution of squared displacements.

1.2.1.2 Hindered diffusion

The diffusion coefficient of free water at body temperature is constant; however, due to the presence of barriers such as cell membranes, myelin sheaths and macromolecules, the water diffusion in certain directions is significantly hindered by the complex environment. As a result, the diffusion coefficient in a restricted environment appears to be much lower than the free-diffusion coefficient. In diffusion MRI, we quantify these apparent diffusion coefficients (ADCs) at least in six directions for each voxel of tissue. These ADCs can be used to infer the underlying geometric structure of the tissue. A relatively high ADC at a certain angle implies a less-restricted path, while a relatively low ADC, found at another diffusion angle, indicates some type of barrier in that direction.

1.2.2 Diffusion weighted imaging

In a spin-echo MRI experiment, the dephasing of spins after the initial 90 degree radiofrequency (rf) pulse excitation is due to field inhomogeneity and dipole interactions. This dephasing is reversed by a 180 degree rf pulse to form an echo. Carefully placed

phase and frequency gradients are used to spatially encode the MRI signal to produce two or three dimensional images. During the experiment, Hahn (1950) noticed an extra reduction of signal in the spin echo and suggested that this was due to translational diffusion within an inhomogeneous magnetic field (Hahn, 1950). A few years later, Carr and Purcell (1954) modified Hahn's spin echo sequence for direct measurement of diffusion by applying a constant field gradient throughout the duration of the experiment (Carr and Purcell, 1954).

Modern diffusion MRI uses a pulsed gradient spin-echo (PGSE) sequence proposed by Stejskal and Tanner (1965). In this sequence the original constant field gradient was split into two matched pulse, one placed on each side of the 180 degree rf pulse (Stejskal and Tanner, 1965) (Figure 1.2). This revision solved the bandwidth and slice-selection problem and also separated the diffusion encoding time (δ, the duration of the gradient) and diffusion time (Δ, the time interval of the application of the first and second gradient) so that the mathematical expression was much simpler. The net phase accrual induced by the two diffusion gradients at the end is expressed by

$$\Delta\emptyset = -\gamma \delta G (x_2 - x_1) \tag{1.2}$$

Where x_1, x_2 are the position of the particles during the first and second diffusion gradient, respectively, and G is the amplitude of the diffusion gradient pulse. If the particles do not move between gradient pulses, the net phase is zero and there is no extra signal attenuation (aside from the intrinsic T2 decay). If the particles diffused randomly, the phase accrual is not fully reversed after the 180 degree refocusing pulse and the second diffusion gradient, thus created additional signal attenuation besides T2 decay. The amount of signal loss from diffusion can be quantified by the ratio of the signal with diffusion gradient S and signal without diffusion weighting S_0. Since the T2 decay stays the same with or without diffusion weighting, the ratio can be solely attributed to diffusion effect. If the particle displacement can be modeled by a Gaussian function and if the particles behave according to Einstein's equation, the relationship between the signal-attenuation ratio and ADC for free particles is single exponential

$$\frac{S}{S_0} = e^{-bADC} \tag{1.3}$$

where the degree of diffusion weighting for a Stejskal-Tanner sequence is characterized by the *b*-factor

$$b = (\gamma \delta G)^2 \left(\Delta - \frac{\delta}{3} \right) \tag{1.4}$$

$\Delta - \frac{\delta}{3}$ is the approximate diffusion time. After taking logarithm, the relationship becomes linear.

$$\ln\left(\frac{S}{S_0}\right) = -bADC \tag{1.5}$$

The typical b-factors used in DTI experiments range from 700-1500 s/mm^2. These sequences have the ability to probe a minimum diffusion distance of about 5-10 μm with a diffusion time around 50-100 ms.
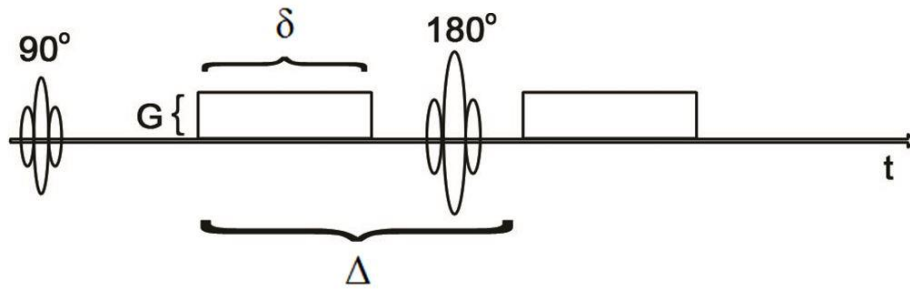
Figure 1.2 The Stejskal-Tanner pulsed gradient spin-echo (PGSE) sequence. Two matched gradients of strength G and duration δ separated by time Δ are placed on each side of the 180 degree rf pulse.

It should be noted that the relationship between the signal attenuation and ADC becomes non-mono-exponential at large b-factors (1500-2000 s/mm^2) in neural tissues.

1.2.3 Diffusion tensor model

One diffusion weighted image with the diffusion sensitizing gradient along a single direction is required to quantify the ADC in case of free-diffusion. Typical direction selected was usually the x, y or z axis. Since 1970s, researchers have started to notice a strong direction dependency of ADC. For the same image location, the degree signal attenuation was not independent of the diffusion direction (Hansen, 1971; Cleveland et al., 1976; Moseley et al., 1990). This indicated faster diffusion along the direction of higher attenuation. This result is also prominent in human white matter where axonal bundles are often highly ordered within the voxel length scale (Doran et al.; Chenevert et al.,

1990). By measuring ADC along many different directions, the underlying microstructure of the tissue can be inferred. The measurement of this anisotropy constitutes DTI.

The diffusion tensor is a simple model of Gaussian diffusion in 3D (Basser et al., 1994b). The geometric representation of the diffusion tensor is an ellipsoid. A particle which begins diffusing at the origin will have an equal probability of ending its motion at any point on the surface of the ellipsoid. If water diffuses primarily along a certain axis, the tensor ellipsoid will be elongated towards that axis (Figure 1.3). Mathematically, the tensor/ellipsoid is a 3×3 symmetric matrix characterizing the displacements in 3D space as

$$D = \begin{bmatrix} D_{xx} & D_{xy} & D_{xz} \\ D_{xy} & D_{yy} & D_{yz} \\ D_{xz} & D_{yz} & D_{zz} \end{bmatrix} \tag{1.6}$$

The three diagonal elements represent diffusivities along the three orthogonal axes and the off-diagonal elements represent the correlation between displacements along x, y, z axes. Some examples of diffusion tensor ellipsoid and corresponding matrix are shown in Figure 1.4.
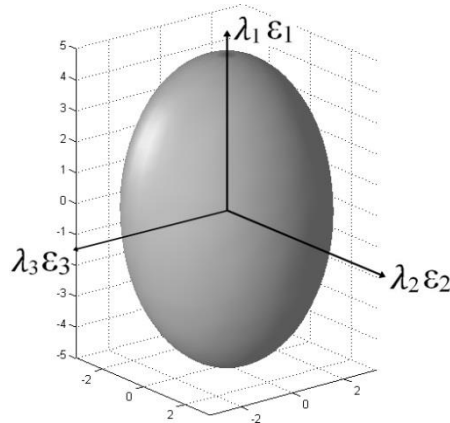
Figure 1.3 Diffusion tensor ellipsoid. The largest axis corresponds to the principle axis ε_1 and the fastest diffusion λ_1.

$$\begin{bmatrix} 4 & 0 & 0 \\ 0 & 4 & 0 \\ 0 & 0 & 4 \end{bmatrix} \qquad \begin{bmatrix} 4 & 0 & 0 \\ 0 & 2 & 0 \\ 0 & 0 & 2 \end{bmatrix} \qquad \begin{bmatrix} 6 & 4 & 0 \\ 4 & 6 & 0 \\ 0 & 0 & 6 \end{bmatrix}$$

$\lambda_1 = 4$	$\lambda_1 = 4$	$\lambda_1 = 10$
$\lambda_2 = 4$	$\lambda_2 = 2$	$\lambda_2 = 6$
$\lambda_3 = 4$	$\lambda_3 = 2$	$\lambda_3 = 2$
FA = 0	FA = 0.41	FA = 0.59
MD = 4	MD = 2.67	MD = 6
$\lambda_\parallel = 4$	$\lambda_\parallel = 4$	$\lambda_\parallel = 10$
$\lambda_\perp = 4$	$\lambda_\perp = 2$	$\lambda_\perp = 4$
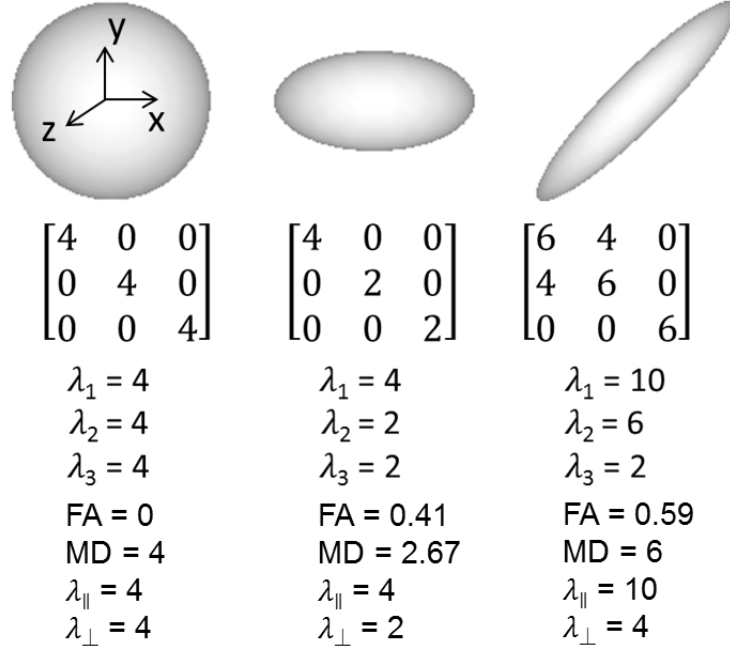
Figure 1.4 Diffusion tensor matrix and the corresponding ellipsoids using the laboratory frame of reference. The non-zero D_{xy} element in the right matrix reflects a correlation in displacements along the x- and y-axes.

The three eigenvalues of the tensor matrix (λ_1, λ_2, λ_3) characterize the diffusivities along the principle axes and the three eigenvectors (ε_1, ε_2, ε_3) denotes the orientation of the principal axes in x, y, z space. The principle eigenvector ε_1 is associated with the largest eigenvalue λ_1. The orientation of the ellipsoid is parallel to the principle eigenvector.

The primary goal for diffusion tensor imaging is to estimate the tensor matrix from diffusion weighted signal. The three dimensional equation becomes

$$\ln\left(\frac{S}{S_0}\right) = -\sum_{i=1}^{3}\sum_{j=1}^{3} b_{ij} ADC_{ij} \tag{1.7}$$

The expanded form will be

$$\ln\left(\frac{S}{S_0}\right) = -(b_{xx} ADC_{xx} + 2b_{xy} ADC_{xy} + 2b_{xz} ADC_{xz}$$

$$+b_{yy} ADC_{yy} + 2b_{yz} ADC_{yz} + b_{zz} ADC_{zz}) \tag{1.8}$$

To solve for the six unknown *ADCs* in the equation, a minimum of six diffusion gradients at non-collinear and non-coplanar directions are required. In addition at least one image must be acquired without diffusion weighting (b0 image). The gradients used for diffusion tensor imaging throughout this thesis follows a seven dual gradient scheme proposed by (Davis et al., 1993) as shown below (Figure 1.5). The three columns correspond to x, y, z axis.

$$
\begin{bmatrix}
0 & 0 & 0 \\
1 & 0 & 1 \\
-1 & 0 & 1 \\
0 & 1 & 1 \\
0 & 1 & -1 \\
1 & 1 & 0 \\
-1 & 1 & 0
\end{bmatrix}
$$
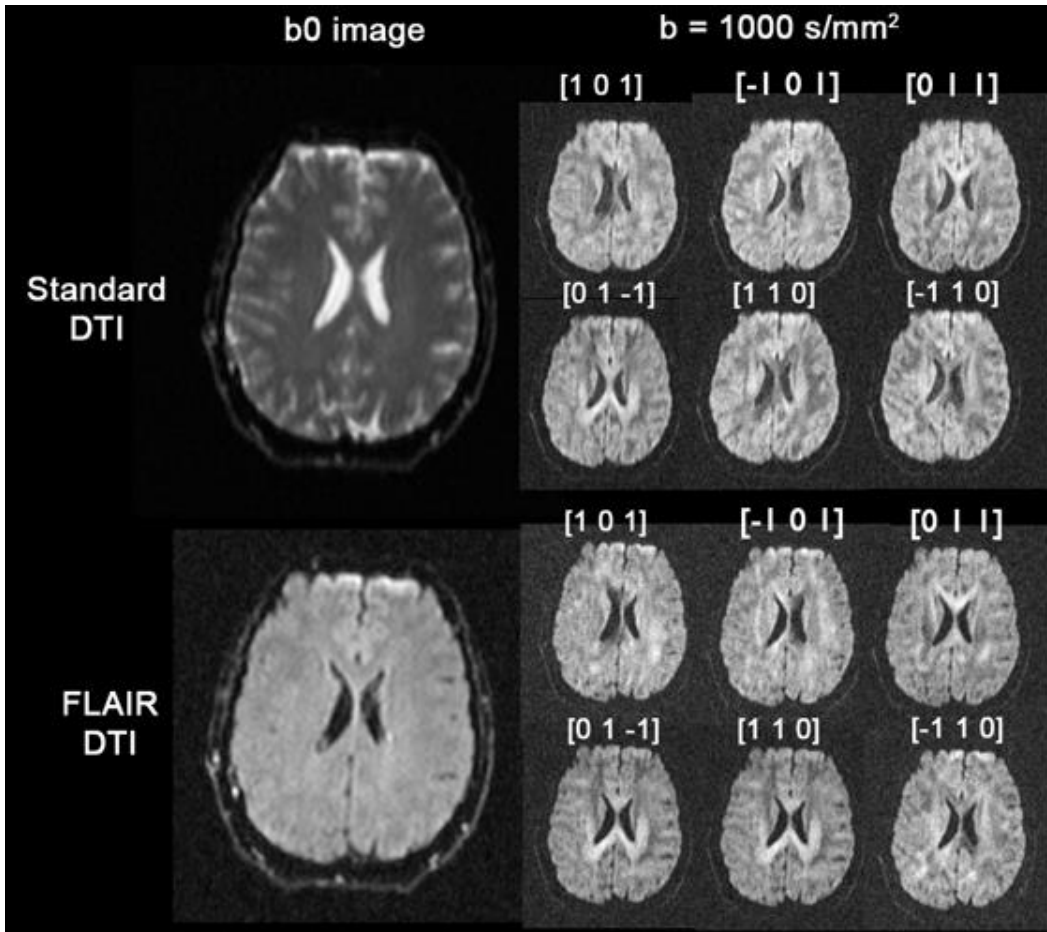
Figure 1.5 Examples of raw DTI images acquired using standard DTI and FLAIR DTI sequence for the studies in this thesis**.** FLAIR DTI suppresses the CSF and the lateral ventricles appear dark in the b0 image.

11

For six direction DTI, each diffusion direction is usually repeated several times to boost the signal–to–noise ratio. An alternative approach is to increase the sampling of gradient directions for a better estimation of diffusion tensor. Experiments using thirty diffusion gradients are common and the number of directions can go beyond thirty to as many as one would like. However, the scan time increases proportionally to the gradient number chosen. It is always a trade-off between optimal imaging parameters and participant's tolerance level of the extended immobility required of long DTI scans. A weighted linear least squares approach is often used to fit the multiple diffusion direction data to the six unknown parameters (Basser et al., 1994a, 1994b).

1.2.4 Water diffusion in the brain

The brain is a complex structure containing 10 billion neuron cells. The neuronal cells are highly organized as a network. The neuronal bodies and glial cells aggregate together forming the outside layer of the cerebral and cerebellar mantle as well as some deep down nuclei groups, called gray matter. Optically, gray matter appears to be gray-brown in color due to the abundant blood supply in this region. The neuronal and glial cell bodies are almost homogeneously distributed in the gray matter. The cell membranes, intracellular content and extracellular matrix are all obstacles to water diffusion. Within a typical DTI resolution volume, around $2 \times 2 \times 2$ mm^3, the hindrance is almost uniform in space. This uniformity leads to an isotropic diffusion pattern in the gray matter although the ADC in gray matter is about 3 times slower than the diffusion of free water.

The inner layer of tissue next to the gray matter is the white matter. Visually, white matter is much lighter in color due to a reduced blood supply and increased lipid content. White matter contains axons, projected from the gray matter, and oligodendrocytes. Oligodendrocytes enhance the speed of action potential propagation by shielding the axons with layers of myelin, i.e. the myelin sheath. Axons traveling to similar destinations are often bundled together by oligodendrocytes and form white matter fibers/tracts that specialize in a certain set of functions. Because of its orderly structure, much more organized than the gray matter, water molecules in white matter find it harder to traverse through layers of axonal membranes and myelin sheaths but easier to diffuse along the axonal fibers. This disproportional hindrance in 3D space creates an anisotropic diffusion pattern in the white matter that is the main target of diffusion tensor imaging. By calculating the diffusion ellipsoid, the structure of the white matter can be estimated

since it is reasonable to assume that the principal axis of the ellipsoid is parallel to the direction of the fiber.

1.2.5 Diffusion tensor metrics

Four scalar measures are widely used to extrapolate the diffusion properties from the tensor model. An overall quantification of diffusion in 3D space is needed to model the underlying tissue structure. Mean diffusivity (MD) is defined by averaging the diffusivity along x, y, z direction of the tensor, which is equal to take an average of the three eigenvalues.

$$MD = \frac{\left(ADC_{xx} + ADC_{yy} + ADC_{zz}\right)}{3}$$

$$= \frac{(\lambda_1 + \lambda_2 + \lambda_3)}{3} \tag{1.9}$$

An example of the MD map of a healthy participant is shown in Figure 1.6. Two acquisition schemes were used, i.e. standard DTI and fluid attenuation inversion recovery (FLAIR) DTI where the cerebrospinal fluid is suppressed (Concha et al., 2005b). As one can perceive immediately, MD is fairly uniform through the parenchyma (Pierpaoli et al., 1996) with a value around 0.7×10^{-3} mm^2/s. It is insensitive to fiber orientation and is widely used in clinical settings to assess acute ischemic lesions (Lythgoe et al., 1997). The cerebrospinal fluid has the highest MD ($\sim 3.13 \times 10^{-3}$ mm^2/s), parallel diffusivity ($\sim 3.1 \times 10^{-3}$ mm^2/s) and perpendicular diffusivities ($\sim 2.97 \times 10^{-3}$ mm^2/s) in standard DTI. The main purpose of FLAIR is to reduce partial volume effects that arise from cerebrospinal fluid mixing with the adjacent white matter structures, such as the fornix, whose dimensions are close to the size of the imaging voxel, i.e. about $2 \times 2 \times 2$ mm^3.

A measure of the extent of anisotropy in the tensor ellipsoid is needed to estimate the extent of orderliness of the structure; a higher anisotropy measurement indicates a greater degree of coherence of direction. Fractional anisotropy is a rotationally scalar variant metric developed for this purpose. It takes the diffusivity from all three axes into consideration and is normalized (0 to 1) to account for regional differences in the overall magnitude of diffusivity.

$$FA = \sqrt{\frac{3}{2}} \sqrt{\frac{(\lambda_1 - MD)^2 + (\lambda_2 - MD)^2 + (\lambda_3 - MD)^2}{\lambda_1^2 + \lambda_2^2 + \lambda_3^2}} \tag{1.10}$$

As shown in Figure 1.6, the white matter has higher FA than gray matter, as expected. The corpus callosum, which contains denser axons bridging the left and right hemisphere, has high FA value, around (0.6 ~ 0.7); white matter, adjacent to the gray matter boundary, has a lower FA value, around (0.3 ~ 0.4). The FA of gray matter is generally below 0.25. The FA of cerebrospinal fluid, in the middle of the brain, has been measured at 0.1. This FA was obtained using standard DTI. The existence of any FA in the fluid is likely due to noise.
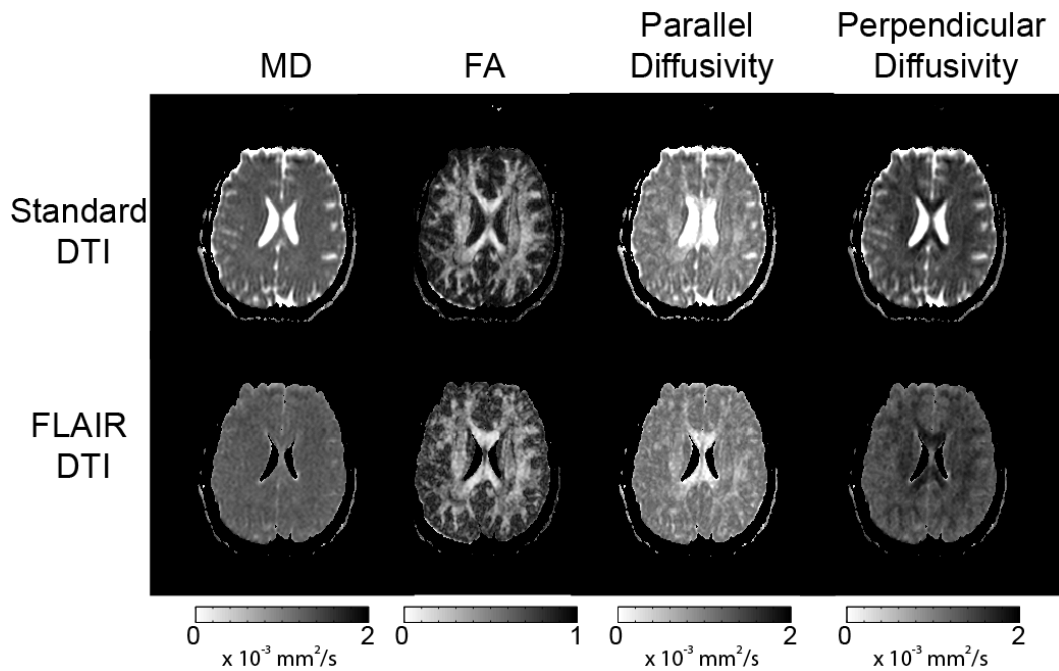
Figure 1.6 Diffusion maps of a 45 year-old healthy male.

Two more diffusion metrics are used to characterize the properties of the diffusion tensor ellipsoid. Parallel (axial) diffusivity is the largest eigenvalue of the diffusion tensor i.e. λ_1, which quantifies water diffusion along the ellipsoid's principal axis. Perpendicular (radial) diffusivity is the average of the second and third eigenvalues of the diffusion tensor, i.e. $(\lambda_2 + \lambda_3)/2$, which quantifies water diffusion perpendicular to the ellipsoid's principal axis. These two metrics further clarify the source of diffusion anisotropy since a high FA can be due to a large parallel diffusivity or a relatively small perpendicular diffusivity (Figure 1.4). Recent studies demonstrated the utility of these two metrics to characterize the distinct structural properties of the white matter tissue.
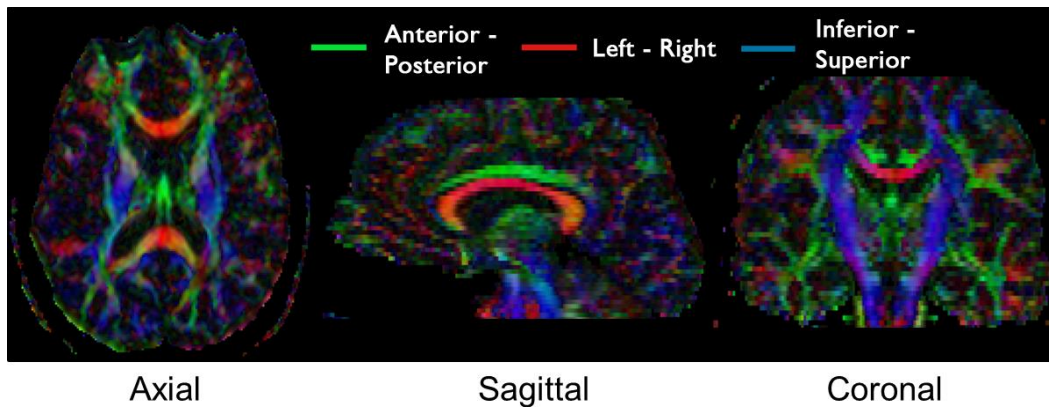
Figure 1.7 The FA-weighted color map of a 45 year-old healthy male.

1.2.6 Diffusion tensor tractography

1.2.6.1 Deterministic tractography

Besides the scalar measurements, the eigenvectors represent the directionality of the tensor ellipsoid. The first eigenvector ε_1 is parallel to the fastest diffusion direction. Presumptively, the primary orientation of the underlying tissue corresponds to ε_1. An FA-weighted color map displays the orientation of the brain using the first eigenvector (Figure 1.7). Left and right direction is denoted in red, anterior and posterior denoted in green and inferior and superior denoted in blue. It is a very informative map where the direction and extent of water diffusion can be appreciated visually by color and brightness. This information can be used in the in vivo reconstruction of white matter tracts. At the end of 20th century, a number of groups (Conturo et al., 1999; Jones et al., 1999; Mori et al., 1999; Basser et al., 2000) contributed to the early development of the deterministic tractography algorithm where tensor ellipsoids above a certain FA baseline and with similar orientation are connected together to reconstruct the white matter pathways in vivo based on a best estimate of underlying fiber orientation. An illustration of tractography is shown in Figure 1.8. Fiber tracking is stopped at voxels where FA is lower than a chosen threshold or the turning angle is greater than a chosen threshold. The common FA threshold used is 0.2 or 0.25 and the angle threshold is between $30° \sim 70°$. The resultant continuous trajectory formed a fiber tract.
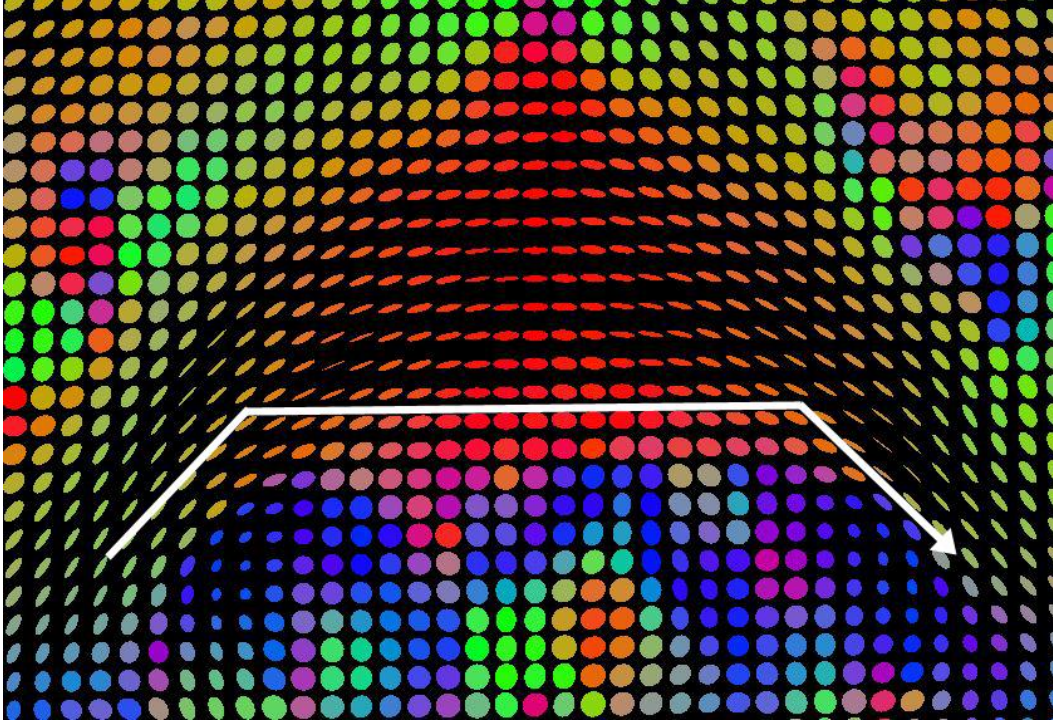
Figure 1.8 An illustration of fiber tracking on ellipsoid glyph at the splenium of corpus callosum. Adjacent ellipsoids with an FA value above 0.25 are connected smoothly without sharp turn larger than 60°. Tracking terminates when FA drops below the threshold (the case here) or encounters an abrupt turn.

To obtain tracts of particular interest, a whole brain tractography is performed first. In whole brain tractography, fibers are launched from every voxel in the brain and then multiple regions of interest are placed at known anatomical locations to select the tracts. Strategies to identify many major white matter tracts have been well established (Wakana et al., 2004). Figure 1.9 demonstrates some white matter tracts studied in this thesis. Although the reconstructed white matter tracts are visually stunning, the deterministic approach has several limitations. First, the errors can accumulate along the estimated pathway due to the inaccurate major eigenvectors. Inaccuracies can be induced by image noise from sources like acquisition, physiological activity, scanner stability, head motion, image distortions, and partial-volume averaging. The dispersion in tract estimates is proportional to the distance from the seed point and inversely proportional to the squares of the eigenvalue differences ($\Delta\lambda_j = \lambda_l - \lambda_j$) and SNR (Anderson, 2001; Lazar and Alexander, 2003). Secondly, diffusion tensor tractography is limited by its single-tensor model which is not able to dissect the trajectories of complicated crossing fibers. For instance, the corticospinal tract derived from deterministic approaches fails to reveal the

16

fibers of the lateral motor cortex because the tensor ellipsoid only yields one single primary direction in centrum semiovale where fibers from superior longitudinal fasciculus, corpus callosum and short U-fibers traverse together.
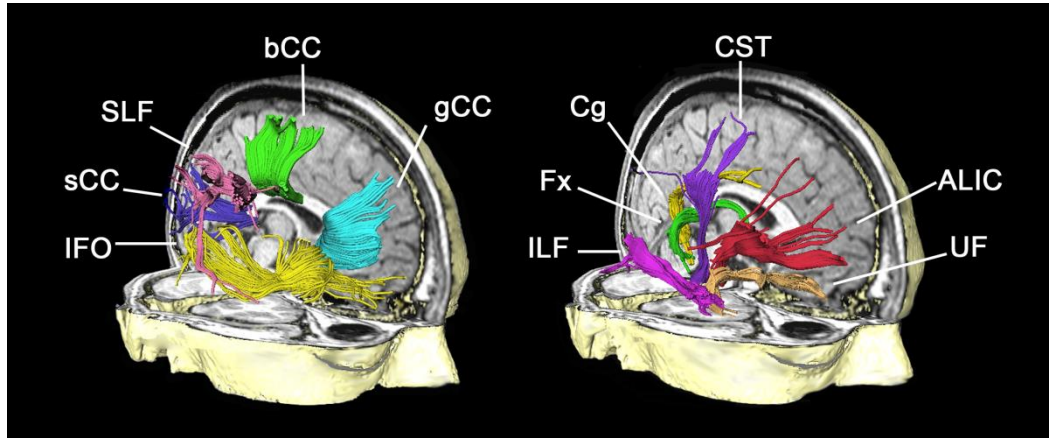
Figure 1.9 Illustration of some white matter tracts derived from deterministic tractography studied in the thesis. gCC/bCC/sCC (genu/body/splenium corpus callosum), SLF (superior longitudinal fasciculus), IFO (inferior fronto-occipital fasciculus), ILF (inferior longitudinal fasciculus), UF (uncinate fasciculus), CST (cerebrospinal tract), Cg (cingulum), Fx (fornix).

1.2.6.2 Probabilistic tractography

The biggest problem of deterministic tractography is that the error associated with the fiber tracking results is unknown. To overcome this, probabilistic tractography methods were proposed to characterize the confidence with which connections may be established through a diffusion MRI dataset (Koch et al., 2002; Parker et al., 2002; Tuch et al., 2002; Batchelor et al., 2003). The key feature of this technique requires the construction of an uncertainty function which indicates the 95% confidence interval of the true dominant fiber orientation, i.e. ε_1, for each voxel. These confidence intervals can be represented graphically as cones. Regions with high anisotropy such as the corpus callosum have small uncertainty of the dominant orientation and are represented using a narrow cone. Crossing fiber regions with isotropic diffusion have large uncertainty of the dominant fiber orientation and this is indicated using a wide cone Figure 1.10. Different strategies have been developed to measure the uncertainty function, including bootstrap (Jones, 2003, 2008; Whitcher et al., 2008) and Bayesian methods (Behrens et al., 2003, 2007)

with the assumption of the diffusion tensor model and the noise structure. Knowing the uncertainty of the dominant fiber orientation for each voxel, a fiber can be propagated from seed point A to its neighbor along the direction drawn from the uncertainty function. Eventually the propagated fiber arrives at a target point B or exits the brain. This procedure needs to be done thousands of time (>5000) to query the probabilities of all possible pathways from seed point A to the target. Unlike deterministic tractography, the propagation does not have terminal criteria, such as an FA threshold, and can travel through low anisotropy area. Probabilistic tractography is also resistant to noisy voxels where the errant paths accidentally taken after encountering the voxel tend to disperse quickly. Only a lenient curvature constraint is placed for probabilistic tractography. This constraint prevents a track from circling back to itself. Finally, the connectivity index is calculated for each voxel as the ratio of the number of times the algorithm produced a tract propagating through that voxel and the total number of sampling times. A larger ratio indicates a more probable actual white matter connection (Ciccarelli et al., 2006). Overall, probabilistic tractography has advantages over deterministic tractography in that multiple possible routes of connection and/or branching of tracts are explored and we know how likely it is that a given pathway exists.

The fiber-tracking method used throughout this thesis is limited to the deterministic tractography since the DTI data were acquired with only six diffusion encoding gradients. Probabilistic tractography, on the other hand, requires at least 12 diffusion encoding gradients to estimate the uncertainty cone.

1.2.6.3 Validation

White matter axons have a very small diameter about 0.1-10 μm compared to a voxel of diffusion MRI ~2 mm. The tracts derived from tractography are subject to validation with the actual anatomical structure. It is impractical (and potentially unethical) to inject tracer into living human brain. However, there are other ways to validate our measurements. Lawes et al. found good correlation between the virtual reconstructed white matter tracts and the dissection of post-mortem brains (Lawes et al., 2008). Where the shape and curve of the dissected inferior occipitofrontal fasciculus changed, the tractography tract changed too. Another way to validate diffusion tractography is through the use of functional mapping. Staempfli et al. detected the brain activation related to the movement of the foot, the hand, and the face. The fMRI and tractography results both showed an

anterior–posterior gradient within the putamen in the connections to these functional areas (Staempfli et al., 2008). Animal tracing studies also lend support to the validity of tractography (Tuch et al., 2005; Dyrby et al., 2007).

Figure 1.10 Uncertainty cone represents 95% confidence interval of the true dominant fiber orientation ε_1.

1.2.7 Interpretation of Diffusion metrics

Although the MD of gray and white matter is similar, the FA of white matter is much larger than that of the gray matter. This is because of the highly ordered axon bundles that restrict water diffusing perpendicular to the axon orientation. Even within white matter, regions with denser axon bundles such as corpus callosum have higher FA value ~0.7 than regions with thinner axon bundles such as fornix ~0.5. However, it is incorrect to say that a voxel of the corpus callosum has more myelin or higher axon density than that of the fornix because axon density, axon size, packing, myelin thickness etc. can all contribute to the FA and comparing different tracts with distinct features is not appropriate. A legitimate use of FA is to compare the same white matter tracts in the same group of subjects before and after an intervention, i.e. longitudinal design. Alternatively the comparison can be made between groups of subjects with and without neurological disorders, i.e. cross-sectional design. The experiments carried out in this thesis mainly utilized the cross-sectional design to detect abnormal white matter structure in epilepsy patients in comparison with healthy controls.

Numerous studies have attempted to identify the source of anisotropy in white matter after the definition was born in the 1990s; these studies have been quite successful. Findings from fish (Beaulieu and Allen, 1994; Beaulieu et al., 1996), rodents (Seo et al., 1999), rabbits (Drobyshevsky et al., 2005), and humans (Partridge et al., 2004) demonstrated that the axonal membranes have a primary role in restricting water diffusion and create sufficient FA while the myelin sheaths play a supporting role in modulating the degree of anisotropy (~20% contribution). This result has been demonstrated in dysmylination animal models (Ono et al., 1995; Song et al., 2002). When experiencing only a matrix of neurofilaments without membranes in big axons, water diffuses isotropically (Beaulieu and Allen, 1994; Takahashi et al., 2002). Associating FA and MD to specific microstructure component is difficult since the axon density and myelin volume are related to each other. FA is found to be correlated with both axon counts and myelin content in two human post-mortem DTI-histology studies (Mottershead et al., 2003; Schmierer et al., 2007). A recent study that correlated DTI and microscopy of freshly resected fornix after temporal lobe surgery also found correlation between FA and myelin thickness, extra-axonal fraction, and cumulative axon membrane circumference with the cumulative axon membrane circumference being the strongest determination of FA (Concha et al., 2010).

Recent observations of Wallerian degeneration in animal models shed light on the issue. Song 2003 found a reduction of parallel diffusivity with no change of perpendicular diffusivity in the acute stage of Wallerian degeneration which corresponds to axonal injury and a dramatic increase of perpendicular diffusivity later on with confirmation of histology which corresponds to myelin degradation (Song et al., 2003). Subsequent DTI-histology/microscopy studies have confirmed this relationship and suggested that the parallel and perpendicular diffusivities are specific markers for white matter components (Budde et al., 2007; Sun et al., 2008). In human epilepsy patients, who underwent callosotomy, similar DTI change have also been found at both the early and late stages (Concha et al., 2006). It is important to note that changes in diffusion can be caused by mechanism other than these specific white matter changes. When changes in DTI are observed, edema, gliosis and inflammation may also be the cause. For example, cytotoxic edema after stroke can cause reduction of MD/parallel/perpendicular diffusivity while vasogenic edema leads to increase of diffusivity.

1.3 Epilepsy

1.3.1 General features

1.3.1.1 Definition and classification

Epilepsy is "a chronic condition of the brain characterized by an enduring propensity to generate epileptic seizures, and by the neurobiological, cognitive, psychological, and social consequences of this condition. The definition of epilepsy requires the occurrence of at least one epileptic seizure" (Fisher et al., 2005). The epileptic seizure is "a transient occurrence of signs and/or symptoms due to abnormal excessive and synchronous neuronal activity in the brain" (Fisher et al., 2005). During seizures, the physiology of the brain deviates from the normal state and its function is affected. It needs to be noted that seizures can occur in people who do not have epilepsy as a consequence of head injury, drug overdose, alcohol withdrawal, toxins, eclampsia or febrile convulsion. Epilepsy is used to refer only to chronic conditions with enduring epileptogenic brain dysfunction (i.e. recurrent unprovoked seizures).

The World Health Organization estimates that 50 million people worldwide have epilepsy (World Health Organization, http://www.who.int/mediacentre/factsheets/fs999/en/index.html). This number likely a gross underestimation of the real prevalence since the disease is underreported in developing countries where medical resources are limited. The incidence rate is between 4-10 per 1000 people at a given time. On par with depression, Alzheimer's disease and substance abuse, epilepsy accounts for 1% of the global burden of disease (Murray and Lopez, 1994). For a normal person, the risk of having at least one seizure in their life time is approximately 10% (Hesdorffer et al., 2011). Around one-third of people who experienced a single seizure will eventually develop epilepsy and this risk is greatest during the early and late years of life (Banerjee and Hauser, 2008).

The classification of epilepsy syndromes and seizure types are undergoing a rapid evolution. The previous terminology system, still in common usage, was based on clinical and scientific observations made prior to 1990 (Angeles, 1981; ILAE, 1989). Seizures were classified into three categories including: (1) partial seizures, where seizures arise in a restricted part of the brain in one hemisphere, (2) generalized seizures

where seizures involve both hemispheres from the beginning, and (3) "unknown type", where seizures cannot be classified because of inadequate or incomplete data or because they defy classification. Based on a determination of the level of subject consciousness, partial seizures were further divided into: (1) simple partial seizures where consciousness is not impaired, (2) complex partial seizures where there is an impairment of consciousness and partial seizures evolving to secondarily generalized seizures. Epilepsies and syndromes, on the other hand, were classified into four categories based on epileptic locations, that is: (1) localization-related, (2) generalized, (3) undetermined, either focal or generalized, and (4) special syndromes. Each category was further divided into subtypes based on etiology, including idiopathic epilepsies, denoting those with a possible hereditary predisposition, symptomatic epilepsies denoting those resulting from a known or suspected disorder, and cryptogenic epilepsies denoting those presumed to be symptomatic but with an unknown etiology.

This old classification system has been deemed antiquated and arbitrary since it is unable to incorporate a vast amount of new information that has been gleaned from genome, molecular cell biology, neuroimaging, neurophysiologic technologies etc in the past 20 years (Berg and Scheffer, 2011). New terminology and concepts for the organization of seizures and epilepsy classified seizures have recently been proposed by the International League Against Epilepsy (ILAE) (Berg et al., 2010) in an attempt to clearly demarcate the nature of different epileptic syndromes and meaningfully translate scientific understanding to clinical practice and research.

In the proposed nomenclature, seizures are categorized into three types:

(1) Generalized seizures are conceptualized as originating at some point within, and rapidly engaging with, bilaterally distributed networks. Such bilateral networks can include cortical and subcortical structures and be asymmetric, but they do not necessarily include the entire cortex. Individual seizure onsets can appear localized but their location and lateralization may be inconsistent. This class includes tonic-clonic, absence (typical, atypical, absence with special features), myoclonic (myoclonic, myoclonic atonic, myoclonic tonic), clonic, tonic, and atonic seizures. Focal seizures are conceptualized as originating within networks limited to one hemisphere, which may be discretely localized or more widely distributed.

(2) Focal seizures may originate in subcortical structures. For each seizure type, ictal onset is consistent from one seizure to another with preferential propagation patterns which can involve the contralateral hemisphere. In some cases, however, there is more than one epileptogenic network, and more than one seizure type, but each individual seizure type has a consistent site of onset. An approach for classification for focal seizures has yet to be developed. The descriptors used for individual patients are based on degree of impairment during seizures. Focal seizure descriptors can include "focal seizures without impairment of consciousness or awareness" (roughly corresponds to previous "simple partial seizure") such as focal clonic, autonomic, hemiconvulsive and "focal seizures with impairment of consciousness or awareness" (roughly corresponds to previous "complex partial seizure") such as dyscognitive seizures, a term proposed by Blume et al (Blume et al., 2001; Berg and Scheffer, 2011).

The etiological classification of the epilepsies has also been proposed for three categories, genetic, structural-metabolic, and unknown cause. These terms would replace the previous terms idiopathic, symptomatic and cryptogenic (Shorvon, 2011).

The genetic class characterizes epilepsies as a direct result of known or inferred genetic defects. Genetic defects such as SCN1A and Dravet syndrome have been demonstrated through specific molecular genetic studies (well replicated) and rigorous family studies. Seizures are the core symptom of all epileptic disorders. It should be noted that the existence of genetic defects does not exclude the possible contribution from environmental factors.

The structure-metabolic class characterizes epilepsies with other structural or metabolic conditions or disease that have been demonstrated to be associated with a substantially increased risk of developing epilepsy. Structural lesions include acquired disorders such as stroke, trauma and infection.

Unknown cause is meant to be taken neutrally and to signify that the nature of the underlying cause is as yet unknown. The epilepsy may be due to fundamental genetic defect or it may be the consequence of a separate disorder or condition not yet recognized.

Although many changes were made to the nomenclature, the list of specific electroclinical syndromes and epilepsy diseases defined previously was not affected. An electroclinical syndrome is a complex of clinical features, signs and symptoms that

together define a distinctive, recognizable clinical disorder. These are distinctive disorders identifiable on the basis of a typical age onset, specific EEG characteristics, seizure types, and often other features which, when taken together, permit a specific diagnosis. Currently, there are 29 types of electroclinical syndromes. Juvenile myoclonic epilepsy is one of them (Berg et al., 2010).

1.3.1.2 Epileptogenesis

Animal experiments and data from patients have greatly advanced our understanding of the mechanism by which an epileptic condition is acquired, i.e. epileptogenesis. In genetic epilepsies, the genetically determined defect may express itself during cerebral maturation and cause behavioral changes. In acquired epilepsies, it is assumed that structural lesion or metabolic disturbance in the brain renders the individual neurons more excitable and enhances synchronization by reorganizing neuronal circuitry. Such synchronized epileptic insult could induce inflammatory mechanisms which might further (1) damage dendritic branching and abolish spinous processes, placing excitatory synapses closer to the axon hillock, (2) rearrange specific ion channel distribution, perhaps rendering Ca^{2+} and Na^+ channels more effective and Cl^- and K^+ channels less effective in influencing membrane events at the axon hillock, (3) destroy synaptic terminals, leading to the sprouting of surviving axon fibers to increase synchronization, and thus create recurrent collateral excitation and inhibition, and/or (4) selectively attenuate and enhance different inhibitory influences, facilitating specific excitatory phenomena and promoting synchronization. The availability of specific neurotransmitters altered by structural or functional changes in afferent input may lead to up- or down-regulation of receptors. Receptors that regulate presynaptic and postsynaptic Ca^{2+}, may be particularly affected and this would have profound effects on synaptic connections. Finally, chronic disturbances in the ionic microenvironment, water balance, pH balance, neuronal energy metabolism and neurotransmitter deactivation could result from glial changes accompanying tissue damage or from alterations in neuronal firing patterns (Jerome Engel, 2013).

1.3.1.3 Diagnosis

The diagnosis of epilepsy requires assessment of the patient's history, physical condition, EEG, and neuroimaging findings to determine the type(s) of epilepsy and possible cause

so that appropriate treatment and prognosis can be made. The patient's history includes details, such as the clinical manifestation of the seizure (prodrome, ictal, postictal and interictal), seizure frequency, age of onset, progression of symptoms, antiepileptic drug history, past medical history, family history, and psychosocial history. If possible, a close relative or friend of the patient, someone who witnessed the seizures, should come along to give the description. EEG remains an important test for diagnosis of epilepsy. The interictal and ictal EEG pattern helps to identify types of seizures and specific epilepsy syndromes. The patterns also help to localize the lesion, although the localization is sometimes difficult given the surface electrodes are not sensitive to discharges deep in the brain. MRI is recommended for almost all patients with chronic recurrent seizures. The T1-, T2- weighted structural images have high resolution and good contrast to enable the detection of abnormal signals in the brain which might be the potential cause of epilepsy. Antiepileptic drugs (discussed below) are prescribed to control the seizures following these assessments.

In cases where antiepileptic drugs fail to control seizures, a more detailed evaluation is administered to decide if epilepsy surgery is an option. The presurgical evaluation includes prolonged EEG-video telemetry, neuropsychological tests or functional imaging (such as ^{18}F-fluorodeoxyglucose (FDG-PET), SPECT and fMRI) to help localize epileptogenic region, assess the risk and benefit of surgery and making prognosis.

1.3.1.4 Treatments

The ultimate goal of epilepsy treatment is to eradicate seizures without side effects. However the desired outcome is often not immediately possible. Only two thirds of patients can get seizure free after medical treatment with acceptable side effects (Kwan and Brodie, 2000; Luciano and Shorvon, 2007). The primary treatment option is antiepileptic drugs (AED) that need to be taken daily. There are more than 25 commonly used AEDs and AEDs must be carefully matched to the type of seizure. These drugs reduce or eliminate seizures by targeting different substrates in the brain. AEDs such as phenytoin, lamotrigine, carbamazepine and eslicarbazpine acetate work by binding with sodium channels of the neuron to stop excessive action potentials. AEDs such as topiramate and pregabalin work by blocking the calcium channel on the synapses to prevent over-release of neurotransmitters. AEDs such as benzodiazepins and phenobarbital increase the activity of gamma amino butyric acid (GABA) receptors;

gabapentin increase the production of GABA; and sodium valproate decrease the breakdown of GABA.

Around one third of the epilepsy population becomes medically refractory, i.e. fails two or three AEDs. The surgical option may be suggested for suitable patients after full evaluation. Around 47% patients undergoing anteriomesial temporal lobectomy become seizure free, with AEDs, 10 years after surgery (De Tisi et al., 2011). There are other palliative treatments for epilepsy. Corpus callosotomy helps to stop epileptic discharges from spreading to the other side of the brain and thus can be used to reduce the severity of the resulting event. Vagus nerve stimulation helps to reduce focal seizures by applying a pulse of 1-3 mA, 500 ms in duration, on the vagus nerve at a frequency of 30 Hz. Deep brain stimulation works by stimulating the anterior nucleus of the thalamus using an electric pulse of 5 V or lower. These treatments result in an average of 40% seizure reduction in 50% of the patients. Other complimentary treatment includes dietary manipulations such as the ketogenic diet, operant conditioning, relaxation, meditation and herbal or folk remedies.

This thesis focuses on using MRI to detect subtle structural abnormalities in the two most common types of epilepsy, juvenile myoclonic epilepsy and temporal lobe epilepsy.

1.3.2 Temporal lobe epilepsy

1.3.2.1 General features

Temporal lobe epilepsy (TLE) is presumed to originate in the temporal lobe. TLE accounts for around 24% of all epilepsies and is the most common type of focal epilepsy (Semah et al., 1998). It affects male and female equally. TLE mainly starts at late childhood to adolescence but can occur in all age groups. About 10% TLE patients are refractory to AEDs (Semah et al., 1998). In these refractory cases, anterior temporal lobe resection (the most successfully surgical remedy for epilepsy so far with a ~47% seizure free rate) can be considered for suitable patients after thorough assessment (De Tisi et al., 2011). Around 70-80% of TLE patients have MRI evidence of mesial temporal sclerosis (MTS). The other 20-30% of patients with TLE is reported to have normal MRI, dubbed as nonlesional MRI (nlTLE). While TLE+MTS and nlTLE have similar seizure semiology, the respective surgical success rate of nlTLE is reduced dramatically (Jack et al., 1992; Antel et al., 2002).

TLE patients may experience three types of seizures, (1) focal seizure without consciousness impairment (known as simple partial seizures previously), such as auras, (2) focal seizure with consciousness impairment (known as complex partial seizures previously), and (3) secondarily generalized seizure. Although auras can occur in isolation, they occur at the onset of a complex partial seizure in the majority of patients. There are different types of auras including déjà-vu experience, psychic, fear, auditory, olfactory auras, and the most common, epigastric aura. The epigastric aura is a 'rising sensation' beginning in the abdomen. The occurrence of any of these indicates a potential temporal lobe onset of the epilepsy but cannot be used to predict the affected side.

More stereotypically, TLE patients experience complex partial seizures with altered consciousness, during which they suddenly stop responding and staring blank for 1-2 minutes. In two thirds of complex partial seizures of mesial temporal lobe onset, automatisms occur along with altered consciousness. There are variant types of automatisms including oro-alimentary automatisms such as chewing and lip smacking, and manual automatisms such as fumbling, grasping, pulling at the bed sheets or manipulating an object within reach. If manual automatisms are unilateral and accompanied by contralateral tonic/dystonic limb posturing or focal clonic jerking, it is likely that the seizure origin lies in the side of hemisphere contralateral to the manual automatisms. After the seizure, patients may not be able to recall the event or even events prior to the seizure. This postictal amnesia may result from bilateral impairment of hippocampal function.

EEG is an important tool to detect temporal lobe seizures. The interictal EEG typically shows abnormal anterior temporal sharp waves, especially in TLE+MTS. In 33% of patients these waves are bilaterally independent with a maximum in the basal areas, such as sphenoidal, true temporal or earlobe electrodes. Ictal onset usually starts with the attenuation of interictal spiking and background. Within 30s of the onset of attenuation, a 5-7 Hz rhythmic pattern starts in the inferior temporal region and then typically develops into intermittent slow waves that increase in frequency until ictal termination (Jerome Engel, 2013). In case of bi-temporal discharges, intracranial electrodes may be used to identify the origin side invasively.

Neuroimaging revolutionized the detection of structural changes, such as tumor, trauma, cortical dysplasia and hippocampal sclerosis in TLE. Hippocampal sclerosis is associated

with MRI evidence of hippocampal atrophy in T1 images and hyperintensity in T2 images. FDG-PET can identify temporal lobe foci hypoperfusion with a high sensitivity and specificity. This identification is particularly good interictally. Quantitative neuroimaging can be used to further locate the specific gray/white matter functional and structural alterations related to TLE. This neuroimaging technique will be discussed in detail in neuroimaging section below.

Neuropsychological testing is useful to assess the affected brain areas, lateralize epileptic lesion, and predict the risk of surgical morbidity in TLE. A battery of tests include, at a minimum, the assessment of intelligence, frontal executive skills, attention, memory, visuo-spatial skills and language. TLE patients typically demonstrate memory and learning problems and those with most intact cognitive function will see greatest deficits after surgery.

TLE+MTS has shown evidence of a progressive nature. This means that seizure control, cognition, behavior, structural abnormalities, EEG patterns and social interactions can worsen over time. There is evidence of progressive damage of clinical (Kwan and Brodie, 2000), cognitive (Helmstaedter et al., 2003; Hermann et al., 2006), EEG (Bartolomei et al., 2008), and neuroimaging metrics (Kälviäinen et al., 1998; Tasch et al., 1999; Briellmann et al., 2002; Fuerst et al., 2003; Coan et al., 2009) in this patient group.

1.3.2.2 Etiology

There are a wide variety of etiologies associated with TLE, such as trauma, neoplasms, brain abscesses, arteriovenous malformations, and encephlomalacia following trauma, stroke, encephalitis or developmental malformations such as heterotopias. In addition, herpes simplex encephalitis can also lead to hippocampal sclerosis and diffuse damage to the temporal lobe.

Hippocampal sclerosis is the most common structural abnormality associated with TLE. It is characterized by neuronal loss and reactive gliosis that range from involvement of only the endfolium or hilus of the dentate gyrus to widespread cell loss in most or all of the hippocampus as well as parts of amygdala and parahippocampal gyrus (Table 1.1, Figure 1.11). Hippocampal atrophy resembling hippocampal sclerosis can also be seen in the absence of epilepsy, for example in cases like dementia and depression. Not all neurons in the hippocampus are affected equally by sclerosis. There is a selective

28

vulnerability where substantial loss of neurons usually happens in CA1 and the endfolium while CA2 and the granule cell layer of the dentate gyrus appear relatively resistant to neuronal insult. The neuronal loss and selective vulnerability is likely due to the excessive release of the excitatory neurotransmitters glutamate and aspartate, acting at calcium-permeable NMDA and AMPA receptors ('excitotoxicity') (Meldrum, 1993). This results in intense depolarization and accumulation of intracellular calcium that elicits multiple cell death pathways.

The mechanisms behind epileptogenesis have long been a subject of debate (Jinde et al., 2013). It is widely known that hilar mossy cells are prone to injury and damage to them has been associated with a change of excitability in the dentate gyrus. So far, three theories have been proposed regarding the mechanisms of mossy cell loss in epileptogenesis, i.e. mossy cell loss-induced sprouting, dormant basket cell and irritable mossy cell. Mossy cell loss-induced sprouting theory hypothesizes that epilepsy-induced loss of mossy cells triggers mossy fiber sprouting. In mossy fiber sprouting, new axons arise from granule cells to establish new synapses in the inner molecular layer of the dentate gyrus. This process creates a recurrent excitatory circuit leading to epileptogenesis (Tauck and Nadler, 1985; Sutula et al., 1992; Dudek et al., 1994; Nadler, 2003). The dormant basket cell theory hypothesizes that the loss of mossy cells deprive the excitatory synapse of interneurons (the basket cells that inhibit granule cells), leading to a disinhibition of granule cells (Sloviter, 1991, 1994; Bernard et al., 1998; Sloviter et al., 2003; Zappone and Sloviter, 2004). The irritable mossy cell theory hypothesizes that the mossy cells that survive insult can generate prolonged trains of action potential discharges that results in dentate hyperexcitability (Santhakumar et al., 2000; Ratzliff et al., 2002, 2004).

It is still unclear how hippocampal sclerosis develops in life. Given the observation that 30% of TLE and hippocampal sclerosis patients experience prolonged febrile seizures during childhood, it is reasonable to postulate that febrile seizures may result in hippocampal sclerosis (Falconer, 1974; French et al., 1993). However, looking at all children who experience febrile seizures between the ages of one and five, very few of them develop epilepsy later in life (Annegers et al., 1979; Neligan et al., 2012). So febrile seizures cannot be fully responsible for epilepsy development. A now popular "two-hit hypothesis" attempts to explain the process. It hypothesizes that there is a genetic

29

predisposition, prenatal or perinatal insult or other predisposition in a certain population, i.e. the first hit, and an injury in these people could be febrile seizure, trauma or infection etc., then the second hit dramatically increases the chance of hippocampal sclerosis and epilepsy (Velísek and Moshé, 2003; Wieser, 2004).
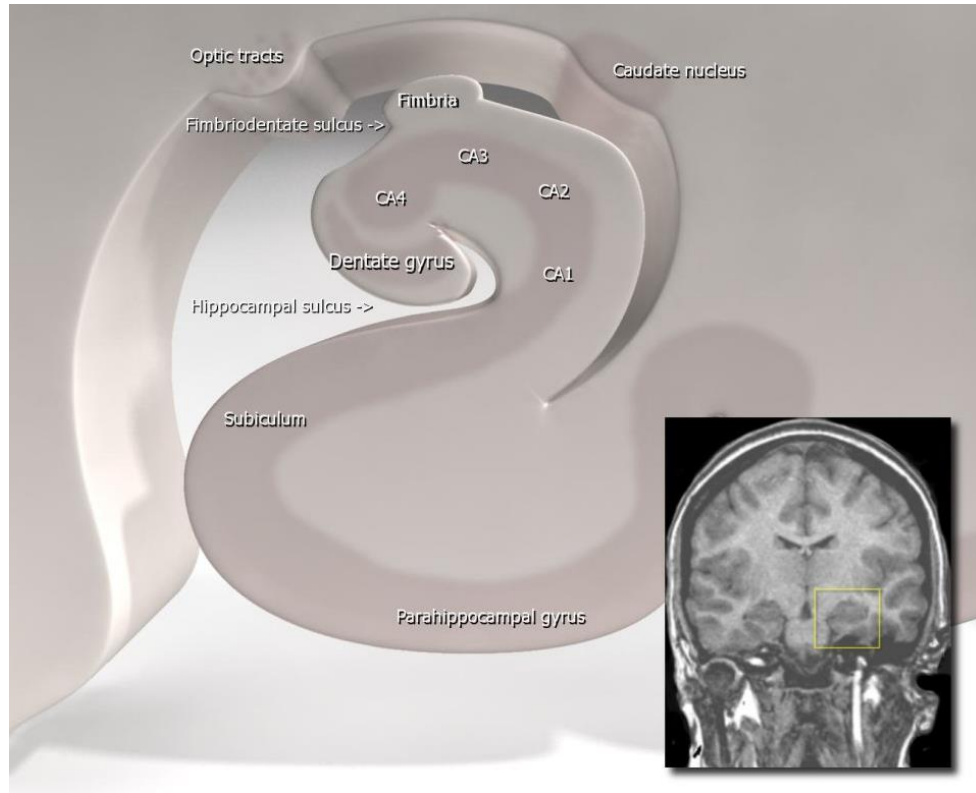
Figure 1.11 The hippocampal anatomy. The hippocampus is an extension of the subiculum of the parahippocampal gyrus. In coronal plane the hippocampus and parahippocampal gyrus form an S-shaped configuration. The hippocampus itself consists of two interlocking C-shaped structures: the cornu ammonis (CA1, CA2, CA3, CA4) and the dentate gyrus. Figure from public domain.

Table 1.1 Simple classification of hippocampal sclerosis

Subtype	Main pathological features
Classical	Neuronal loss and gliosis mainly in CA1, CA3 and endfolium
Total	Severe neuronal loss in all hippocampal subfields and the dentate gyrus
Endfolium	Neuronal loss and gliosis restricted to the hilum of the dentate gyrus

1.3.2.3 Treatment and prognosis

The common AEDs used to treat TLE are carbamazepine, oxcarbazepine, lamotrigine, topiramate, and levetiracetam. The seizures can often be controlled for several years. About half of the children with TLE outgrow the disorder. For 10% intractable TLE cases, surgery is considered. Other complimentary therapies include vagus nerve stimulation or a ketogenic diet.

1.3.2.4 Neuroimaging findings

Neuroimaging plays an important role in the diagnosis and pre-surgical evaluation of TLE. Structural MRI can be visually examined or quantitatively measured to reveal evidence of volume or signal changes that might indicate hippocampal sclerosis. When MRI is not effective, for example in nlTLE, other imaging modality may be employed. FDG-PET is the most sensitive interictal imaging technique for identifying the focal functional deficit in nlTLE. Hypometabolism is usually found in the epileptogenic temporal lobe and also ipsilateral thalamus, basal ganglia and other cortical structures. PET has been shown to correctly lateralize the lesion in 80% of TLE cases that present with normal MRI (Won et al., 1999). "Negative MRI and positive PET" has been distinguished as a unique category of TLE associated with good surgical outcome (Carne et al., 2004). FDG-PET can also help with equivocal cases like bitemporal seizure onset by lateralizing the origin base on asymmetric hypometabolism (Liew et al., 2009).

Other PET ligands can be used in research to improve our understanding of the neurochemistry of TLE. ^{11}C-flumazanil PET is able to identify focal abnormalities in 80% of patients with TLE and normal MRI (Koepp et al., 2000). Reduction of binding of ^{11}C-flumazanil has been shown to be confined to the hippocampus in TLE patients with hippocampal sclerosis (Koepp et al., 1997). ^{18}F-MPPF (2'-methoxyphenyl-(N-2'-pyridinyl)-p-^{18}F-fluorobenzamidoethylpiperazine) PET measures the binding potential of the 5-HT$_{1A}$ receptors. These receptors mediate serotonin and measures of their binding potential have shown promise as a marker of the epileptogenic lobe. The sensitivity of this technique (90%) is higher higher than the sensitivity of FDG-PET (Didelot et al., 2008). Further, the binding potential of dopaminergic receptors D2/D3, measured by ^{18}F-Fallypride PET, was found to be reduced in the lateral temporal and temporal pole in mTLE patients with hippocampal sclerosis (Werhahn et al., 2006).

The ictal SPECT is commonly used to investigate relative cerebral blood flow during seizures in patients with TLE. ^{99}mTc-HMPAO and ^{99}mTc-ECD are two common tracers that have a quick uptake in the brain. They reach peak uptake within 2 mins of injection without redistribution up to at least 2h. So the SPECT image, taken within this period, reflects the cerebral blood flow at the time of seizure. Ictal SPECT is more effective in the identification of the epileptic side/location in TLE patient (sensitivity $> 73\%$) than interictal SPECT (sensitivity ~50%) (Devous et al., 1998; Spanaki et al., 1999; Weil et al., 2001; Zaknun et al., 2008).

Structural MRI is widely used to study the substrates of TLE and previous research has focused on the hippocampus. Extratemporal pathology has also been recognized for decades and it has been suggested as an explanation for the lack of surgical success in some TLE+MTS patients. With the advent of quantitative MRI, recent studies have demonstrated widespread extratemporal gray matter volume/concentration, white matter volume/concentration and cortical thickness abnormalities spanning mesial temporal, temporal neocortex, thalamus, frontocentral, parietal areas and cerebellum. The relevance of these extratemporal subtle lesions to surgical outcomes remains uncertain. A brief review of previous studies regarding to quantitative analysis of structural MRI images is listed in Table 1.2.

Table 1.2 Previous studies of structural abnormalities in TLE detected by structural MRI. Abbreviations: L (left), R (right), GM (gray matter), WM (white matter), TBSS (Tract-based spatial statistics), ROI (Region of interest), VBA (Voxel based analysis), VBM (Voxel based morphology).

Study	Modality	Subjects	Findings of TLE
(Lee et al., 1995)	Volumetry, cortical thickness	6 left mTLE vs. 10 Controls	Bilateral decrease in white matter surface area and a small left-sided decrease in white matter volume.
(Marsh et al., 1997)	Volumetry	14 TLE vs. 49 Controls	Smaller temporal and frontoparietal GM volume bilaterally and temporal lobe WM volume bilaterally
(DeCarli et al., 1998)	Volumetry	21 left TLE (11 L, 9 R) vs. 19 Controls	No significant differences in total cerebral, left temporal lobe, right temporal lobe, or total temporal lobe volumes were found. Left hippocampal volumes and left hippocampus-to-right hippocampus volume ratio, left hippocampal volumes, mean left thalamic, left caudate, and bilateral lenticular volumes, left-to-right thalamic volume ratio were significantly lower in

			patients.
(Lee et al., 1998)	Volumetry, surface analysis (curvature)	27 uTLE (12 L, 15 R) vs. 42 Controls	Bilateral temporal lobe and total GM volume reduction, ipsilateral temporal lobe reduction
(Bernasconi et al., 1999)	Volumetry	20 TLE vs. 18 Controls	Bilateral reduction in the volume of the entorhinal cortex and greater reduction was seen in the ipsilateral side. The volumes of the ipsilateral hippocampus and the amygdala were smaller.
(Bernasconi et al., 2000)	Volumetry	6 TLE with hippocampal atrophy vs. 20 Controls	Volume reduction in ipsilateral entorhinal cortex in all patients; ipsilateral reduction of the perirhinal cortex in 2/6 (33%) patients; no reduction of the volume of left posterior parahippocampal cortex in any patient. (50%) of patients, the EC was also abnormally small contralateral to the seizure focus.
(Sandok et al., 2000)	Volumetry	185 TLE vs. 80 Controls	Reduction of cerebellar volumes.
(Woermann et al., 2000)	VBM	24 TLE with aggression vs. 24 TLE without aggression vs. 35 Controls	The patients with TLE with aggressive episodes had a decrease of GM, most markedly in the left frontal lobe, compared with the control group and with patients with TLE without aggressive episodes
(Bernasconi et al., 2001)	Volumetry	22 TLE with normal hippocampal volume vs. 24 Controls	Reduction in the volume of the entorhinal cortex ipsilateral to the seizure focus in patients with left and right temporal lobe epilepsy.
(Dreifuss et al., 2001)	Volumetry	27 TLE vs. 14 Controls	The patient group had smaller thalamic and striatal volumes in both hemispheres, mostly ipsilateral to the epileptic focus.
(Jutila et al., 2001)	Volumetry	27 TLE vs. 10 extratemporal partial epilepsy vs. 20 Controls	In left TLE, the mean volume of the ipsilateral entorhinal cortex was reduced by 17% and that of the ipsilateral temporopolar cortex by 17%. In right TLE, the mean ipsilateral entorhinal volume was reduced by 13%, but only in patients with hippocampal atrophy. Asymmetry ratios also indicated ipsilateral cortical atrophy.
(Moran et al., 2001)	Volumetry	62 TLE vs. 20 Controls	Mesial and lateral temporal lobe substructures showed atrophy.
(Keller et al., 2002b)	VBM, stereological analysis	58 left TLE vs. 58 right TLE vs. 58 Controls	Bilateral thalamic, prefrontal, and cerebellar GM concentration reduction in patients, which correlated with duration and age of onset of epilepsy.
(Coste et al., 2002)	Volumetry	30 TLE (15 L, 15 R) vs. 30 Controls	Reduction of the ipsilateral temporopolar white and gray matter volumes in both left and

			right TLE
(Keller et al., 2002a)	VBM	40 left TLE with hippocampal atrophy vs. 36 right TLE with hippocampal atrophy vs. 85 Controls	GM concentration reduced in anterior hippocampus in left TLE and posterior hippocampus in right TLE and right dorsal prefrontal in both TLE. Bilateral temporal lobe GMC excess was observed in left HA patients, while ipsilateral temporal lobe GMC excess was observed in right HA patients.
(Bernasconi et al., 2003b)	Volumetry	70 TLE vs. 18 extratemporal lobe epilepsy vs. 20 idiopathic generalized epilepsy	Entorhinal cortex volume was smaller ipsilateral but not contralateral. No difference in the entorhinal cortex volumes ipsilateral and contralateral to the seizure focus was seen in patients with extratemporal lobe epilepsy and idiopathic generalized epilepsy.
(Bernasconi et al., 2003c)	Volumetry	25 TLE vs. 20 Controls	The volume of ipsilateral hippocampal head, body and tail and the entorhinal and perirhinal cortices were smaller with hippocampal head and entorhinal cortex mostly affected. The mean volume of the posterior parahippocampal cortex was not different from that of normal controls.
(Hogan et al., 2003)	Deformation-based hippocampal shape analysis	15 left TLE+MTS vs. 15 right TLE+MTS	Both the right- and left-MTS groups showed similar shape changes, with maximal inward deformation in the medial and lateral hippocampal head and the hippocampal tail. However, more extensive involvement was seen in the lateral hippocampal body in the right-MTS group as compared with the left.
(Lambert et al., 2003)	Volumetry	10 TLE	The volumes of the amygdala and hippocampus on the operated side were significantly smaller than on the unoperated side. More severe astrocytosis appeared to go along with smaller volume ratios but the relationship was not significant.
(Hermann et al., 2003)	Volumetry	58 TLE vs. 62 Controls	Significant volumetric reductions were evident across frontal, temporal and parietal but not occipital lobe regions. Subarachnoid but not total ventricular CSF was significantly increased in epilepsy patients.
(Bernasconi et al., 2004)	VBM	85 TLE (45 L, 40 R) vs. 47 Controls	Atrophy in TLE extends beyond the hippocampus involving other limbic areas such as the cingulum and the thalamus, as well as extralimbic areas, particularly the frontal lobe. White matter reduction was found in ipsilateral temporopolar, entorhinal, and perirhinal areas.

(Hogan et al., 2004)	Volumetry, deformation-based hippocampal segmentations	30 mTLE+MTS (15 L, 15 R) vs. 15 Controls	MTS hippocampi showed significant ipsilateral but not contralateral volume loss in TLE+MTS.
(McMillan et al., 2004)	VBM	25 TLE (13 L, 12 R) vs. 62 Controls	GM abnormalities were evident in ipsilateral hippocampus and ipsilateral thalamus. Temporal and extratemporal white matter was affected ipsilateral to the side of seizure onset, in both left and right temporal lobe epilepsy groups.
(Bonilha et al., 2004)	VBM	43 mTLE (22 L, 21 R) vs. 49 Controls	Left and right MTLE exhibited GM concentration reduction in the ipsilateral hippocampus, ipsilateral parahippocampal and isocortical temporal regions. Patients with MTLE also showed GM concentration reduction in subcortical nuclei such as the thalamus and caudate, in the cerebellum, in the midbrain, and in parieto-occipital regions.
(Bonilha et al., 2005)	VBM	43 mTLE (22 L, 21 R) vs. 49 Controls	GM concentration reduction in the anterior portion relative to posterior thalami. Thalamic atrophy was greater ipsilateral to the MTLE origin than on the contralateral side.
(Cormack et al., 2005)	VBM	20 left TLE vs. 10 right TLE vs. 22 Controls	Reduced GM ipsilateral to the seizure focus not in the hippocampus, lateral temporal lobe and in extra-temporal regions including the thalamus, posterior cingulate cortex and cerebellum. Bilateral differences were present in the frontal and parietal opercular cortices and lateral temporal regions.
(Seidenberg et al., 2005)	Volumetry	24 TLE (15 L, 19 R) vs. 65 Controls	Abnormalities extend beyond the ipsilateral hippocampus and temporal lobe with extratemporal (frontal and parietal lobe) reductions in cerebral white matter, especially ipsilateral but also contralateral to the side of seizure onset.
(Mueller et al., 2006)	VBM	26 TLE+MTS vs. 17 nonlesional TLE vs. 30 Controls	In TLE+MTS, GM/WM volume and concentration reductions in the ipsilateral limbic system, ipsi- and contralateral neocortical regions, thalamus, cerebellum, internal capsule, and brainstem when compared with controls. In contrast, no differences of GM/WM volumes/concentrations were found between nonlesional TLE and controls or between nonlesional TLE and TLE+MTS.
(Lin et al., 2007)	Cortical thickness	15 left mTLE vs. 15 right mTLE	Both mTLE groups showed up to 30% bilateral decrease in cortical thickness,

		vs. 19 Controls	in the frontal poles, frontal operculum, orbitofrontal, lateral temporal, and occipital regions. In both groups, cortical complexity was decreased in multiple lobar regions.
(Bonilha et al., 2007)	VBM	36 mTLE vs. 49 Controls	mTLE showed a more intense correlation between hippocampal gray matter volume and regional gray matter volume in locations such as the contralateral hippocampus, bilateral parahippocampal gyri and frontal and parietal areas. Compared with right mTLE, patients with left mTLE exhibited a wider area of atrophy related to hippocampal gray matter loss, encompassing both the contralateral and ipsilateral hemispheres, particularly affecting the contralateral hippocampus.
(Pell et al., 2008)	VBM, voxel-based relaxometry (VBR)	19 TLE vs. 115 Controls	The volume and T2 changes obtained using the combined univariate approach were found in an extensive area, prominently in the ipsilateral hippocampus and amygdala (overlap of GM-VBM and VBR), and in the remaining temporal lobe (overlap of WM-VBR and VBR).
(Riederer et al., 2008)	VBM	22 mTLE vs. 17 cryptogenic TLE vs. 12 Controls	Decreased GM volume beyond the hippocampus in the ipsilateral thalamus in mTLE. GM volume decrease was more widespread in patients with left-sided seizure focus including the left parahippocampal and superior temporal gyrus, frontal regions, cerebellum, and the right cingulum. In cryptogenic TLE, decreased GM volume was observed in the frontal and orbitofrontal cortex, the cerebellum, neocortical temporal regions, and in the right parahippocampal cortex. Again, patients with left-sided seizure focus had a more widespread and extensive GM volume decrease including regions such as the right and left cingulum.
(Gong et al., 2008a)	Volumetry, DTI	17 TLE+MTS vs. 10 nonlesional TLE vs. 26 Controls	No significant changes were found in either DTI parameters or volume of thalamus in nonlesional TLE patients, as compared to healthy controls. However, both DTI parameters and MRI volumetry showed bilateral thalamic pathology in TLE+MTS patients. Also, TLE+MTS patients showed significant reduction of thalamic volume as compared to nonlesional TLE patients.
(Labate et al.,	VBM	95 mild TLE (34	Reduction in GM volume in the

2008)		MTS, 61 nonlesional) vs. 37 Controls	hippocampus and thalami in midl TLE and more severe in TLE+MTS patients than nonlesional TLE and controls.
(McDonald et al., 2008b)	Volumetry (Freesurfer)	21 mTLE (10 L, 11 R) vs. 21 Controls	Hippocampal volume reduction on the side ipsilateral to the seizure focus, as well as bilateral reductions in thalamic and cerebellar GM volume. Significant asymmetry in the hippocampus and putamen in patients compared to controls.
(McDonald et al., 2008c)	Cortical thickness	21 mTLE vs. 21 Controls	Bilateral thinning was observed within frontal and lateral temporal regions in mTLE. The most striking finding was bilateral cortical thinning in the precentral gyrus and immediately adjacent paracentral region and pars opercularis of the inferior frontal gyrus, extending to the orbital region.
(Keller et al., 2009)	VBM, stereological analysis	43 TLE vs. 30 Controls	TLE had volume atrophy of the ipsilateral hippocampus and bilateral dorsal prefrontal cortex.
(Bonilha et al., 2009)	VBM	23 mTLE vs. 58 Controls	The ipsilateral hippocampi of patients with MTLE displayed a significantly lower mean Z-score compared to the hippocampi of controls
(Brázdil et al., 2009)	VBM	20 mTLE+HS vs. 20 Controls	Extensive GM volume reduction than GM concentration reduction in patients' affected hippocampus. In addition, significant GMV reduction was observed in the ipsilateral thalamus in mTLE+HS patients.
(Das et al., 2009)	Hippocampal thickness	20 TLE	Pronounced disease-related decrease in thickness is found in posterior and anterior hippocampus. A region in the body also shows increased thickness in patients' healthy hippocampi compared with controls.
(Mueller et al., 2010)	Coritcal thickness	15 TLE+MTS vs. 16 nonlesional TLE vs. 35 Controls	Both TLE+MTS and nonlesional TLE showed both widespread temporal and extratemporal corticalthinning. In TLE+MTS, the inferior medial and posterior temporal regions were most prominently affected while lateral temporal and opercular regions were more affected in nonlesional TLE.
(Bonilha et al., 2010)	VBM, DTI/probabilistic tractogrpahy	23 mTLE(8 L, 15 R) vs. 34 Controls	Reduction in GM volume and FA in perihippocampal and limbic areas. There was a decrease in hippocampal probabilistic tractography in patients with mTLE in limbic areas.
(Pail et al., 2010)	VBM	20 left TLE+HS vs. 20 right TLE+HS vs. 40 Controls	Right mTLE+HS had reduction of GM volume in the mesiotemporal structures and the ipsilateral thalamus (as in left mTLE+HS), but also notably in the

			ipsilateral insula and contralateral thalamus. A statistical analysis revealed a significantly more extensive reduction of GM volume in the ipsilateral/contralateral insula and the contralateral thalamus in the subgroup with right-sided compared to left-sided mTLE+HS.
(Labate et al., 2011)	VBM	19 mild TLE with MTS vs. 19 refractory TLE with MTS vs. 37 Controls	Both mild TLE and refractory TLE patients showed GM volume reduction of the bilateral thalamus, left hippocampus, and sensorimotor cortex compared with controls. No significant GM difference was found between refractory TLE and mild TLE groups.
(Mueller et al., 2010)	Cortical thickness, volumetry	15 TLE+MTS vs. 14 nonlesional TLE vs. 29 Controls	TLE+MTS had bilateral volume loss in the anterior thalamus, which was correlated with CA1 volume and cortical thinning in the mesiotemporal lobe. Nonlesional TLE had less severe volume loss in the dorsal lateral nucleus, which was correlated with thinning in the mesiotemporal region but not with extratemporal thinning.
(Kaaden et al., 2011)	VBM	38 early onset TLE vs. 52 late onset TLE	GM excess in the early-onset group which were found mainly in frontal regions.
(Oyegbile et al., 2011)	Volumetry	46 TLE vs. 31 Controls	Bilateral reductions in the superior and inferior posterior lobes, whereas volume was significantly increased in the anterior lobes, especially in patients with early onset TLE, and not significantly different in the corpus medullare.
(Kemmotsu et al., 2011)	Cortical thickness, DTI	18 left TLE vs. 18 right TLE vs. 36 Controls	Cortical thinning and white matter compromise, predominately on the side ipsilateral to the seizure onset. Relative to RTLE, patients with LTLE showed more widespread abnormalities, particularly in white matter fiber tracts.
(Labate et al., 2011)	Cortical thickness	32 benign TLE with MTS vs. 16 benign TLE wihout MTS vs. 44 Controls	Cortical thinning was found in benigh TLE with MTS in the sensorimotorcortex bilaterally but was more extensive in the left hemisphere and other areas including occipital cortex, left supramarginal gyrus, left superior parietal gyrus, left paracentral sulcus, left inferior/middle/superior frontal gyrus, left inferior frontal sulcus, right cingulate cortex, right superior frontal gyrus, right inferior parietal gyrus, right fusiform gyrus, and cuneus/precuneus. In the benign TLE without MTS, a

			similar neurodegenerative pattern was detected, although not surviving correction for multiple comparisons. Direct comparison between the two TLE groups did not reveal significant changes.
(Ronan et al., 2011)	Cortical curvature, thickness, volumetry	29 TLE with negative MRI vs. 40 Controls	Abnormal cortical curvature in the basal left temporal lobe. The presence of whole-brain volume loss in TLE was confirmed and found not to contribute to the cortical curvature abnormality in the temporal lobe.
(Alhusaini et al., 2012)	Cortical surface area, surface geometric distortion, thickness	70 TLE+HS vs. 40 Controls	Asymmetric reduction in cortical surface area, predominantly in ipsilateral mesial and anterior temporal lobe subregions, of patients with TLE+HS. Changes in surface geometric features were also evident and closely mirrored surface area patterns. In contrast, cortical thinning appeared dispersed across the cortex bilaterally. The regression models revealed that ipsilateral hippocampal volume was a significant predictor of temporal lobe surface area changes.
(Bernhardt et al., 2012)	Cortical thickness	36 TLE vs. 19 Controls	TLE showed ipsilateral thalamic atrophy that was located along the medial surface, encompassing anterior, medial, and posterior divisions. Unbiased analysis correlating the degree of medial thalamic atrophy with cortical thickness measurements mapped bilateral frontocentral, lateral temporal, and mesiotemporal cortices. These areas overlapped with those of cortical thinning found when patients were compared with control subjects.
(Butler et al., 2013)	Volumetry	20 TLE+MTS vs. 24 nonlesional TLE vs. 20 extratemporal epilepsy vs. 114 Controls	Patients with TLE without MTS had significantly larger septal nuclei than patients with extratemporal epilepsy and controls. This was not true for patients with MTS.

Diffusion tensor imaging, on the other hand, has revealed widespread white matter alteration shown by decreased FA and increased MD. Deterministic tractography has been used in previous studies to examine the diffusion properties of some tracts. One important finding consistent with gray matter studies is that TLE+MTS has more

extensive white matter changes than nlTLE patients (Concha et al., 2009; Liacu et al., 2012). Major findings of specific tracts are summarized in Table 1.3.

Table 1.3 Previous findings of reduced FA in white matter using diffusion tensor tractography in TLE patients

Tracts	Ipsilateral FA ↓	Contralateral FA ↓	Bilateral FA ↓	Combined FA↓	No difference
Fornix	(Focke et al., 2008; Ahmadi et al., 2009)		(Concha et al., 2005a); (Kemmotsu et al., 2011); (Concha et al., 2005a)	(Concha et al., 2009)	(McDonald et al., 2008a)
Parahippocampal cingulum	(Thivard et al., 2005; McDonald et al., 2008a)		(Concha et al., 2005a); (Ahmadi et al., 2009);(Focke et al., 2008)	(Concha et al., 2009)	
dorsal Cingulum	(Ahmadi et al., 2009)				
Uncinate Fasciculus	(Rodrigo et al., 2007); (Diehl et al., 2008b) in left TLE; (Lin et al., 2008); (McDonald et al., 2008a); (Kim et al., 2011)	(Diehl et al., 2008b) in right TLE;	(Govindan et al., 2008)	(Concha et al., 2009)	(Ahmadi et al., 2009)
Inferior Longitudinal Fasciculus	(Ahmadi et al., 2009)		(Govindan et al., 2008); (McDonald et al., 2008a)	(Concha et al., 2009)	
Arcuate Fasciculus	(Lin et al., 2008)		(Govindan et al., 2008)		
Superior Longitudinal Fasciculus	(Ahmadi et al., 2009)			(Concha et al., 2009)	
Corticospinal Tract			(Govindan et al., 2008)	(Concha et al., 2009)	(McDonald et al., 2008a)
Inferior Fronto-occipital Fasciculus	(Ahmadi et al., 2009)			(Concha et al., 2009)	
Anterior Thalamic Radiation	(Ahmadi et al., 2009)				
Anterior Limb of Internal Capsule				(Concha et al., 2009)	

External Capsule			(Arfanakis et al., 2002; Gross et al., 2006)
Genu of Corpus Callosum		(Knake et al., 2009)	(Gross et al., 2006)
Body of Corpus Callosum		(Knake et al., 2009)	(Concha et al., 2009)
Posterior Corpus Callosum			(Arfanakis et al., 2002)

1.3.3 Juvenile myoclonic epilepsy

1.3.3.1 General features

Juvenile myoclonic epilepsy (JME) is the most common syndrome of idiopathic generalized epilepsies (~26%) that have a clear but complex genetic basis (Kobayashi et al., 2008). JME affects up to 10% of all epilepsies and is equally prevalent in both boys and girls. Onset of JME typically occurs between the ages of 12 and 19 and most frequently between the ages of 13 and 16. JME is characterized by bilaterally synchronous single or repetitive massive myoclonic jerks, i.e. myoclonic seizures or myoclonus, during which consciousness is well preserved, and also generalized tonic-clonic seizures characterized by impaired consciousness, violent movement and a long tonic phase. The myoclonic jerks predominantly involve the extensor muscles of the arms and, sometimes legs, in an irregular and arrhythmic manner. Seizures commonly occur shortly after awakening. Fifteen to thirty percent of patients also have absence seizures. Alcohol, sleep deprivation, emotional stress and fatigue often trigger the seizures. Thirty percent of patients are also photosensitive (Wolf and Goosses, 1986).

EEGs in JME typically show 4-6 Hz bilateral spike-and-wave or polyspike-and-wave discharges with a fronto-central predominance on a normal background (Montalenti et al., 2001). The spikes may occur without associated myoclonic jerks. Other patterns such as slow sharp waves, bursts of slow waves, groups of spikes and a fast rhythm may also be found. Recent dense array EEG and quantitative analysis suggested that the epileptiform discharges have a source localized in orbitofrontal, mesiofrontal, and, to a lesser extent, basal-medial temporal lobe regions (Holmes et al., 2010).

41

By definition, JME patients have normal qualitative MRI; however, advanced image analysis on high resolution MRI images recently pinpointed structural and metabolic abnormalities in JME patients.

Persons with JME may show frontal lobe dysfunction and immature personalities, but they have normal intelligence and behavioral adjustment (Wandschneider et al., 2010). Most studies reported average IQs in JME patients (Sonmez et al., 2004; Iqbal et al., 2009; Roebling et al., 2009; O'Muircheartaigh et al., 2011) however some studies have shown lower verbal IQs in JME subjects when compared to healthy controls (Pascalicchio et al., 2007; Wandschneider et al., 2010). Global attention was reported as normal in some studies (Sonmez et al., 2004; Roebling et al., 2009) while others have shown impairment in JME (Pascalicchio et al., 2007; Wandschneider et al., 2010). Verbal and non-verbal episodic memory are generally spared in JME (Roebling et al., 2009; Wandschneider et al., 2010). Frontal lobe functions have been reported abnormal in JME patients including working memory (Swartz et al., 1994), executive functions (Devinsky et al., 1997; Sonmez et al., 2004; Pascalicchio et al., 2007; Wandschneider et al., 2010), and prospective memory (Wandschneider et al., 2010).

1.3.3.2 Genetic causes

JME has been associated with heterogeneous genetic causes. Various inheritance models have been reported including autosomal dominant, autosomal recessive and multifactorial and complex models (Gardiner, 2005); however, the cause of vast majority of JME has not been identified. Interestingly, the clinical manifestation of these different genetic mutations is indistinguishable.

The $GABA_A$ receptor is a ligand-gated chloride channel that mediates fast inhibition in the adult central nervous system. It consists of 19 different classes of subunits (α1-6, β1-4, γ1-3, δ, ϵ, π, θ, and ρ1-2). JME has been associated with mutation of GABRA1(Cossette et al., 2002) and GABRD (Dibbens et al., 2004), encoding the α1 and δ subunits, respectively. These mutations result in a reduction of GABA-activated chloride currents and thus reduce inhibition of normal excitation (Macdonald et al., 2004). It has been shown that at least two mutations in GABRA1 (p.A322D, p.S326fs328X) cause reduced surface expression of receptor protein since the mutant receptors are retained in the endoplasmic reticulum (Krampfl et al., 2005; Maljevic et al., 2006).

Previous studies found polymorphism of the potassium channel gene KCNQ3 (8q24) may be an important predisposing factor for JME in Indian probands (Zifkin et al., 2005). The late expression of this gene may account for the adolescent onset of JME (Vijai et al., 2003). The potassium channel is involved in the slow inhibitory post-synaptic potential and regulates the fast repolarization phase of action potentials. Decreased activity of this potassium channel delays the repolarizing action potential and thus lowers the excitation threshold for subsequent action potentials. This delay predisposes the system to undesirable discharges (Vijai et al., 2003). Another potassium channel gene, KCNJ10, has been found to be related with the susceptibility of several other common seizure types (Buono et al., 2004).

Another study associated mutation of CLCN2 (3q26) with decreased GABA inhibition and increased probability of seizures (Haug et al., 2003; Kleefuss-Lie et al., 2009). Whether or not this study is valid is still being debated (D'Agostino et al., 2004; Niemeyer et al., 2010). Nevertheless, they have reported that the gene CLCN2 is responsible for the synthesis of voltage-gated chloride channel ClC-2, which is specially expressed in neurons inhibited by GABA. The mutation of CLCN2 causes loss of function in the chloride channel ClC-2. This dysfunction results in intracellular accumulation of chloride and decreased response to GABA inhibition (Haug et al., 2003; Kleefuss-Lie et al., 2009).

Five mutations of gene EFHC1 (6p12) have been uncovered in familiar JME (Suzuki et al., 2004; Annesi et al., 2007; Medina et al., 2008; Jara-Prado et al., 2012). In animal models, the EFHG1 protein is not an ion channel protein but it increases calcium currents in type R voltage-dependent calcium channels and promotes calcium-related apoptosis (Suzuki et al., 2009). The mutations may interfere with apoptotic activity and prevent normal neuronal death during postnatal development of the central nervous system in human, increasing the density of neurons and the formation of hyperexcitable circuits. Homozygous mutation in EFHC1 has also been associated with intractable epilepsy (Berger et al., 2012).

BRD2 (RING3) has been identified as a putative nuclear transcriptional regulator from a family of genes that are expressed during development. A mutation of this gene may be relevant to the age-related onset of JME (Pal et al., 2003; Velíšek et al., 2011).

Malic enzyme 2 (ME2), a genome-coded mitochondrial enzyme involved in neuronal synthesis of the neurotransmitter GABA, was found to increase the risk of IGE when present with nine single-nucleotide polymorphism (SNP) haplotype homozygously (Greenberg et al., 2005).

1.3.3.3 Thalamocortical circuit and spike-and-wave discharges

The 3-5 Hz bilaterally synchronous spike-and-wave discharges related to absence and 4-6 Hz spike-and-wave related to generalized tonic-clonic seizures in JME are reminiscent of normal oscillatory brain activity, sleep spindles. The sleep spindles are generated by thalamocortical system. Gloor conducted electrophysiological studies and postulated that the underlying diffuse mild cortical hyperexcitability and activation of the intracortical recurrent inhibitory pathway cause spike-and-wave discharges in generalized epilepsy (Gloor, 1979).
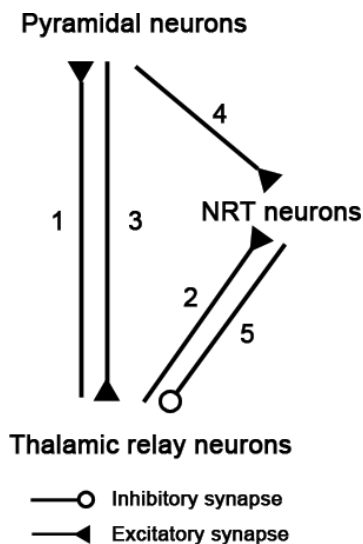
Figure 1.12 The basic synaptic circuit of the thalamocortical system is shown in the schematic diagram. NRT neurons are from nucleus reticularis thalami.

The dorsal thalamus consists of four main nuclear masses: anterior, medial, lateral and midline thalamic nuclei. An important functional partner of the thalamus is a thin layer of cells surrounding the thalamus on its lateral and rostral extent called nucleus reticularis thalami (NRT). The thalamocortical cells in the thalamic nuclei relay information from the midbrain to cerebral cortex and also receive massive reciprocal connections returning

from the cortical areas to which they project. The NRT receives input from the cerebral cortex but does not send output to it.

The basic synaptic circuit of the thalamocortical system is shown in the schematic diagram Figure 1.12. The thalamic relay neurons receive sensory afferent input from midbrain, brain stem and other sources. The principal sensory relay neurons within the thalamus send projections to the pyramidal neurons in the cortex (synapse 1) and receive a feedback from pyramidal neurons in the same cortical area (synapse 3). Pyramidal neurons also send projections to NRT neurons (synapse 4); however, NRT neurons have no reciprocal connections to pyramidal neurons. The thalamic relay neurons send collateral axons to (synapse 2) and receive inhibitory feedback from NRT neurons (synapse 5). The corticothalamic and thalamocortical projections are excitatory and use glutamate or aspartate as a neurotransmitter. NRT projections are inhibitory and use GABA as a neurotransmitter.

The spindle at the stage II sleep consists of 11-15 Hz oscillations that wax and wanes in amplitude and is usually 2-4 seconds in duration, reappearing every 3-10 seconds. The spindle is triggered by an oscillatory interaction between the thalamus and NRT neurons (Steriade and Contreras, 1995). NRT neurons fire in a series of bursts during spindle discharges and elicit synchronized GABAergic inhibitory postsynaptic potentials (IPSPs) in thalamic relay neurons (synapse 5), mediated by activation of both $GABA_A$ and $GABA_B$ receptors. These IPSPs induce T-type Ca-dependent spike and then Na-dependent action potentials in thalamic neurons. In turn, these spikes repeatedly activate NRT neurons (synapse 2) and form spindle rhythm. The NRT neurons serve as the pacemaker in the cycle. The oscillation terminates when Ca-dependent spike is inactivated due to intracellular Ca^{2+} accumulation.

The thalamocortical system also participates in generating pathologic rhythms like 3-4 Hz spike-and-wave activity of absence seizure. The spike-and-wave activity consists of repetitive cycles of an early sharp spike, associated with action potential firing in the thalamus and cortex, and a following slower wave, associated with prolonged inhibition in the cerebral cortex (Pollen, 1964) and probably also in the thalamus (Steriade and Contreras, 1995). In a feline penicillin-generalized epilepsy model of generalized absence epilepsy, 3-4 Hz spike-and-wave discharges have been shown to gradually evolve from 7-14 Hz spindle rhythms accompanied by the behavioral symptoms of absence (Gloor

and Fariello, 1988). In slices of ferret lateral geniculate nucleus, blocking $GABA_A$-mediated inhibition by ethosuximide, a generalized absence anticonvulsant, is associated with a transition from faster, smaller, spindle-like rhythms to slower, larger, spike-and-wave like rhythms (Von Krosigk et al., 1993). Spontaneous thalamocortical oscillations are also recorded in thin slices of rodent brain maintaining reciprocal connections between thalamus, cortex, and NRT (Coulter and Lee, 1993).

Under normal condition, cortical inputs to NRT neurons (synapse 7) may produce brief firing of NRT cells, with approximately 0.1 second IPSPs in the thalamus that produce 10 Hz or higher oscillations, as is seen in normal sleep spindles. Pathologically enhanced cortical firing may produce sustained NRT firing, with approximately 0.3 second thalamic IPSPs that produce 3-4 Hz oscillations. This sustained firing is seen in a typical absence seizure. The switch from normal sleep spindles to 3-4 Hz oscillations is dependent on enhanced cortical firing.

1.3.3.4 Treatment and prognosis

The majority of JME patients respond to antiepileptic medications and have benign outcomes with no other neurologic disturbances. Valproate is the most commonly used AED and the newer drugs such as lamotrigine and topiramate yield good control of generalized tonic-clonic seizures. AEDs can be withdrawn in only a minority (10-20%) of patients and others tend to continue on JME drugs for life (Kobayashi et al., 2008).

1.3.3.5 Neuroimaging findings

Although conventional MRI of JME patients show no abnormality, recent advances in quantitative neuroimaging techniques have started to reveal the insights into the disorder. Positron emission tomography (PET), single photon emission computed tomography (SPECT), structural MRI, DTI, fMRI and MR spectroscopy (MRS) have uncovered structural, functional and metabolic aspects of JME.

PET is a functional imaging method that detects positron decay of radio-labeled ligands injected in the subject intravenously. PET images reveal the physiological distribution of the injected ligands in the brain. The ^{18}F-fluoro-2-deoxyglucose (FDG) is a standard ligand, used in PET, to assess cerebral glucose metabolism in epilepsy. FDG-PET shows increased interictal glucose metabolism in bilateral thalami which has been correlated

with the amount of spike-wave activity on EEGs of JME patients (Kim et al., 2005). Additionally, reduced glucose metabolism in the dorsolateral prefrontal cortex, premotor cortex, and basal frontal cortex during a visual working memory paradigm has been shown in JME patients compared to controls (Swartz et al., 1996). Frontal lobe glucose metabolic values have been shown to be strong predictors of executive function in JME patients (McDonald et al., 2006).

Other PET ligands that measure receptor density or neurotransmitter and related enzyme activity also helped underpin the neurobiological basis of epilepsy. A study using PET with ^{11}C-diprenorphine, an opioid-receptor ligand, revealed increased diprenorphine elimination from the association cortex during absence seizures. This result suggests that an increased opioid-receptor occupancy of the association cortex may play a role in pathophysiology of absences (Bartenstein et al., 1993). PET with serotonin 1A receptor antagonist carbonyl-carbon 11-WAY-100635 measures serotonin 1A receptor binding potentials and reveals reduced binding potential in dorsolateral prefrontal cortex, raphe nuclei, and hippocampus. These results suggest a disruption of the serotonin system in JME (Meschaks et al., 2005). 11C-flumazanil PET measures the density of GABA$_A$ receptors and have been used to uncover a globally increase of GABA$_A$ receptors in the cortex of JME patients, especially the frontal lobe (Koepp, 2005). The dopaminergic system is also involved in JME. The binding potential of the dopamine transporter and D2/D3 receptor was reduced in the substantia nigra and midbrain (Ciumas et al., 2008, 2010; Odano et al., 2012), and the bilateral posterior putamen (Landvogt et al., 2010), respectively.

SPECT is used to measure cerebral blood flow by detecting γ rays emitted by injected radiotracers, typically hexamethyl propylene-amine-oxime (^{99m}Tc-HMPAO) or ethylcysteinate dimer (^{99m}Tc-ECD). SPECT is primarily used in presurgical evaluation of the epileptogenic zone. A previous ^{99m}Tc-ECD SPECT study has found reduced regional cerebral blood flow in bilateral thalami, red nucleus, midbrain, pons, left hippocampus, and in the cerebella whereas increased regional cerebral blood flow was found in the left superior frontal gyrus (Tae et al., 2007).

Structural MRI helps identify subtle gray matter abnormalities related to JME that are not obvious on conventional MRI while DTI examines the integrity of white matter microstructure. There is a growing body of literature showing converging evidence of

47

frontal and thalamic abnormalities in JME summarized below (Table 1.4). fMRI, however, is seldom performed on JME patients.

Table 1.4 Previous studies of structural abnormalities in JME detected by structural MRI (sMRI) and DTI. Abbreviations: GM (gray matter), WM (white matter), CT (cortical thickness), TBSS (Tract-based spatial statistics), ROI (Region of interest), VBA (Voxel based analysis), VBM (Voxel based morphology).

Study	Modality	Subjects	Findings of JME
(Woermann et al., 1999b)	sMRI (VBM)	20 JME vs. 30 Controls	GM volume ↑ in bilateral mesial frontal lobes
(Betting et al., 2006)	sMRI (VBM)	44 JME vs. 47 Controls (and other IGE subgroups)	GM concentration↑ in frontobasal region; GM concentration ↑ in anterior thalamus in JME with absence seizures
(Tae et al., 2006)	sMRI (VBM & Volumetry)	19 JME vs. 19 Controls	GM concentration↓ in prefrontal lobe; GM volume↓ in rostrum and rostral body of the corpus callosum
(Kim et al., 2007a)	sMRI (VBM)	25 JME vs. 44 Controls	GM volume↑ in bilateral superior mesiofrontal region; GM ↓ in bilateral thalamus; Bilateral thalamic GM volume is negatively correlated with epilepsy duration
(Tae et al., 2008)	sMRI (Cortical thickness)	19 JME vs. 18 Controls	CT↓ in superior/middle/medial frontal gyri and superior/middle/inferior temporal gyri; CT of precentral gyrus and medial orbital gyrus of right hemisphere were negatively correlated with disease duration
(Deppe et al., 2008)	DTI (VBA of FA maps)	10 JME vs. 67 Controls (vs. 8 Cryptogenic partial epilepsy)	FA↓ in thalamocortical WM; FA reduction was correlated with the frequency of generalized tonic-clonic seizures.
(Roebling et al., 2009)	sMRI (VBM), fMRI(working memory)	19 JME vs. 20 Controls	No significant findings of GM or working memory fMRI
(De Araújo Filho et al., 2009)	sMRI (VBM)	16 JME with class B personality disorder (PD) vs. 38 JME without PD vs. 30 Controls	GM volume↓ in bilateral thalami, insular and cerebellar hemispheres. GM volume ↑ in right superior and medial frontal gyrus; WM volume↓ in bilateral cerebellar hemispheres
(Pulsipher et al., 2009)	sMRI (ROI)	20 recent-onset JME vs. 51 Controls (vs. 12	GM volume↓ in thalami and frontal CSF↑ in JME relative to other groups

		benign childhood epilepsy with centrotemporal spikes)	
(Filho et al., 2010)	sMRI (ROI)	16 JME with class B personality disorder (PD) vs. 38 JME without PD vs. 30 Controls	Corpus callosum volume↓ was found in JME with PD group relative to other groups
(O'Muircheartaigh et al., 2011)	sMRI (VBM), DTI (TBSS)	28 JME vs. 55 Controls (55 had MRI and 38 had DTI)	GM volume↓ in supplementary motor area and posterior cingulate cortex; FA↓ in corpus callosum
(Keller et al., 2011b)	sMRI (Stereological analysis), DTI (ROI)	10 JME (same patients in Deppe 2008) vs. 59 Controls	FA↓ in frontal lobe and thalamocortical WM; FA↑ in bilateral putamen; Putamen FA negatively correlated with putamen volume and age of onset, duration and thalamocortical WM FA
(Vulliemoz et al., 2011)	DTI (probabilistic tractography of supplementary motor area defined by motor fMRI)	15 JME vs. 18 Controls (vs. 36 Frontal lobe epilepsy)	Structural connectivity of supplementary motor area is reduced (FA↓ and MD↑) in JME but not in frontal lobe epilepsy
(Mory et al., 2011)	sMRI (VBM, volumetry, shape analysis of thalami)	21 JME vs. 20 Controls	VBM showed atrophy in the anterior thalamus while shape analysis identified changes in the anterior and inferior thalamus
(Saini et al., 2013)	sMRI (VBM, volumetry, shape analysis)	40 JME vs. 19 Controls	GM volume ↓ in bilateral anteriomesial thalami; Shape of medial and lateral thalami changed
(O'Muircheartaigh et al., 2012)	DTI (probabilistic tractography of thalamus), fMRI(phonemic verbal fluency)	28 JME vs. 38 Controls (38 had DTI, 27 had fMRI)	The impaired anterior thalamocortical WM is overlapped with the region detected by reduced functional connectivity between thalamus and frontal lobe using task phonemic verbal fluency
(Kim et al., 2012)	DTI (TBSS)	25 JME vs. 30 Controls	FA↓ and MD↑ in bilateral anterior and superior corona radiata, genu and body of corpus callosum, and multiple frontal WM tracts. Disease severity, as assessed by the number of generalized tonic–clonic seizures in given years, was negatively correlated with FA and positively correlated with MD extracted from

			regions of significant differences between patients and controls in TBSS
(Vollmar et al., 2012)	DTI (probabilistic tractography), fMRI	29 JME vs. 28 Controls	DTI showed pre-SMA cluster showed reduced connectivity to the prefrontal and frontopolar areas and increased connectivity to the central region and descending motor pathways; SMA cluster showed decreased connectivity to the primary motor cortex and increased connectivity to the occipital lobe and lateral temporal neocortex
(Ronan et al., 2012)	sMRI (Cortical thickness/surface area/curvature)	24 JME vs. 40 Controls	Changes to cortical morphology were detected in several regions. In the left hemisphere, these were in insular and cingulate cortices, occipital pole, and middle temporal and fusiform gyri. In the right hemisphere, changes were detected in insular cortex, inferior temporal gyrus, and precuneus. Further analysis of ROIs revealed that these changes are related to differences in surface area rather than average cortical thickness. In addition, mean curvature abnormalities were detected in the insula bilaterally, the left cingulate cortex, and right inferior temporal gyrus.
(De Araujo Filho et al., 2013)	sMRI (Cortical thickness/pial area/depth of sulcus/curvature/metric distortion)	66 JME (22 with cluster B personality disorder and 44 without) vs. 23 Controls	CT and pial area↓ mainly in frontal and temporal regions in JME (with and without cluster B personality disorder combined)
(De Oliveira et al., 2013)	sMRI (Texture analysis)	24 JME vs. 20 Controls	Texture parameters were different in right thalamus between JME and controls

Magnetic resonance spectroscopy yields information on the metabolites of brain tissue including N-acetyl aspartate (NAA), creatine plus phosphocreatine (Cr), choline (Cho) and lactate (Lac). Previous findings revealed metabolic changes in frontal and thalamus supporting thalamocortical involvement in JME (Savic et al., 2000; Mory et al., 2003;

Haki et al., 2007; Lin et al., 2009), as well as in primary motor cortex, posterior cingulate gyrus (Lin et al., 2009), and hippocampus (Ristić et al., 2011). These metabolic changes may comprise the epileptic network in generalized seizures.

<p style="text-align:center">*　　*　　*</p>

The goal of this thesis is to reveal the white matter changes associated with temporal lobe epilepsy and idiopathic generalized epilepsy using DTI. Chapter 4 tracks the acute diffusion change at one to seven days of Wallerian degeneration and relates the observation to known physiological processes. Chapters 5, 6, 7 studied the white matter alterations, the disrupted brain topological organization, and the progression of the white matter change related to temporal lobe epilepsy. Chapter 8 examines the gray and white matter changes in subsyndromes of idiopathic generalized epilepsy.

Chapter 2   The acute phase of Wallerian degeneration: Longitudinal diffusion tensor imaging of the fornix following temporal lobe surgery[1]

2.1   Introduction

Non-invasive measures of water diffusion and its anisotropy in neural fibers have long been shown to be a sensitive indicator of micro-structural changes associated with Wallerian degeneration (Ford et al., 1994; Beaulieu et al., 1996). These studies in both central and peripheral nervous systems demonstrated concurrent reductions of parallel diffusivity (axial, $\lambda_{\parallel}$) and increases of perpendicular diffusivity (radial, $\lambda\perp$) yielding reductions in anisotropy that were linked with histology to both axonal injury and demyelination. However, the diffusion measurements were performed late at 7 days after the spinal cord injury in rats (Ford et al., 1994) or after 1 month for the sciatic nerve injury in frogs (Beaulieu et al., 1996). This combined set of diffusion changes was also observed in ipsilateral internal capsule in chronic stroke patients (Pierpaoli et al., 2001).

Serial measurements including early time points in an optic nerve injury model led to the observation that the individual diffusivities may yield more specific tissue indicators as the reduction of $\lambda_{\parallel}$ early post retinal ischemia, without a change in $\lambda\perp$, correlated with axonal damage and the elevation of $\lambda\perp$ later was associated with myelin break down (Song et al., 2003). This diffusion eigenvalue hypothesis has been supported by similar observations in other experimental models including trauma, multiple sclerosis and stroke (Mac Donald et al., 2007b; Budde et al., 2008; Kozlowski et al., 2008; Sun et al., 2008; Zhang et al., 2009).

Since a series of histological examinations are not generally applicable in humans in vivo, could diffusion tensor imaging (DTI) provide similar insights into the progression of

Wallerian degeneration that is otherwise not evident with conventional MRI? In patients with atonic seizures, transection of the anterior 2/3 of the corpus callosum resulted in a markedly similar evolution of the diffusion eigenvalues as shown in the experimental models, namely reduction of $\lambda_\parallel$ with little change of $\lambda_\perp$ at 1 week and then major increases of $\lambda_\perp$ at 2 months (Concha et al., 2006). However, the pattern and time course of water diffusion within the first week following white matter injury remains unknown in human brain. Surgical transection studies such as this have the advantage of being able to perform pre-operative DTI and have a definitive injury to the tract at a precise time.

Anterior temporal lobectomy (ATL) and selective amygdalohippocampectomy (SelAH) are surgical treatments for intractable temporal lobe epilepsy (TLE). In standard ATL, the anterior portion of the temporal lobe is completely removed while during SelAH, mesial temporal structures that are involved with seizures are selectively removed and much of the lateral temporal lobe is spared with the goal of reducing postoperative morbidity (Wheatley, 2008). During both procedures, the crus of the fornix is completely resected anterior to the surgical margin under direct visualization with hippocampal efferent fibers originating anterior to the resection margin expected to then undergo Wallerian degeneration. Other DTI studies have shown post-surgical reductions of anisotropy in the ipsilateral fornix of epilepsy patients; however, the diffusion parameters have been measured greater than 2 months post-surgery (Concha et al., 2007; McDonald et al., 2010; Yogarajah et al., 2010; Nguyen et al., 2011). While there are challenges in performing MRI on patients within the first week after brain surgery, this time frame is needed to understand what diffusion changes occur at the early phases of Wallerian degeneration. The objective of this study was to assess the acute changes of water diffusion in a white matter bundle, namely the ipsilateral crus of the fimbria-fornix, after a transection injury in temporal lobe epilepsy patients.

2.2   Material and methods

Approval of the research protocol was obtained from the University of Alberta Health Research Ethics Board, and informed consent was obtained from all participants.

2.2.1 Subjects

Six patients with medically intractable epilepsy as well as three healthy individuals were included in this study. Sutures were used instead of the conventional staples to enable the MRI scanning post-surgery. All patients were entirely seizure free after surgery throughout the imaging period. The postoperative T1 weighted MPRAGE scans clearly show the surgical cavities (Figure 2.1). Surgical pathology was available in four of six subjects. For the remaining two subjects, hippocampal T2 relaxometry, which has been demonstrated to correlate strongly with hippocampal sclerosis, was used to define presumptive hippocampal sclerosis using a T2 value of >120ms (Concha et al., 2005a, 2009).

Patient 1 (33 years, right-handed male) suffered medically refractory complex partial seizure originating from the left mesiotemporal lobe as revealed by EEG-video telemetry. Clinical MRI showed clear evidence of left mesiotemporal sclerosis. The patient demonstrated elevated T2 relaxometry value in the left hippocampus (left 128 ms, right 113 ms). He underwent left selective amygdalohippocampectomy and was scanned with our imaging protocol 6 months before surgery and 1, 2, 3, 6 days, 2 months, and 4 months after surgery. Post-operative histological examination of the resected hippocampus confirmed typical hippocampal sclerosis.

Patient 2 (55 years, right-handed female) suffered frequent generalized and complex partial seizures. Intracranial EEG-video telemetry demonstrated an epileptic generator in the left mesiotemporal region. Clinical MRI showed diffuse atrophy without obvious focal lateralized structural abnormality. The patient demonstrated elevated T2 relaxometry value in the left hippocampus (left 126 ms, right 110 ms). She underwent left anterior temporal lobectomy and was scanned 3 months before surgery and 2, 3, 6, 7 days, and 2 months after surgery. Post-operative histological examination of the resected left hippocampus confirmed typical hippocampal sclerosis.

Patient 3 (45 years, right-handed male) suffered typical complex partial seizures and was demonstrated to have a right temporal ictal generator on EEG-video telemetry. Clinical MRI showed clear evidence of right mesiotemporal sclerosis. The patient demonstrated elevated T2 relaxometry value in the right hippocampus (left 114 ms, right 139 ms). He underwent right selective amygdalohippocampectomy and was scanned 12 months before

surgery and 1, 5, 6 days, and 2 months after surgery. Post-operative histological examination of the resected right hippocampus confirmed hippocampal sclerosis.

Patient 4 (39 years, right-handed female) suffered medically refractory complex partial seizures originating from the right temporal lobe detected with EEG-video telemetry. Clinical MRI showed increased signal in right hippocampus consistent with MTS, however the patient did not show elevated T2 relaxometry value in either side of the hippocampus (left 114 ms, right 113 ms). She underwent right anterior temporal lobectomy and was scanned 7 months before surgery and 1, 2, 3, 7 days, and 2 months after surgery. Post-operative histological examination of the resected right hippocampus showed no evidence of hippocampal sclerosis.

Patient 5 (29 years, left-handed male) suffered complex partial seizures with a focal ictal onset in the right temporal lobe demonstrated on EEG-video telemetry. Clinical MRI suggested right hippocampal sclerosis; however, the patient did not present elevated T2 relaxometry value in either side of the hippocampus (left 113 ms, right 103 ms). He underwent right anterior temporal lobectomy and was scanned twice (10 months and 4 days) before surgery and 1, 2, 3, 6 days, 1 month, and 4 months after surgery.

Patient 6 (26 years, left-handed male) suffered complex partial seizures with ictal and interictal epileptic discharges confined to the left temporal lobe as demonstrated with EEG-video telemetry. Clinical MRI suggested left hippocampal sclerosis. The patient demonstrated elevated T2 relaxometry value in the left hippocampus (left 148 ms, right 114 ms). He underwent left anterior temporal lobectomy and was scanned 1 month before surgery and 1, 2, 3, 6 days, and 2 months after surgery.

Three controls (age: 20, 22 and 33 years, all right-handed male) were scanned six times corresponding to the scan time points in patients: initial, and 1, 2, 3, 6 days and 2 months after to investigate the variability of the diffusion measurements in the absence of surgery. One scan acquired at 1 day after the initial time point from a control was excluded due to a MRI data acquisition problem. A total of 17 scans from controls were used in the variability analysis.

2.2.2 Image acquisition

Fluid-attenuated inversion recovery (FLAIR) DTI was performed on a 1.5T Siemens Sonata (Erlangen, Germany) using a dual spin-echo, single shot echo planar imaging sequence with the following parameters: 2 mm thick slices with no inter-slice gap, TR = 10 s, TE = 88 ms, TI = 2200 ms, acquisition matrix = 128×128 with 75% phase partial Fourier (interpolated to 256×256), FOV = 256 mm $\times$ 256 mm, voxel dimension $2 \times 2 \times 2$ mm^3 (interpolated to $1 \times 1 \times 2$ mm^3), 26 axial slices with coverage of fornices, 6 diffusion directions, b = 1000 s/mm^2, 8 averages, scan time = 8:30 min (Concha et al., 2005b). The FLAIR DTI was adopted for its advantages of suppressing signal from cerebrospinal fluid and minimizing partial volume artifacts (Papadakis et al., 2002), which is very important for the fornix (Concha et al., 2005b). The SNR of the non-diffusion weighted images in this study was ~56.
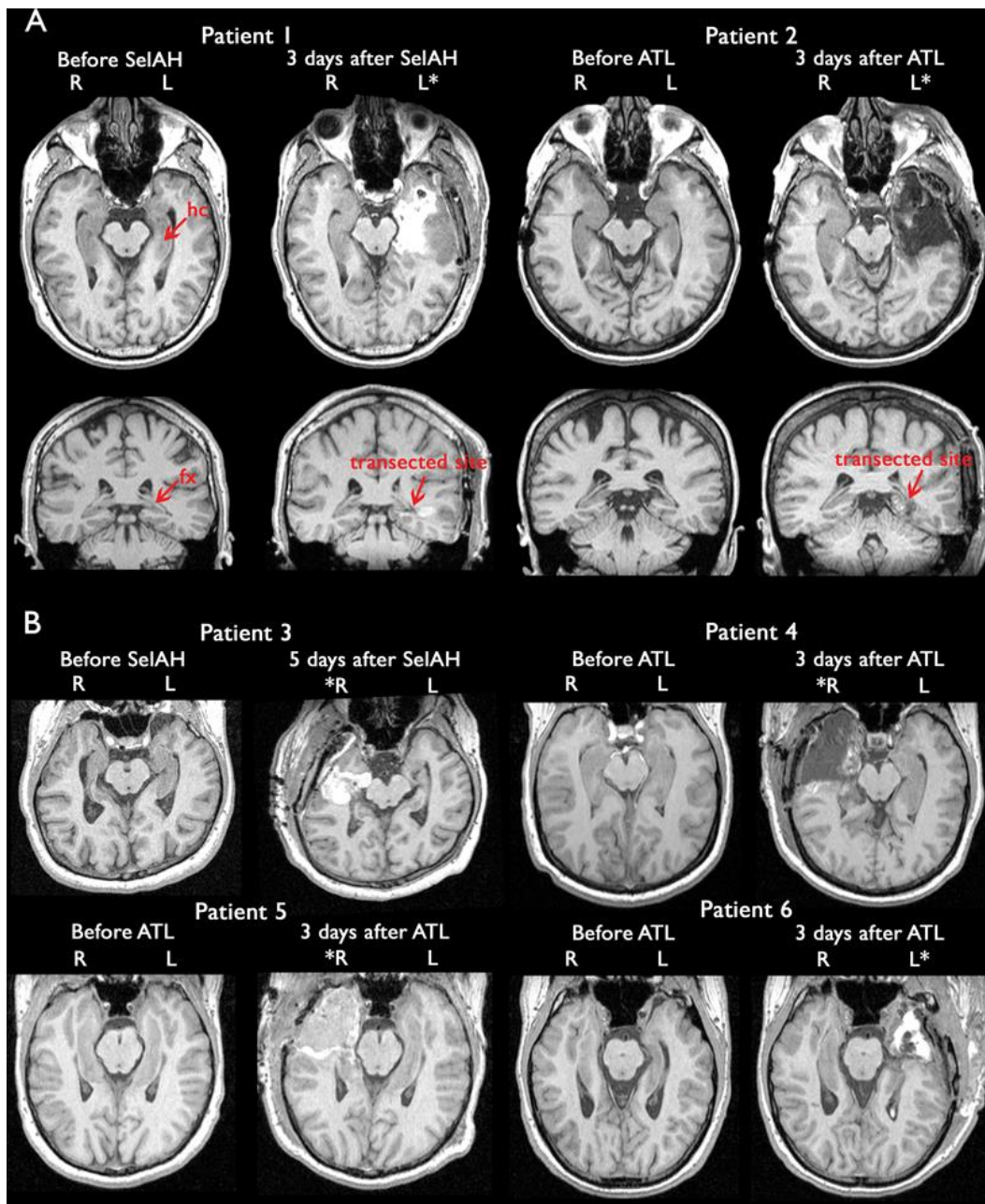
Figure 2.1 Demonstration of resection site before and after surgery (side indicated by *) on T1-weighted MPRAGE scans. (A) Axial (top row) and coronal (bottom row) slices on Patient 1 who underwent a left selective amygdalohippocampectomy (SelAH) and Patient 2 who underwent a left anterior temporal lobectomy (ATL). Part of the head of the left hippocampus (hc) was removed and the left fimbria-fornix (fx) was transected in both surgery techniques. (B) Axial slices for the other four patients who underwent surgery.

2.2.3 Diffusion tensor tractography and measurements of diffusivity and T2-intensity ratio

Fractional anisotropy and diffusion maps were calculated with DTIstudio V2.4 (Johns Hopkins University, Baltimore, USA). For each time point before the surgery and within the first week after surgery, diffusion tensor tractography of fimbria-fornix crus (fornix for short) both ipsilateral and contralateral to the surgery side was performed manually and separately using the fiber assignment by continuous tracking (FACT) algorithm adopted by DTIstudio with FA threshold 0.25 and angular threshold 70° (Mori et al., 1999). The region-of-interests used to select the tracts were drawn on color maps based on the methods and anatomy described before (Concha et al., 2005b). Each fornix was defined as the portion posterior to the most anterior coronal slice where the two crura were separated and only contained fibers traveling from the corresponding hippocampus to the body of the fornix. The manual tracing has an inter-rater reliability of 0.80 and intra-rater reliability of 0.81 (Malykhin et al., 2008). For the chronic scans, because deterministic tractography was unable to trace the middle portion of the fornix which was severely degenerated, the pre-surgical non-diffusion-weighted images (i.e., b0 images) in patients or the initial scans in controls were nonlinearly registered to their corresponding chronic scans using diffeomorphic demons algorithm (Vercauteren et al., 2009) in MedINRIA (v1.6, INRIA-Asclepios Research Team, France). The same deformation was applied to the tract from the pre-surgical/initial time point to derive an approximate fornix for the chronic scans. An FA threshold of 0.25 was applied to the quantitative analysis of the approximate fornix in order to exclude a small number of voxels misregistered to the adjacent gray matter. This approach yielded consistent measurements for the chronic scans in controls (see section 2.4); however, given the FA threshold, it may lead to an underestimation of the change in fornix. Four diffusion parameters including fractional anisotropy (FA), mean diffusivity (MD), $\lambda_{\parallel}$ and $\lambda\perp$ were obtained by overlaying the tracts on the corresponding diffusion maps and averaging across all voxels occupied by the tracts in order to generate a single value for each fornix using an in-house program. The diffusion parameters of the left and right fornix were also queried in controls by the aforementioned method to define a normal variation range of the four diffusion parameters. The occipital callosal fibers that were not transected during surgery were analyzed as an internal reference in patients by the same method since the FLAIR

DTI covers this structure completely. No apparent diffusion changes were expected since occipital callosal fibers are not injured during either anterior temporal lobectomy or selective amygdalohippocampectomy.

The longitudinal T2-weighted signal intensity of the fornix was measured in each tractography defined fornix on the non-diffusion-weighted FLAIR images (b = 0 s/mm^2) that have a long echo time of 88 ms. To account for scanner variability in different imaging sessions, the fornix T2 signal intensity was normalized by the non-transected occipital callosal fibers T2 signal intensity, yielding a T2-intensity ratio of 1.01 ± 0.03 in the 3 healthy volunteers over all time points.

2.2.4 Quantitative analysis

The absolute difference of later scans relative to the first scan was calculated for each side of the fornix of each control. Left and right fornices showed similar longitudinal variability for all diffusion parameters in the healthy controls (Figure 2.2). The normal variation range was defined as twice the average absolute deviation relative to zero for all three controls which was 0.031 for FA, 0.033×10^{-3} mm^2/s for MD, 0.063×10^{-3} mm^2/s for $\lambda_{\parallel}$, 0.031×10^{-3} mm^2/s for $\lambda\perp$, and 0.049 for T2-intensity ratio. For patients, the absolute difference of each post-surgery scan relative to the pre-surgical baseline was calculated to query the longitudinal alteration of the ipsilateral and contralateral fornix separately as well as occipital callosal fibers. The change was considered significant if it surpassed the normal variation range.
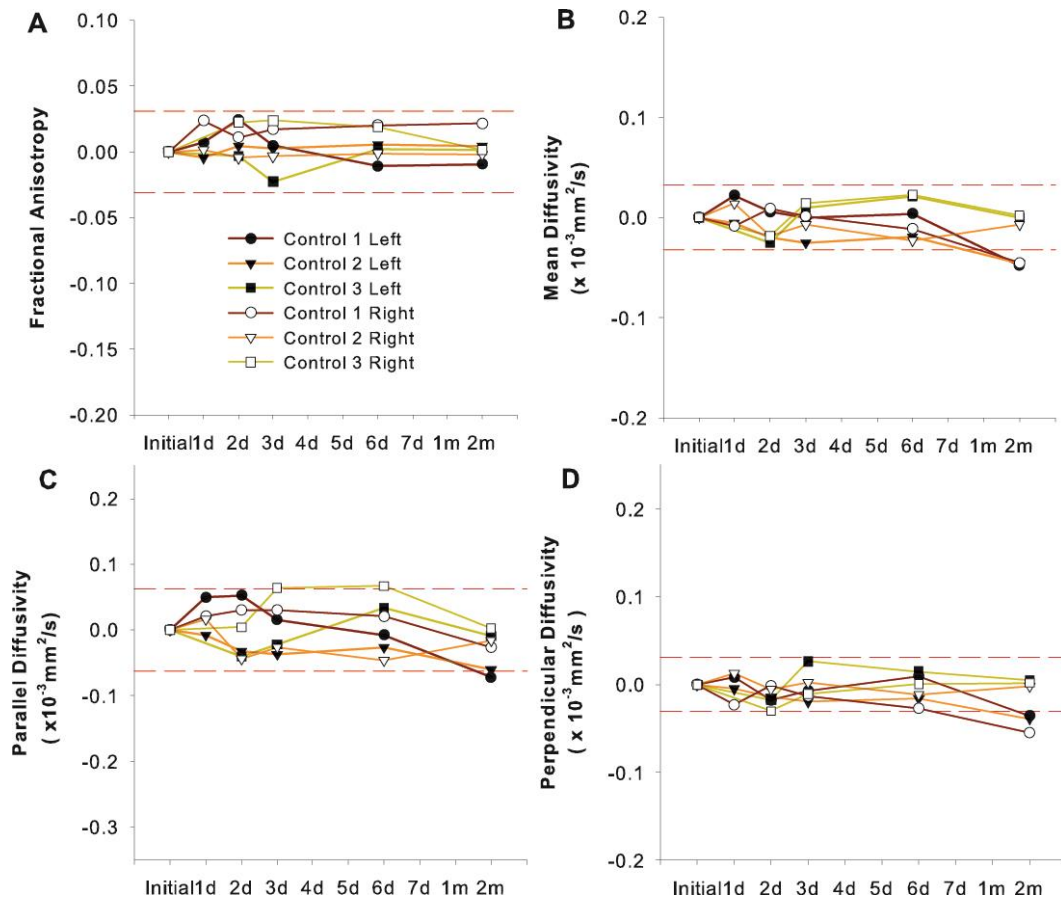
Figure 2.2 Time course of normalized DTI parameters of crus of fimbria-fornices in each hemisphere from three controls repeatedly measured over a similar time span as patients. The four DTI parameters were normalized to the first scan. The normal variation range was defined as twice the average absolute deviation from the initial time point of the six fornices (shown by the two red dashed lines). Vertical scales are kept the same as subsequent patient plots.

2.3   Results

2.3.1 Qualitative visualization of diffusion changes on tractography

As expected, the non-transected callosal fibers of patients showed minimal changes of the four diffusion parameters by visual inspection of the color-coded tracts (Figure 2.3). There was some small variation of the shape of the fornix at different time points in patients within the first week resulting from the displacement of brain after surgery

(Figure 2.4) yet the tract volume did not differ from each other by more than 10% (data not shown). It was not possible to measure the fornix volume at the chronic stage as the low FA values made the tractography algorithm ineffective. The four diffusion parameters of the ipsilateral fornix showed unique changes over time (details in section 3.2 below). All parts of the ipsilateral crus of the fornix appeared to demonstrate simultaneous changes, rather than a graded change along the tract. These changes were similar for patients who underwent either anterior temporal lobectomy or selective amygdalohippocampectomy. The diffusion maps of the contralateral fornix (not shown) appeared quite consistent over time.
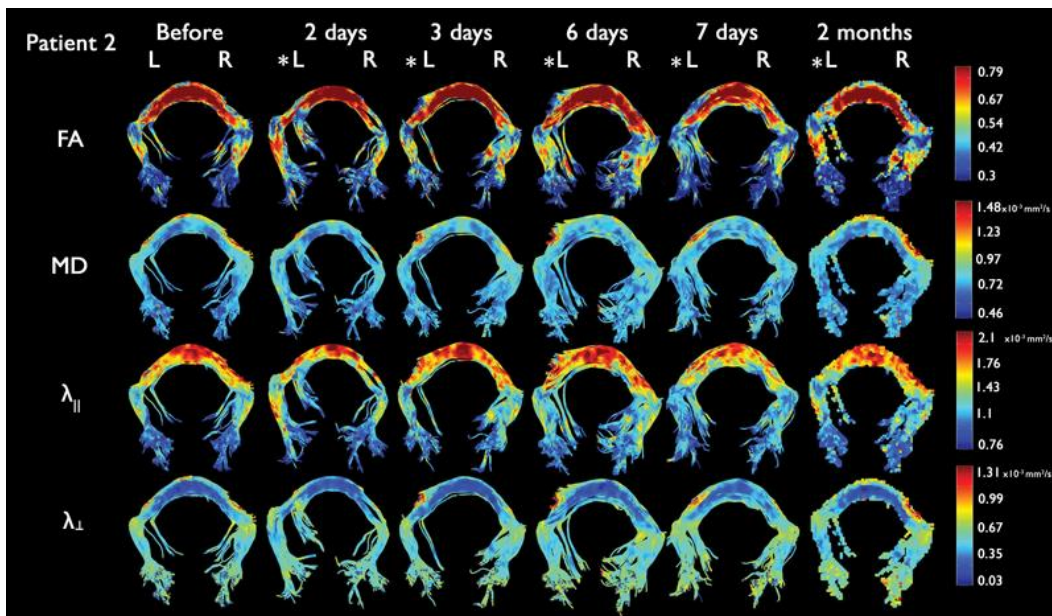
Figure 2.3 Visualization of non-transected occipital callosal fibers (viewed from above) before and after left anterior temporal lobectomy surgery in Patient 2 where FA, MD, $\lambda_{\parallel}$, and $\lambda\perp$ values are color-coded for each voxel. The parameters showed minimal changes as expected. The occipital callosal fibers at 2 months were coregistered from the pre-surgical fibers and are displayed as voxels rather than streamlines at the earlier time points. L, left; R, right. The surgery side is marked by asterisks.

2.3.2 Quantitative assessment of fornix parameters post-surgery

All four diffusion parameters were within the normal variation range in the non-transected occipital callosal fibers over all time points (Figure 2.5). The mean percentage

of the absolute variation across all time points and patients was 2% for FA (range: 1-3%), 2% for MD (range: 1-2%), 2% for $\lambda_\parallel$ (range: 0.1-2%) and 3% for $\lambda\perp$ (range: 2-4%).

In contrast, the transected ipsilateral fornix crus had alterations in the four diffusion parameters post-surgery, although with different timing patterns (individual participant data normalized to their first scan in Figure 2.6). The FA was relatively stable within the first week after surgery except Patient 1 that showed a decrease beyond normal variation range at 6 days. All six patients had major reductions of FA (19%, range 10-30%) at 1-4 months post-operative. In contrast, immediate reductions of MD, $\lambda_\parallel$, and/or $\lambda\perp$ were observed in all six patients as early as the first one or two days after surgery. Specifically, MD was reduced within the first two days (reduced by 8%, range: 4-13%) and rebounded back to some extent at 6-7 days post-operative yet still remained lower than the initial. At 1-4 months, five out of six patients showed an elevated MD (7%, range: 4-12%) with only Patient 3 presenting MD at pre-surgery levels. A reduction of $\lambda_\parallel$ occurred in the first two days for five out of six patients (reduced by 10%, range: 5-15%) except Patient 5 that remained within the normal variation range. The $\lambda_\parallel$ stayed low for the rest of the week. At the chronic stage, $\lambda_\parallel$ remained low in four of six patients and did not reverse back to baseline, but Patients 2 and 5 rebounded back to the pre-surgical level. For $\lambda\perp$, an acute reduction occurred at 1-2 days after surgery (8%; range: 6-11%) for five of six patients, which then showed a rebound pattern closer to baseline by the end of the first week whereas Patient 4 remained within the normal variation over the first week. At 6-7 days, $\lambda\perp$ in four patients recovered to pre-surgical level while $\lambda\perp$ in Patients 2 and 3 stayed unrecovered (reduced by 9% and 6%, respectively). At 2 months post-operation, $\lambda\perp$ increased beyond pre-surgical levels in all patients (increased by 17%, range: 10-33%).

In contrast, the contralateral fornix showed very little change over time (Figure 2.7) in five of six patients with the exception of Patient 1. Patient 1, who had a left selective amygdalohippocampectomy, demonstrated FA reduction and MD and $\lambda\perp$ elevation beyond the normal variation range from 6 days to 4 months. Notably, Patient 1 also showed the greatest FA reductions in the ipsilateral fornix. Patient 2 and Patient 3 showed some changes slightly beyond the normal variation range at one or two time points but they were not consistent over time.

An increase of the normalized ipsilateral fornix T2-intensity (normalized to the non-transected occipital corpus callosum) was observed within the first two days after surgery

(increased by 10%, range: 8-16%) except Patient 4 who showed a slight decrease of 5% (Figure 2.8A). T2-intensity peaked at two days and gradually returned to its pre-surgical level in four out of six patients at the end of the first week except Patients 2 and 3. At 1-4 months, the ratio in four patients totally returned to its pre-surgical state while Patients 4 and 6 had a decrease of 11% and 7%, respectively. The contralateral fornix of five patients had relatively stable T2-intensity ratios except Patient 6 who showed a consistent ~6% decrease post-surgery (Figure 2.8B).

Compared to Patients 1-3 and 6 who demonstrated T2 evidence of hippocampal sclerosis, Patients 4 and 5 who did not exhibit T2 evidence of hippocampal sclerosis showed an absolute reduction of mean, parallel and perpendicular diffusivities to a lesser extent within the first week after surgery (Figure 2.9); in many cases the values were still within the normal variation range of controls.
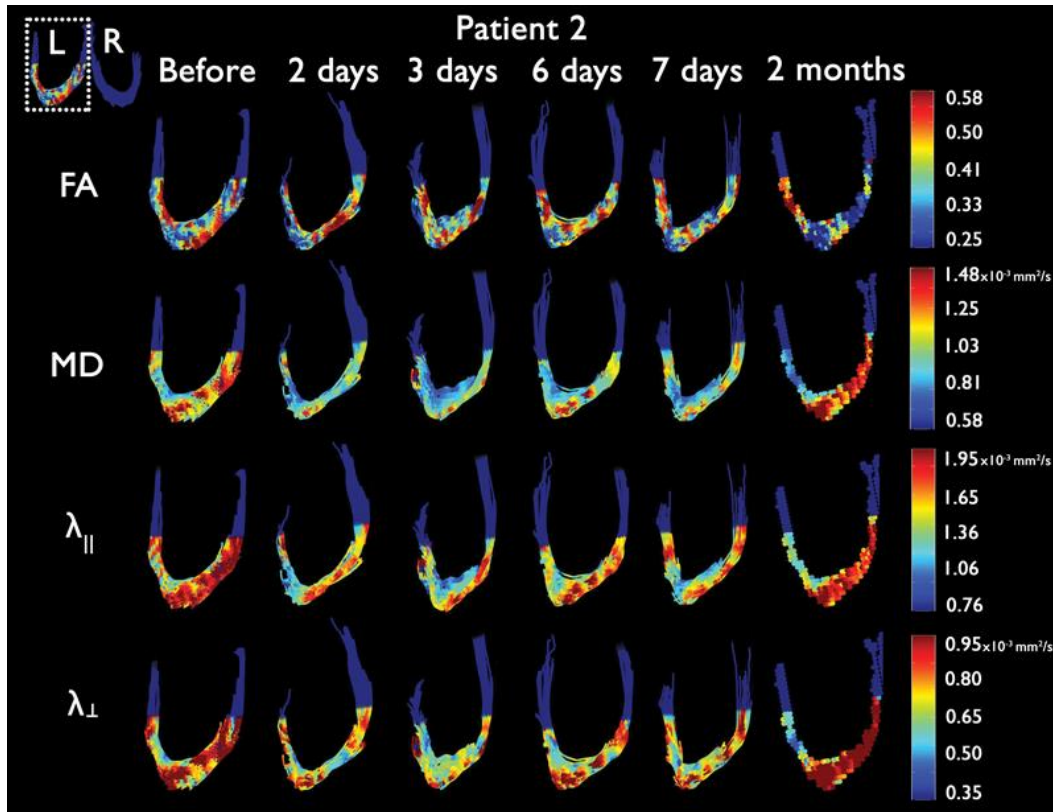
Figure 2.4 Visualization of the ipsilateral/left crus of fimbria-fornices (viewed from above) before and after surgery in Patient 2 where FA, MD, $\lambda_{\parallel}$, and $\lambda\perp$ values are color-coded for each voxel. The non-measured part (i.e. the body of fornix and the fimbria-fornix adjacent to hippocampi) is colored in uniform dark purple. The FA was relatively stable within the first week after surgery and decreased at 2 months. The $\lambda_{\parallel}$, $\lambda\perp$, and MD was reduced at 2 days, stayed low up to 7 days, and then increased at least to ($\lambda_{\parallel}$) or beyond ($\lambda\perp$, MD) the pre-surgical values at 2 months.
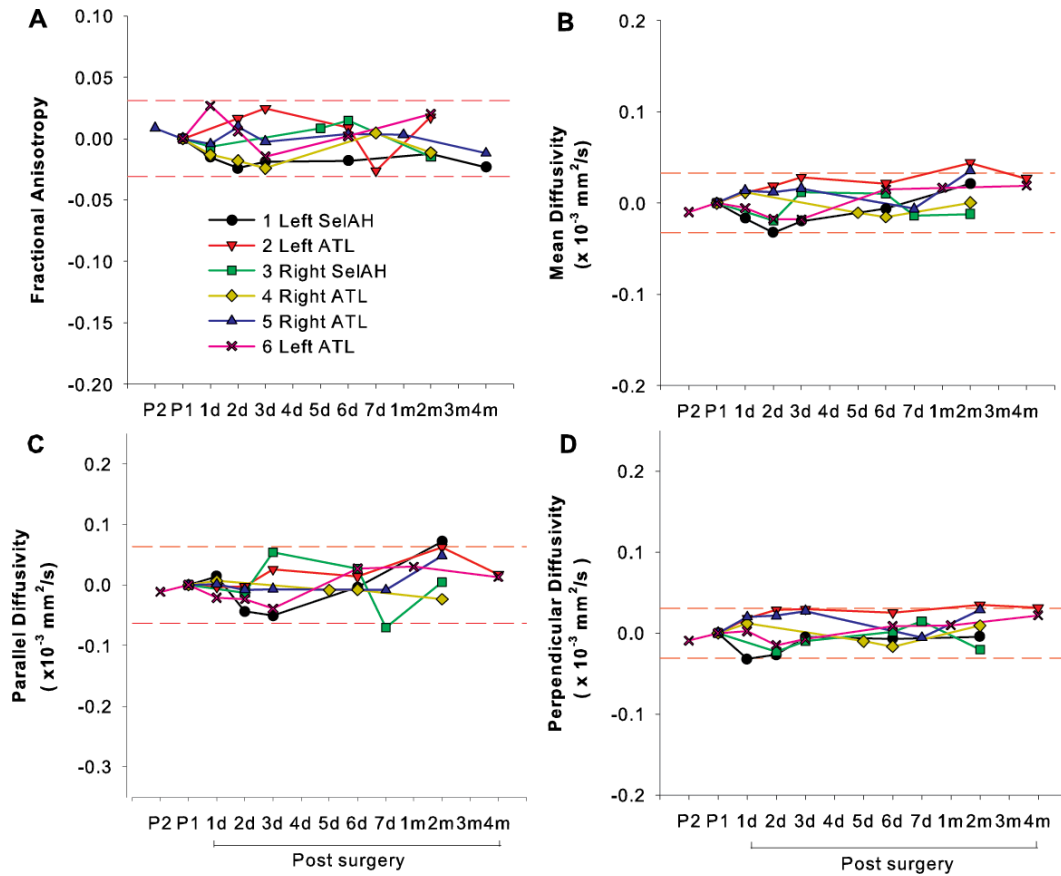
Figure 2.5 Time course of normalized DTI parameters of the non-transected occipital callosal fibers from six patients with temporal lobe epilepsy prior to (P1, P2) and after (days, d and months, m) surgery. The time point prior to surgery serves as a baseline. DTI parameters were normalized by subtracting the baseline value from each time point. The red dashed lines showed the normal variation range defined from repeated measures of three controls spanning a similar period of time. The diffusion parameters showed minimal changes within the normal variation range over time. SelAH, selective amygdalohippocampectomy; ATL, anterior temporal lobectomy.

65
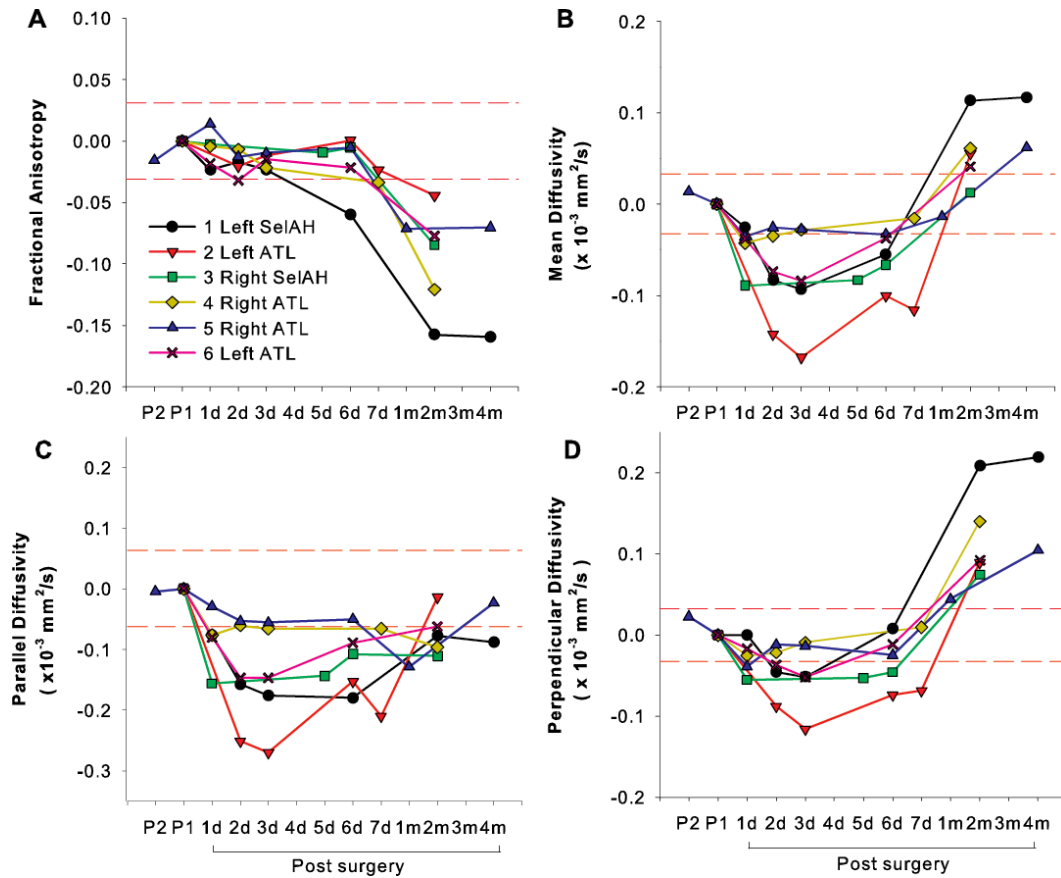
Figure 2.6 Time course of normalized DTI parameters of the ipsilateral crus of fimbria-fornices from six patients with temporal lobe epilepsy prior to (P1, P2) and after (days, d and months, m) surgery. DTI parameters post-surgery were normalized by subtracting the baseline value prior to surgery. The red dashed lines show the normal variation range defined from repeated measures of three controls spanning a similar period of time. (A) The FA was relatively stable within the first week after surgery and dramatically decreased at 1-4 months. (B) The MD dropped markedly within the first two days, recovered slightly but still remained lower than the pre-surgical level at the end of the first week and increased at 1-4 months. (C) The $\lambda_{\parallel}$ decreased within the first two days, stayed low at the end of the first week, and rebounded slightly but remained still lower than the pre-surgical level at 1-4 months. (D) The $\lambda_{\perp}$ decreased within the first two days, recovered to its pre-surgical level in most cases at the end of the first week, and increased markedly at 1-4 months. SelAH, selective amygdalohippocampectomy; ATL, anterior temporal lobectomy.

66
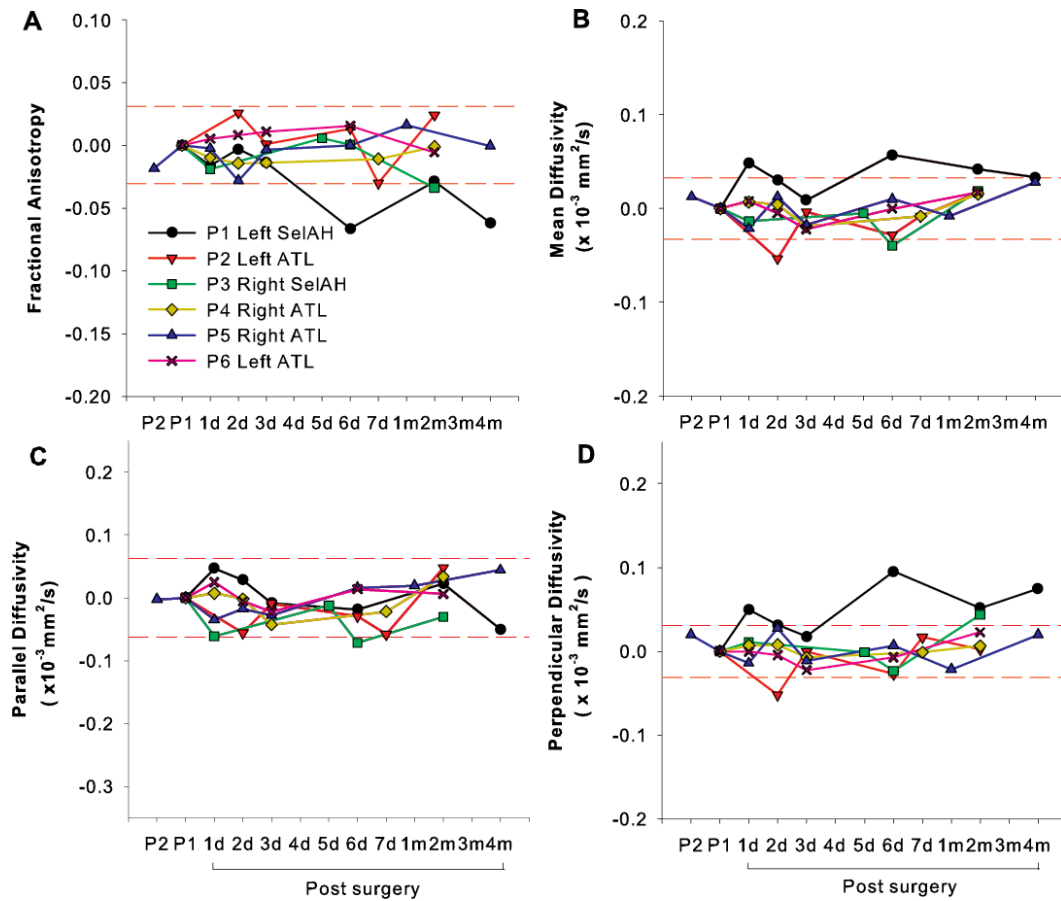
Figure 2.7 Time course of normalized DTI parameters of the contralateral crus of fimbria-fornices from six patients with temporal lobe epilepsy before and after surgery. Although most measurements were within the normal variation, the main exception was Patient 1 with decreased FA and elevated MD and $\lambda_\perp$ beyond the normal variation range at a number of time points after surgery. SelAH, selective amygdalohippocampectomy; ATL, anterior temporal lobectomy.

Table 2.1 Baseline diffusion measurements prior to surgery (time point P1) for six patients and three controls.

	FA	MD (10^-3 mm²/s)	$\lambda_{\parallel}$ (10^-3 mm²/s)	$\lambda_{\perp}$ (10^-3 mm²/s)	FA	MD (10^-3 mm²/s)	$\lambda_{\parallel}$ (10^-3 mm²/s)	$\lambda_{\perp}$ (10^-3 mm²/s)
		Ipsilateral fornix				Contralateral fornix		
Patient 1	0.52	0.98	1.61	0.66	0.54	0.93	1.57	0.61
Patient 2	0.43	1.08	1.64	0.80	0.42	1.08	1.62	0.80
Patient 3	0.45	1.00	1.53	0.73	0.46	0.97	1.51	0.70
Patient 4	0.48	0.97	1.53	0.69	0.47	0.99	1.54	0.71
Patient 5	0.49	0.93	1.49	0.66	0.50	0.92	1.48	0.64
Patient 6	0.47	1.07	1.66	0.77	0.46	1.04	1.61	0.75
Mean	0.47	1.01	1.58	0.72	0.48	0.99	1.56	0.70
Std	0.03	0.06	0.07	0.06	0.04	0.06	0.06	0.07
		Left fornix				Right fornix		
Control 1	0.46	0.97	1.51	0.71	0.44	1.00	1.52	0.74
Control 2	0.51	0.98	1.60	0.67	0.51	0.98	1.60	0.66
Control 3	0.50	0.99	1.61	0.69	0.47	1.00	1.58	0.71
Mean	0.49	0.98	1.57	0.69	0.47	0.99	1.57	0.70
Std	0.03	0.01	0.06	0.02	0.04	0.01	0.04	0.04
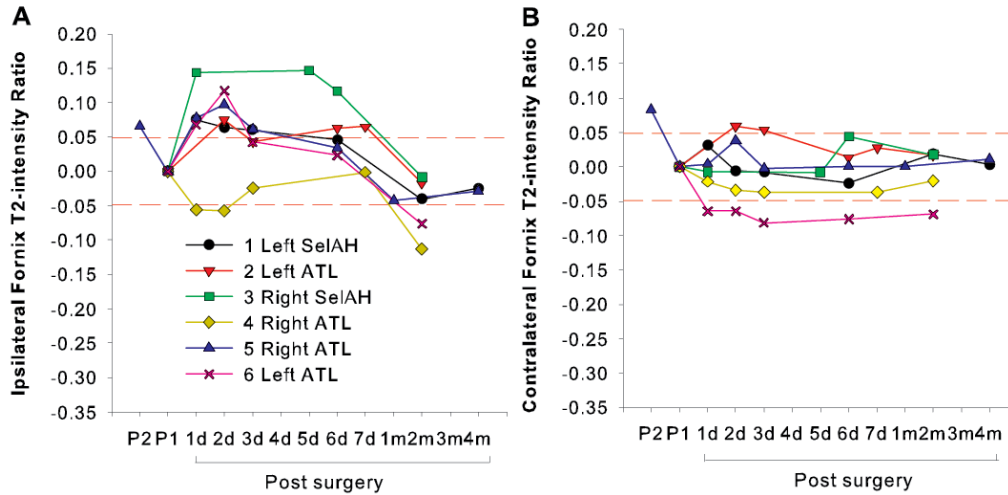
Figure 2.8 Time course of normalized T2-weighted intensity from b0 images of the ipsilateral (A) and contralateral (B) crus of fimbria-fornices (normalized to occipital corpus callosum T2-weighted intensity per scan) from six patients with temporal lobe epilepsy before and after surgery. The time point prior to surgery serves as a baseline and was subtracted from each time point. The red dashed lines show the normal variation range defined from repeated measures of three controls spanning a similar period of time. (A) The ipsilateral fornix T2-intensity ratio immediately increased within the first two days after surgery and then returned to its pre-surgical level at 1-4 months in four out of six patients and below normal at 1-4 months in Patients 4 and 6. Notably, Patient 4 did not show increases of T2-intensity at any time point. (B) The contralateral fornix T2-intensity ratio was relatively stable over time in five out of six patients, but was actually reduced in Patient 6 consistently over time. SelAH, selective amygdalohippocampectomy; ATL, anterior temporal lobectomy.
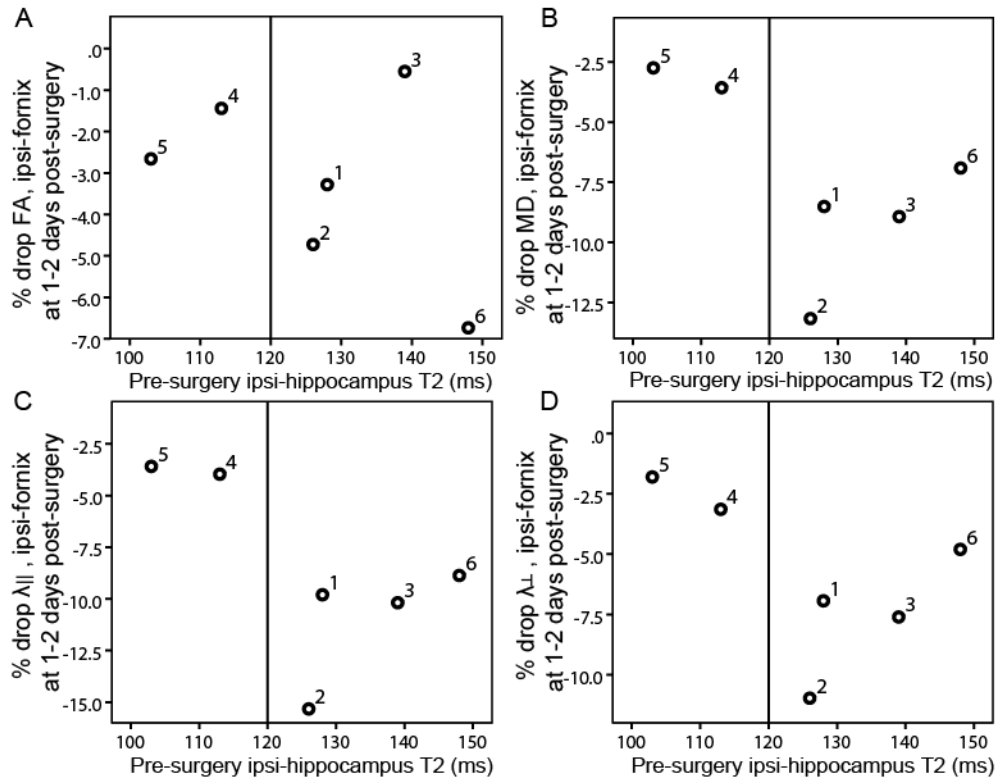
Figure 2.9 Scatter plots of percentage reduction of ipsilateral diffusion parameters of fornix at 1-2 days after surgery (the data at 2 days was used if both data at 1 and 2 days were available) versus pre-surgical ipsilateral T2 of hippocampus. Patients 1-3 and 6 had elevated ipsilateral T2 above 120 ms, amongst whom Patients 1-3 had histologically confirmed hippocampal sclerosis. Notably, Patients 4 and 5 did not show elevated T2 (and patient 4 had no histological evidence of hippocampal sclerosis) showed less reduction of mean, parallel and perpendicular diffusivities acutely.

2.4 Discussion

Wallerian degeneration can be caused by a variety of axonal injuries such as trauma, ischemia, metabolic abnormalities, toxins and inflammation (Coleman and Perry, 2002; Raff et al., 2002; Vargas and Barres, 2007). It is characterized by a series of chronological events, namely, axonal degeneration at both the proximal and distal ends as early as 30 minutes post injury (Kerschensteiner et al., 2005), axonal beading and swelling close to the injury site between 1 and 48 hours (George et al., 1995; Sievers et al., 2003; Zhai et al., 2003; Beirowski et al., 2010), granular disintegration of axonal cytoskeleton resulting in axon fragmentation with the initiation of narrowing and dilating

myelin sheath, myelin ovoid formation, and clearance of myelin debris in the long term (George and Griffin, 1994). In this study, distinct acute (1-7 days) and chronic (1-4 months) water diffusion changes were shown after transection of the ipsilateral fornix during temporal lobe epilepsy surgery. These diffusion changes reflect presumably the different stages of Wallerian degeneration. The reduced FA and elevated perpendicular diffusivity ($\lambda\perp$) were expected at chronic stages. The acute reduction of parallel diffusivity ($\lambda_{\parallel}$) within the first week is also in line with previous literature, but the concomitant reduction of $\lambda\perp$ yielding reduced mean diffusivity (MD) and preserved fractional anisotropy (FA) are new observations.

2.4.1 Acute diffusion changes within the first week post-surgery

Temporal lobe surgery serves as a unique opportunity to examine the process of Wallerian degeneration since the timing of the transection of fimbria-fornix crus is known, requirements not usually met by naturally occurring neurological disease. To date, there is a lack of literature investigating acute diffusion changes within days of axonal transection in human brain; not surprising given the practical issues of performing an MRI on a patient so soon after brain surgery. Experimental models have been used to explore the acute DTI changes post injury. An early decrease of $\lambda_{\parallel}$ and FA without significant increase of $\lambda\perp$ until later time points has been reported in the white matter after neuronal injury from retinal ischemia (Song et al., 2003; Sun et al., 2008), trauma (Kim et al., 2007b; Mac Donald et al., 2007a, 2007b; Zhang et al., 2009) and experimental autoimmune encephalomyelitis (EAE) (Budde et al., 2008). Immunohistochemistry and optical/electron microscopy examinations in these studies confirmed axonal injury without demyelination at an early post-injury stage, strongly suggesting $\lambda_{\parallel}$ as an imaging marker for axonal degeneration.

In contrast, we observed concurrent reduction of both parallel and perpendicular diffusivities, which reduces mean diffusivity, with a relatively stable fractional anisotropy of the transected fornix within the first two days after surgery. This acute diffusion change may reflect the axonal swelling/spheroid formation immediately after axonal injury. Demonstrated recently, axonal swellings arise as soon as 1 hour post injury starting from the surrounding of the injury to more distal sites after transection of the optic nerve in rats and mice (Beirowski et al., 2010). Swelling persists at least for 24 hours post injury with clear continuity of the axons and no appearance of axonal

fragmentation. Confocal imaging revealed that axonal swellings extended over the entire corpus callosum fiber of the mice by 24 hours, marking its rapid progression in the central nervous system. A simulation biophysical model showed that the morphometric changes of axons such as neurite beading was sufficient enough to hinder water mobility and thereby decrease $\lambda_\parallel$ in both the intra- and extracellular compartments and $\lambda_\perp$ mainly in the extracellular compartment (Budde and Frank, 2010). The simulations predicted that $\lambda_\parallel$ would decrease to a greater extent than $\lambda_\perp$; this was confirmed in axons injured by stretching although FA was not significantly reduced. However, here the transected fornix showed similar percentage reductions of both $\lambda_\parallel$ and $\lambda_\perp$ also leading to a lack of change of FA in the first week. These reduced diffusion coefficients, particularly parallel, are consistent with disintegration of the axonal cytoskeleton. It is unclear why earlier experimental studies performing DTI within days after injury do not observe a reduction of $\lambda_\perp$. This may be partly due to the fact that the magnitude of $\lambda_\perp$ in rodent white matter is only about one-fifth of $\lambda_\parallel$ which increases the difficulty of detecting a change in $\lambda_\perp$ (Xu et al., 2008), while the magnitude of $\lambda_\perp$ in the fornix in human is only about half of the magnitude of $\lambda_\parallel$ (Table 2.1).

Alternatively, the concomitant reduction of both parallel and perpendicular diffusivities in the transected fornix at 1-2 days post-surgery could also be a result of other factors such as inflammation and cytotoxic edema. Inflammation has been shown to occur rapidly at the nerve distal stump including microglia activation, macrophage infiltration and massive astrocytic reaction within hours after neural injury such as transection of the fornix in the rat (Stichel and Müller, 1994). The influx of a large population of "isotropic" glial cells in the injured tract could concurrently reduce both parallel and perpendicular diffusivities. Although the major blood supply to the fornix, i.e. medial central arteries, was not injured during surgery, the hippocampal transection might cause some vasospasm in the anterior choroidal artery that could lead to ischemia in the fornix. Our observation of a limited decrease of MD (~8%) within the first two days after surgery is not of sufficient magnitude to be attributed to cytotoxic edema alone. Vasogenic edema as a result of surgery may counteract reductions of diffusion due to the Wallerian degeneration mechanisms, cytotoxic edema, or inflammation. The elevated T2-weighted signal intensity of the ipsilateral fornix in the first few days after surgery (Figure 2.8) and its resolution at a week is consistent with vasogenic edema. Overall, all the

72

abovementioned physiological processes could happen with Wallerian degeneration simultaneously and play a part in the acute diffusion changes we observed in the study.

It is interesting to note that Patients 1, 2, 3 and 6, who presented with histologically confirmed hippocampal sclerosis or elevated T2 relaxometry value, showed a greater reduction of the diffusivities at 1-2 days after surgery than Patients 4 and 5 who did not present with evidence of hippocampal sclerosis (Figure 2.9). Electron microscopy of the excised fimbria-fornix has shown that TLE patients with hippocampal sclerosis have increased extra-axonal space, less myelin fraction, and decreased number of axons in the fimbria-fornix compared to patients without hippocampal sclerosis (Concha et al., 2010). While a larger sample size is needed to confirm the apparent differences in the longitudinal diffusion parameters post-surgery in patients with and without hippocampal sclerosis, these findings suggest that the acute diffusion changes (less than a week after surgery) may be driven by extra-axonal processes (inflammation etc).

At 6-7 days after transection, parallel diffusivity remains reduced in all six subjects. This is in contrast to perpendicular diffusivity where 4 of 6 subjects pseudo-normalize to within the normal range at this time point. This may be due to persistent discontinuities along the disrupted tracts whereas demyelination and reduced membrane integrity may be slowly causing perpendicular diffusion to increase towards its chronic elevated values. This result of reduced parallel diffusivity and relatively unchanged perpendicular diffusivity fits well with our earlier finding of the corpus callosum one week after its transection (Concha et al., 2006); although there the corpus callosum showed slightly elevated $\lambda_\perp$ at 1 week. Note that no scans were performed within six days after corpus callosotomy and it is unknown whether similar reductions of $\lambda_\perp$ would have been observed.

2.4.2 Chronic diffusion changes post-surgery

Past efforts have focused mainly on chronic diffusion changes of white matter tracts several months or years after transection in epilepsy patients (Wieshmann et al., 1999; Taoka et al., 2005; Concha et al., 2007; Schoene-Bake et al., 2009; McDonald et al., 2010; Yogarajah et al., 2010; Nguyen et al., 2011). Our findings of reduced fractional anisotropy and elevated mean diffusivity in the ipsilateral fornix 1-4 months after surgery are in agreement with the previous studies that compared post- to pre-operative fornix as

early as 2 months after anterior temporal lobectomy (Concha et al., 2007; McDonald et al., 2010; Yogarajah et al., 2010; Nguyen et al., 2011). Interestingly, one study acquired DTI at two time points, 2 months and 1 year, and the reduction of FA and elevation of MD did not progress further in the ipsilateral fornix at 1 year relative to at 2 months following transection (McDonald et al., 2010), which suggests a completion of Wallerian degeneration within 2 months post injury in human central nervous system. The same pattern of diffusion changes was also observed in other white matter tracts including both directly transected (parahippocampal cingulum, uncinate fasciculus, inferior longitudinal fasciculus, geniculo-calcarine tracts) and other non-transected tracts (inferior fronto-occipital fasciculus, corpus callosum, anterior commissure) more than 2 months after anterior temporal lobectomy (Taoka et al., 2005; McDonald et al., 2010; Yogarajah et al., 2010). The chronic FA reduction in this study was driven by both a decrease of $\lambda_{\parallel}$ in 4 of 6 subjects (pseudo-normal in the other 2) and increase of $\lambda\bot$ in all subjects, which is compatible with myelin degradation and slow clearance of axonal and myelin debris (George and Griffin, 1994; Vargas and Barres, 2007) and/or the persistence of isotropic cells associated with gliosis, as previously shown in a rat model of fornix transection (Stichel and Müller, 1994). A previous study on chronic stroke patients discussed that the diffusion "signature" of reduced $\lambda_{\parallel}$, elevated $\lambda\bot$, and limited increase of MD was consistent with gliosis (Pierpaoli et al., 2001).

2.4.3 Minimal diffusion change in the contralateral fornix

The contralateral fornix, on the other hand, did not show much change in five out of six patients. Since fornices contains commissural fibers as well as bidirectional fibers linking hippocampus and septal regions in each hemisphere, it is unclear whether the contralateral fornix would be affected by Wallerian degeneration initiated from the cut lesion on the ipsilateral side. From six days to 4 months, Patient 1 showed elevated perpendicular (12%) and mean diffusivity (5%), normal parallel diffusivity, and reduced FA (10%) in the contralateral fornix. The lack of T2-intensity changes in this contralateral tract in Patient 1 (Figure 2.8) would argue against possible edema. The remaining five patients did not have alterations of these diffusion parameters in the contralateral fornix over this period of time. Previous findings regarding the contralateral fornix at the chronic stage vary. In accordance with the current observation, our previous study did not observe significant diffusion changes of the contralateral side at 1 year post-

surgery in comparison with its presurgical level (Concha et al., 2007). On the other hand, significant FA reduction in the contralateral fornix, was observed at 2 months post-surgery in temporal lobe epilepsy patients, and was sustained at 1 year (McDonald et al., 2010). Similarly, relative to pre-surgical measurements, reduced FA in the contralateral fornix was shown in both left and right temporal lobe epilepsy patients at 4.5 months post-surgery (Yogarajah et al., 2010). However, increased FA in the contralateral fornix was reported at 4 months after surgery, suggestive of a structural reorganization in response to epilepsy surgery (Nguyen et al., 2011). Further investigation is required to elucidate the diffusion changes of the contralateral fornix at both acute and chronic stages after temporal lobe surgery.

2.5 Limitations

Due to the extreme difficulties of scanning patients within days after brain surgery, the sample size of the current study is small. Therefore, little can be inferred on potential responses due to type of surgery since two had selective amygdalohippocampectomy and four had anterior temporal lobe resection. However, in the four patients with hippocampal sclerosis, the responses of the diffusion parameters of Patients 1 and 3 with selective amygdalohippocampectomy is similar to that of Patients 2 and 6 with anterior temporal lobe resection (Figure 2.6 and Figure 2.9). In addition, more frequent post-operative DTI acquisitions, e.g. between 7-30 days after surgery, might facilitate catching the transition of perpendicular diffusivity from reduction to elevation compared to the pre-surgical level, which could help in understanding the timing of Wallerian degeneration in the central nervous system. Because of severe Wallerian degeneration at 1-4 months following surgery and subsequent reduction in FA, a middle portion of the fornix was unable to be traced by tractography; instead the fornix measured for the chronic scans was nonlinearly deformed from the one tracked from the pre-surgical scan based on coregistration of the b0 images between the two time points. Such transformation might not be accurate due to the brain shift and incomplete resolution of subdural edema at the chronic scans. To help minimize quantitative errors, we attempted to eliminate voxels located outside of the fornix by excluding voxels with fractional anisotropy lower than 0.25; however, this approach may lead to an underestimation of the change in fornix fractional anisotropy (19% change in FA at the chronic time point) since those heavily degenerated tract voxels would be excluded from the overall tract mean. Without setting

a fractional anisotropy threshold of 0.25, the fractional anisotropy would be reduced by 29% (range 23-42%); mean diffusivity would be elevated by 12% (range 7-17%) and perpendicular diffusivity would be elevated by 29% (range 20-46%) in all patients at the chronic time points. A further explanation for the observation that the changes in diffusion parameters are perhaps less than expected following transection of a fiber bundle is the fact that the portion of fimbria-fornix posterior to the surgical margin was preserved. While the efferent axons originating from the resected hippocampus anterior to the surgical margin were expected to undergo Wallerian degeneration, the remaining efferent axons originating from the unresected hippocampus posterior to the surgical margin as well as the afferent axons coming from the septal region were expected to remain intact. As the surgical transection would not disconnect these axons from their cell bodies, the axons would be expected to be preserved following surgery and not undergo Wallerian degeneration. The presurgical DTI scan of some patients was acquired months before surgery and then served as a baseline for all post-surgical analyses. The time gap in which epilepsy may still evolve and cause seizure related degenerative changes may contribute to the variation seen post-surgically. This concern is partly addressed by the demonstration of similar diffusion parameters derived from the two presurgical scans (at 10 months and 4 days prior to the surgery) for Patient 4.

2.6   Conclusions

In summary, Wallerian degeneration can be followed by diffusion tensor imaging. In this paper, we report novel diffusion changes of transected white matter in the challenging hyperacute (1-2 days), acute (3-7 days), and chronic (1-4 months) periods following temporal lobe epilepsy surgery in human brain. A unique pattern was observed in the ipsilateral fimbria-fornix crus featuring a notable decrease of both parallel and perpendicular diffusivities within the first two days, followed by a pseudo-recovery over the first week, and then highly elevated perpendicular diffusion at several months with a reduced or normal parallel diffusivity. While the reduced parallel diffusivity (sub)acutely and elevated perpendicular diffusivity chronically fit with the notion of using the diffusion eigenvalues as markers of axon and myelin health, respectively, the reduced perpendicular diffusivity in the acute phase is tougher to rationalize but may reflect a number of pathologies including axon swelling, increased axoplasmic viscosity, ischemia-induced cytotoxic edema, and/or infiltration of inflammatory cells. Fractional

anisotropy did not change during the first week post-transection necessitating the use of other complementary diffusion metrics for monitoring the white matter degeneration process in vivo in human brain.

2.7   Appendix[2]

Here is some additional information of the study that is not published but is useful to better interpret the results.

The volume of the fornix was within 10% variation for time points within the first week.
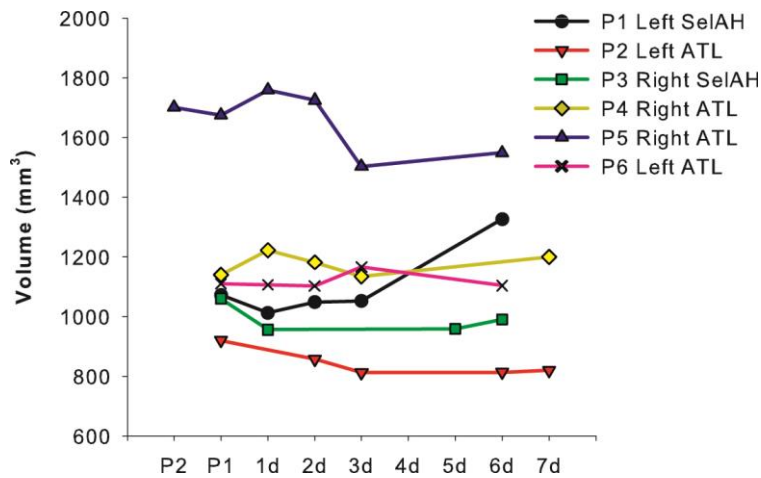
Appendix Figure 2.1 Time course of the volume of the ipsilateral crus of fimbria-fornices from six patients with temporal lobe epilepsy prior to (P1, P2) and within the first week (days, d) after surgery. The volume showed limited variation within 10% of the pre-surgical baseline (P1). SelAH, selective amygdalohippocampectomy; ATL, anterior temporal lobectomy.

---

[2] The appendix did not appear in the published version of this Chapter.

Figure 2.4 in the published version of the study only showed the ipsilateral fornix after surgery to illustrate its dynamic diffusion change. The contralateral side showed little change at all. The following figure gives additional illustration of the contralateral side.
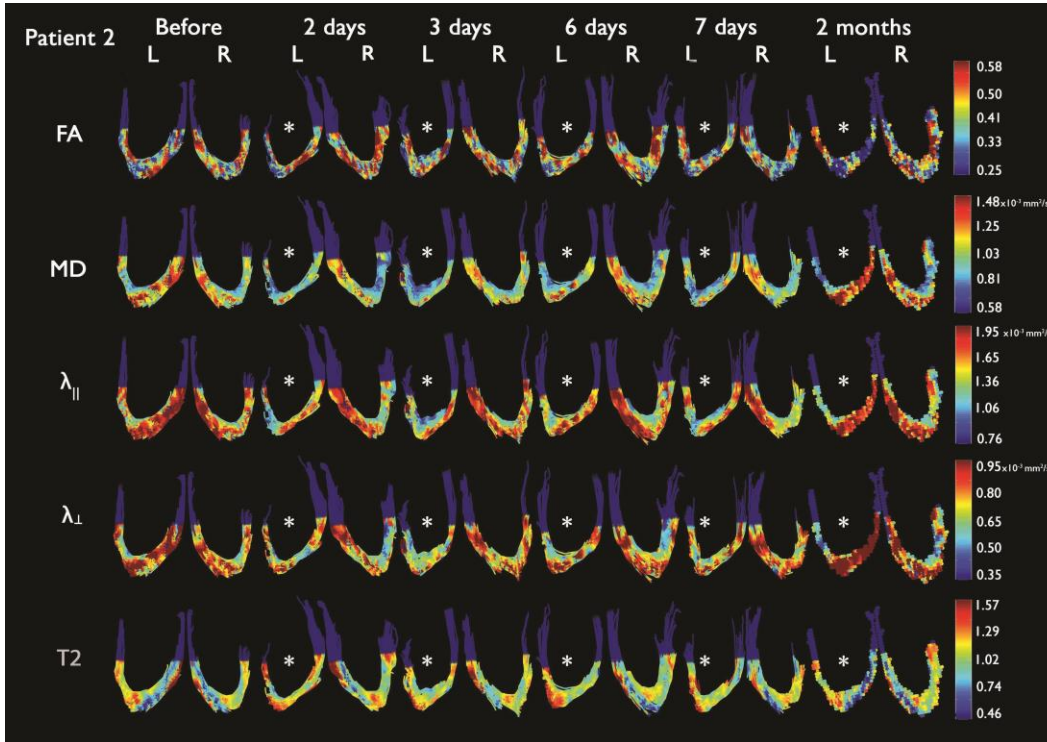
Appendix Figure 2.2 Visualization of the crus of fimbria-fornices (viewed from above) before and after surgery in Patient 2 where FA, MD, $\lambda_{\parallel}$, $\lambda\perp$ and T2 ratio are color-coded for each voxel. The non-measured part (i.e. the body of fornix and the fimbria-fornix adjacent to hippocampi) is colored in uniform dark purple. For the ipsilateral/left side, the FA was relatively stable within the first week after surgery and decreased at 2 months. The $\lambda_{\parallel}$, $\lambda\perp$, and MD was reduced at 2 days, stayed low up to 7 days, and then increased at least to ($\lambda_{\parallel}$) or beyond ($\lambda\perp$, MD) the pre-surgical values at 2 months. The diffusion and T2 ratio for the contralateral side was quite stable.

Chapter 3 Mesial temporal sclerosis is linked with more widespread white matter changes in temporal lobe epilepsy[3]

3.1 Introduction

Temporal lobe epilepsy (TLE) is the most common localization related epilepsy syndrome. Most TLE cases are associated with mesial temporal sclerosis (MTS) which can be detected by abnormal signal intensity and reduced volume of the hippocampus on magnetic resonance imaging (MRI) (Van Paesschen et al., 1997). Along with mesial temporal abnormalities, TLE patients have also demonstrated extensive grey and white matter abnormalities both ipsilateral and contralateral to the seizure onset zone (Keller and Roberts, 2008; Otte et al., 2012). Patients with TLE and unilateral MTS (TLE+uMTS) often demonstrate gray matter atrophy within and beyond the ipsilateral temporal lobe including inferior-medial and posterior temporal, limbic system, insular, frontal regions, basal ganglia, and thalamus ipsilateral, and not uncommonly contralateral to the seizure onset zone (Keller and Roberts, 2008; Riederer et al., 2008; Pail et al., 2010). White matter abnormalities have been demonstrated with volumetry and voxel-based morphometry (VBM) (Coste et al., 2002; Keller and Roberts, 2008) and diffusion tensor imaging (DTI) in the fornix, parahippocampal cingulum, dorsal cingulum, uncinate fasciculus, inferior/superior longitudinal fasciculus, inferior fronto-occipital fasciculus, corticospinal tracts, anterior thalamic radiation, and splenium of the corpus callosum in TLE patients (Thivard et al., 2005; Gross et al., 2006; Focke et al., 2008; Kim et al., 2008; Shon et al., 2010; Kemmotsu et al., 2011; Otte et al., 2012).

Although MTS is observed in most TLE patients, some patients do not demonstrate evidence of MTS on MRI. While it is assumed that some of these non-lesional TLE patients (nl-TLE) have subtle pathological features of MTS that cannot be detected with MRI, Carne *et al*. have demonstrated a strong correlation between negative MRI findings

---

[3] A version of this chapter has been published. Liu M, Concha L, Lebel C, Beaulieu C, Gross DW. Mesial temporal sclerosis is linked with more widespread white matter changes in temporal lobe epilepsy. NeuroImage: Clinical 2012; 1: 99–105.

and the absence of histological features of MTS in surgical specimens (Carne et al., 2004). Although most reports of imaging findings outside of the mesial temporal regions in TLE have focused on TLE+uMTS or have not clearly separated TLE+uMTS and nl-TLE, we have recently reported more extensive white matter abnormalities in TLE+uMTS as compared to nl-TLE in a small number of white matter tracts (Concha et al., 2009). Whether TLE+uMTS and nl-TLE demonstrate differences in other white matter tracts previously reported as abnormal in TLE remains unknown (Thivard et al., 2005; Gross et al., 2006; Focke et al., 2008; Kim et al., 2008; Shon et al., 2010; Kemmotsu et al., 2011; Otte et al., 2012).

The purpose of the current study is to compare the diffusion properties (i.e., fractional anisotropy and mean, parallel and perpendicular diffusivities) of thirteen major white matter tracts in patients with temporal lobe epilepsy and unilateral mesial temporal sclerosis (TLE+uMTS) versus patients with non-lesional TLE (nl-TLE) using diffusion tensor tractography.

3.2 Materials and Methods

Approval of the research protocol was obtained from local Health Research Ethics Board, and informed consent was obtained from all participants.

3.2.1 Subjects

TLE with unilateral MTS (TLE+uMTS, n = 23, age 40 ± 11 years, range 19-58 years, 14F/9M): Electroencephalogram (EEG) video-telemetry demonstrated unilateral temporal lobe ictal onset in all patients, among which 15 were left (n = 15, age 39 ± 13 years, range 19-58 years, 8F/7M) and eight were right (n = 8, age 42 ± 5 years, range 36-48 years, 6F/2M). Hippocampal sclerosis was defined based on T2 relaxometry analysis where the ipsilateral hippocampal T2 values were above two standard deviations of the overall mean of the controls (i.e., 120 ms using the methodology below). Patients with contralateral hippocampal T2 greater than two standard deviations of controls were included if the ipsilateral hippocampal T2 was greater than that of the contralateral value and EEG demonstrated ictal EEG onset solely from the ipsilateral temporal region. No other lesions were identified from the clinical imaging for all subjects.

Non-lesional TLE (nl-TLE, n = 15, age 35 ± 8 years, range 17-45 years, 6F/9M): All patients had temporal lobe epileptic EEG abnormalities. EEG lateralization was left temporal for four patients, right temporal for seven, and bitemporal for four. No lesions were visually identified on the clinical imaging and hippocampal T2 was within two standard deviations of controls bilaterally.

Healthy controls (n = 21, age 37 ± 12 years, range 19-58 years, 8F/13M): All control subjects had no history of any neurological or psychiatric disorders and had no evidence of structural lesions on T1 weighted MRI.

There were no significant age differences among the three groups (analysis of variance (ANOVA), p = 0.31). The TLE+uMTS patients had an earlier age of seizure onset than the nl-TLE patients (TLE+uMTS: 14 ± 12 years; nl-TLE: 23 ± 10 years; Mann-Whitney U, p = 0.033) and longer disease duration than the nl-TLE patients (TLE+uMTS: 26 ± 14 years; nl-TLE: 12 ± 9 years, Mann-Whitney U, p = 0.006).

Note that 17 of the 23 patients in the TLE+uMTS group and 10 of the 15 in the nl-TLE have been previously reported in a more restricted analysis of the thalamus, limbic tracts (fornix, cingulum), external capsule, and corpus callosum (Gong et al., 2008a; Concha et al., 2009).

3.2.2 Image acquisition

All imaging was performed on a 1.5T Siemens Sonata scanner (Siemens Medical Systems, Erlangen, Germany). T2 relaxometry with coverage of the hippocampus used a high-resolution, multi-echo sequence with 32 echoes, 10 coronal slices, 3 mm slice thickness with 3 mm inter-slice gap, TR = 4430 ms, TE_1 = 9.1 ms, TE spacing = 9.1 ms, NEX = 1, acquisition matrix = 192×176 (interpolated to 384×352), FOV = 230 mm × 210 mm, scan time = 8 min 13 sec. Both standard DTI and fluid-attenuated inversion recovery (FLAIR) DTI were acquired using the same dual spin-echo, single shot echo planar imaging sequence except FLAIR DTI used an extra inversion pulse and fewer slices. The common parameters include 2 mm slice thickness with no inter-slice gap, TR = 10 s, TE = 88 ms, six diffusion directions with b = 1000 s/mm^2, NEX = 8, acquisition matrix = 128×128 (interpolated to 256×256), FOV = 256 mm × 256 mm. Fifty two axial slices with coverage of whole brain were acquired for standard DTI and 26 axial slices with coverage of the fornix plus an inversion time of 2200 ms were used for FLAIR DTI

(Concha et al., 2005b). Scan times for standard DTI and FLAIR DTI were 9:30 min and 8:30 min, respectively.
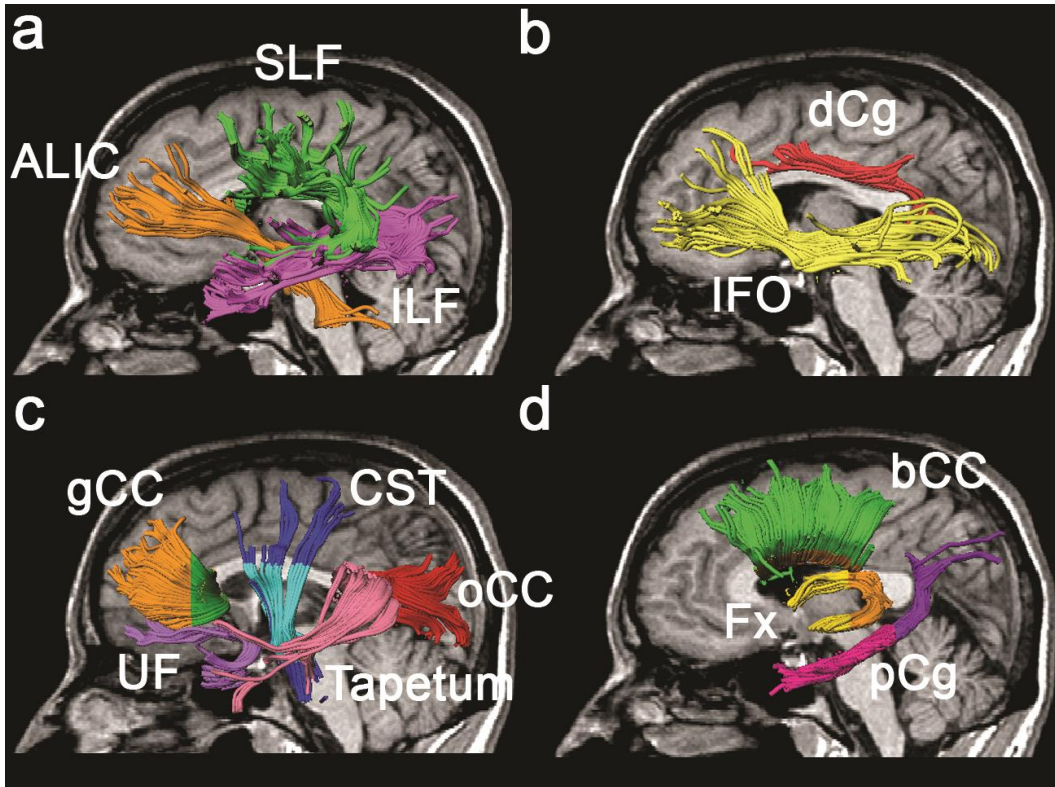
Figure 3.1 Three-dimensional visualization of thirteen tracts derived from tractography on a mid-sagittal slice in a 36-year-old male TLE+uMTS patient including: a) anterior limb of internal capsule (ALIC) and inferior/superior longitudinal fasciculi (ILF/SLF), b) dorsal cingulum (dCg) and inferior fronto-occipital fasciculus (IFO), c) uncinate fasciculus (UF), frontal, occipital and temporal part of the corpus callosum (gCC/oCC/Tapetum) and corticospinal tracts (CST), and d) body of corpus callosum (bCC), fornix (Fx) and parahippocampal cingulum (pCg). For some tracts, only a portion was analyzed and is indicated by a different color, namely the portion between the decussation and the body of the corpus callosum in light blue for CST, the crus of the Fx posterior to the coronal slice placed at the fusion of the two crura in orange for Fx, the portion anterior to the most anterior slice of the splenium of the corpus callosum in pink for pCg, and, the medial central part before the fibers fan out to the cortices (~15 mm from the midline) for all callosal fibers (gCC/bCC/oCC/Tapetum) are colored differently.

3.2.3 Quantitative hippocampal T2 relaxometry

The T2 signal decay was fitted to a mono-exponential curve voxel by voxel across the multi-echo coronal images. T2 values for the left and right hippocampi were calculated

by averaging within the regions of interest manually drawn on two consecutive slices (Concha et al., 2005a).

3.2.4 Diffusion tensor tractography

In total, thirteen major white matter tracts were analyzed in this study. Limbic tracts (i.e. fornix and parahippocampal cingulum) and genu, occipital and temporal callosal tracts were included in order to verify our previous findings (Concha et al., 2009) and the other eight tracts were chosen based on previously reported abnormalities from other groups (Thivard et al., 2005; Gross et al., 2006; Focke et al., 2008; Kim et al., 2008; Shon et al., 2010; Kemmotsu et al., 2011; Otte et al., 2012). The tracts were also selected due to their well-established tracking protocols using deterministic tractography (Wakana et al., 2004). Tensor calculation and tractography of the parahippocampal cingulum (pCg), dorsal cingulum (dCg), uncinate fasciculus (UF), inferior/superior longitudinal fasciculus (ILF/SLF), inferior fronto-occipital fasciculus (IFO), anterior limb of the internal capsule (ALIC), corticospinal tracts (CST) and genu and body of the corpus callosum (gCC/bCC) on the whole brain DTI dataset and the occipital and temporal part of the corpus callosum (oCC/Tapetum) on the FLAIR DTI dataset (to be consistent with our previous study) (Concha et al., 2009) were identified using a semiautomatic deterministic tractography method fully described before (Lebel et al., 2008) (Figure 3.1). In brief, a non-diffusion weighted image template was created based on six scans of a 33-year-old male control subject coregistered to each other and averaged together for both whole brain DTI and FLAIR DTI datasets. Regions-of-interest (ROIs) for selecting specific tracts were manually drawn on the template subject based on known anatomical landmarks (Wakana et al., 2004). Each subject's non-diffusion weighted images were nonlinearly normalized to the custom template using SPM8 (Wellcome Department of Cognitive Neurology, London, United Kingdom). The estimated deformation map from normalization step was then inverted and applied to transform the template's ROIs into each subject's native space. Fiber tracking was performed in the subject's native space using the deformed ROIs and a deterministic streamline method provided by ExploreDTI (Leemans et al., 2009). All resultant tracts were visually examined and a limited number of spurious tracts which deviated into other distant anatomical locations were excluded manually. The tractography of the crus of the fornix (Fx) was performed manually (due to the requirement of finer ROIs for this small structure) (Malykhin et al., 2008) on the FLAIR

DTI dataset to reduce the signal contamination from the adjacent cerebrospinal fluid (Concha et al., 2005b). Fractional anisotropy threshold was set to 0.25 and the angle threshold was set to 60 degrees for all tracts. In order to reduce the effects of crossing fibers and tract variability near the gray matter boundaries, only the portion between the decussation and the body of the corpus callosum axially and the medial central part before the lateral corpus callosum fibers turning up to the primary cortices were analyzed in CST and bCC, respectively (Figure 3.1). The oCC and tapetum were also analyzed using the same method as our previous study (Concha et al., 2009). Fractional anisotropy (FA), mean diffusivity (MD), and parallel and perpendicular diffusivities were obtained by averaging over all voxels within the tract.

3.2.5 Statistical analyses

Statistical analyses were performed using SPSS version 18. Paired Student's t test on FA was performed in control group to evaluate the left and right symmetry of the nine paired tracts (except gCC, bCC, oCC and tapetum). A left-greater-than-right asymmetry was observed for FA in the dCg (left = 0.54 ± 0.02; right = 0.52 ± 0.02; p = 0.001) and ILF (left = 0.48 ± 0.02; right = 0.47 ± 0.02; p = 0.03), while a right-greater-than-left asymmetry was observed in the UF (left = 0.44 ± 0.03; right = 0.46 ± 0.02; p = 0.021). The lateralization of nl-TLE patients was complicated due to the presence of independent bilateral seizure onset in four subjects. The analyses of left and right symmetry in our previous study (Concha et al., 2009) further demonstrated low dependence of seizure lateralization on FA of Fx, pCg and external capsule in nl-TLE patients with different onset sides. As our primary interest in the current study was to look for differences between patients with TLE+uMTS and nl-TLE, and given the fact that the right to left differences for the control group were small (all less than 0.02) and to simplify the analysis from a practical perspective, the paired tracts were collapsed by averaging the value from each hemisphere to yield a single value per tract. The between-group differences of FA were tested by multivariate analysis of covariance (MANCOVA) with age included as a covariate for all thirteen tracts together among TLE+uMTS, nl-TLE and controls. To better understand the basis of any FA differences, the mean, parallel and perpendicular diffusivities were also compared between-groups secondarily. Only if Wilks' Lambda was significant at p = 0.05, then univariate analysis of covariance (ANCOVA) was performed for each tract followed by post-hoc t-tests for those tracts

that survived ANCOVA at $p = 0.05$ between groups. All the post-hoc tests for each diffusion measurement were corrected with False Discovery Rate (FDR) at $p = 0.05$. Additionally, the FA of the white matter tracts with significant between-group differences were evaluated for linear correlations with disease duration (controlling for age) and age of seizure onset (controlling for disease duration) in each patient group. The correlation between the ipsilateral FA of the white matter tracts and ipsilateral hippocampal T2 were also examined in all TLE+uMTS patients ($n = 23$) and 11 of the 15 nl-TLE patients excluding the four patients with bitemporal seizure onset. Both correlation results with and without FDR correction at $p = 0.05$ level were reported.

To probe the effect of laterality of MTS, the TLE+uMTS patients were divided into TLE with left MTS (left TLE+uMTS, $n = 15$) and TLE with right MTS (right TLE+uMTS, $n = 8$) and compared to controls ($n = 21$). Statistical tests showed neither age differences among the three groups (left TLE+uMTS: 39 ± 13 years; right TLE+uMTS: 42 ± 5 years; controls: 37 ± 12 years; Student's t test $p = 0.5$), nor differences of age of seizure onset and duration of epilepsy between the two TLE+uMTS subgroups (left TLE+uMTS: onset 15 ± 12 years, duration: 24 ± 15 years; right TLE+uMTS: onset 14 ± 13 years, duration: 29 ± 12 years; onset Mann-Whitney U, $p = 0.87$; duration Mann-Whitney U, $p = 0.52$). For this analysis, each side of the nine paired tracts (except the four commissural tracts, i.e. gCC, bCC, oCC and Tapetum) was considered separately to yield an FA value per side. Z-scores of FA (zFA) were calculated for each side of the nine paired fiber tracts in patients based on the mean FA and standard deviation of the corresponding side of controls. MANCOVA and following ANCOVA and post hoc tests were performed for each side of the tracts to compare the zFA between patients and controls separately for left TLE+uMTS and right TLE+uMTS with age included as a covariate. All post hoc tests were corrected by FDR at $p = 0.05$. To probe tract asymmetry, the left and right zFA for each tract were tested by paired t tests for each patient group. For the other four commissural tracts, i.e. gCC, bCC, oCC and Tapetum, the FA of the whole tract was compared among left TLE+uMTS, right TLE+uMTS and controls using ANCOVA and post hoc tests with age included as a covariate.

3.3 Results

The hippocampal T2 values of controls were 112 ± 4 ms for the left side and 111 ± 4 ms for the right side. The overall mean of both sides was 112 ± 4 ms. All TLE+uMTS patients demonstrated ipsilateral hippocampal T2 more than two standard deviations greater than controls (mean: 135 ms, range: 122-160 ms); these differences were highly significant (Student's t test, $p < 0.000001$). T2 of the contralateral side was also significantly larger than that of controls (mean: 117 ms, range: 107-129 ms, $p = 0.0001$). Four TLE+uMTS patients had contralateral T2 equal to or higher than 120 ms; however, in each case ipsilateral hippocampal T2 was greater than contralateral T2 (range difference in T2 ipsilateral – contralateral: 6-10 ms). None of the nl-TLE patients demonstrated elevated T2 on either side by definition. The average hippocampal T2 for the nl-TLE group was 114 ms (range: 106-118 ms) for the left and 112 (range: 103-118 ms) for the right side, both of which were not significantly different from the overall mean of controls (left side $p = 0.07$, right side $p = 0.87$).

Primary analysis: The MANCOVA test on FA showed a significant Wilks' Lambda at $p < 0.001$. ANCOVA and post-hoc tests revealed that ten tracts had significantly lower FA in TLE+uMTS relative to controls (all tracts except gCC, oCC and tapetum) and seven of these (all except the CST, UF and SLF) had lower FA with respect to nl-TLE group (Figure 3.2a). The nl-TLE group demonstrated significantly reduced FA of pCg and tapetum only with respect to controls.

Secondary analysis: The MANCOVA test on MD also demonstrated significant Wilks' Lambda at $p < 0.001$. The subsequent univariate analyses revealed four tracts (pCg, ILF, IFO and bCC) with significantly higher MD in TLE+uMTS compared to controls, among which, the bCC also showed higher MD relative to nl-TLE group (Figure 3.2b). There were no significant MD differences between nl-TLE patients and controls. The MANCOVA test on parallel diffusivity showed significant Wilks' Lambda at $p = 0.002$. The ANCOVA tests further showed the CST with reduced parallel diffusivity in the TLE+uMTS group versus controls and the bCC with significantly higher parallel diffusivity in TLE+uMTS versus nl-TLE (Figure 3.2c). Wilks' Lambda for perpendicular diffusivity was significant at $p < 0.001$. The elevation of perpendicular diffusivity was observed in ten tracts (all except the CST, gCC and oCC) in TLE+uMTS patients

compared to controls, among which the elevation in Fx, pCg, dCg, ILF, IFO and bCC was also significant with respect to nl-TLE patients (Figure 3.2d). Only the tapetum showed elevated perpendicular diffusivity in nl-TLE group relative to controls. Uncorrected correlations between disease duration and FA demonstrated no significant findings in 11 of 13 tracts with positive findings being observed in dCg (r = -0.58, p = 0.029) and bCC (r = -0.59, p = 0.027) in nl-TLE patients. However, neither results approached significance following FDR correction (FDR corrected dCg p = 0.19, bCC p = 0.35). For hippocampal T2 versus FA, no significant correlation was found before or after FDR correction.
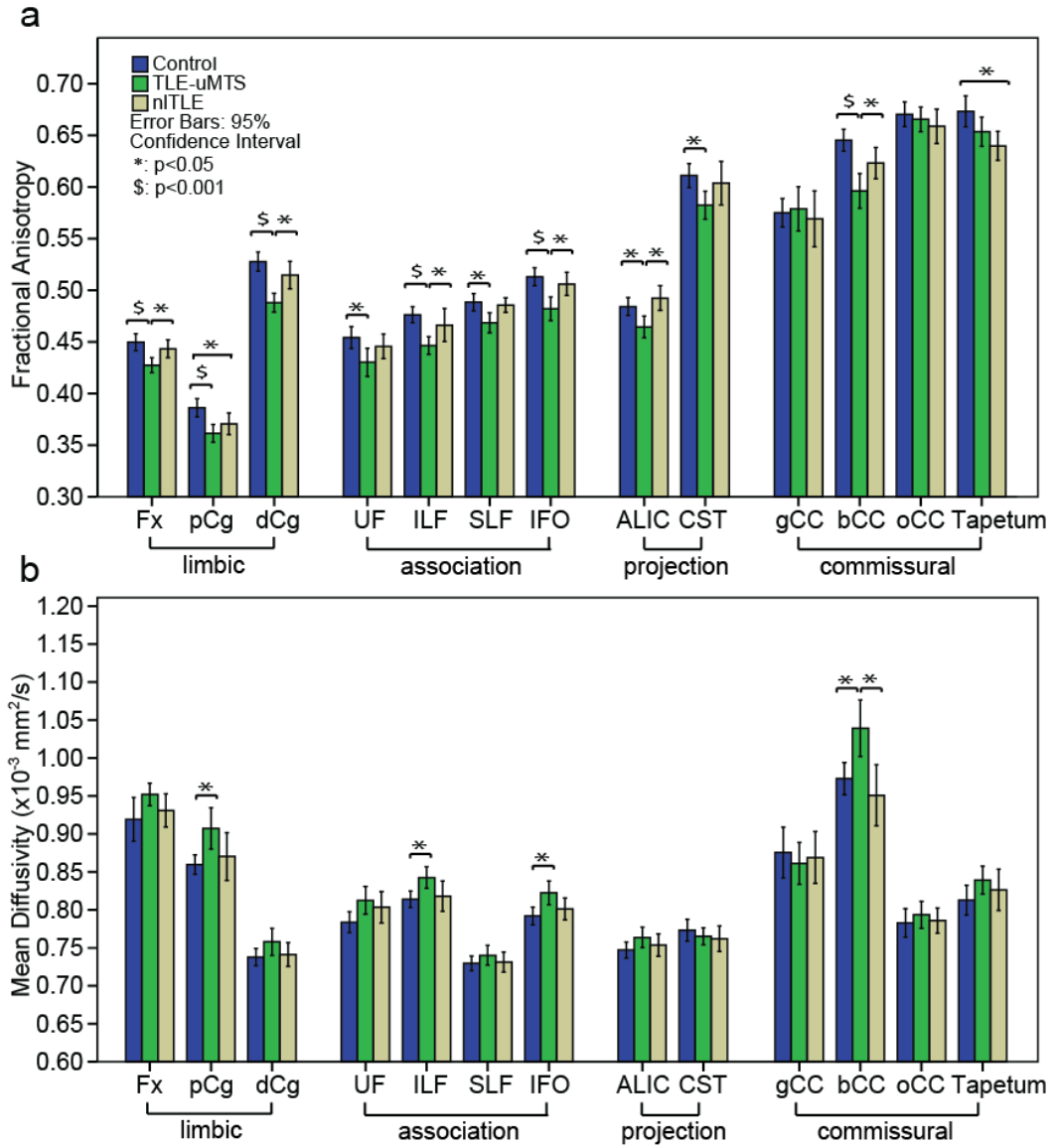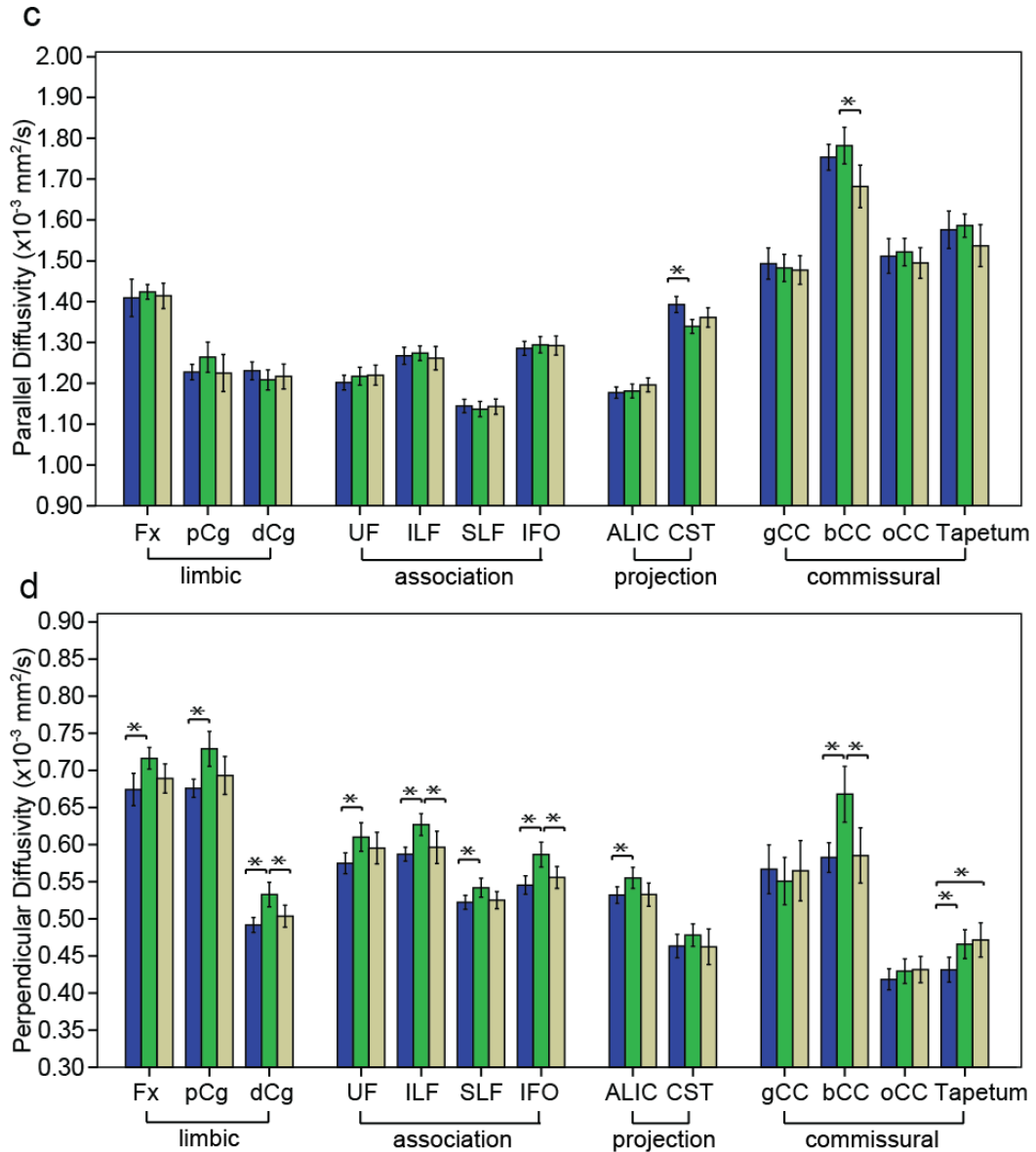
Figure 3.2 The mean and 95% confidence interval of a) FA, b) MD, c) parallel and d) perpendicular diffusivities of the thirteen white matter tracts (averaged across left and right) in TLE+uMTS (n=23), nl-TLE (n=15) and controls (n=21). The tracts were categorized into limbic, association, projection and commissural fibers. Significant between-group differences after FDR correction are marked. Many tracts show reduction of FA or elevations of perpendicular diffusivity, although this is more prevalent for the TLE+uMTS patients with the reduction in FA being primarily explained by increased perpendicular diffusivity.

89
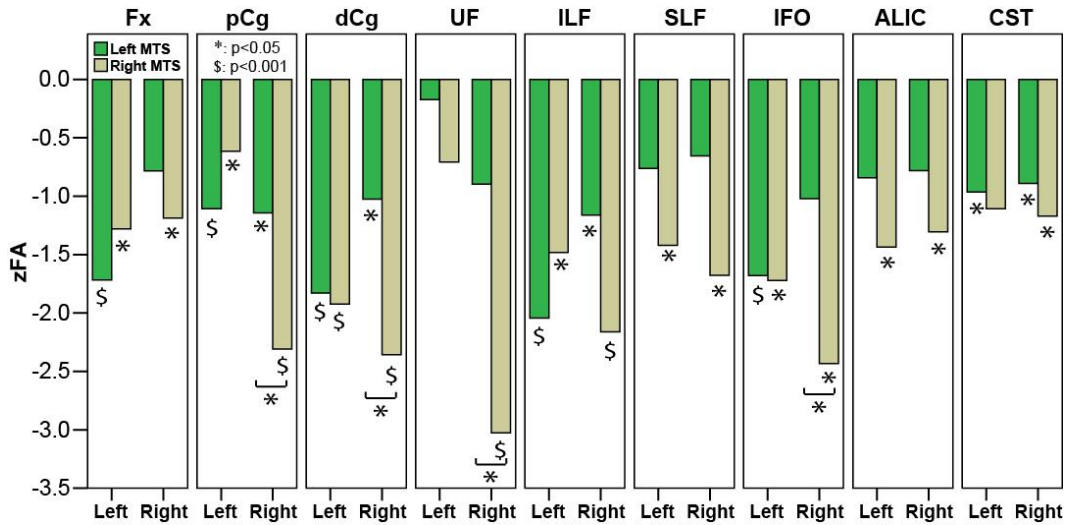
Figure 3.3 The z scores of FA (zFA, based on the mean and standard deviation of the corresponding side in control subjects) of the nine paired tracts with left and right sides assessed in patients with TLE and left MTS and with TLE and right MTS. Significant differences between patients and controls are marked beneath the individual bars and significant differences between the two patient groups are denoted by brackets. Right MTS shows FA reductions in all 9 tracts with 7 bilateral and 2 right only. Left MTS shows FA reductions in 6 tracts with 4 bilateral and 2 left only.

Analysis of right and left TLE+uMTS: For the nine paired tracts, right TLE+uMTS had FA reductions in all with seven bilateral and two right only whereas left TLE+uMTS had FA reductions in six tracts with four bilateral and two left only (Figure 3.3). Specifically, for patients with left TLE+uMTS (n = 15), four tracts (pCg, dCg, ILF and CST) demonstrated bilateral FA reduction and two tracts (Fx and IFO) showed ipsilateral FA reduction. For patients with right TLE+uMTS (n = 8), significant bilateral FA reduction was shown in seven tracts (Fx, pCg, dCg, ILF, SLF, IFO and ALIC) and ipsilateral FA reduction was shown in two tracts (UF and CST). Among the six tracts with significant changes in the left TLE+uMTS group, paired t tests revealed four tracts (dCg, ILF, Fx and IFO) with greater FA reduction on the left side, the UF with greater FA reduction on the right side and two tracts (pCg and CST) without significant asymmetry. Among all the nine paired tracts showing significant change in the right TLE+uMTS group, paired t tests revealed two tracts (pCg and UF) with greater FA reduction on the right side with the other seven tracts not showing any asymmetry. For the four commissural tracts, the only between group difference was shown in bCC (ANOVA, p < 0.001) where the FA of

all three groups was significantly different from each other with right TLE+uMTS showing the most FA reduction compared to controls (controls: 0.65 ± 0.02, left TLE+uMTS: 0.61 ± 0.03, right TLE+uMTS: 0.58 ± 0.05).

3.4 Discussion

In the current study, widespread abnormalities of white matter tracts within and beyond the temporal lobe were demonstrated in TLE+uMTS patients, while nl-TLE patients demonstrated fewer white matter abnormalities. These results suggest disruption of brain networks in TLE patients with and without MTS, although the affected network was more extensive in TLE+uMTS. Interestingly, in our cohort of subjects, TLE patients with right MTS showed more extensive bilateral changes than in TLE patients with left MTS, despite similar ages of onsets or disease durations.

These findings on a larger sample (an additional 6 TLE+uMTS and 5 nl-TLE patients) confirm our previous findings of FA reduction in the Fx and pCg in TLE+uMTS patients (Concha et al., 2005a, 2009). Furthermore, the nl-TLE patients here showed abnormalities of the pCg and tapetum, in agreement with our previous report (Concha et al., 2009). However, the gCC and oCC did not show any changes in either the TLE+uMTS or the nl-TLE groups, as was demonstrated before (Gross et al., 2006; Concha et al., 2009). Along with the increased sample size, the different methodologies used for gCC in the previous studies (ROI drawing on a single slice) and here (three-dimensional tractography) may contribute to the discrepancy of results.

The current observation of the abnormal frontal lobe (ALIC) and temporal lobe connected tracts (IFO, ILF, SLF and UF) as well as limbic system involvement (Fx, pCg and dCg) in TLE+uMTS are in agreement with several former DTI reports on cohorts of purely or largely TLE+uMTS patients (Thivard et al., 2005; Rodrigo et al., 2007; McDonald et al., 2008a; Ahmadi et al., 2009; Kim et al., 2011). The diffusion abnormalities identified in the central part of the bCC are in accordance with a previous voxel-based study (Knake et al., 2009). Interestingly, the CST has not been measured in many previous studies in TLE or has been used as a 'control' tract (no significant FA or MD changes in 17 unilateral TLE patients, 14 of whom had MTS, in a recent paper) (McDonald et al., 2008a); this is in contrast to our study where the CST had reduced anisotropy in adult TLE+uMTS patients. Our results are however consistent with findings

of bilaterally decreased FA of CST in 13 children with left TLE (Govindan et al., 2008). Discrepancy between our CST findings and McDonald *et al*. (McDonald et al., 2008a) could relate to differences in methodology. For example, our CST measurement was restricted to the central part of the tract (as shown by the blue highlight in Figure 3.1) where the fiber orientation is expected to be most uniform while they measured the full extent of the tracts. Our findings are also compatible with a number of earlier MRI-based volumetric and VBM studies in which white matter volume in total (Hermann et al., 2003), ipsilateral temporal lobe and body of the corpus callosum (Bernasconi et al., 2004), temporal pole (Coste et al., 2002), and ipsilateral frontal and parietal lobes and cerebellum (Mueller et al., 2006) was reduced in TLE+uMTS.

The reduction of FA observed here was mainly driven by an increase of perpendicular diffusivity, which is consistent with previous reports (Arfanakis et al., 2002; Gross et al., 2006; Lin et al., 2008; Concha et al., 2009). A few histopathological studies based on animal models proposed parallel and perpendicular diffusivities as surrogate indices of axonal membrane and myelination status, respectively (Song et al., 2002, 2003, 2005; Sun et al., 2006; Wu et al., 2007; Budde et al., 2009). Previous human in vivo DTI studies lent support to the notion by demonstrating increased perpendicular diffusivity with unchanged parallel diffusivity at the chronic stage of Wallerian degeneration when the myelin degradation is expected (Pierpaoli et al., 2001; Concha et al., 2006). These observations would suggest that the observed increase in perpendicular diffusion reflects reduced myelin in the chronically degenerated fibers; however, the expected disruption of axonal membranes associated with degeneration could also impact the perpendicular diffusivity (Concha et al., 2010).

The white matter findings in the pCg and tapetum in nl-TLE patients are in line with a previous VBM study demonstrating white matter concentration/volume reduction in the ipsilateral temporal lobe of nl-TLE patients (McMillan et al., 2004). In contrast to our more limited findings in nl-TLE, a recent DTI study detected widespread and bilateral reduction of white matter FA in the temporal lobes, the entire corpus callosum and the thalamus in a group of ten nl-TLE patients using voxel-based statistics (Keller et al., 2011a). A possible explanation for the more extensive findings in the Keller *et al*. study is the fact that qualitative as opposed to quantitative methods were used to classify subjects as non-lesional and therefore, it is possible that their patient group included some

TLE+uMTS patients. One other recent voxel-based DTI study reported significant MD elevation in the ipsilateral posterior fornix and posterior cingulum in ten left nl-TLE patients without changes in seven right nl-TLE patients (Shon et al., 2010). We did not look at left and right nl-TLE patients separately due to a small sample size. This, together with the different patient selection criteria and methodologies used (voxel-based statistics for them and tractography here), may account for the discrepancy among the aforementioned DTI studies.

Overall, we found that the white matter abnormalities were extensive and dramatic in TLE+uMTS and more limited in nl-TLE patients. Given the differences in age of seizure onset and disease duration between our TLE+uMTS and nl-TLE patients, where the MTS patient's onset was 9 years earlier and had 14 years longer disease duration, a possible explanation for the distinct white matter abnormalities observed is that these changes are secondary to seizure related white matter injury; however, the lack of correlations between FA and age of seizure onset/disease duration would argue against this hypothesis. That said, given the known changes of diffusion parameters in white matter during neurodevelopment (Lebel et al., 2008), it is possible that seizure onset during critical neurodevelopment periods of childhood and adolescence in the TLE+uMTS patients may have caused aberrant white matter development that is not evident if the seizures occur after the wiring is mostly laid down by adulthood (Hermann et al., 2002; Kaaden et al., 2011). The distinct white matter differences between TLE+uMTS and nl-TLE agrees with previous reports on structural and functional MRI and EEG. A more widespread gray matter volume reduction or white matter diffusivity elevation was seen in TLE+uMTS while nl-TLE patients showed either no change (Mueller et al., 2006) or a less extensive pattern (Riederer et al., 2008; Shon et al., 2010). Evidence from EEG recording analysis (Zaveri et al., 2001), multi-slice proton magnetic resonance spectroscopic imaging (Mueller et al., 2004) and structure-function correlation (Mueller et al., 2012) indicate differences between the two TLE sub-syndromes. Our findings further support the idea that TLE+uMTS and nl-TLE are associated with different epileptic networks. Along with more extensive structural changes, TLE+uMTS have also demonstrated more extensive cognitive dysfunction including measures not only of temporal lobe dysfunction (memory and language) but also executive function [22, 47–50]. Further study is required to assess a possible relationship between white matter integrity and cognitive function in TLE. It has been hypothesized that extratemporal

structural abnormalities may predict poor surgical outcome in TLE (Sisodiya et al., 1997). Our observation of more extensive white matter abnormalities in TLE+uMTS (who are expected to have a better surgical outcome (Sisodiya et al., 1997)) however contradicts this hypothesis.

An increasing number of studies suggest that patients with left TLE have greater impairment of learning and memory (Bell and Davies, 1998) and more distributed grey and white matter changes than patients with right TLE (Bonilha et al., 2007; Riederer et al., 2008; Ahmadi et al., 2009; Coan et al., 2009). One recent DTI study focusing on TLE patients with unilateral MTS reported more widespread diffusion changes in the ipsilateral temporal lobe and bilateral limbic system in 21 patients with left TLE+uMTS than in 12 patients with right TLE+uMTS, while more prominent contralateral changes were observed in the temporal lobe and the inferior frontal gyrus in the right TLE+uMTS group (Focke et al., 2008). Another DTI tractography study reported overall smaller FA in Fx, pCg, UF, ILF, IFO and arcuate fasciculus in 18 patients with left TLE, among which 14 had left MTS, relative to controls and 18 right TLE patients, among which 11 had right MTS (Kemmotsu et al., 2011). The exact mechanism of this asymmetry remains unknown. Focke *et al.* (Focke et al., 2008) suggested that the seizure propagation may be more widespread in the language dominant hemisphere, commonly the left side, on the basis of a pre-existing better connectivity (Powell et al., 2007) and Kemmotsu *et al.* (Kemmotsu et al., 2011) speculated that the left hemisphere undergoes a more prolonged maturation process than the right and is therefore more vulnerable to early brain insults (Corballis and Morgan, 1978). Interestingly, despite the comparable age, disease duration, age of seizure onset and ipsilateral T2 relaxometry time (left TLE+uMTS: 135 ± 10 ms, right TLE+uMTS: 132 ± 6 ms, $p = 0.45$) of the two TLE+uMTS subgroups in our study, more extensive white matter abnormalities were observed in patients with right TLE+uMTS in comparison to left TLE+uMTS. The discrepancy between our study and previous reports may be partly attributed to the tighter age range of our right TLE+uMTS patients (mean 42 ± 5 years, range 36-48 years) compared to the other two studies with a wider age range (22-54 years for the right TLE+uMTS group in (Focke et al., 2008) and 38 ± 11 years for right TLE group in (Kemmotsu et al., 2011)). While many reports suggest more extensive structural changes in left TLE+uMTS, two recent studies using VBM of T1-weighted images or SPECT have demonstrated more extensive abnormalities in right TLE+uMTS (Tae et al., 2005; Pail et al., 2010). More frequent interictal

hypoperfusion of the contralateral hippocampus on SPECT was seen in right TLE+uMTS as compared to left TLE+uMTS (Tae et al., 2005) and gray matter volume reduction was significantly more extensive in right TLE+uMTS than left TLE+uMTS (Pail et al., 2010). Given the conflicting observations in the literature more work is needed to better characterize the differences in the extent of structural changes associated with right and left TLE+uMTS.

3.5 Conclusion

In summary, the current study demonstrated widespread diffusion abnormalities of white matter tracts within and beyond the temporal lobe in patients with TLE and unilateral MTS while, in contrast, patients with non-lesional TLE showed fewer changes. Specifically, patients with TLE and right MTS showed a more extensive bilateral white matter disruption than patients with left MTS. In conjunction with previous findings of white and gray matter abnormalities reported by other independent investigators, there is considerable evidence to suggest different dysfunctional networks in TLE patients with and without MTS.

Chapter 4 Disrupted anatomical white matter network in left mesial temporal lobe epilepsy[4]

4.1 Introduction

Temporal lobe epilepsy (TLE) is the most common focal epilepsy syndrome. Most TLE cases are associated with mesial temporal sclerosis (MTS) where hippocampal atrophy and/or T2 hyperintensity is observed on magnetic resonance imaging (MRI) images. Recently, quantitative MRI studies provided new structural information in TLE by demonstrating extensive abnormalities within and beyond the temporal lobe, including reduced gray matter concentration/atrophy (Keller and Roberts, 2008), decreased cortical thickness (Bernhardt et al., 2011), and abnormal white matter in the temporal, frontal and parietal lobes (Concha et al., 2005a; Yogarajah et al., 2008). The language and memory impairments seen in TLE patients have also been related to altered blood-oxygen-level-dependent (BOLD) activations during memory and language tasks compared to healthy controls in functional MRI (fMRI) studies (Dupont et al., 2000; Waites et al., 2006).

The growing knowledge of the brain structural and functional changes related to TLE have led to the notion that TLE is a network disorder that affects large neural networks involved in normal brain functions (Spencer, 2002). With the implementation of graph theoretical analysis on brain functional and structural measurements the complex brain can be quantified as an integrated system and infer its capacity of information integration and segregation (Sporns et al., 2005). Graph theoretical analysis enables the abstraction and examination of the brain topological architecture and properties at the network level, which provides a macroscopic perspective rather than the previously performed investigations at the level of local connections. Past network analysis in epilepsy has focused on the functional connectivity in TLE patients where several studies measured the brain functional network constructed from the coherence of electroencephalography

---

[4] A brief version of this chapter has been presented. Liu M, Chen Z, Concha L, Beaulieu C, Gross DW (2012). Disrupted anatomical white matter network in left mesial temporal lobe epilepsy. Poster presentation at American epilepsy society (AES) 66th annual meeting, Nov 30 - Dec 4, 2012, San Diego, CA, USA.

(EEG) signals between different regions. These studies have demonstrated that the network in TLE had a small-world configuration and transited from a more random configuration towards a regular configuration at seizure onset (Ponten et al., 2007, 2009; Kramer et al., 2008; Schindler et al., 2008). A recent study based on single photon emission tomography demonstrated increased connectivity and clustering within the medial temporal and subcortical regions with an overall reduction of connectivity in the remaining cortex and the whole network in mesial TLE patients during the ictal compared to the inter-ictal state (Sequeira et al., 2013). Other studies based on inter-ictal functional MRI (fMRI) showed decreased global efficiency in TLE patients in comparison with healthy controls (Waites et al., 2006; Liao et al., 2010).

While functional network analysis offers insights into the dynamics of the brain, it is also necessary to examine the structural network that provides anatomical substrate for the functional change. One recent structural brain network study based on regional cortical thickness correlation reported increased path length and clustering in TLE patients (Bernhardt et al., 2011). Two other network studies based on white matter fiber connection derived from diffusion tensor imaging (DTI) tractography specifically examined the default network (Liao et al., 2011) and limbic network (Bonilha et al., 2012) in TLE patients. They reported significantly decreased connection density among default network cortical regions (Liao et al., 2011) and increased cluster coefficient in the limbic network (Bonilha et al., 2012), respectively. However, the alterations in the topological properties of a whole brain white matter network in TLE patients remain unknown.

The purpose of this study was to examine the topological properties of the white matter structural network in a cohort of left TLE patients with MTS (mTLE) in comparison with healthy controls.

4.2   Materials and Methods

Approval of the research protocol was obtained from University of Alberta Health Research Ethics Board, and informed consent was obtained from all participants.

4.2.1 Participants

Sixteen patients with left mTLE and 21 healthy volunteers were recruited from the epilepsy clinic of the University of Alberta Hospital (Table 4.1). All left mTLE patients demonstrated left temporal lobe ictal seizure onset on EEG-video telemetry and left mesial temporal sclerosis defined by left hippocampal T2 greater than two standard deviations above the mean of controls (i.e. above 120 ms; see the method used in our previous study (Liu et al., 2012)). Note that 15 of the 16 left mTLE patients have been previously reported in group comparisons of tractography derived parameters in individual tracts versus controls (Concha et al., 2009; Liu et al., 2012). Three cognitive tests were administered to the left mTLE patients including processing speed (PS, a Wechsler Adult Intelligence Scale III measure that is sensitive to white matter abnormalities (Axelrod et al., 2001; Drew et al., 2009)), auditory-verbal learning test (AVLT-VII) and continuous visual memory test (CVMT). The standardized scores (to the same age groups) were later used for correlation analysis. Cognitive assessments were not performed on controls.

4.2.2 Image acquisition

All participants were scanned on a 1.5T Siemens Sonata scanner (Erlangen, Germany). Whole brain magnetization prepared rapid acquisition gradient echo (MPRAGE) and standard DTI were acquired. MPRAGE provided high resolution 3D T1-weighted images with 144 axial slices, 1 mm slice thickness with no inter-slice gap, TR = 1890 ms, TE = 4.38 ms, TI = 1100 ms, flip angle = 15°, NEX = 1, acquisition matrix = 256×192 (interpolated to 512×384), FOV = 256 mm $\times$ 192 mm, voxel dimension $1 \times 1 \times 1$ mm^3 (interpolated to $0.5 \times 0.5 \times 1$ mm^3), scan time = 6 min 3 sec. Standard DTI used a dual spin-echo, single shot echo planar imaging sequence with 52 axial slices, 2 mm slice thickness with no inter-slice gap, TR = 10 s, TE = 88 ms, six diffusion directions with b = 1000 s/mm^2, NEX = 8, acquisition matrix = 128×128 (interpolated to 256×256), FOV = 256 mm $\times$ 256 mm, voxel dimension $2 \times 2 \times 2$ mm^3 (interpolated to $1 \times 1 \times 2$ mm^3), scan time = 9 min 30 sec.

Table 4.1 Demographic and clinical data of left mTLE patients and controls.

	left mTLE (n = 16)	Controls (n = 21)
Age (years)	38 ± 13 $(19 - 58)$	37 ± 12 $(19 - 58)$
Males	8	13
Age of seizure onset (years)	13 ± 11 $(1 - 29)$	-
Disease duration (years)	26 ± 14 $(4 - 51)$	-
Left hippocampal T2 (ms)	136 ± 10 $(126 - 160)$	112 ± 4 $(102 - 120)$
PS	75 ± 9	-
AVLT-VII	29 ± 10	-
CVMT	14 ± 16	-

4.2.3 Construction of weighted cortical networks

4.2.3.1 Pre-processing

Motion and eddy current corrections for all DTI images were performed using FSL (v5.0, FMRIB, Oxford, UK). Using SPM8 (Wellcome Department of Cognitive Neurology, London, UK), the structural images (MPRAGE) were linearly coregistered to the b0 image of each subject so that they were aligned in the DTI native space (Figure 4.1).
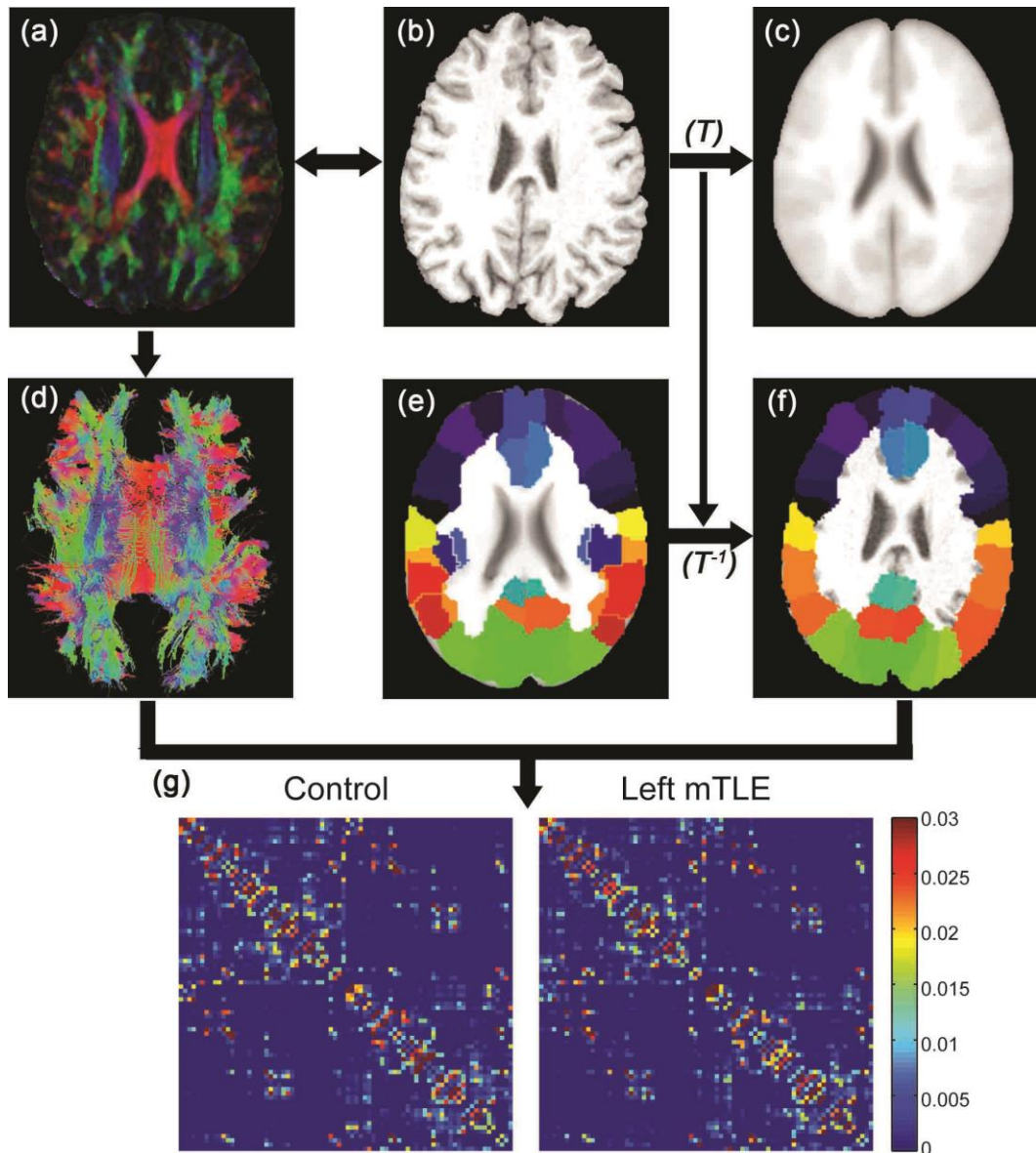
Figure 4.1 A flowchart for the construction of DTI white matter structural network. 1) The T1-weighted structural image for each subject (b) was coregistered into DTI native space (a) using rigid transformation. 2) The resultant structural image was nonlinear registered to the ICBM 152 T1 template (c) in the MNI space. 3) The AAL template including 78 cortical regions in the MNI space was inversely warped back to the individual DTI space (f) using the inverse transformation (T-1). 4) Whole brain white matter fibers were reconstructed using a deterministic tractography method. 5) The white matter fibers connecting any pair of the 78 regions were found and the FA, fiber number (FN) and average volume of the two cortical regions were counted to construct the white matter matrix for each subject. The mean matrices averaging from all participants from each group are shown (g).

4.2.3.2 Definition of network nodes

The automatic anatomical labeling (AAL) template was used to parcellate the cerebral cortex into 78 predefined cortical regions (39 for each hemisphere, Supplementary Table 4.1) (Tzourio-Mazoyer et al., 2002), each representing a node of the cortical network. This parcellation scheme has been used for several previous brain network studies (Gong et al., 2008b, 2009; Lo et al., 2010; Yan et al., 2011). Specifically, the T1-weighted structural image of each subject was nonlinearly transformed to ICBM 152 T1 template in the Montreal Neurological Institute (MNI) space (SPM8). The resulting inverse deformation map for each subject was then applied to warp the AAL template to the DTI native space using nearest neighbor interpolation method to preserve the discrete labeling values (SPM8).

4.2.3.3 Whole brain white matter tractography

The diffusion tensors were estimated and three eigenvalues and eigenvectors were derived from the diagnolization of the tensor matrix for each subject (Basser and Pierpaoli, 1996). Whole brain white matter tractography was performed in DTI-TK TractTool (v2.3.1) using a brute-force streamline-tracking method (Basser et al., 2000) seeding from every voxel in the brain with a fractional anisotropy (FA) greater than 0.2. The tract propagation terminated when it reached a voxel with FA less than 0.2 or with primary eigenvector turning more than 45 degrees.

4.2.3.4 Definition of network edges

The deformed AAL template for each subject marked 78 cortical regions in the DTI native space. The number of white matter fibers whose two terminal voxels fell within the area of any pair of the 78 cortical regions, conjointly, was counted. Two cortical regions were deemed connected if at least three connecting fibers were found between them. The counting threshold was applied to minimize false positive connections among regions (Lo et al., 2010; Brown et al., 2011; Shu et al., 2011).

4.2.3.5 Construction of weighted network

To quantify the strength of each connection/edge between two cortical regions (node i and j) we defined the edge weight by the product of the number of connecting fibers (fiber number, FN) and mean FA of the connecting fibers, divided by the average volume

of the two cortical regions to counteract the bias where larger cortical regions inherently project/receive more fibers (i.e. $w_{ij} = \frac{FN \times FA}{volume}$). This weighting factor has been adopted by several previous brain network studies (Lo et al., 2010; Brown et al., 2011).

4.2.4 Graph theoretical metrics

Several topological properties were measured for the weighted anatomical brain network derived from each participant, including small world properties originally proposed by (Watts and Strogatz, 1998) and efficiency measurements proposed by (Latora and Marchiori, 2003). A summary of graph theoretical metrics and their interpretations are listed in Table 4.2. For each white matter network, the connection weights w were normalized by the mean of all weights in the network to keep each participant's cost at the same level.

The strength S of a weighted network G with N nodes and K edges were defined as the mean of all edge weights in the network as follows:

$$S(G) = \frac{1}{N}\sum_{i \neq j \in G} w_{ij} \qquad (4.1)$$

where i and j are two distinct nodes in graph G. It characterizes the overall strength of connections between regions in the network.

The weighted clustering coefficient C_i of a node i in a weighted network G quantifies the likelihood whether the neighboring nodes j and k of node i were connected with each other, was defined as follows:

$$C_i = \frac{\sum_{j,k \in G}\left(w_{ij}w_{jk}w_{ik}\right)^{\frac{1}{3}}}{\frac{k_i(k_i-1)}{2}} \qquad (4.2)$$

where w_{ij} was the weight between node i and j and k_i was the number of connected neighbors of node i. The clustering coefficient is zero, i.e. $C_i = 0$, if node i was isolated or only had one connection, i.e. $k_i \in \{0,1\}$. The weighted clustering coefficient C of the network G with N nodes was defined as the mean of C_i averaging over all nodes in the network.

$$C = \frac{1}{N}\sum_{i \in G} C_i \qquad (4.3)$$

The weighted clustering coefficient (C) measures the probability that neighbors of a node are connected with each other, indicating the extent of cliquishness in a network (Watts and Strogatz, 1998).

The weighted characteristic path length L_{ij} between node i and j was defined as the shortest path length between the two nodes. The length of each weighted length was computed as the reciprocal of the edge weight $1/w_{ij}$. The weighted characteristic shortest path length L of a network G was defined as the harmonic mean length between any pair of nodes to overcome the problem of dramatically increased L between disconnected nodes (Newman, 2003).

$$L = \frac{1}{N(N-1)}\sum_{i=1}^{N}\sum_{j\neq i}^{N}\frac{1}{L_{ij}} \tag{4.4}$$

The weighted characteristic shortest path length (L) quantifies the average minimum weighted length that must be taken to go from one node to another of the network, reflecting the network's ability for information propagation in parallel.

The global efficiency E_{glob} of a weighted network G is defined as the inverse of the mean harmonic shortest path length between each pair of nodes within the network. The path length is computed as the reciprocal of the edge weight, thus

$$E_{glob}(G) = \frac{1}{N(N-1)}\sum_{i\neq j\in G}w_{ij} \tag{4.5}$$

where N is the number of nodes. It characterizes the efficiency of a system transporting information in parallel (Latora and Marchiori, 2003).

The local efficiency E_{loc} of a weighted network G is defined as the mean of the local efficiency of all nodes within the network, while the local efficiency of a node i is the global efficiency of its subgraph G_i which is comprised of the nearest neighbors of node i.

$$E_{loc}(G) = \frac{1}{N}\sum_{i\in G}E_{glob}(G_i) \tag{4.6}$$

The local efficiency represents the capacity of fault tolerance of the network in response to the removal of a node (Latora and Marchiori, 2003).

103

The small world property of a network can be examined by comparing its *C* and *L* with C_{rand} and L_{rand} of random networks that have the same number of nodes, edges, and degree and weight distribution. For each subject's white matter network, 1000 random networks were generated by a random rewiring procedure with the weight distribution of the real network preserved using Brain Connectivity Toolbox (Rubinov and Sporns, 2010). The weighted network can be categorized as small world if the normalized weighted clustering coefficient $\gamma = C/C_{rand} \gg 1$ and the normalized weighted characteristic shortest path length $\lambda = L/L_{rand} \approx 1$ (Watts and Strogatz, 1998). The two measurements can be combined into a single metric, small-worldness, $\sigma = \gamma/\lambda > 1$ (Humphries et al., 2006).

The regional global efficiency E_{reg} of a given node *i* is defined as the inverse of mean harmonic shortest path length between this node and all other nodes in the network (Achard and Bullmore, 2007). With the shortest path length being the reciprocal of the edge weight $1/w_{ij}$,

$$E_{reg}(i) = \frac{1}{N-1}\sum_{i \neq j \in G} \frac{1}{L_{ij}} \tag{4.7}$$

It measures the connectivity of the node to all other nodes of the network. Highly connected nodes have high regional efficiency and play pivotal role in the network (Achard and Bullmore, 2007). In this study, nodes with E_{reg} > group mean + group standard deviation (SD) is defined as network hubs in each participant group (Lo et al., 2010; Shu et al., 2011).

4.3   Statistical analysis

General linear model was used to compare the network topological properties (*S*, *C*, *L*, E_{glob}, E_{loc}, E_{reg}) between patients and controls with age and gender included as nuisance variables. The results of each E_{reg} of the 78 regions are corrected by false discovery rate at q = 0.05 (Genovese et al., 2002; Zeisel et al., 2011). For left mTLE group, significantly different topological properties were correlated with the left hippocampal T2, age of seizure onset, disease duration, PS, AVLT-VII and CVMT controlling for age and gender. Multiple comparison correction was also applied on correlation results using false discovery rate at q = 0.05.

4.4 Reliability test

The confidence intervals of graph theoretical metrics measured in this study were estimated by the sampling with replacement bootstrap approach with 10,000 randomizations for each group.

4.5 Results

4.5.1 Global property of the WM network

The mean WM network for controls and left mTLE patients were shown in Figure 4.2 and Figure 4.3, separately. Both controls and left mTLE patients demonstrated 'small-world' properties ($\gamma_{controls} = 2.52$, $\gamma_{LmTLE} = 2.81$, $\lambda_{controls} = 1.18$, $\lambda_{LmTLE} = 1.19$, $\sigma_{controls} = 2.14$, $\sigma_{LmTLE} = 2.35$). The patient-versus-control comparisons showed significantly increased L and decreased E_{glob} and E_{loc} in left mTLE patients relative to controls (Table 4.3).

4.5.2 Nodal property of the WM network

4.5.2.1 Hub regions

In controls, 13 hubs were identified by regional efficiency E_{reg}, including 11 association cortical regions, one paralimbic cortical region and one primary cortical region (Figure 4.4 and Figure 4.5). In left mTLE patients, 13 hubs were identified including 11 association cortical regions, one paralimbic cortical regions and one primary cortical region. However, compared to controls, left precuneus and paracentral lobule hubs were replaced by left cuneus and superior frontal medial part in left mTLE patients. The other hubs were shared by both groups including bilateral supplementary motor area, superior occipital gyrus, left superior frontal gyrus dorsolateral part, left middle occipital gyrus, right superior frontal gyrus medial part, precuneus, calcarine fissure and surrounding cortex, cuneus and median cingulate and paracingulate gyrus.

4.5.2.2 Group differences in regional efficiency

Compared to controls, left mTLE patients showed significantly reduced E_{reg} ($p < 0.05$, FDR corrected) in 17 cortical regions of the temporal, frontal and parietal lobes involving both hemispheres. The left precuneus and left medial superior frontal gyrus were identified as hubs only in controls while the left cuneus and left paracentral lobule were

identified as hubs in the left mTLE group only. The right supplementary motor area and the right precuneus were hubs identified in both groups (Table 4.4, Figure 4.6).
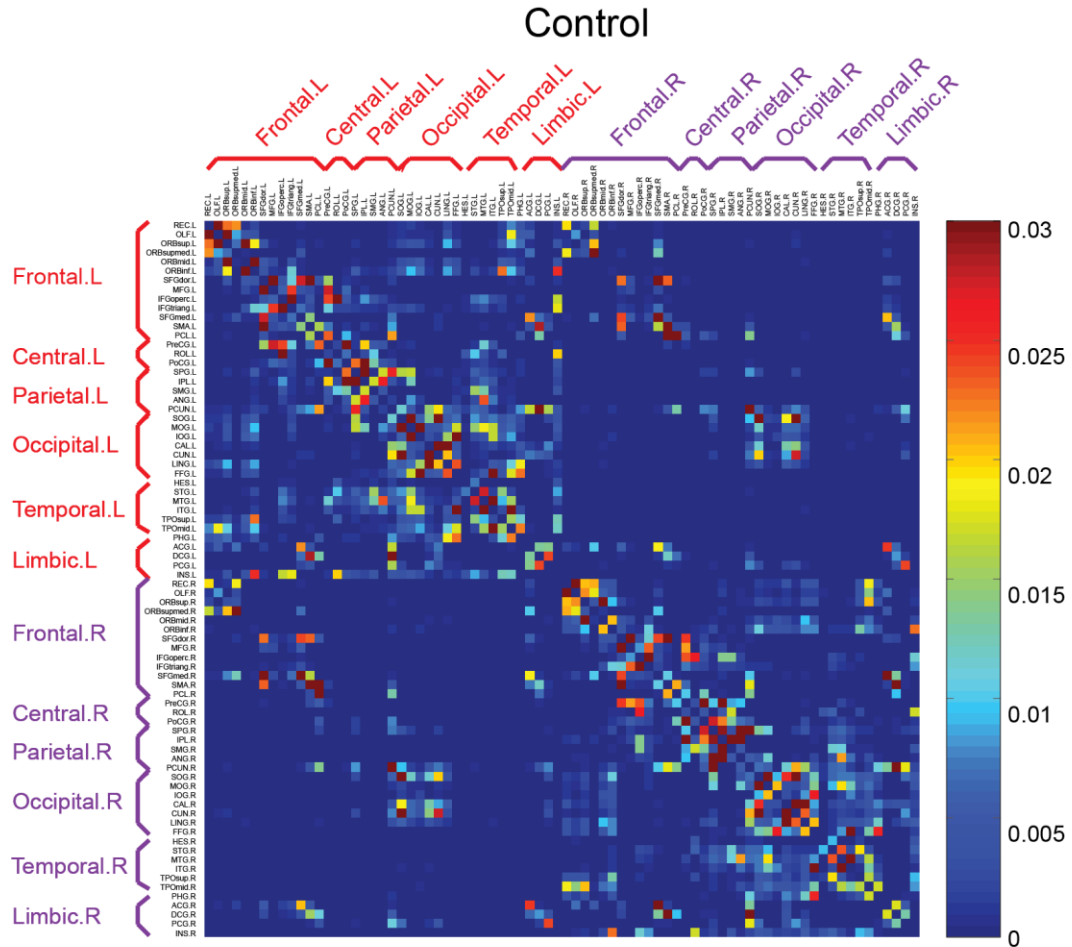
Figure 4.2 The mean cortical connection matrices of the 78 regions (39 left and 39 right) for controls. The bright diagonal strip revealed the dense connectivity among neighboring cortical regions.
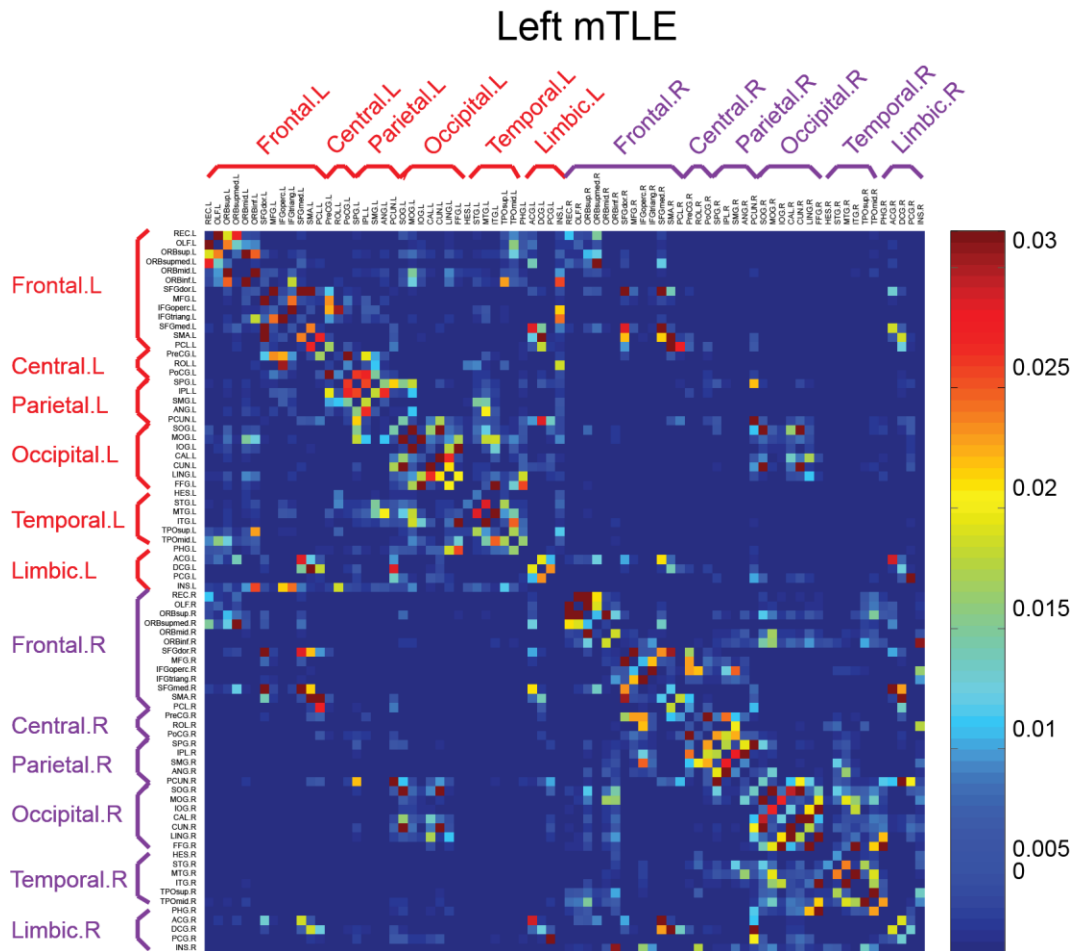
Figure 4.3 The mean cortical connection matrices of the 78 regions (39 left and 39 right) for left mTLE patients. The bright diagonal strip revealed the dense connectivity among neighboring cortical regions.

Table 4.2 Description of the global and regional network parameters examined in this study.

Graph theoretical metrics		Interpretation
S	Total strength	The overall strength of connections between regions in the network
C	Clustering coefficient	The probability that neighbors of a node are also connected
L	Characteristic path length	The network's ability for information propagation in parallel
γ	Normalized clustering coefficient	C/C_{rand}[1]. For a small world architecture[2], $\gamma \gg 1$
λ	Normalized shortest path length	L/L_{rand}. For a small world architecture, $\lambda \approx 1$
σ	Small-worldness	γ / λ. For a small world architecture, $\sigma \gg 1$
E_{glob}	Global efficiency	The effectiveness of the network transporting information in parallel
E_{loc}	Local efficiency	The measurement of network fault tolerance capacity[3]
E_{reg}	Regional efficiency	The efficiency of a particular cortical region in the network
Hubs	Pivotal nodes	Regions with E_{reg} higher than mean + std of all regions

[1]C_{rand} and L_{rand} are the clustering coefficient and characteristic path length of the random network which is generated by a random rewiring procedure with the number of nodes, edges, weight and degree distribution of the real network preserved. [2]A small world architecture has high clustering of a lattice (each node of the lattice is connected to its nearest neighbors) and short path length of a random graph (each node of the random graph is connected to a remote node). [3]Fault tolerance capacity is the network's resistance ability to function efficiently even after the weakening or removal of some nodes.

Table 4.3 Global network properties and between-group comparison results between left mTLE and controls.

	left mTLE	Controls	T	p
S	0.18 ± 0.06	0.19 ± 0.03	-0.83	0.42
C	0.38 ± 0.02	0.38 ± 0.01	1.14	0.26
L	1.06 ± 0.10	0.97 ± 0.05	3.70	0.0008*
E_{glob}	0.95 ± 0.09	1.03 ± 0.06	-3.51	0.001*
E_{loc}	1.32 ± 0.08	1.41 ± 0.05	-3.69	0.0008*
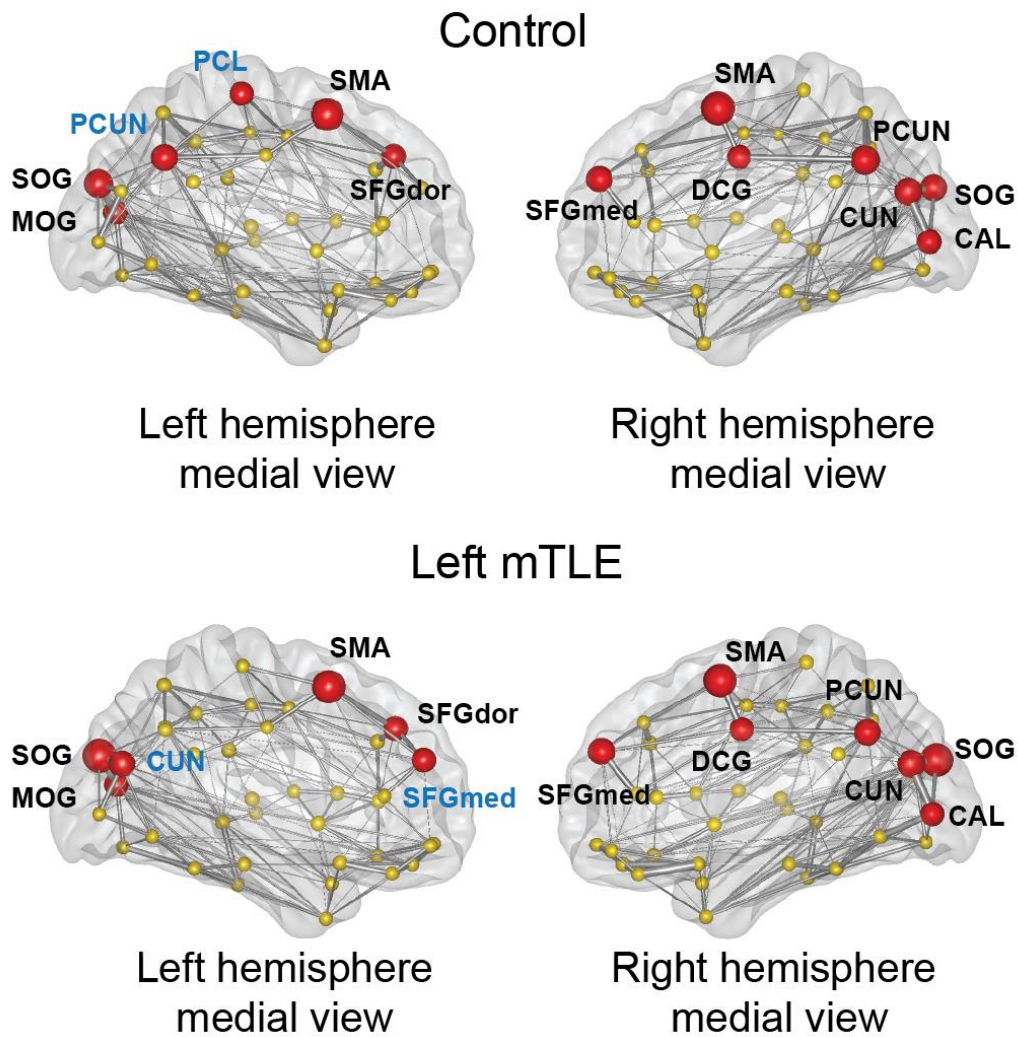
Figure 4.4 White matter network hubs in left mTLE patients and controls. Hubs were shown as red balls whose size was proportional to its regional efficiency value. Compared to controls, left mTLE patients lost the hubs at left precuneus (PCUN) and paracentral lobule (PCL) but gained hubs at left cuneus (CUN) and superior frontal medial part (SFGmed).
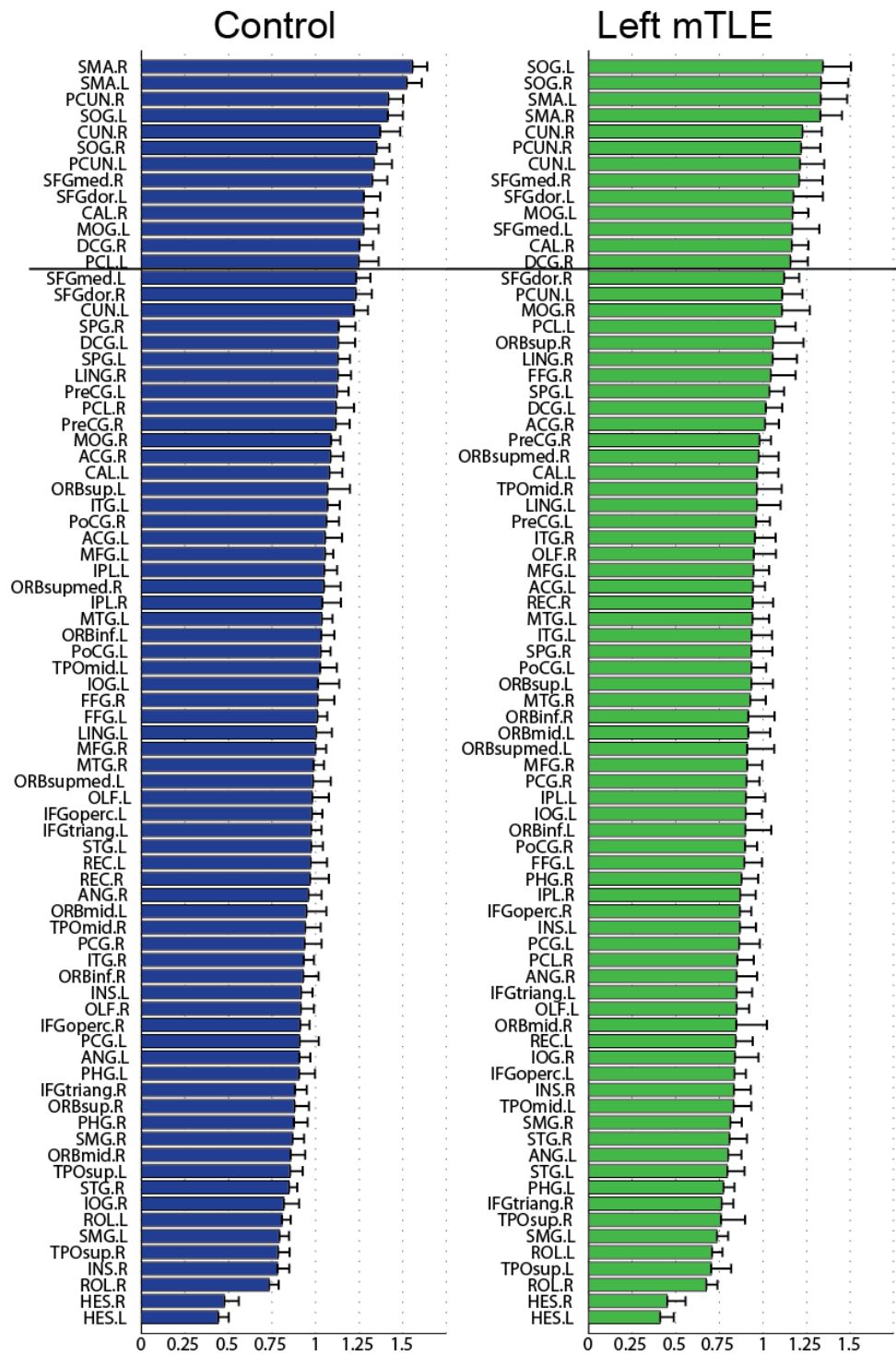
Figure 4.5 Regional efficiencies of the 78 cortical regions in left mTLE patients and controls. The mean regional efficiencies of the 78 cortical regions sorted in descending order. Nodes with regional efficiency one standard deviation greater than the group mean was defined as network hubs in each group, which were the regions above the cut-off bar.
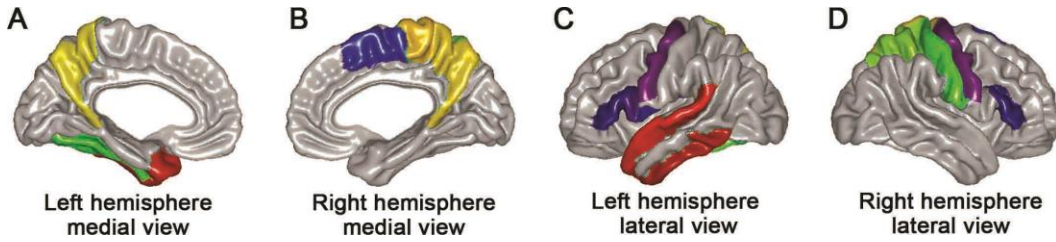
Figure 4.6 Seventeen regions with significantly reduced Ereg in left mTLE patients compared to controls. (A) Left hemisphere medial view: precuneus, temporal pole middle and superior temporal gyri, fusiform gyrus; (B) Right hemisphere medial view: paracentral lobule, supplementary motor area, precuneus; (C) Left hemisphere lateral view: precentral gyrus, inferior frontal gyrus opercular and triangular parts, Rolandic operculum, superior and inferior temporal gyri; (D) precentral and postcentral gyri, superior parietal gyrus, inferior frontal gyrus triangular part.

4.5.3 Clinical correlation

For left mTLE patients, no significant correlation was found between global properties L, E_{glob} and E_{loc} (which showed significant between-group difference) and clinical variables or neuropsychological score. However, there are some trends between E_{reg} of the left inferior frontal opercular gyrus and processing speed (r = 0.65, uncorrected p = 0.016) and between L and processing speed (r = -0.51, uncorrected p = 0.077) (Figure 4.7).

4.5.4 Reliability

The bootstrapped graph theoretical metrics across 10,000 randomizations were very close to the original values for controls and patients (Table 4.2, Supplementary Table 4.2). The significant between-group differences in L, E_{glob} and E_{loc} were verified by the boundary of the bootstrapped confidence intervals.

Table 4.4 Regions with significantly reduced regional efficiency Ereg in left mTLE patients. The cortical regions were categorized as primary sensorimotor, association and paralimbic regions (Mesulam, 1998).

	Region	Category	Hub	T	p
Temporal	Left Superior temporal gyrus	Association		-3.55	0.001
	Left Temporal pole: middle temporal	Paralimbic		-2.99	0.005
	Left Inferior temporal gyrus	Association		-2.62	0.013
	Left Fusiform gyrus	Association		-2.6	0.014
	Left Temporal pole: superior temporal	Paralimbic		-2.56	0.015
Frontal lobe	Right Paracentral lobule	Association		-3.58	0.001
	Left Inferior frontal gyrus, opercular part	Association		-3.4	0.002
	Left Precentral gyrus	Primary		-3.36	0.002
	Right Supplementary motor area	Association	Yes	-3.21	0.003
	Right Inferior frontal gyrus, triangular part	Association		-2.54	0.016
	Right Precentral gyrus	Primary		-2.48	0.018
	Left Inferior frontal gyrus, triangular part	Association		-2.42	0.021
Frontoparietal	Left Rolandic operculum	Association		-2.6	0.014
Parietal lobe	Right Postcentral gyrus	Primary		-3.19	0.003
	Right Precuneus	Association	Yes	-2.85	0.007
	Left Precuneus	Association	Yes	-2.82	0.008
	Right Superior parietal gyrus	Association		-2.72	0.01
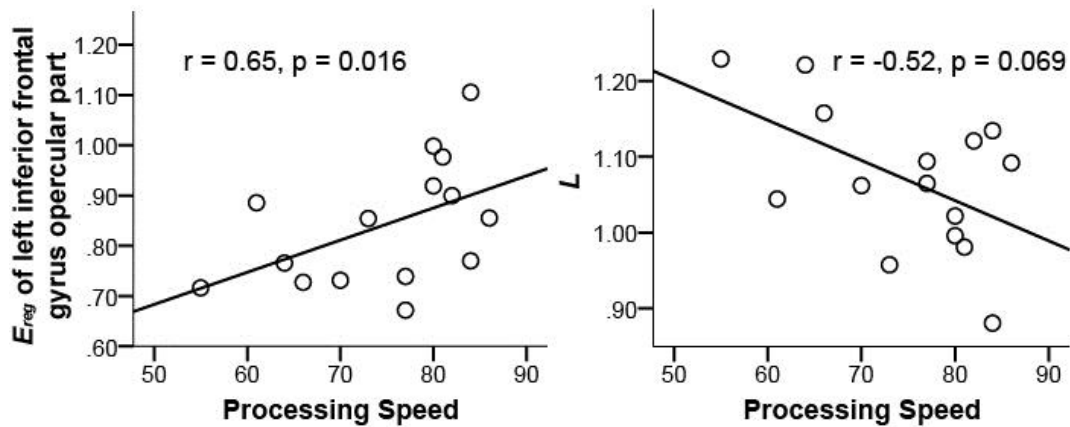
Figure 4.7 Trend correlation between processing speed and two graph theoretical metrics in left mTLE patients.

4.6   Discussion

In the current study, graph theoretical analysis provided direct evidence of large scale network disruption in temporal lobe epilepsy with left mesial temporal sclerosis. These patients demonstrated impaired global (E_{glob}) and local (E_{loc}) communication efficiency and reduced regional efficiency (E_{reg}) at a number of cortical regions of the temporal, frontal and parietal lobes. Network roles of highly connected heteromodal regions (hubs) such as left precuneus were altered in mTLE patients, indicating a reorganization of the underlying brain anatomical network. Albeit a type of focal epilepsy with a presumed well circumscribed seizure onset zone, temporal lobe epilepsy demonstrated changes in the brain network both locally and globally.

4.6.1 Disrupted global properties in left mTLE

Both patient and control groups demonstrate small-world topological organization, indicating a balance between global integration and local specification of information transfer in the complex brain network. Small-world properties were first demonstrated in functional (Salvador et al., 2005) and anatomical networks (He et al., 2007) in the human brain with these properties being confirmed in both normal participants with a wide age range and patients with neurological conditions such as Alzheimer's disease (Lo et al., 2010), multiple sclerosis (Shu et al., 2011) and schizophrenia (Bassett et al., 2008). Although the small-world configuration was preserved in the left mTLE patients, increased L and decreased Eglob and Eloc were observed as compared to controls (Table 4.3). Both E_{glob} and E_{loc} are metrics derived from the inverse *L*. A relatively short *L* reflects efficient information transfer between distant regions that is believed to constitute the basis of cognitive processes (Sporns and Zwi, 2004). In contrast, an increase of *L* reflects the disturbance of the long-range connections and thus decreased global efficiency in information communication. The left mTLE patients also showed decreased E_{loc}, suggestive of impaired fault tolerant capacity of the network resulting from a loss of effective compensatory circuitry. These global changes indicate a suboptimal, more regular small-world configuration in left mTLE.

These findings add a new perspective to the literature about the anatomical network of temporal lobe epilepsy where the whole brain physical white matter connections were reconstructed and abstracted for topological evaluation. Previous graph theoretical

113

analysis of cortical thickness, EEG and functional imaging has shown diverging results. A recent study based on cortical thickness correlation also found a more regular network configuration in 63 left and 59 right temporal lobe epilepsy (Bernhardt et al., 2011). Consistent with our study a trend towards increased L was observed, however, while we found no difference in C between patients and controls, Bernhardt et al. demonstrated increased C (Bernhardt et al., 2011). Along with the difference in data analyzed, (DTI vs cortical thickness), the two different network construction approaches may also contribute to the discrepancy in findings. The previous study chose to binarize the network matrix to make each connection either exist or not exist (Bernhardt et al., 2011). This approach would be expected to yield different results from that of a weighted network where the strength information of each connection is preserved and taken into account. A graph theoretical analysis of interictal resting-state fMRI reported decreased clustering coefficient C and shortest path length L in 18 temporal lobe epilepsy patients with bilateral mesial temporal sclerosis (Liao et al., 2010). As this was an fMRI study, it is again not surprising that different results were observed as compared to our DTI study and the previously discussed cortical thickness analysis. Another possible explanation for the difference in the Liao et al. study relates to the study population. While we and Bernhardt et al. studied patients with unilateral mTLE, Liao et al. restricted their analysis to patients with bilateral MTS who have been documented to have more extensive (bilateral mesial temporal) abnormalities and therefore could also have different network properties as compared to patients with unilateral MTS. The functional network configuration derived from EEG recordings showed dependency on the state of the seizure. One study showed a more regular network structure at the interictal stage (Horstmann et al., 2010) while others observed a transition of the network from a random configuration towards a more regular configuration at seizure onset and during seizure (Ponten et al., 2007, 2009; Kramer et al., 2008; Schindler et al., 2008; Wilke et al., 2011). A recent graph theoretical analysis based on single photon emission tomography further examined the region-specific change during seizures where the epileptogenic regions including medial temporal and adjacent subcortical and limbic regions showed increased clustering and nodal efficiency after seizure onset while the remaining cortex exhibited reduced connectivity. The overall whole brain network showed reduced clustering coefficient compared to the inter-ictal state (Sequeira et al., 2013). The different modalities used in network construction may contribute to the discrepancy between these

114

findings. Despite the differences in observations, however, graph theoretical analysis based on both structural and functional datasets has consistently demonstrated differences in the brain network in TLE.

4.6.2 Disrupted regional properties in left mTLE

Hubs play pivotal roles in information communication within the network (Achard and Bullmore, 2007). The majority of hubs in both patients and controls were association areas that share connections with other brain regions to integrate information for higher level mental activities. Areas such as precuneus and superior frontal regions were also identified as hubs in previous white matter network studies (Lo et al., 2010; Shu et al., 2011). The precuneus area has drawn a lot of attention in recent years following the revelation of its important role in a wide spectrum of highly integrated tasks such as visuo-spatial imagery and episodic memory retrieval (Cavanna and Trimble, 2006). It has the most complex columnar cortical organization and is among the last regions to myelinate (Goldman-Rakic, 1987). In our study, the left mTLE patients have shifted the left precuneus gyrus hub towards a more posterior location (left cuneus gyrus) compared to controls (Figure 4.4 and Figure 4.5). It has been demonstrated that TLE patients had decreased functional connectivity between the precuneus and the hippocampus (Pittau et al., 2012), mesial temporal lobe (Liao et al., 2011), and the rest of the brain (Liao et al., 2010). Studies also revealed local gray matter atrophy (Coan et al., 2009; Mueller et al., 2009) and underlying white matter impairment in the cingulum bundle which contains fibers connecting regions of the frontal lobe with the precuneus. Thus, we suspect that our findings of reduced hub role for left precuneus in left mTLE patients can be attributed to the reduced functional connectivity and structural abnormalities of the region.

Left mTLE patients further showed decreased regional efficiency in a number of cortical regions (**Error! Reference source not found.**) in the temporal, frontal and parietal lobes. ll temporal regions were located on the same side of the mesial temporal sclerosis, indicating a decreased communication efficiency of the temporal lobe within the whole brain network. Frontal and parietal lobes were bilaterally involved and bilateral precuneus and right supplementary motor area were identified as hubs in the corresponding control groups. There is converging literature demonstrating the widespread nature of structural abnormalities in TLE (Keller and Roberts, 2008).

Reduced gray matter volume/concentration was also reported in the bilateral frontal and parietal lobes of TLE patients (Keller and Roberts, 2008). White matter abnormalities were observed in limbic (fornix and cingulum), fronto-temporal (uncinate fasciculus), temporal-occipital (inferior longitudinal fasciculus, superior longitudinal fasciculus), fronto-occipital (inferior fronto-occipital fasciculus) and projection tract (cerebrospinal tracts) (Otte et al., 2012). These structural changes could have a profound impact on the regional as well as global properties of the anatomical brain network of TLE.

4.6.3 Regional efficiency vs. clinical and neuropsychological variables

No significant correlation between disease duration, age of seizure onset and network metrics was observed, arguing against the observed changes in network properties being a consequence of seizures. Given the relatively early age of seizure onset for these patients (Table 4.1), it raises the possibility that the network reorganized with seizures, i.e. "firing and wiring together", during the critical childhood development period. One other possibility is that large scale network disruption was present prior to the onset of epilepsy and may have had a role in the pathogenesis of TLE.

Although no significant correlation was found between graph theoretical metrics and cognitive performance, the interesting trend observed between processing speed and L, γ and E_{reg} in the inferior frontal gyrus opercular part in left mTLE patients suggests that the network parameters could be potential predictors of cognitive function. Indeed, correlations between cognitive function and graph theoretical metrics have been observed before in both normal intelligent population (Van den Heuvel et al., 2009) and people with neurological disorders (Lo et al., 2010; Shu et al., 2011). A larger sample size is warranted to further explore the relationship in epilepsy patients.

4.6.4 Methodological issue

In this study, the DTI sequence was acquired with six diffusion directions and eight repetitions. Although the data quality was high (b0 SNR = 56), the low diffusion direction sampling scheme limited our white matter construction method to deterministic tractography. Our group has previously published reproducible network properties using similar data acquisition scheme (Gong et al., 2008b). Recent studies adopted probabilistic

116

tractography method to ameliorate "crossing fiber" issue (Iturria-Medina et al., 2008; Gong et al., 2009). It may provide more complete information of the brain white matter network. To minimize random connections between two cortical regions, a fiber number threshold of three was set to construct the brain network. To examine the influence of the threshold, we also tested a range of thresholds from three to ten and the results were stable. Similar to our previous study, the subcortical regions in the AAL template were not considered in white matter network construction. Given the known low FA in these structures (Lebel et al., 2008), there is a concern that fiber propagation would yield erroneous trajectory when approaching these areas.

4.7 Conclusion

In this study, the white matter structural network properties of temporal lobe epilepsy with left mesial temporal sclerosis were examined. Patients exhibited decreased global and local efficiencies and widespread reduction of regional efficiency in temporal, frontal and parietal areas. Shift of important hubs, especially the left precuneus gyrus suggested a reorganization of the brain network. Our results demonstrated extensive network disruption in left mTLE patients, consistent with the widespread grey and white matter structural abnormalities and altered functional connectivity previously found in these patients. The findings support that mTLE is a network disorder.

Supplementary Table 4.1 Seventy eight cortical regions of interest defined by the AAL template in the study (39 on each hemisphere).

Index	Region	Abbreviation	Index	Regions	Abbreviation
(1 , 40)	Gyrus Rectus	REC	(21 , 60)	Precuneus	PCUN
(2 , 41)	Olfactory Cortex	OLF	(22 , 61)	Superior occipital gyrus	SOG
(3 , 42)	Superior frontal gyrus, orbital part	ORBsup	(23 , 62)	Middle occipital gyrus	MOG
(4 , 43)	Superior frontal gyrus, medial orbital	ORBsupmed	(24 , 63)	Inferior occipital gyrus	IOG
(5 , 44)	Middle frontal gyrus orbital part	ORBmid	(25 , 64)	Calcarine fissure and surrounding cortex	CAL
(6 , 45)	Inferior frontal gyrus, orbital part	ORBinf	(26 , 65)	Cuneus	CUN
(7 , 46)	Superior frontal gyrus, dorsolateral	SFGdor	(27 , 66)	Lingual gyrus	LING
(8 , 47)	Middle frontal gyrus	MFG	(28 , 67)	Fusiform gyrus	FFG
(9 , 48)	Inferior frontal gyrus, opercular part	IFGoperc	(29 , 68)	Heschl gyrus	HES
(10 , 49)	Inferior frontal gyrus, triangular part	IFGtriang	(30 , 69)	Superior temporal gyrus	STG
(11 , 50)	Superior frontal gyrus, medial	SFGmed	(31 , 70)	Middle temporal gyrus	MTG
(12 , 51)	Supplementary motor area	SMA	(32 , 71)	Inferior temporal	ITG

				gyrus	
(13 , 52)	Paracentral lobule	PCL	(33 , 72)	Temporal pole: superior temporal gyrus	TPOsup
(14 , 53)	Precentral gyrus	PreCG	(34 , 73)	Temporal pole: middle temporal gyrus	TPOmid
(15 , 54)	Rolandic operculum	ROL	(35 , 74)	Parahippocampal gyrus	PHG
(16 , 55)	Postcentral gyrus	PoCG	(36 , 75)	Anterior cingulate and paracingulate gyrus	ACG
(17 , 56)	Superior parietal gyrus	SPG	(37 , 76)	Median cingulate and paracingulate gyrus	DCG
(18 , 57)	Inferior parietal, but supramarginal and angular gyri	IPL	(38 , 77)	Posterior cingulate gyrus	PCG
(19 , 58)	Supramarginal gyrus	SMG	(39 , 78)	Insula	INS
(20 , 59)	Angular gyrus	ANG			

Supplementary Table 4.2 Reliability of the graph theoretical metrics queried in left mTLE patients and controls. The mean and 95% confidence interval of the network parameters derived from 10000 bootstraps for each group.

	left mTLE (n = 16)	Controls (n = 21)
S	0.18 (0.16-0.21)	0.19 (0.18-0.20)
C	0.38 (0.38-0.39)	0.38 (0.37-0.38)
L	1.06 (1.02-1.11)	0.97 (0.95-0.99)
E_{glob}	0.95 (0.91-0.99)	1.03 (1.01-1.06)
E_{loc}	1.32 (1.29-1.37)	1.41 (1.39-1.43)

Chapter 5   Long term white matter change in temporal lobe epilepsy[5]

5.1   Introduction

Refractory temporal lobe epilepsy (TLE), especially those with mesial temporal sclerosis (TLE+MTS), has shown evidence of progressive damage in clinical manifestation (Kwan and Brodie, 2000), cognitive impairment (Helmstaedter et al., 2003; Hermann et al., 2006) and experimental model (Pitkänen et al., 2002). The structural substrates that are associated with the progressive changes have been the research focus for the past decade. Two methods were used to investigate the progressive nature of the disorder, either correlation analysis of gray matter volume/concentration and clinical parameters of TLE patients or practically more difficult longitudinal design to track the structural change over time. Several studies using correlation analysis have found negative correlation between duration of epilepsy and gray matter volume reduction in hippocampus, amygdala, thalamus and other extratemporal alterations within and beyond the temporal lobe (Tasch et al., 1999; Salmenperä et al., 2001; Keller et al., 2002b; Seidenberg et al., 2005; Bonilha et al., 2006; Bernhardt et al., 2009a). However, some studies did not observe this correlation (Cendes et al., 1993) or correlation between duration of epilepsy and the extra-temporal abnormalities (Moran et al., 2001). While correlation analysis is easy to perform based on a cross-sectional design, it is susceptible to outliers and small sample size. Longitudinal analysis, on the other hand, is powerful to show the actual changes happened on the exact same subjects over a period of time. Previous longitudinal studies have demonstrated progressive volume reduction in the ipsilateral hippocampus (Briellmann et al., 2002) and widespread neocortical regions (Fuerst et al., 2003; Liu et al., 2003b; Bernhardt et al., 2009b; Coan et al., 2009) within a mean of 3.5 years.

While there is increasing evidence of widespread white matter abnormalities in TLE patients revealed by diffusion tensor imaging (DTI) (Otte et al., 2012) , especially those with TLE+MTS (Concha et al., 2009; Liu et al., 2012), it is unclear whether these changes have a progressive nature similar to gray matter abnormalities. Correlation

---

[5] This are the preliminary results from an ongoing project that has not been published.

analyses provide some evidence of association between degraded white matter integrity and earlier age of seizure onset (Lin et al., 2008; Jeffrey et al., 2010; Kemmotsu et al., 2011) or longer duration of epilepsy (Govindan et al., 2008; Meng et al., 2010; Keller et al., 2012) while some did not observe the correlation (Liu et al., 2012). As far as we know, long term longitudinal study has not been carried out for the white matter change in TLE. Repeated DTI scans have been performed on TLE patients who underwent surgical resection where our group previously reported signs of Wallerian degeneration in the fornix and cingulum ipsilateral to the resected temporal lobe (Concha et al., 2007). Interestingly, the pre-operative abnormalities in the contralateral fornix, cingulum, external capsules and the genu of the corpus callosum sustained after one year follow up (Concha et al., 2007). Later studies further identified Wallerian degeneration in other ipsilateral tracts such as uncinate fasciculus and inferior longitudinal 3-6 months post-surgery (McDonald et al., 2010; Yogarajah et al., 2010; Nguyen et al., 2011; Faber et al., 2013). Interestingly, Yogarajah et al observed an increase of fractional anisotropy (FA) in the ipsilateral external capsule, posterior limb of the internal capsule, and corona radiata 4.5 months after surgery (Yogarajah et al., 2010). The extent of FA increase was correlated with diminished decline of postoperative verbal fluency and naming test scores, suggesting post-injury rehabilitation (Yogarajah et al., 2010). Faber et al also observed diffuse FA reduction of ipsilateral white matter and some FA increase in the left corticospinal tract (Faber et al., 2013). However, it is of note that these two studies yielded results from direct comparison between the post- and pre-surgical images of the patients without including repeated scans for healthy control, which raises the possibility that the findings may suffer from drifting scan quality. Nevertheless, these findings induce the question whether such white matter changes could be seen in a longer period after surgery.

The purpose of this study is to examine the longitudinal white matter change in temporal lobe epilepsy patients with and without surgery over a mean of 6.5 years.

5.2 Materials and Methods

5.2.1 Subjects

Fifteen TLE patients who underwent either anterior temporal lobectomy or selective amygdalohippocampectomy, seven TLE patients without any surgery and nine controls

were included in the study (Table 5.1). Each participant was scanned twice on the same Siemens 1.5T scanner over an average of 6.5 years. The operated group was composed of seven left TLE+MTS, five right TLE+MTS, one left nonlesional TLE and two right nonlesional TLE. The unoperated group was composed of four bilateral nonlesional TLE, one left TLE+MTS and one right TLE+MTS. The 1st scan of the TLE+MTS and nonlesional TLE patients was acquired before surgery and the 2nd scan was acquired at least 2.4 years after surgery. There are no significant differences of age at the 1st scan or time interval between the 1st and 2nd scans.

Table 5.1 Subjects information.

Groups	N	Duration (years)	Age at the 1st scan (years)	Time between 1st and 2nd Scan (months)	Time between surgery and 2nd scan (months)	Seizure Free at 2nd scan
Operated	15	16 ± 12 $(4 - 43)$	35 ± 9 $(19 - 46)$	78 ± 25 $(34 - 104)$	68 ± 25 $(29 - 99)$	11 seizure free
Unoperated	7	26 ± 16 $(6 - 45)$	37 ± 10 $(17 - 46)$	69 ± 8 $(61 - 85)$	-	4 seizure free
Controls	9	-	38 ± 13 $(23 - 58)$	83 ± 26 $(43 - 109)$	-	-

5.2.2 Image acquisition

All participants were scanned by the same 1.5T Siemens Sonata scanner (Erlangen, Germany) twice. MPRAGE provides high resolution 3D T1-weighted images that were acquired with the following parameters: 1 mm slice thickness with no inter-slice gap, 144 axial slices, TR = 1890 ms, TE = 4.38 ms, TI = 1100 ms, flip angle = 15°, NEX = 1, acquisition matrix = 256×192 (interpolated to 512×384), FOV = 256 mm $\times$ 192 mm, voxel dimension $1 \times 1 \times 1$ mm^3 (interpolated to $0.5 \times 0.5 \times 1$ mm^3), scan time = 6:03 min. Standard DTI used a dual spin-echo, single shot echo planar imaging sequence with 52 axial slices, 2 mm slice thickness with no inter-slice gap, TR = 10 s, TE = 88 ms, six diffusion directions with b = 1000 s/mm^2, NEX = 8, acquisition matrix = 128×128 (interpolated to 256×256), FOV = 256 mm $\times$ 256 mm, voxel dimension $2 \times 2 \times 2$ mm^3 (interpolated to $1 \times 1 \times 2$ mm^3), scan time = 9 min 30 sec.

5.2.3 Image processing

5.2.3.1 Gray matter volumes

An estimate of the volume of cortical gray matter, white matter, hippocampus and amygdala was provided by FreeSurfer (v5.1, https://surfer.nmr.mgh.harvard.edu/) based on the transformation of each subject's brain into Talairach space (Fischl et al., 2002, 2004).

5.2.3.2 White matter measurements

Motion and eddy current corrections for all DTI images were performed using FSL (v5.0, FMRIB, Oxford, UK). Tensor calculation was performed for each dataset in DTI-TK (Zhang et al., 2007). The 2nd scan was registered to the 1st scan in DTI-TK using a top-performing tensor based registration method (Wang et al., 2011).

To create a common surgical cavity map, each 2nd mean diffusivity (MD) map was thresholded by 2×10^{-3} mm^2/s to reveal the cavity and then mapped into a common space depicted by the IXI adult template using DTI-TK. The registered surgical cavity map was overlaid onto each other and the largest empty space was outlined to make sure the most extensive surgical cavity is included. This common cavity map was deformed back to each DTI dataset (both 1st and 2nd scan) and used to exclude that area from measurements.

The tensor images of the 1st scan were then loaded in DTIStudio (v3.03, Dr. Hangyi Jiang and Susumu Mori, John Hopkins University), in which 12 major white matter tracts including the crus of fornix (Fx), dorsal cingulum (dCg), parahippocampal cingulum (pCg), genu/body/splenium of corpus callosum (gCC/bCC/sCC), tapetum, inferior fronto-occipital fasciculi (IFO), inferior/superior longitudinal fasciculi (ILF/SLF), uncinate fasciculi (UF), and anterior limb of the internal capsule (ALIC) were identified with tractography here. The FA threshold was set to 0.25 and the angular threshold to 60° for Fx, UF and SLF and 30° for all other tracts. ROIs were manually placed using a two ROI approach for each tract based on the methods and anatomy described before (Wakana et al., 2007; Malykhin et al., 2008). The visualization of the tracts can be found in Figure 3.1.

The masks of the 12 tracts of the 1st scan were deformed back onto the 2nd scan using the inverse deformation derived in DTI-TK, with the nearest interpolation method to obtain tract masks for the 2nd time point.

Two additional structures, internal capsule (IC) and external capsule (EC), were examined using regions-of-interest (ROIs) to test whether the ipsilateral IC and EC were strengthened after surgery in the operated patients as observed previously by another group (Yogarajah et al., 2010). To maintain the accuracy of the location, ROIs of IC and EC were manually drawn on both 1st and 2nd scans for each hemisphere.

FA was obtained for each tract and ROI at each time point by overlaying the tract mask on FA maps with the exclusion of the surgical cavity, and averaging all the voxels within each hemisphere to generate a single value per side of a tract.

5.2.4 Statistical analysis

Statistical analyses were administered using IBM SPSS v20. The structure ipsilateral and contralateral to the side of the seizure focus was quantified separately. For controls and bilateral TLE patients, left side corresponded to the ipsilateral side and right side corresponded to the contralateral side for comparison between groups.

To visually examine changes over time, the FA of white matter structures and the volume of cortical and subcortical gray matter for each subject were plotted as a function of age. To examine if any significant change happened between the 1st and 2nd scan for the structures in each group, the FA/gray matter volume at the 1st time point was subtracted from the 2nd time point to calculate the difference ($\Delta FA/\Delta MD/\Delta V$) and one sample T test was used to test $\Delta FA/\Delta MD/\Delta V$ against zero. To test whether the change in the operated and unoperated patients were greater than that of the controls, analysis of variance with covariate (ANCOVA) was used to compare $\Delta FA/\Delta MD/\Delta V$ between groups with time interval of the 1st and 2nd scans included as a covariate. Post-hoc analysis was performed to test difference of $\Delta FA/\Delta MD/\Delta V$ between any pair of the three groups.

5.3 Results

The change of gray matter volume, FA and MD as a function of age were shown in Figure 5.1, Figure 5.2, Figure 5.3 and Figure 5.4. Generally, the cortical gray matter

volume decreased with age (Figure 5.1); the FA decreased and the MD increased with age for white matter (Figure 5.2 and Figure 5.3) except IC and EC (Figure 5.4). IC and EC showed the reversed pattern where FA increased and MD reduced with age in most subjects (Figure 5.4). The operated TLE patients showed dramatic gray matter volume reduction on the operated side due to surgical resection and significant FA decrease and MD increase of the white matter tracts that were directly resected (Fx, pCg) during surgery or closely connected to the resection site (IFO, ILF).

One sample T test showed significant change of FA, MD and gray matter volume from the 1st to 2nd time point in some areas (Table 5.2). The cortical gray matter reduced for all three groups. In addition, controls showed volume reduction of the left/ipsilateral hippocampus. The operated patients presented volume reduction of bilateral hippocampus, ipsilateral white matter and amygdala. The change of FA and MD of the white matter structures showed different patterns for each group. Controls showed bilateral FA reduction of UF, contralateral FA reduction of ILF and IFO, ipsilateral FA reduction of gCC, and contralateral FA increase of IC from the 1st to 2nd time point. The operated TLE patients showed bilateral FA reduction of the Fx, UF, ILF, IFO, ipsilateral FA reduction of pCg and ALIC, and FA increase of the ipsilateral IC and EC. The unoperated group showed bilateral MD increase of dCg and FA increase of IC.

ANCOVA revealed greater change in the operated patients relative to controls and the unoperated patients. The operated patients presented greater volume reduction of the ipsilateral cortical gray matter, white matter, hippocampus and amygdala, as well as the contralateral hippocampus, than controls and the unoperated group (Figure 5.5). Among the 14 white matter structures measured, the FA of the ipsilateral Fx, pCg and IFO showed significant reduction in the operated group than the unoperated TLE and controls over time (Figure 5.6). The operated patients also showed greater FA reduction in the ipsilateral ILF more than that of the unoperated TLE patients. The MD showed similar pattern where the operated group showed greater MD increase in Fx and pCg than the other two groups and in ILF than the unoperated group (Figure 5.7). No significant greater-than-controls inter-scan change was found in any contralateral tract of the operated group. No such change was seen in any tract of the unoperated patients compared to controls.

126
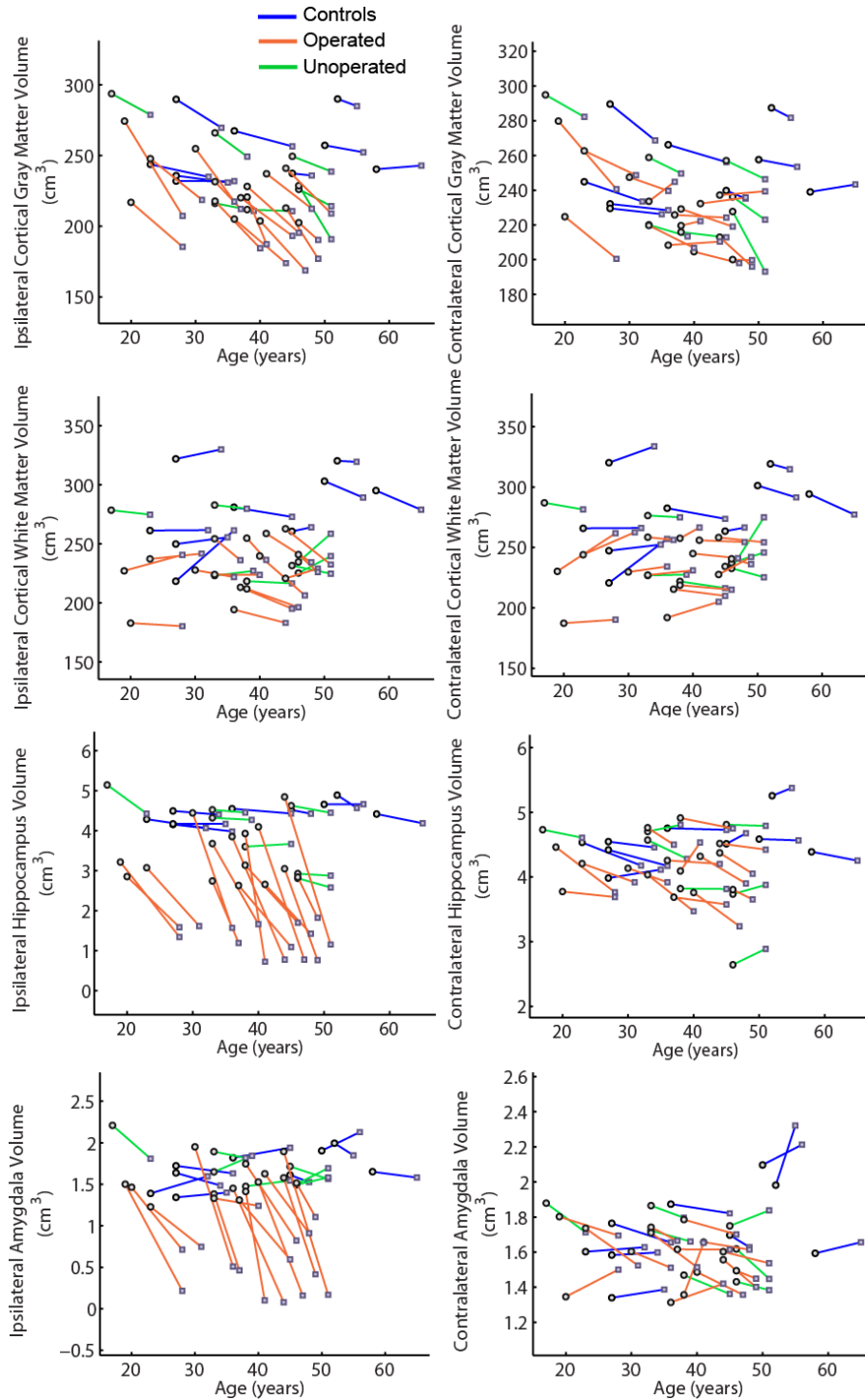
Figure 5.1 The volume change of cortical gray matter, white matter, hippocampus and amygadala for controls, operated and unoperated TLE patients plotted as a function of age. All three groups showed decreased cortical gray matter volume over time which was not apparent for the volume of white matter, hippocampus or amygdala. The operated patients also showed dramatic gray matter volume reduction on the operated side due to surgical resection.
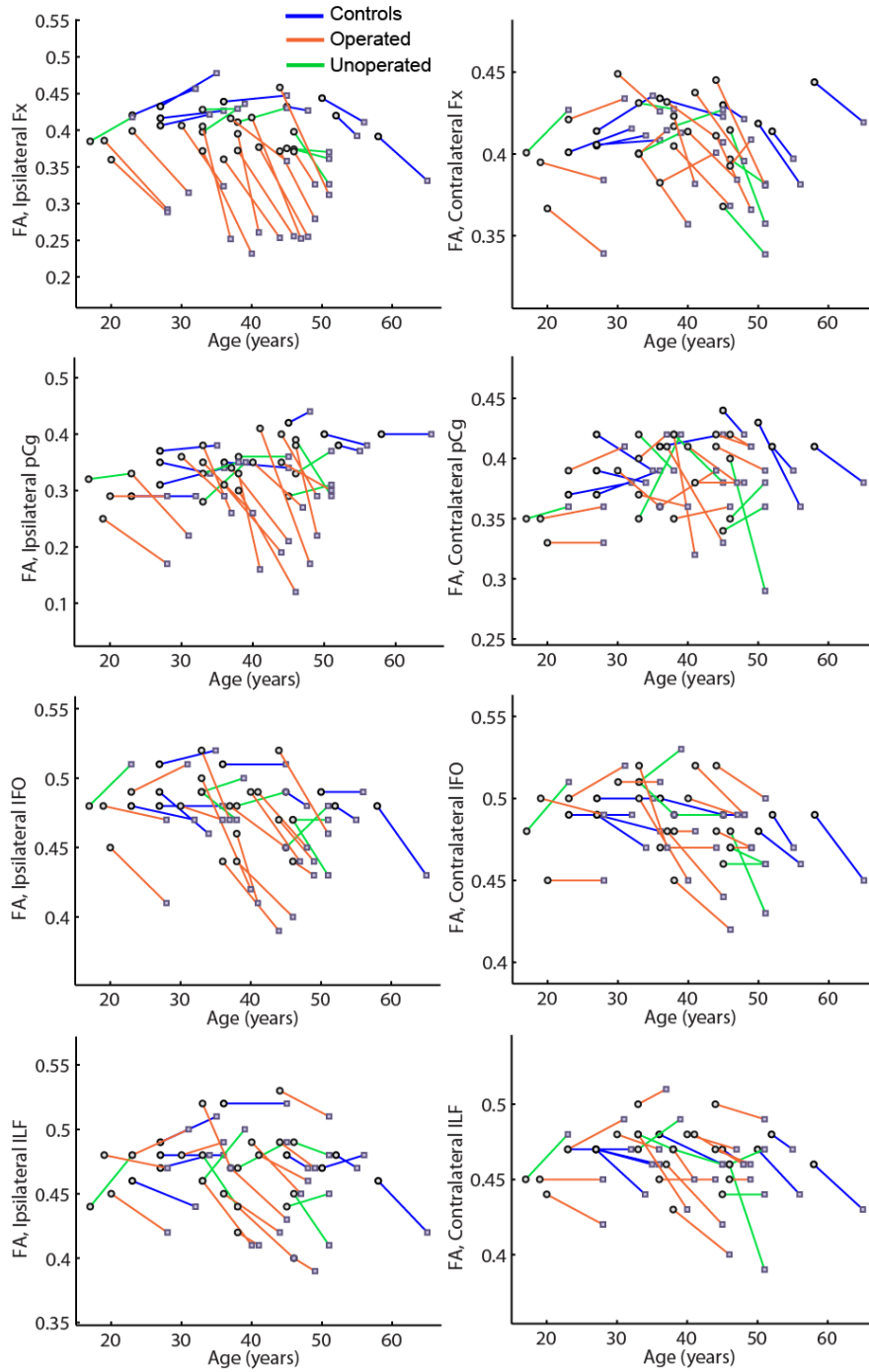
Figure 5.2 The FA change of four white matter tracts (Fx, pCg, IFO and ILF) for controls, operated and unoperated TLE patients plotted as a function of age. Overall, the FA decreased as age increased. The operated patients showed dramatic FA decrease on the operated side.

128
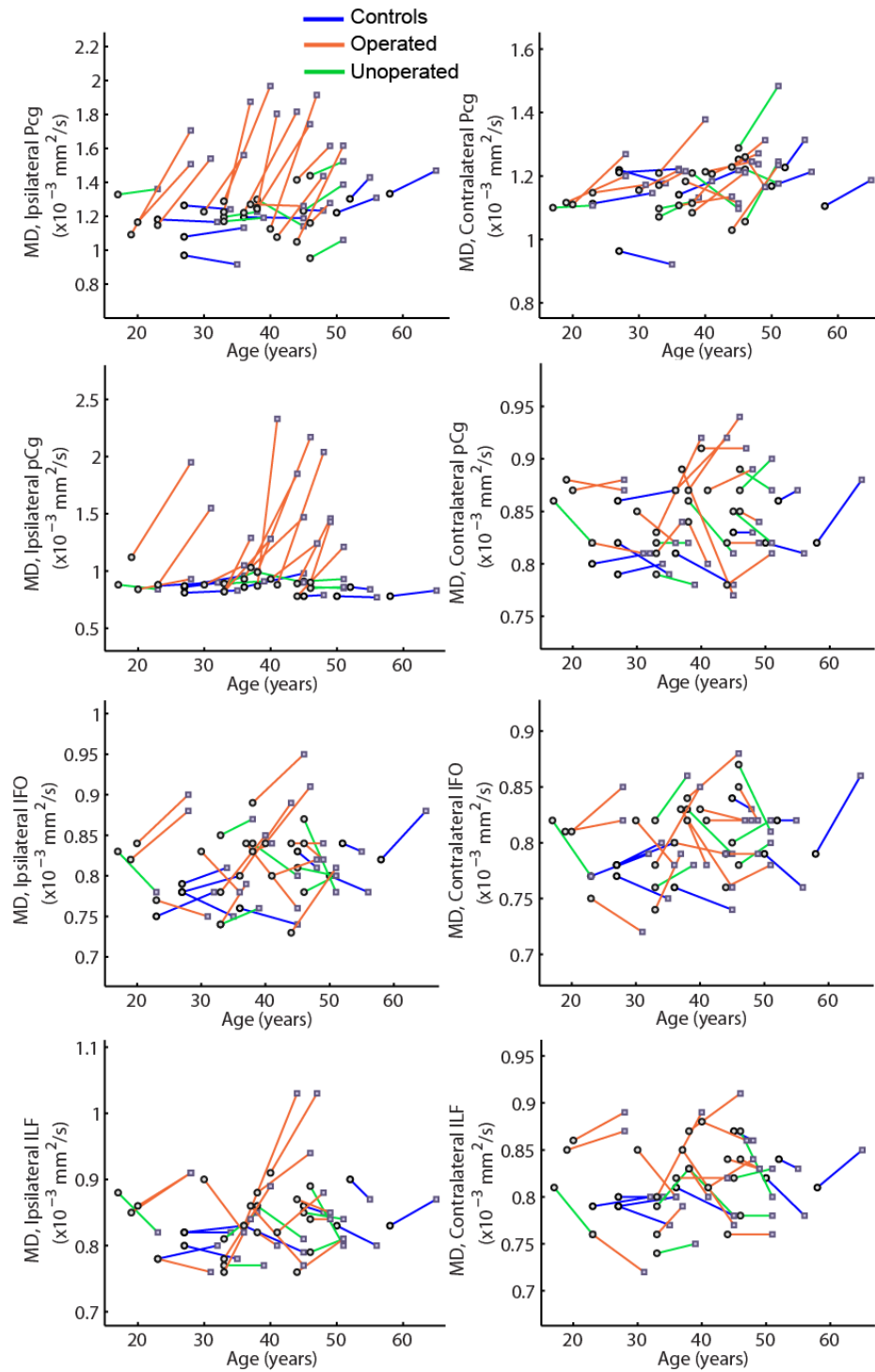
Figure 5.3 The MD change of four white matter tracts (Fx, pCg, IFO and ILF) for controls, operated and unoperated TLE patients plotted as a function of age. Overall, the MD increased with age. The operated patients showed dramatic MD increase on the operated side.
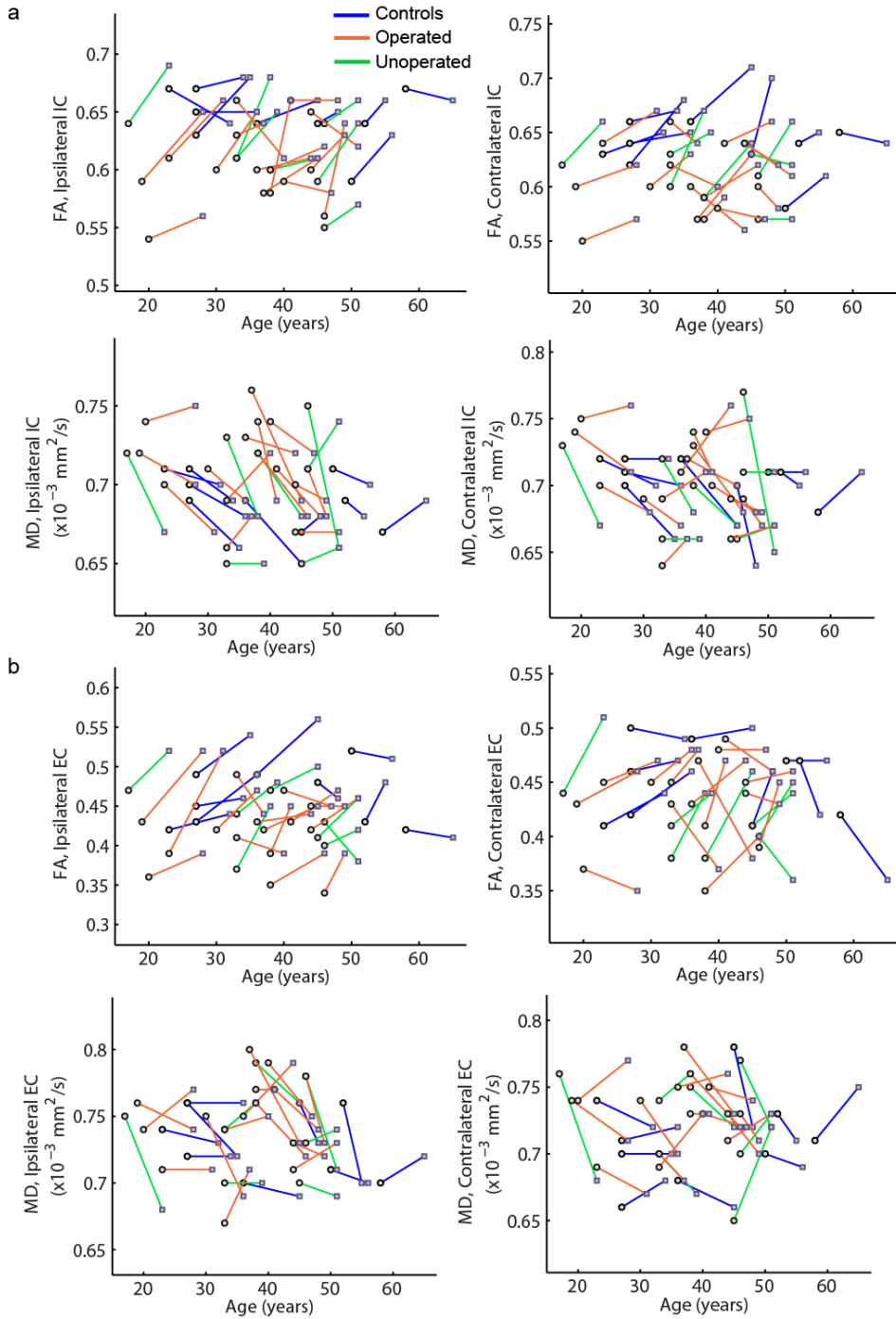
Figure 5.4 a) The FA and MD of internal capsule (IC) for all subjects plotted as a function of age. b) The FA and MD of external capsule (EC) for all subjects plotted as a function of age. Both IC and EC showed increased FA and decreased MD over time.

Table 5.2 The p values of the one sample T test for each structure of the three groups showing significant changes (in bold) from 1st to 2st time point.

		Ipsilateral p values			Contralateral p values		
		Control	Operated	Unoperated	Control	Operated	Unoperated
Cortical gray matter	ΔV↓	**0.03**	**<0.001**	**0.02**	**0.02**	**0.04**	**0.02**
White matter	ΔV↓	0.69	**0.01**	0.40	0.71	0.10	0.54
Hippo-campus	ΔV↓	**0.005**	**<0.001**	0.12	0.41	**0.005**	0.92
Amyg-dala	ΔV↓	0.89	**<0.001**	0.89	0.37	0.24	0.06
Fx	ΔFA↓	0.92	**<0.001**	0.98	0.38	**0.01**	0.48
	ΔMD↑	0.18	**<0.001**	0.34	0.16	**0.01**	0.33
pCg	ΔFA↓	0.86	**<0.001**	0.77	0.07	0.16	0.78
	ΔMD↑	0.06	**<0.001**	0.96	0.71	0.61	0.14
dCg	ΔFA↓	0.41	0.38	0.48	0.57	0.61	0.86
	ΔMD↑	0.08	0.08	**0.003**	0.16	0.11	**0.003**
UF	ΔFA↓	**0.02**	**<0.001**	0.69	**0.003**	**0.01**	0.79
	ΔMD↑	0.72	**0.04**	0.59	0.90	0.60	0.93
ILF	ΔFA↓	0.56	**<0.001**	0.89	**0.002**	**0.02**	0.73
	ΔMD↑	0.59	0.07	0.23	0.80	0.98	0.44
SLF	ΔFA↓	0.58	0.06	0.84	0.58	0.95	0.49
	ΔMD↑	0.52	0.41	0.06	0.92	0.25	0.34
IFO	ΔFA↓	0.07	**<0.001**	0.78	**0.02**	**0.01**	0.67
	ΔMD↑	0.80	0.07	0.41	0.76	0.99	0.70
ALIC	ΔFA↓	0.39	**0.05**	0.90	0.09	0.19	0.75
	ΔMD↑	0.46	0.70	0.86	0.95	0.30	0.69
gCC	ΔFA↓	**0.04**	0.23	0.35	0.50	0.69	0.88
	ΔMD↑	0.20	0.59	0.59	0.19	0.37	0.28
oCC	ΔFA↓	0.37	0.13	0.47	0.43	0.40	0.06
	ΔMD↑	0.68	0.17	0.63	0.62	0.33	0.21
IC	**ΔFA↑**	0.08	**0.04**	**0.004**	**0.02**	0.38	**0.03**
	ΔMD↓	0.07	**0.01**	0.12	0.08	0.41	0.11
EC	**ΔFA↑**	0.06	**0.02**	0.09	0.86	0.54	0.06
	ΔMD↓	0.10	0.19	0.16	0.56	0.14	0.66
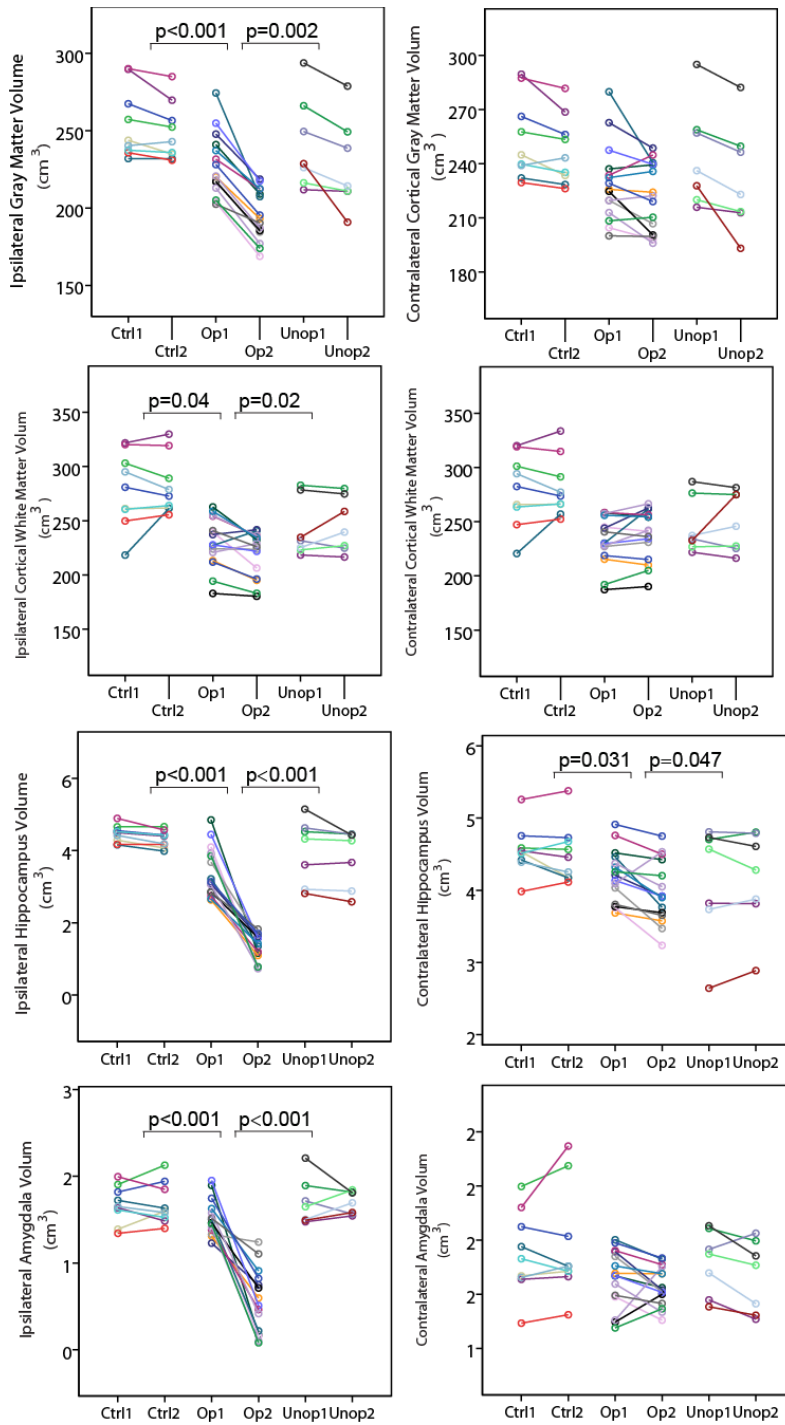
Figure 5.5 The longitudinal volume change of cortical gray matter, white matter, hippocampus and amygdala in controls, operated and unoperated group. The operated patients showed greater inter-scan change than the other groups, which was marked with p value. The operated patients presented greater volume reduction of the ipsilateral cortical gray matter, white matter, hippocampus and amygdala, as well as the contralateral hippocampus, than controls and the unoperated group.
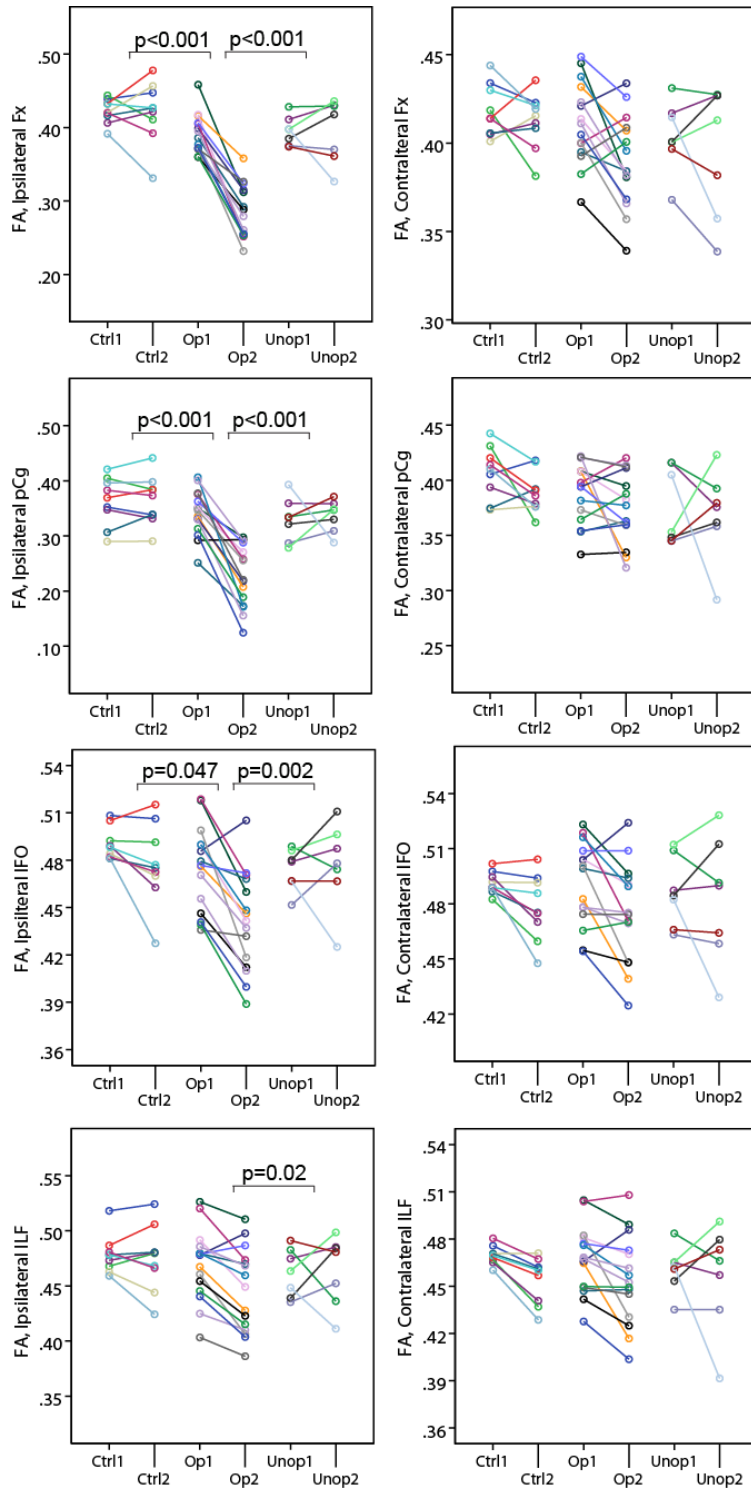
Figure 5.6 The longitudinal FA change of Fx, pCg, IFO and ILF in controls, operated and unoperated group. The operated patients showed greater inter-scan change than the other groups, which was marked with p value.
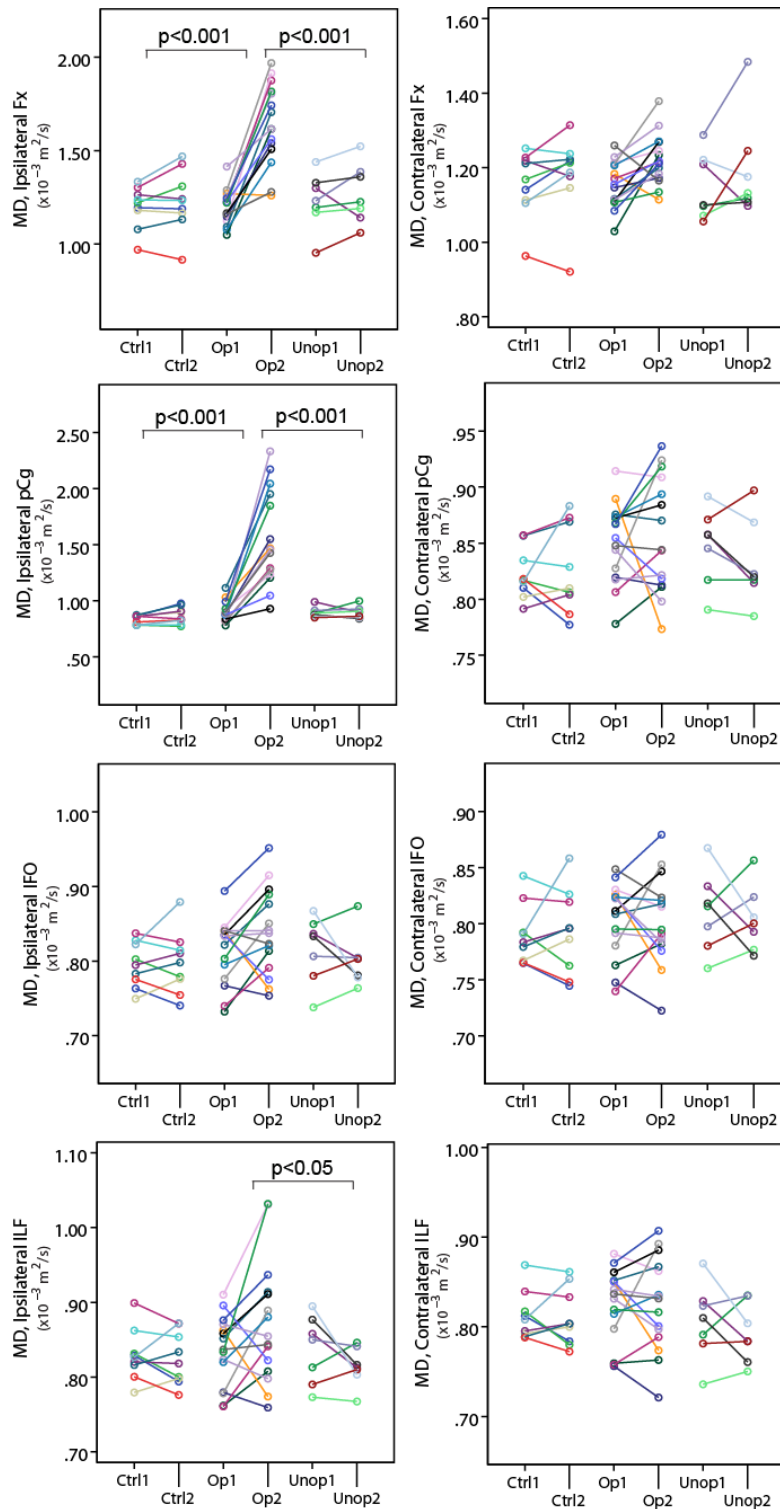
Figure 5.7 The longitudinal MD change of Fx, pCg, IFO and ILF in controls, operated and unoperated group. The operated patients showed greater inter-scan change than the other groups, which was marked with p value.

134

5.4 Discussion and Future direction

In this preliminary study, the gray and white matter changes over a mean of 6.5 years were studied for a group of healthy controls, operated TLE patients (before and at least 2.4 years after surgery) and unoperated TLE patients. All participants demonstrated reduced cortical gray matter volume over time. Controls and the unoperated patients showed few white matter changes from the 1st to the 2nd time point, while the unoperated patients presented dramatic ipsilateral change due to surgery. Between group comparisons of the inter-scan changes showed significant greater volume reduction of the ipsilateral cortical gray matter, white matter, hippocampus and amygdala, and FA reduction of the ipsilateral temporal lobe tracts including fornix, parahippocampal cingulum, inferior frontooccipital fasciculus and inferior longitudinal fasciculus in the operated TLE patients after surgery compared to the unoperated patients and controls. The contralateral side did not show greater inter-scan change than controls over a mean of 6.5 years. The unoperated TLE patients did not show any greater inter-scan change than controls over time.

For the operated TLE patients, consistent with previous studies, the remaining white matter tracts on the operated hemisphere experienced Wallerian degeneration after injury and showed significant FA reduction (McDonald et al., 2010; Nguyen et al., 2011). The Fx and pCg were directly resected during both anterior temporal lobectomy and selective amygdalohippocampectomy and showed the greatest amount of reduction as expected. The ILF is resected during anterior temporal lobectomy and IFO formed the posterior-medial boundary of surgical cavity. These two tracts also showed degeneration after surgery but to a lesser extent. Previously Yogarajah et al. found increased FA in the ipsilateral internal and external capsule in TLE patients after surgery (Yogarajah et al., 2010). We found no greater FA change of the ipsilateral IC and EC compared to controls. While the Yogarajah data is intriguing, suggesting the possibility of plasticity, our results do not support this observation. Change of the white matter structure contralateral to the surgical side did not show progressive degradation than controls, which is consistent with previous results (McDonald et al., 2010; Nguyen et al., 2011).

The lack of greater structural change in the unoperated TLE patients than controls over a mean of 6.5 years was probably because the seizures in four of seven patients were well

controlled by medications. It may also indicate that TLE does not necessarily lead to further structural changes. Previous quantitative MRI studies failed to provide evidence that chronic TLE progressively adds damage to the brain (Liu et al., 2003a, 2005). One recent neuropsychological study provided evidenc that TLE is a neurodevelopmental disease rather than a progressively dementing one (Helmstaedter and Elger, 2009). In their study, TLE patients did not show more progressive memory damage than their healthy peers after 25 years old.

Further analysis would be to look at the T2 relaxometry change of the contralateral hippocampus in all patients. Neocortical and other subcortical volumes are also interesting to be examined in this cohort.

Chapter 6   Distinct white matter abnormalities in different idiopathic generalized epilepsy syndromes[6]

6.1   Introduction

The underlying cause of idiopathic generalized epilepsy (IGE) remains unknown. By definition IGE is not associated with structural abnormalities on conventional magnetic resonance imaging (MRI) (ILAE, 1989). This, together with recent genetic studies demonstrating ion channel and neurotransmitter receptor defects in a small number of pedigrees with autosomal dominant inherited juvenile myoclonic epilepsy (JME) (Cossette et al., 2002), has led to the notion that the underlying pathophysiological mechanisms responsible for sporadic IGE occur at the molecular / membrane level. IGE is subdivided into different syndromes based on the predominant seizure type and age of onset (ILAE, 1989; Engel Jr., 2001). JME, the most common IGE subsyndrome, is associated with the occurrence of "impulsive petit mal" or myoclonus which is the primary clinical feature that distinguishes it from IGE with generalized tonic clonic convulsions only (IGE-GTC) (Janz, 1985; Engel Jr., 2001; Camfield and Camfield, 2010). Recent genetic studies suggest that JME should be considered separately from other subtypes of IGE based on its distinct genetic bases (Zifkin et al., 2005). On the other hand, the overlapping clinical phenotypes and lack of specificity of electroencephalogram (EEG) manifestations makes the differentiation between the two syndromes difficult (Janz, 1985; Andermann and Berkovic, 2001; Koutroumanidis and Smith, 2005).

Recent advances in quantitative neuroimaging enable detailed investigation of the brain *in vivo*. A few studies in single voxel magnetic resonance spectroscopy (MRS) or magnetic resonance spectroscopic imaging (MRSI) have provided evidence of both cortical and deep gray matter (GM) abnormalities, particularly in frontal lobe and

---

[6] A version of this chapter has been published. Liu M, Concha L, Beaulieu C, Gross DW. Distinct white matter abnormalities in different idiopathic generalized epilepsy syndromes. Epilepsia 2011; 52: 2267–75.

thalamus, in IGE patients (Savic et al., 2000, 2004; Bernasconi et al., 2003a; Mory et al., 2003; Helms et al., 2006; Haki et al., 2007; Lin et al., 2009; Doelken et al., 2010). However, findings in IGE using MRI volumetry and voxel-based morphometry (VBM) methods on T1-weighted images have been inconsistent. The first quantitative MRI study on IGE reported significantly larger cortical GM volumes (GMV) in 45 syndrome-mixed IGE patients compared to controls using a semi-automatic segmentation method (Woermann et al., 1998). More recently, a VBM study of 22 syndrome-mixed IGE patients reported 17 of them with increased cortical GMV and seven patients with either enlargement or atrophy of thalamus (Betting et al., 2010). Two volumetry studies of the thalami in mixed IGE patients did not detect differences (Natsume et al., 2003; Seeck et al., 2005). In studies investigating JME independently, some reported increased cortical GM in mesial frontal lobes (Woermann et al., 1999b; Kim et al., 2007a) or the frontobasal region (Betting et al., 2006). Other studies suggest decreased GM concentration in the prefrontal lobe (Tae et al., 2006) and thinner cortical thickness of frontal and temporal gyri in the same group of 20 JME patients (Tae et al., 2008). A more recent study reported decreased GM volume in the supplementary motor area and posterior cingulate cortex of 28 JME patients (O'Muircheartaigh et al., 2011). On the other hand, a recent VBM study failed to demonstrate significant GM differences between a group of 19 JME patients and age, sex, and education matched controls (Roebling et al., 2009). Bilateral thalamic atrophy was detected in only one VBM study of JME (Kim et al., 2007a) but not in the other groups (Woermann et al., 1999a; Betting et al., 2006; Tae et al., 2006). Some studies also explored underlying GM abnormalities in IGE with generalized tonic-clonic seizures as the predominant seizure type with inconclusive results. One MRI volumetry and VBM study of 19 patients with IGE-GTC revealed reduced cortical GM in the frontal, parietal, temporal cortices, cerebellum and reduced subcortical GM in the thalamus, caudate and putamen (Ciumas and Savic, 2006). Another study on 23 patients with IGE-GTC showed widespread cortical thinning in the fronto-central areas and bilateral thalamic atrophy (Bernhardt et al., 2009a). A more recent study on 14 patients with IGE-GTC reported atrophy in the left thalamus, left putamen and bilateral globus pallidus (Du et al., 2011). However, a VBM study showed no GM abnormality in the patients with generalized tonic clonic seizures on awakening compared to controls although, as mentioned above, increased GM was seen in JME (Betting et al., 2006).

In contrast to the numerous studies with a focus on GM, there is a paucity of research on the white matter (WM) in IGE. Diffusion tensor imaging (DTI) is a technique that measures the diffusion and directionality of water (Basser et al., 1994a) which is in turn an indirect marker of key microstructural components of the WM tracts such as axon packing, myelination and cumulative membrane circumference (Beaulieu, 2002; Concha et al., 2010). While there have been numerous DTI studies highlighting extensive WM abnormalities in temporal lobe epilepsy (Arfanakis et al., 2002; Concha et al., 2005a, 2009; Thivard et al., 2005; Ahmadi et al., 2009; Yogarajah et al., 2009), it is unknown if similar findings will be observed in IGE. There are four previous DTI studies of JME patients: (1) voxel-based analysis (VBA) of FA maps identified bilateral FA reduction in the anterior limb of the internal capsule that also correlated with the frequency of generalized tonic-clonic seizures (Deppe et al., 2008); (2) region-of-interest (ROI) analysis showed reduced FA in frontal lobe and thalamocortical WM fibers and increased FA in bilateral putamen correlated with decreasing putamen volume in the same group of JME patients studied in (1) (Keller et al., 2011b); (3) probabilistic tractography identified an FA reduction and mean diffusivity (MD) elevation of the white matter tracts connecting to the left supplementary motor area which include the callosal tracts bridging the left and right supplementary motor areas, left corticospinal tracts and a small number of fibers connecting the primary motor cortex, although other tracts were not examined (Vulliemoz et al., 2011); and (4) tract-based spatial statistics (TBSS) showed reduced FA in the rostral body and splenium of the corpus callosum (O'Muircheartaigh et al., 2011). There is only one DTI study on IGE-GTC showing decreased FA in cerebellum confirmed by VBA, TBSS, probabilistic tractography and ROI analyses (Li et al., 2011).

The purpose of this study was to investigate whether there are white and/or gray matter structural differences between controls and two subsets of IGE, namely JME, and IGE-GTC. White matter microstructure as indicated by fractional anisotropy (FA) was analyzed using diffusion tensor tractography and region of interest analysis of 13 major white matter tracts. Regional gray matter volume was assessed using whole-brain voxel-based morphometry of 3D T1-weighted images. Correlations of FA with lifetime seizures were measured in both IGE groups.

6.2   Subjects and methods

Approval of the research protocol was obtained from the University of Alberta Health Research Ethics Board, and informed consent was obtained from all participants.

6.2.1 Subjects

Participants included 15 patients with JME (12F/3M, age 21±4 years, range 17-32 years) and 10 patients with IGE-GTC (3F/7M, age 21±4 years, range 18-31 years) who were recruited from the epilepsy clinic of the University of Alberta Hospital. All patients had a history of generalized tonic-clonic seizures (GTC), normal intelligence, normal neurologic examination, absence of focal EEG abnormalities and normal clinical MRI scans. Among the 15 JME patients, four were on two antiepileptic drugs and all the others were on a single medication. Among the 10 IGE-GTC patients, three were on two antiepileptic drugs and all the others were on one medication. Precise total lifetime GTC number was available for 23 of 25 patients. For the remaining two patients who had 12-16 and 12-14 seizures, respectively, mean values of 14 and 13 were chosen for the correlation analysis. There was no difference in the number of lifetime GTC between the two patient groups (for JME, 6±4 lifetime GTC, range 1-14; for IGE-GTC, 6±4 lifetime GTC, range 1-12; Student's t test, $p = 0.98$). The 15 JME patients were compared to a group of 15 age-matched controls (12F/3M, age 21±4 years, range 17-31 years). The 10 IGE-GTC patients were compared to another group of 10 age-matched controls (3F/7M, age 21±4 years, range 18-30 years) distinct from the 15 controls paired with JME patients. All 25 control subjects had no history of any neurological or psychiatric disorders.

6.2.2 Image acquisition

All imaging was performed on a 1.5T Siemens Sonata scanner (Erlangen, Germany). Three imaging protocols were used including magnetization prepared rapid acquisition gradient echo (MPRAGE), standard DTI, and fluid-attenuated inversion recovery (FLAIR) DTI. MPRAGE provides high resolution 3D T1-weighted images that were acquired with the following parameters: 1 mm slice thickness with no inter-slice gap, 144 axial slices, TR = 1890 ms, TE = 4.38 ms, TI = 1100 ms, flip angle = 15°, NEX = 1, acquisition matrix = 256×192 (interpolated to 512×384), FOV = 256 mm×192 mm, voxel dimension $1 \times 1 \times 1$ mm^3 (interpolated to $0.5 \times 0.5 \times 1$ mm^3), scan time = 6:03 min. The

two DTI protocols used the same dual spin-echo, single shot echo planar imaging (EPI) sequence except an extra inversion pulse and fewer slices for FLAIR DTI. The common parameters are: 2 mm thick axial oblique slices with no inter-slice gap; TR = 10 s, TE = 88 ms, acquisition matrix = 128×128 with 75% phase partial Fourier (interpolated to 256×256), FOV = 256 mm $\times$ 256 mm, voxel dimension $2 \times 2 \times 2$ mm^3 (interpolated to $1 \times 1 \times 2$ mm^3), 6 diffusion directions, b = 1000 s/mm^2, 8 averages. The protocol differences are 52 axial slices with coverage of whole brain for standard DTI and 26 axial slices with coverage of fornix and cingulum plus an inversion time of 2200 ms for FLAIR DTI (Concha et al., 2005b). Scan time for standard DTI and FLAIR DTI was 9:30 min and 8:30 min, respectively. The SNR of the b0 images in this study was high (average 66 for standard DTI and 51 for FLAIR DTI).

6.2.3 Diffusion tensor tractography and region of interest analysis

Tensor calculation and tractography were performed on a PC running ExploreDTI (A. Leemans, University Medical Center, Utrecht, Netherlands). White matter tracts were chosen for analysis based on abnormal findings previously demonstrated in patients with temporal lobe epilepsy so that a comparison could be made to evaluate consistencies of white matter pathology in various epilepsy syndromes. In addition, from a practical perspective we focussed on major white matter tracts that can be identified well with deterministic tractography. Our group previously reported abnormal limbic tracts, i.e. fornix and cingulum, corpus callosum and external capsule in mesial temporal lobe epilepsy patients (Concha et al., 2005a, 2009; Gross et al., 2006). Several DTI tractography studies conducted by others also suggest extensive abnormalities in a number of major WM tracts not restricted to the temporal lobe (Rodrigo et al., 2007; Diehl et al., 2008a; Lin et al., 2008; McDonald et al., 2008a; Tae et al., 2008; Ahmadi et al., 2009). Based on these findings, twelve major white matter tracts including the crus of fornix (Fx), dorsal cingulum (dCg), parahippocampal cingulum (pCg), genu/body/splenium of corpus callosum (gCC/bCC/sCC), inferior fronto-occipital fasciculi (IFO), inferior/superior longitudinal fasciculi (ILF/SLF), uncinate fasciculi (UF), anterior limb of the internal capsule (ALIC), and corticospinal tracts (CST) were identified with tractography here (Figure 6.1) and external capsule (EC) which cannot be reliably delineated with tractography was analyzed with ROI. ExploreDTI, which adopts

141

a deterministic streamline method to obtain fibers, was used to identify the Fx using the 26 slice FLAIR DTI datasets while all the other tracts were delineated using the 52 slice standard DTI by setting the FA thresholds to 0.25 and the angular threshold to 60° for UF and SLF and 30° for all other tracts. ROIs were manually placed using a two ROI approach for each tract based on the methods and anatomy described before (Wakana et al., 2007; Malykhin et al., 2008). The bCC was defined as the central section of the corpus callosum excluding the genu, splenium and tapetum. As a result, the bCC mainly contains fibers associated with premotor, supplementary motor, motor and somatosensory cortices. Fractional anisotropy (FA) was obtained by overlaying the tracts on FA maps and averaging all the voxels for both hemispheres to generate a single value per tract using an in-house program written by L.C. The EC was analyzed by manually drawing a ROI on a single axial FA map where the structure shows the clearest boundary.

Statistical analyses were administered using SPSS version 18. Paired Student's t test was used to evaluate the right and left symmetry of ten paired tracts within JME patients, IGE-GTC patients and each control group (the commissural tracts gCC/bCC/sCC are not included). The FA of Fx showed a small but significant asymmetry in JME patients (right = 0.42 ± 0.03; left = 0.43 ± 0.03; p = 0.03) and their corresponding 15 controls (right = 0.45 ± 0.02; left = 0.47 ± 0.02; p = 0.01) but not in IGE-GTC patients (right = 0.44 ± 0.03; left = 0.45 ± 0.02; p = 0.47) or their 10 matched controls (right = 0.46 ± 0.02; left = 0.45 ± 0.02; p = 0.6). The FA of SLF differed between left and right side only in the 10 control group (right = 0.51 ± 0.02; left = 0.50 ± 0.02; p = 0.04) but not in the others. No asymmetry was observed for the other eight tracts. For simplicity, given the fact that most tracts were not asymmetric and those that were showed minimal FA differences, subsequent analysis was performed using collapsed data (i.e., a single mean value per subject combining both sides for each tract).

Before proceeding to the comparisons between patients and controls, the two control groups (n_1= 15, n_2 = 10) were first tested against each other on FA value of each of the 13 WM structures using independent student t-test. The FA did not show a difference between the two control groups and the minimum p value among the 13 tracts was 0.23. FA was then compared between the JME group (n = 15) and its corresponding control group (n = 15) and between the IGE-GTC group (n = 10) and its corresponding control group (n = 10) for each of the 13WM structures using independent t-test. Because the age

and gender distributions were similar in the two comparisons, these variables were not included in the statistical model. False discovery rate (FDR) at $p = 0.05$ level was used to adjust for multiple comparison correction. To better understand the FA changes, parallel diffusivity ($\lambda_{\parallel}$) and perpendicular diffusivity ($\lambda\perp$), as well as mean diffusivity (MD), were queried subsequently for the tracts demonstrating significant between group differences using independent student t-test. Furthermore, correlation between total lifetime GTC and FA of each abnormal tract within each patient group and in all patients combined was computed using Pearson's correlation coefficient at $p < 0.05$ with FDR correction.
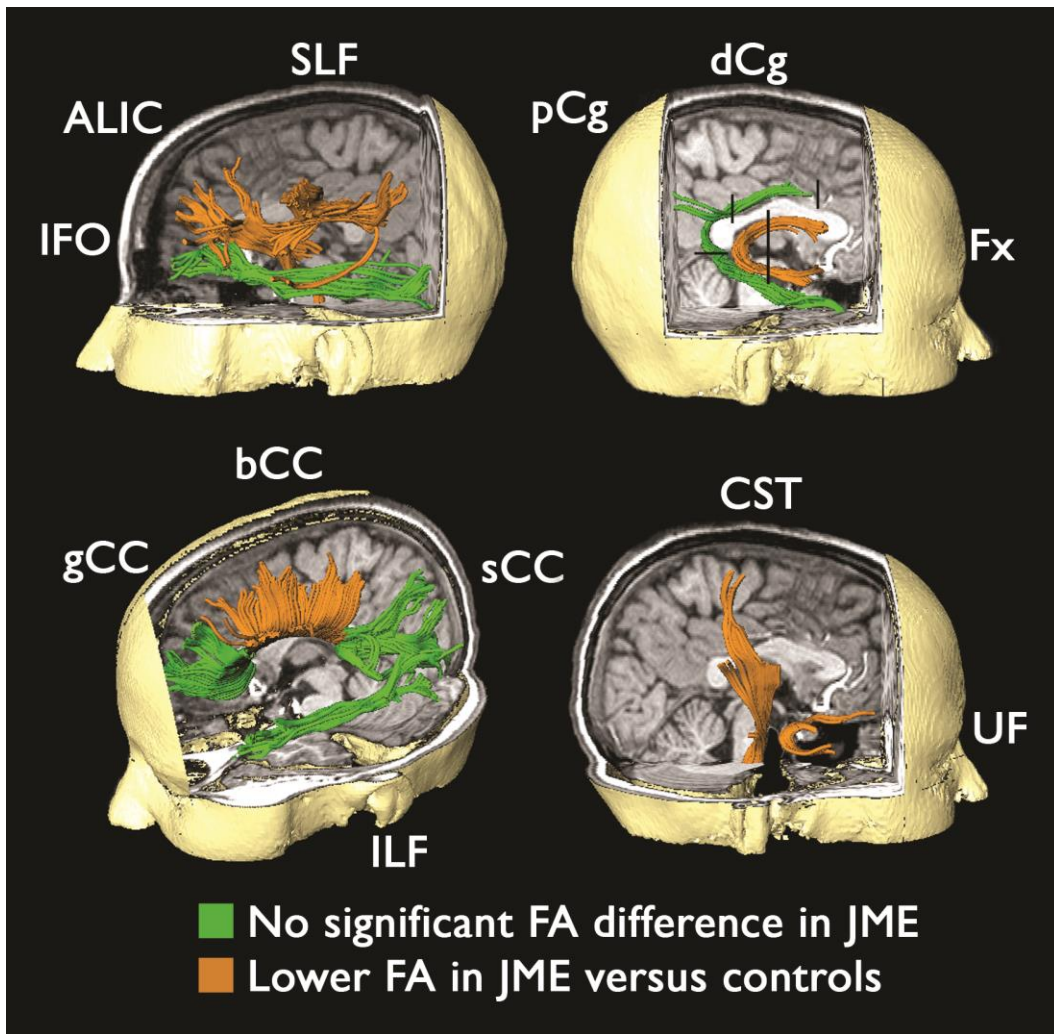
Figure 6.1 Three dimensional visualization of 12 tracts derived from tractography in a 17-year-old female JME patient. Tracts in green did not have significant differences between JME and controls while tracts in orange had significantly lower FA in JME. Measurement of the fornix was constrained to the crus part as indicated by black lines cutting coronally at the fusion of left and right fornices. The dorsal cingulum was limited

between the most posterior coronal slice of genu of corpus callosum and the most anterior coronal slice of splenium of the corpus callosum. The parahippocampal cingulum was limited below the lower body of the splenium. Abbreviations: the crus of fornix (Fx), dorsal cingulum (dCg), parahippocampal cingulum (pCg), genu/body/splenium of corpus callosum (gCC/bCC/sCC), inferior fronto-occipital fasciculi (IFO), inferior/superior longitudinal fasciculi (ILF/SLF), uncinate fasciculi (UF), anterior limb of the internal capsule (ALIC), and corticospinal tracts (CST).

6.2.4 Voxel-based morphometry on gray matter

Automated, whole brain VBM was performed on T1-weighted structural images using SPM8 (Wellcome Department of Cognitive Neurology, London, UK) and VBM8 toolbox (Revision 343, Christian Gaser, http://dbm.neuro.uni-jena.de/vbm/). In summary, all images were spatially normalized into the stereotaxic space using high-dimensional Dartel method (Ashburner, 2007) and segmented into GM/WM/cerebrospinal fluid (CSF).The resultant GM images were modulated by Jacobian determinant only for the non-linear terms so that not only the quantity of tissue that was deformed during non-linear normalization was preserved but also individual brain sizes were corrected. This step yielded inference about regional GMV change in the following statistical analysis. The modulated GM images were smoothed using a 10mm isotropic Gaussian Kernel. Relative GMV differences were assessed between JME group (n = 15) and its corresponding control group (n = 15) and between IGE-GTC group (n = 10) and its corresponding control group (n = 10) on a voxel wise basis using analysis of variance (ANOVA). An absolute GM threshold masking of 0.1 was applied to avoid confounding results around GM and WM edges. Two T-contrast {1, -1} and {-1, 1} were defined for the comparisons to detect regional GMV increases or reductions. The voxel wise multiple comparisons were corrected using a false discovery rate at $p < 0.05$ (Genovese et al., 2002). If no difference was found after FDR correction, a less stringent uncorrected threshold ($p < 0.001$) and extent threshold (k) defined by the expected number of voxels per cluster based on random field theory (readable from SPM output, $k_{JME} = 106$ voxels in the JME comparison and $k_{IGE-GTC} = 90$ voxels in the IGE-GTC comparison) were used to detect potential GMV difference between groups. To probe a possible relationship between the identified GMV abnormality and total lifetime GTC, a correlation analysis was conducted by extracting the mean GMV within each abnormal cluster for each

patient and correlating them with total lifetime GTC using Pearson's correlation coefficient at $p < 0.05$ with Bonferroni correction.

6.3 Results

6.3.1 Diffusion tensor tractography and region of interest analysis

No subjective differences of the 12 tracts between JME, IGE-GTC and their corresponding controls was observed in terms of tract shape nor were there differences in tract volume (data not shown, tested by independent t-test and $p < 0.05$). The FDR corrected t-tests demonstrated six tracts with significantly lower FA values in JME group with respect to its control group, while there were no significant differences between IGE-GTC group and its corresponding control group (Figure 6.1, Figure 6.2). The six tracts and their FDR corrected significance values as well as the percentages of FA reduction were as follows: Fx ($p = 0.036$, 6.9%), bCC ($p = 0.042$, 2.6%), UF ($p = 0.029$, 6.7%), SLF ($p = 0.043$, 2.9%), ALIC ($p = 0.019$, 3.5%) and CST ($p = 0.042$, 3.6%). The FA reduction in these tracts resulted from an elevation of $\lambda_\perp$ in all ($p < 0.05$ in each individual tract without multiple comparison correction). There was no significant correlation between FA and lifetime GTC number in the six abnormal tracts for either JME group, IGE-GTC group or in all epilepsy patients combined.
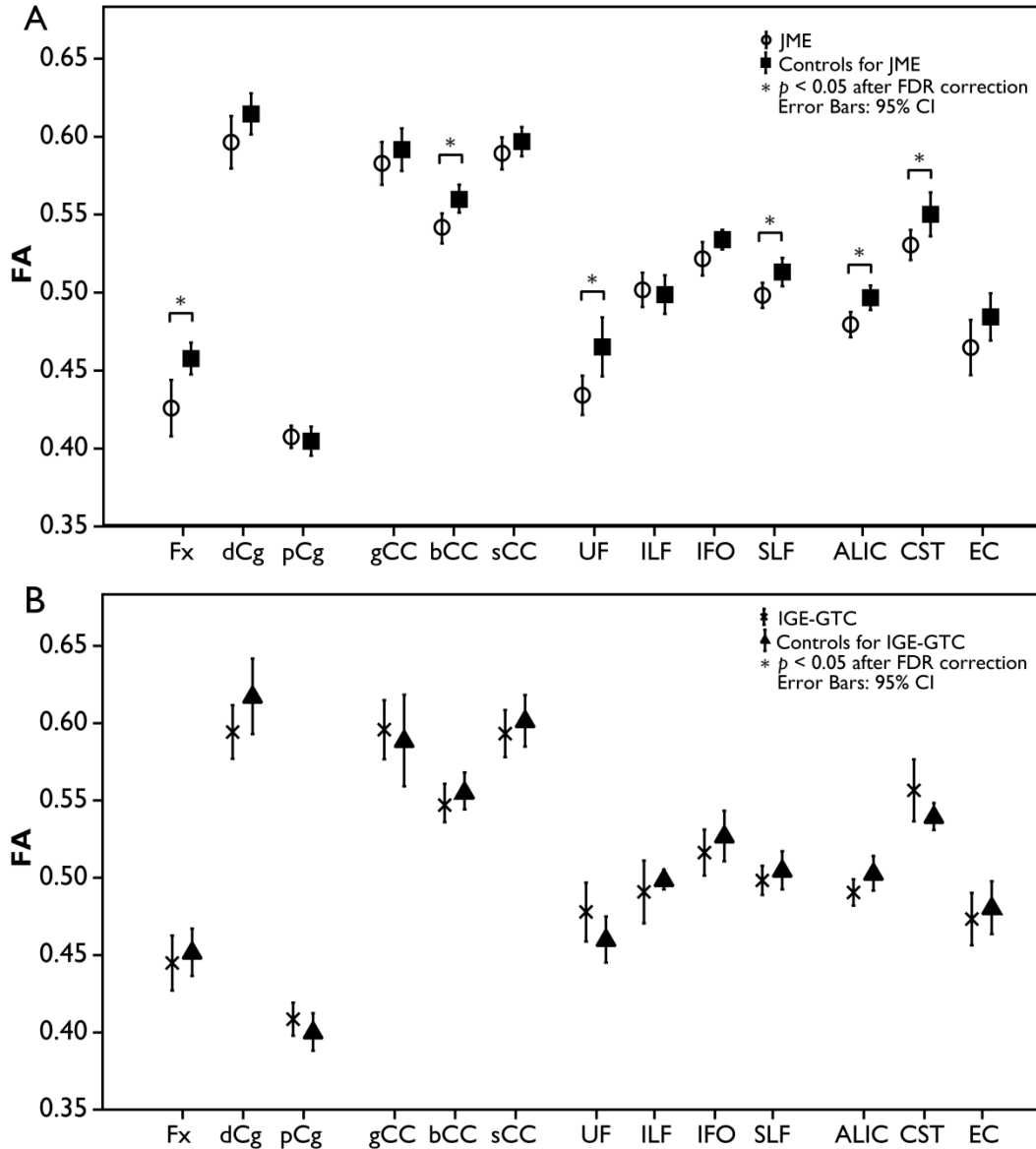
Figure 6.2 Mean and 95% confidence interval of fractional anisotropy (FA) for the 13 white matter structures (12 tracts analyzed with tractography as well as the external capsule which was analyzed with ROIs) examined in JME with respect to its corresponding control group (panel A, n=15 in each group) and in IGE-GTC with respect to its corresponding control group (panel B, n=10 in each group). Significantly lower FA was observed in the six tracts marked by asterisks in JME while no significant FA differences were detected in IGE-GTC. Abbreviations: the crus of fornix (Fx), dorsal cingulum (dCg), parahippocampal cingulum (pCg), genu/body/splenium of corpus callosum (gCC/bCC/sCC), inferior fronto-occipital fasciculi (IFO), inferior/superior longitudinal fasciculi (ILF/SLF), uncinate fasciculi (UF), anterior limb of the internal capsule (ALIC), and corticospinal tracts (CST).

6.3.2 Voxel-based morphometry on gray matter

Neither regional GMV increases nor decreases were detected in JME or IGE-GTC patients as compared to their corresponding controls after FDR correction ($p < 0.05$)**.** However, the uncorrected threshold showed GMV reduction in both JME and IGE-GTC albeit in different regions (Figure 6.3). JME patients showed GMV loss in right precentral gyrus (peak voxel, x, y, z = 33, -18, 49; T = 4.4), left and right middle frontal gyri (peak voxel, left x, y, z = -32, 15, 46, T = 4.53; right x, y, z = 35, 0, 51, T = 4.34), left temporal pole (peak voxel, x, y, z = -51, 18, -29, T = 3.86), and left superior parietal gyrus (peak voxel, x, y, z = -12, -76, 49, T = 4.02). IGE-GTC patients showed GMV reduction in left and right supplementary motor areas (peak voxel, left x, y, z = -5, 9, 70, T = 5.22; right x, y, z = 3, 8, 51; T = 4.95), left and right frontal lobes (peak voxel, left x, y, z = -44, 18, -12, T = 5.56; right x, y, z = 26, -7, 61; T = 5.16), left paracentral lobule (peak voxel, x, y, z = 0, -19, 67, T = 6.23), and right middle temporal gyrus (peak voxel, x, y, z = 69, -7, -17, T = 4.24). The detected regions in both patient groups were concentrated in frontal and central regions yet were separate from each other. JME GMV areas were more lateral while IGE-GTC GMV areas were more medial. No significant correlation between the decreased GM region volumes of the significant clusters in JME and IGE-GTC patients and their total lifetime GTC number was observed at $p < 0.05$.

6.4 Discussion

The main finding of the study was that the two IGE subsyndromes, i.e. JME and IGE-GTC, had distinct white matter abnormalities, with JME demonstrating reduction of FA in six particular white matter tracts with four of them related to the temporal and/or frontal lobes while IGE-GTC showed no such white matter changes. While corrected VBM analysis showed no differences between patient and control groups, the uncorrected VBM analysis suggested a trend of regionally disparate gray matter volume reduction in frontal and central regions in both patient groups with JME showing more lateral areas and IGE-GTC showing more medial areas.
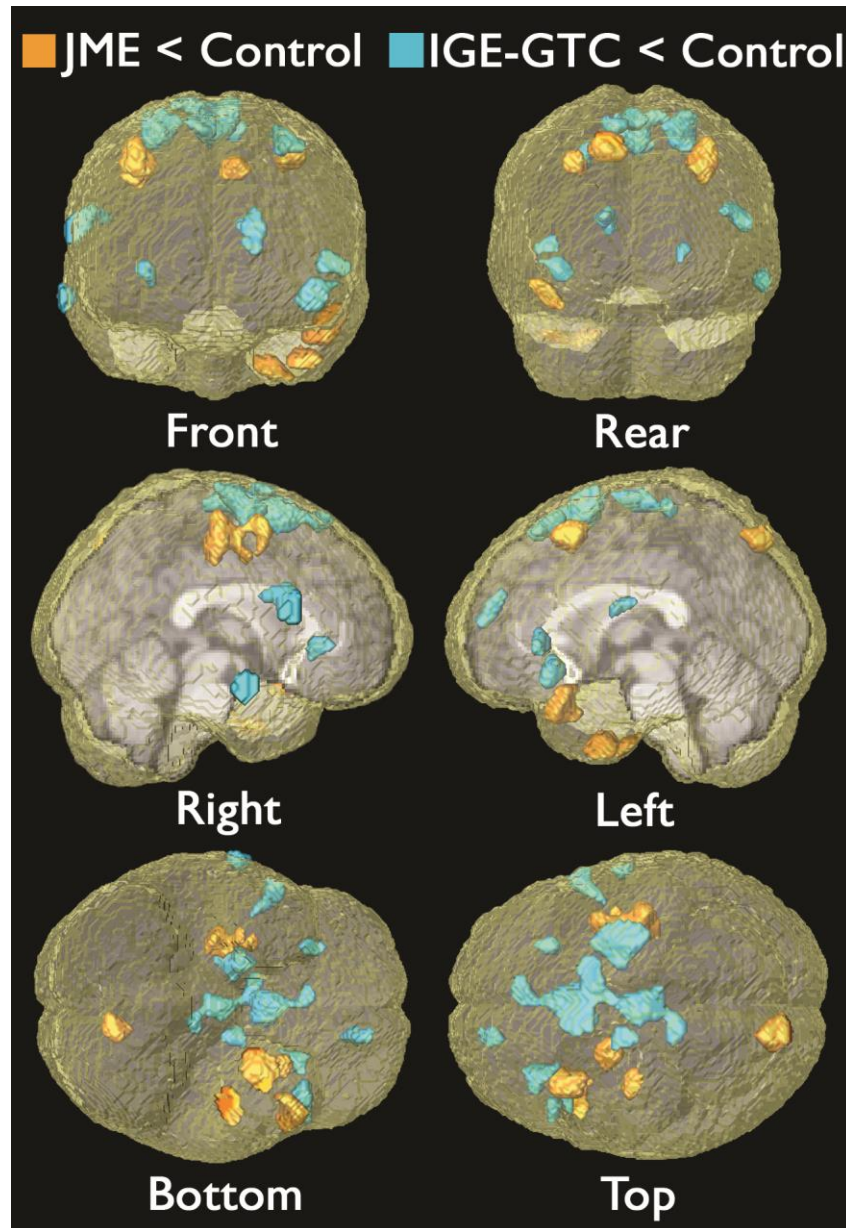
Figure 6.3 VBM analyses detected regions that showed reduced gray matter volume (GMV) in JME (orange), IGE-GTC (blue) at uncorrected statistical threshold ($p < 0.001$, $k_{JME} = 106$ voxels, $k_{IGE-GTC} = 90$ voxels) presented on the same 17-year-old female JME patient presented in Figure 6.1 after the T1-weighted image was transformed into MNI space. Regions of GMV reduction in JME included right precentral gyrus, left and right middle frontal gyri, left temporal pole, and left superior parietal gyrus. Regions of GMV reduction in IGE-GTC included left and right supplementary motor areas, left and right frontal lobes, left paracentral lobule, and right middle temporal gyrus. The detected regions in both patient groups were concentrated in frontal and central regions yet were separate from each other. JME GMV areas were more lateral while IGE-GTC GMV areas were more medial.

Impaired white matter structures were demonstrated previously in JME patients based on a voxel-by-voxel comparison of FA maps (Deppe et al., 2008) and a ROI analysis in the frontal lobe and thalamocortical white matter (Keller et al., 2011a). Our tractography findings of significant FA reductions in anterior limb of internal capsule (collapsed left and right) in JME were in concordance with the major observation of lowered FA in bilateral anterior limb of internal capsule (Deppe et al., 2008) and reduced FA in thalamocortical white matter fibers (Keller et al., 2011a). Another DTI study of JME using probabilistic tractography demonstrated decreased FA in the connection of the supplementary motor area which mainly consists of a portion of body of corpus callosum connecting to the contralateral supplementary motor area and some ipsilateral descending corticospinal tracts (Vulliemoz et al., 2011). The same research group extended these findings on a larger JME sample by using TBSS to show FA reduction in the part of body of corpus callosum which projects to superior frontal regions including the supplementary motor area (O'Muircheartaigh et al., 2011). Our finding of reduced FA in the body of corpus callosum was in agreement with these two studies. We also found reduced FA in the fornix, uncinate fasciculi, superior longitudinal fasciculi and cortical spinal tracts in JME related to controls. It is interesting to note that the fornix, uncinate fasciculi, superior longitudinal fasciculi and anterior limb of internal capsule were also reported abnormal in temporal lobe epilepsy (McDonald et al., 2008a; Ahmadi et al., 2009; Concha et al., 2009), suggesting the susceptibility of these white matter tracts in distinctly different epilepsy syndromes, while other affected tracts in temporal lobe epilepsy such as inferior longitudinal fasciculi, inferior fronto-occipital fasciculi and cingulum were spared in JME. The percentage of FA reduction in the fornix observed in our JME patients (6.9%) was not as large as that of temporal lobe epilepsy patients with unilateral mesial temporal sclerosis (10%) previously reported by our group (Concha et al., 2005a, 2009). This could explain the mild or absent memory impairment reported in JME (O'Muircheartaigh et al., 2011) that is typically more severe in temporal lobe epilepsy (Oyegbile et al., 2004). On the other hand, the corticospinal tracts seem to be exclusively affected in JME but not in temporal lobe epilepsy (McDonald et al., 2008a). The body of the corpus callosum which connects bilateral motor regions was abnormal in JME but not in temporal lobe epilepsy (Kim et al., 2008) while the genu and splenium were affected in temporal lobe epilepsy but not in JME (Deppe et al., 2008; O'Muircheartaigh et al., 2011; Vulliemoz et al., 2011). Adopting VBA, TBSS,

149

probabilistic tractography and ROI analysis, the only DTI study on IGE-GTC showed reduced FA in cerebellum but not in the other white matter area (Li et al., 2011). Our negative white matter finding on IGE-GTC was in agreement with this study. Because some of our DTI data did not cover the whole cerebellum due to the variation of individual brain size (cerebrums were fully covered primarily in these cases), we did not perform tractography for cerebellum tracts such as medial cerebellar peduncle.

The fact that the primary clinical difference between JME and IGE-GTC is the occurrence of myoclonus, raises the possibility that disruption of white matter integrity may be the underlying mechanism responsible for myoclonus in JME. Further to this, interestingly one tract where FA was significantly reduced in JME but not in IGE-GTC patients was the corticospinal tracts which would be consistent with a disruption of the primary motor pathways in JME. While it is impossible to confirm what underlying mechanism is responsible for the reduced FA observed in JME patients, an intriguing hypothesis would be that disruption of myelination is present which in turn results in abnormal conduction of impulses in motor pathways resulting in ephaptic transmission as a possible explanation for the occurrence of myoclonus in JME.

The demonstration of ion channel and neurotransmitter receptor defects in Mendelian inherited IGE pedigrees has supported the assumption that changes in membrane excitability that occur at the molecular level are the primary pathophysiological mechanism resulting in IGE (Cossette et al., 2002). Although previously considered to have no structural abnormalities, there is a growing body of quantitative imaging literature demonstrating such differences in IGE patients. Two reports on IGE patients with GTC as the predominant seizure type have demonstrated reduced GM (Ciumas and Savic, 2006; Bernhardt et al., 2009a).The reported GM findings in JME have been more variable with some studies suggesting increased gray matter volume while others report decreased gray matter volume in different regions or no difference between JME and controls (Woermann et al., 1998, 1999a; Ciumas and Savic, 2006; Tae et al., 2006; Roebling et al., 2009; O'Muircheartaigh et al., 2011). We did not find significant gray matter changes after multiple comparison correction, which is likely related to our relatively small sample size. However, the uncorrected VBM analysis suggests reduced cortical gray matter volume bilaterally in both syndromes, which is in agreement with a number of previous studies (Ciumas and Savic, 2006; Tae et al., 2006; Bernhardt et al.,

2009a; O'Muircheartaigh et al., 2011). As opposed to previous reports (Ciumas and Savic, 2006; Kim et al., 2007a; Betting et al., 2010; Du et al., 2011), we did not observe volume difference of any subcortical gray matter in either patient group which again may be explained by the relatively small sample size.

As previously stated, the current assumption is that sporadic JME and IGE-GTC are most likely caused by defects at the molecular level. As it is difficult to directly associate an ion channel or neurotransmitter receptor defect with structural changes, the most reasonable explanation for the gray matter atrophy reported in both JME and IGE-GTC and the white matter abnormalities reported solely in JME by us and the other four previous studies is that these structural changes are a secondary effect of seizures (Deppe et al., 2008; Keller et al., 2011a; O'Muircheartaigh et al., 2011; Vulliemoz et al., 2011). This concept was supported by Deppe et al's finding of a negative correlation between lifetime seizure number and FA. In contrast to their study, we did not find any correlations between lifetime seizures and FA for any white matter region nor did we find any significant correlations between lifetime seizures and gray matter atrophy. Differences in subjects may account for this disagreement, in particular the fact that three of ten subjects in the Deppe et al. JME group had never experienced a generalized convulsion. While the cross sectional study design and relatively small number of subjects limit the conclusions that can be drawn from our study, our finding of an absence of a correlation do not support the idea that either the grey or white matter abnormalities seen in IGE-GTC and JME respectively are secondary to seizures. As both the JME and IGE-GTC groups had experienced a similar number of lifetime generalized seizures (mean of 6, range 1-12 for JME and range 1-14 for IGE-GTC), the most compelling argument against the structural changes being secondary to seizures is that the two groups had distinctly different anatomical findings (different gray matter abnormalities in JME and IGE-GTC and white matter abnormalities in JME only) while experiencing a the same number of lifetime generalized tonic clonic convulsions.

In summary, our findings demonstrate white matter abnormalities in JME but not in IGE-GTC and potential gray matter atrophy in both JME and IGE-GTC which support the idea that JME and IGE-GTC may be associated with distinctly different anatomical substrates.

6.5   Appendix[7]

No significant findings were observed by the VBM analysis with FDR correction in either patient group. Nevertheless, it remains interesting to look at the VBM analyses as previous studies had reported varying grey matter deficits. The uncorrected VBM analysis revealed a trend of reduced grey matter bilaterally in both JME and IGE-GTC patients, but the regions identified had no overlap. Please refer to Figure 6.3 for illustration.

The absolute grey matter volume of the significant clusters detected in JME and IGE-GTC were extracted from the two patients groups and two control groups and are shown in Appendix Figure 6.1.
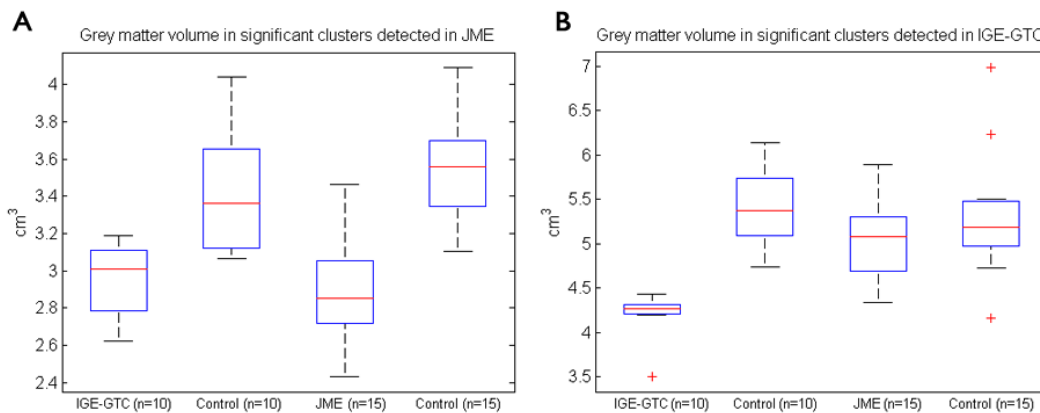
Appendix Figure 6.1 The boxplot (A) lists the volume values of the JME, IGE-GTC and their matching control groups in regions showing grey matter loss in JME. In these areas, IGE-GTC group also showed a trend towards volume decrease. The bloxplot (B) lists the volume values of the JME, IGE-GTC and their matching control groups in regions showing grey matter loss in IGE-GTC. In these areas, the JME group did not show volume decrease suggesting these reduction areas are unique to IGE-GTC group.

---

[7] The appendix did not appear in the published version of this Chapter.

Chapter 7   Discussion and Conclusion

7.1   Limitations

While diffusion tensor imaging and quantitative methods have been proven to have great value in identifying gray and white matter changes in the brain with neurological disorders, one should be aware of the limitations related to the techniques to thoughtfully interpret any findings. Our diffusion tensor imaging acquisition adopts a twice-refocused spin-echo echo-planar imaging (EPI) sequence to reduce eddy-current-induced distortion (Reese et al., 2003). However, susceptibility distortion still exists at the basofrontal regions where the air-tissue interface around the sinuses is located. Single shot EPI has other shortcomings, such as limited spatial resolution (e.g. $2 \times 2 \times 2$ mm^3 as used in this thesis; at 1.5T the signal-to-noise ratio becomes poor when pushing the resolution below this), due to the limited number of echoes that can be acquired in a single shot. The $2 \times 2 \times 2$ mm^3 spatial resolution impairs imaging white matter structures smaller than this dimension; thus, tractography of the mammillo-thalamic tract and fibers streaming into the border of gray and white matter was precluded. The smallest tracts analyzed in this thesis was the fornix. Because its width is only 2-3 mm, tractography suffered slightly from partial volume effects due to tissue signal mixing with signal from the adjacent cerebrospinal fluid (CSF). FLAIR DTI dramatically alleviates this problem by suppressing the signal from the CSF and thus yields better tractography of the fornix. Chemical shift can also cause signal misregistration at the fat layer around the scalp.

Deterministic tractography based on images of high signal-to-noise ratio (~55 for averaged b0 images in data acquired in this thesis) yields clear-cut tracts (Mori et al., 2009). There is debate over whether it is beneficial to use more than six diffusion gradient directions (e.g. 30 directions) to give better tensor estimation and thus more accurate tracts (Ni et al., 2006; Landman et al., 2007). We argue that data with six gradient directions with 10 repetitions can yield as robust results as 30 gradient directions with two repetitions (Lebel et al., 2012); although, absolute difference exists between the FA and MD values (see also for the study of fornix in the Appendix).

The other fundamental limitation of deterministic tractography lies within the tensor model. As stated in Section 1.2.6.2, the biggest problem associated with deterministic

tractography is that only one possible direction with highest probability is picked during streamline propagation and thus the confidence/uncertainty of the tractography result is unknown. Probabilistic tractography better handles the problem by exploring every possible path from a starting point to any other regions of the brain. Thus, the tracts that traverse through crossing fiber regions can be revealed while deterministic tractography stops at this confusing region with low FA value.

Last but not least, the experiments performed in this thesis did not address gender effects on brain structures in epilepsy patients. Previous MRI studies have shown structural differences between healthy males and females in both gray and white matter (Sowell et al., 2007; Bava et al., 2011). A recent study found the total number of voxels with decreased FA was higher in women with right hippocampal sclerosis and in men with left hippocampal sclerosis (Oguz et al., 2012). It is difficult to acquire the same number of male and female patients and controls at our community-based research center. Controlling gender effects using a general linear model oversimplifies the case. In particular, it would be interesting to investigate the gender effect on the brain in temporal lobe epilepsy and idiopathic generalized epilepsy patients with a larger sample size.

7.2 Conclusion

The recent development of quantitative magnetic resonance imaging techniques has make the detection of subtle brain changes that are not visible on conventional MRI images possible. These methods greatly enhance our understanding of epilepsy by locating structural change, quantifying the relationship between different regions and correlating with clinical parameters. The research in this thesis took advantage of one of the techniques, diffusion tensor imaging, to quantify the integrity of white matter tracts in epilepsy, which is conventionally deemed a gray matter disorder. Experiments were conducted to identify structural change, aberrant brain networks and progression of white matter in different types of epilepsy syndromes.

The parallel and perpendicular diffusivities derived from DTI have the potential to be specific biomarkers for axonal and myelin statuses, respectively. DTI has demonstrated the ability to detect acute water diffusion changes within days of transection of the fornix that are not just limited to parallel diffusivity. While the chronically elevated perpendicular diffusivity and reduced parallel diffusivity in the fornix are compatible

with myelin degradation, the acute reduction of both parallel and perpendicular diffusivities may reflect a number of physiological process including beading and swelling of axolemma, granular disintegration of the axonal neurofilaments, ischemia induced cytotoxic edema, and/or changes in the extra-axonal space including inflammatory changes and gliosis.

Disrupted white matter compared to controls was detected in ten tracts for temporal lobe epilepsy and mesial temporal sclerosis (TLE+MTS), but only in the parahippocampal cingulum and tapetum for those without mesial temporal sclerosis (nonlesional TLE, nlTLE). Interestingly, right TLE+MTS patients showed more changes than left TLE+MTS patients despite similar ages of onsets or disease durations. The underlying mechanism remains unclear.

Graph theoretical analysis based on white matter tractography has provided a new perspective to evaluate the connectivity of the brain. Left TLE+MTS patients exhibited concurrent decreases of global and local efficiencies and widespread reduction of regional efficiency in temporal, frontal and parietal areas. Communication hubs, such as the left precuneus, were also altered. These findings further support the notion that TLE is a network disease.

The next important question is whether the white matter changes observed in TLE patients is progressive over time. Over a 6.5 year span, TLE+MTS patients who underwent surgery showed significant white matter degeneration ipsilateral to the surgical side secondary to Wallerian degeneration while the contralateral side did not show more change than controls. The unoperated TLE patients did not present progressive white matter change greater than controls either.

A similar question is whether the subsyndromes of idiopathic generalized epilepsy have different structural substrates. Idiopathic generalized epilepsy, the most common type of generalized epilepsy, is by definition not associated with qualitative MRI change. The two subsyndromes, juvenile myoclonic epilepsy (JME) and idiopathic generalized epilepsy with generalized tonic clonic seizures only (IGE-GTC), share very similar clinical traits except that patients with JME experience myoclonic jerks. MRI structural analysis here revealed distinct abnormality patterns associated with the two syndromes, with JME having more widespread white matter changes and IGE-GTC having more gray

matter changes. This suggests that there are different networks involved in these two similar clinical syndromes.

Overall, the thesis showed great usefulness of diffusion tensor imaging in detecting abnormalities in epilepsy. With the rapid development of more advanced techniques, this research tool has great potential to be applied in routine clinical settings. The structural abnormalities shown in this thesis may provide a better understanding of the various epileptic disorders themselves.

7.3   Future direction

Many other questions regarding to epilepsy have not been answered yet. Does the white matter change seen in epilepsy occur at the very beginning, or is it secondary to seizures? While temporal lobe epilepsy patients have been demonstrated to have widespread white matter alterations, is the extent of abnormality very widespread at the very beginning or gradually becomes extensive due to uncontrolled seizures later? Which areas are the most severely affected? Do these white matter changes account for different cognitive functions? What are the structural and functional substrates of epilepsy patients with comorbidity such as depression?

As MRI techniques advance, higher magnetic field and stronger diffusion gradients are able to generate more detailed structural and functional images to facilitate the detection of alterations in epileptic brain. Better predictors of surgical outcome and new pharmaceutical targets can become possible with the MRI research of epilepsy.

Bibliography

Achard, S., and Bullmore, E. (2007). Efficiency and cost of economical brain functional networks. PLoS Comput Biol *3*, e17.

Ahmadi, M.E., Hagler, D.J., McDonald, C.R., Tecoma, E.S., Iragui, V.J., Dale, A.M., and Halgren, E. (2009). Side matters: diffusion tensor imaging tractography in left and right temporal lobe epilepsy. AJNR Am J Neuroradiol *30*, 1740–1747.

Alhusaini, S., Doherty, C.P., Palaniyappan, L., Scanlon, C., Maguire, S., Brennan, P., Delanty, N., Fitzsimons, M., and Cavalleri, G.L. (2012). Asymmetric cortical surface area and morphology changes in mesial temporal lobe epilepsy with hippocampal sclerosis. Epilepsia *53*, 995–1003.

Andermann, F., and Berkovic, S.F. (2001). Idiopathic generalized epilepsy with generalized and other seizures in adolescence. Epilepsia *42*, 317–320.

Anderson, A.W. (2001). Theoretical analysis of the effects of noise on diffusion tensor imaging. Magn Reson Med *46*, 1174–1188.

Angeles, D. (1981). Proposal for revised clinical and electroencephalographic classification of epileptic seizures. From the Commission on Classification and Terminology of the International League Against Epilepsy. Epilepsia *22*, 489–501.

Annegers, J.F., Hauser, W.A., Elveback, L.R., and Kurland, L.T. (1979). The risk of epilepsy following febrile convulsions. Neurology *29*, 297–303.

Annesi, F., Gambardella, A., Michelucci, R., Bianchi, A., Marini, C., Canevini, M.P., Capovilla, G., Elia, M., Buti, D., Chifari, R., et al. (2007). Mutational analysis of EFHC1 gene in Italian families with juvenile myoclonic epilepsy. Epilepsia *48*, 1686–1690.

Antel, S.B., Li, L.M., Cendes, F., Collins, D.L., Kearney, R.E., Shinghal, R., and Arnold, D.L. (2002). Predicting surgical outcome in temporal lobe epilepsy patients using MRI and MRSI. Neurology *58*, 1505–1512.

De Araujo Filho, G.M., De Araujo, T.B., Sato, J.R., Silva, I. Da, Lin, K., Júnior, H.C., Yacubian, E.M.T., and Jackowski, A.P. (2013). Personality traits in juvenile myoclonic epilepsy: Evidence of cortical abnormalities from a surface morphometry study. Epilepsy Behav.

De Araújo Filho, G.M., Jackowski, A.P., Lin, K., Guaranha, M.S.B., Guilhoto, L.M.F.F., Da Silva, H.H., Caboclo, L.O.S.F., Júnior, H.C., Bressan, R.A., Yacubian, E.M.T., et al. (2009). Personality traits related to juvenile myoclonic epilepsy: MRI reveals prefrontal abnormalities through a voxel-based morphometry study. Epilepsy Behav *15*, 202–207.

Arfanakis, K., Hermann, B.P., Rogers, B.P., Carew, J.D., Seidenberg, M., and Meyerand, M.E. (2002). Diffusion tensor MRI in temporal lobe epilepsy. Magn Reson Imaging *20*, 511–519.

Ashburner, J. (2007). A fast diffeomorphic image registration algorithm. Neuroimage *38*, 95–113.

Assaf, Y., and Cohen, Y. (1998). Non-mono-exponential attenuation of water and N-acetyl aspartate signals due to diffusion in brain tissue. J Magn Reson *131*, 69–85.

Assaf, Y., Freidlin, R.Z., Rohde, G.K., and Basser, P.J. (2004). New modeling and experimental framework to characterize hindered and restricted water diffusion in brain white matter. Magn Reson Med *52*, 965–978.

Axelrod, B.N., Fichtenberg, N.L., Liethen, P.C., Czarnota, M.A., and Stucky, K. (2001). Performance characteristics of postacute traumatic brain injury patients on the WAIS-III and WMS-III. Clin Neuropsychol *15*, 516–520.

Banerjee, P., and Hauser, W. (2008). Incidence and prevalence. In Epilepsy: A Comprehensive Textbook, J.J. Engel, and T. Pedley, eds. (Philadelphia: Lippincott Williams & Wilkins),.

Bartenstein, P.A., Duncan, J.S., Prevett, M.C., Cunningham, V.J., Fish, D.R., Jones, A.K., Luthra, S.K., Sawle, G. V, and Brooks, D.J. (1993). Investigation of the opioid system in absence seizures with positron emission tomography. J Neurol Neurosurg Psychiatry *56*, 1295–1302.

Bartolomei, F., Chauvel, P., and Wendling, F. (2008). Epileptogenicity of brain structures in human temporal lobe epilepsy: a quantified study from intracerebral EEG. Brain *131*, 1818–1830.

Basser, P.J., Mattiello, J., and LeBihan, D. (1994a). Estimation of the effective self-diffusion tensor from the NMR spin echo. J Magn Reson B *103*, 247–254.

Basser, P.J., Mattiello, J., and LeBihan, D. (1994b). MR diffusion tensor spectroscopy and imaging. Biophys J *66*, 259–267.

Basser, P.J., Pajevic, S., Pierpaoli, C., Duda, J., and Aldroubi, A. (2000). In vivo fiber tractography using DT-MRI data. Magn Reson Med *44*, 625–632.

Basser, P.J., and Pierpaoli, C. (1996). Microstructural and physiological features of tissues elucidated by quantitative-diffusion-tensor MRI. J Magn Reson B *111*, 209–219.

Bassett, D.S., Bullmore, E., Verchinski, B. a, Mattay, V.S., Weinberger, D.R., and Meyer-Lindenberg, A. (2008). Hierarchical organization of human cortical networks in health and schizophrenia. J Neurosci *28*, 9239–9248.

158

Batchelor, P.G., Atkinson, D., Hill, D.L., Calamante, F., and Connelly, A. (2003). Anisotropic noise propagation in diffusion tensor MRI sampling schemes. Magn Reson Med *49*, 1143–1151.

Bava, S., Boucquey, V., Goldenberg, D., Thayer, R.E., Ward, M., Jacobus, J., and Tapert, S.F. (2011). Sex differences in adolescent white matter architecture. Brain Res *1375*, 41–48.

Beaulieu, C. (2002). The basis of anisotropic water diffusion in the nervous system - a technical review. NMR Biomed *15*, 435–455.

Beaulieu, C., and Allen, P.S. (1994). Water diffusion in the giant axon of the squid: implications for diffusion-weighted MRI of the nervous system. Magn Reson Med *32*, 579–583.

Beaulieu, C., Does, M.D., Snyder, R.E., and Allen, P.S. (1996). Changes in water diffusion due to Wallerian degeneration in peripheral nerve. Magn Reson Med *36*, 627–631.

Behrens, T.E., Berg, H.J., Jbabdi, S., Rushworth, M.F., and Woolrich, M.W. (2007). Probabilistic diffusion tractography with multiple fibre orientations: What can we gain? Neuroimage *34*, 144–155.

Behrens, T.E.J., Woolrich, M.W., Jenkinson, M., Johansen-Berg, H., Nunes, R.G., Clare, S., Matthews, P.M., Brady, J.M., and Smith, S.M. (2003). Characterization and propagation of uncertainty in diffusion-weighted MR imaging. Magn Reson Med *50*, 1077–1088.

Beirowski, B., Nógrádi, A., Babetto, E., Garcia-Alias, G., and Coleman, M.P. (2010). Mechanisms of axonal spheroid formation in central nervous system Wallerian degeneration. J Neuropathol Exp Neurol *69*, 455–472.

Bell, B.D., and Davies, K.G. (1998). Anterior temporal lobectomy, hippocampal sclerosis, and memory: recent neuropsychological findings. Neuropsychol Rev *8*, 25–41.

Berg, A.T., Berkovic, S.F., Brodie, M.J., Buchhalter, J., Cross, J.H., Van Emde Boas, W., Engel, J., French, J., Glauser, T.A., Mathern, G.W., et al. (2010). Revised terminology and concepts for organization of seizures and epilepsies: report of the ILAE Commission on Classification and Terminology, 2005-2009. Epilepsia *51*, 676–685.

Berg, A.T., and Scheffer, I.E. (2011). New concepts in classification of the epilepsies: entering the 21st century. Epilepsia *52*, 1058–1062.

Berger, I., Dor, T., Halvardson, J., Edvardson, S., Shaag, A., Feuk, L., and Elpeleg, O. (2012). Intractable epilepsy of infancy due to homozygous mutation in the EFHC1 gene. Epilepsia *53*, 1436–1440.

Bernard, C., Esclapez, M., Hirsch, J.C., and Ben-Ari, Y. (1998). Interneurones are not so dormant in temporal lobe epilepsy: a critical reappraisal of the dormant basket cell hypothesis. Epilepsy Res *32*, 93–103.

Bernasconi, A., Bernasconi, N., Natsume, J., Antel, S.B., Andermann, F., and Arnold, D.L. (2003a). Magnetic resonance spectroscopy and imaging of the thalamus in idiopathic generalized epilepsy. Brain *126*, 2447–2454.

Bernasconi, N., Andermann, F., Arnold, D.L., and Bernasconi, A. (2003b). Entorhinal cortex MRI assessment in temporal, extratemporal, and idiopathic generalized epilepsy. Epilepsia *44*, 1070–1074.

Bernasconi, N., Bernasconi, A., Andermann, F., Dubeau, F., Feindel, W., and Reutens, D.C. (1999). Entorhinal cortex in temporal lobe epilepsy: a quantitative MRI study. Neurology *52*, 1870–1876.

Bernasconi, N., Bernasconi, A., Caramanos, Z., Andermann, F., Dubeau, F., and Arnold, D.L. (2000). Morphometric MRI analysis of the parahippocampal region in temporal lobe epilepsy. Ann N Y Acad Sci *911*, 495–500.

Bernasconi, N., Bernasconi, A., Caramanos, Z., Antel, S.B., Andermann, F., and Arnold, D.L. (2003c). Mesial temporal damage in temporal lobe epilepsy: a volumetric MRI study of the hippocampus, amygdala and parahippocampal region. Brain *126*, 462–469.

Bernasconi, N., Bernasconi, A., Caramanos, Z., Dubeau, F., Richardson, J., Andermann, F., and Arnold, D.L. (2001). Entorhinal cortex atrophy in epilepsy patients exhibiting normal hippocampal volumes. Neurology *56*, 1335–1339.

Bernasconi, N., Duchesne, S., Janke, A., Lerch, J., Collins, D.L., and Bernasconi, A. (2004). Whole-brain voxel-based statistical analysis of gray matter and white matter in temporal lobe epilepsy. Neuroimage *23*, 717–723.

Bernhardt, B.C., Bernasconi, N., Kim, H., and Bernasconi, A. (2012). Mapping thalamocortical network pathology in temporal lobe epilepsy. Neurology *78*, 129–136.

Bernhardt, B.C., Chen, Z., He, Y., Evans, A.C., and Bernasconi, N. (2011). Graph-theoretical analysis reveals disrupted small-world organization of cortical thickness correlation networks in temporal lobe epilepsy. Cereb Cortex *21*, 2147–2157.

Bernhardt, B.C., Rozen, D.A., Worsley, K.J., Evans, A.C., Bernasconi, N., and Bernasconi, A. (2009a). Thalamo-cortical network pathology in idiopathic generalized epilepsy: insights from MRI-based morphometric correlation analysis. Neuroimage *46*, 373–381.

Bernhardt, B.C., Worsley, K.J., Kim, H., Evans, A.C., Bernasconi, A., and Bernasconi, N. (2009b). Longitudinal and cross-sectional analysis of atrophy in pharmacoresistant temporal lobe epilepsy. Neurology *72*, 1747–1754.

Betting, L.E., Li, L.M., Lopes-Cendes, I., Guerreiro, M.M., Guerreiro, C.A., and Cendes, F. (2010). Correlation between quantitative EEG and MRI in idiopathic generalized epilepsy. Hum Brain Mapp.

Betting, L.E., Mory, S.B., Li, L.M., Lopes-Cendes, I., Guerreiro, M.M., Guerreiro, C.A., and Cendes, F. (2006). Voxel-based morphometry in patients with idiopathic generalized epilepsies. Neuroimage *32*, 498–502.

Blume, W.T., Lüders, H.O., Mizrahi, E., Tassinari, C., Van Emde Boas, W., and Engel, J. (2001). Glossary of descriptive terminology for ictal semiology: report of the ILAE task force on classification and terminology. Epilepsia *42*, 1212–1218.

Bonilha, L., Edwards, J.C., Kinsman, S.L., Morgan, P.S., Fridriksson, J., Rorden, C., Rumboldt, Z., Roberts, D.R., Eckert, M.A., and Halford, J.J. (2010). Extrahippocampal gray matter loss and hippocampal deafferentation in patients with temporal lobe epilepsy. Epilepsia *51*, 519–528.

Bonilha, L., Halford, J.J., Rorden, C., Roberts, D.R., Rumboldt, Z., and Eckert, M.A. (2009). Automated MRI analysis for identification of hippocampal atrophy in temporal lobe epilepsy. Epilepsia *50*, 228–233.

Bonilha, L., Nesland, T., Martz, G.U., Joseph, J.E., Spampinato, M. V, Edwards, J.C., and Tabesh, A. (2012). Medial temporal lobe epilepsy is associated with neuronal fibre loss and paradoxical increase in structural connectivity of limbic structures. J Neurol Neurosurg Psychiatry.

Bonilha, L., Rorden, C., Appenzeller, S., Coan, A.C., Cendes, F., and Li, L.M. (2006). Gray matter atrophy associated with duration of temporal lobe epilepsy. Neuroimage *32*, 1070–1079.

Bonilha, L., Rorden, C., Castellano, G., Cendes, F., and Li, L.M. (2005). Voxel-based morphometry of the thalamus in patients with refractory medial temporal lobe epilepsy. Neuroimage *25*, 1016–1021.

Bonilha, L., Rorden, C., Castellano, G., Pereira, F., Rio, P.A., Cendes, F., and Li, L.M. (2004). Voxel-based morphometry reveals gray matter network atrophy in refractory medial temporal lobe epilepsy. Arch Neurol *61*, 1379–1384.

Bonilha, L., Rorden, C., Halford, J.J., Eckert, M., Appenzeller, S., Cendes, F., and Li, L.M. (2007). Asymmetrical extra-hippocampal grey matter loss related to hippocampal atrophy in patients with medial temporal lobe epilepsy. J Neurol Neurosurg Psychiatry *78*, 286–294.

Brázdil, M., Marecek, R., Fojtíková, D., Mikl, M., Kuba, R., Krupa, P., and Rektor, I. (2009). Correlation study of optimized voxel-based morphometry and (1)H MRS in patients with mesial temporal lobe epilepsy and hippocampal sclerosis. Hum Brain Mapp *30*, 1226–1235.

Briellmann, R.S., Berkovic, S.F., Syngeniotis, A., King, M.A., and Jackson, G.D. (2002). Seizure-associated hippocampal volume loss: a longitudinal magnetic resonance study of temporal lobe epilepsy. Ann Neurol *51*, 641–644.

Brown, J. a., Terashima, K.H., Burggren, A.C., Ercoli, L.M., Miller, K.J., Small, G.W., and Bookheimer, S.Y. (2011). Brain network local interconnectivity loss in aging APOE-4 allele carriers. Proc Natl Acad Sci U S A *108*, 20760–20765.

Brown, R. (1828). A brief account of microscopical observations made in the months of June, July and August, 1827, on the particles contained in the pollen of plants; and on the general existence of active molecules in organic and inorganic bodies. Phil. Mag. *4*, 161–173.

Budde, M.D., and Frank, J.A. (2010). Neurite beading is sufficient to decrease the apparent diffusion coefficient after ischemic stroke. Proc Natl Acad Sci U S A *107*, 14472–14477.

Budde, M.D., Kim, J.H., Liang, H.F., Russell, J.H., Cross, A.H., and Song, S.K. (2008). Axonal injury detected by in vivo diffusion tensor imaging correlates with neurological disability in a mouse model of multiple sclerosis. NMR Biomed *21*, 589–597.

Budde, M.D., Kim, J.H., Liang, H.F., Schmidt, R.E., Russell, J.H., Cross, A.H., and Song, S.K. (2007). Toward accurate diagnosis of white matter pathology using diffusion tensor imaging. Magn Reson Med *57*, 688–695.

Budde, M.D., Xie, M., Cross, A.H., and Song, S.K. (2009). Axial diffusivity is the primary correlate of axonal injury in the experimental autoimmune encephalomyelitis spinal cord: a quantitative pixelwise analysis. J Neurosci *29*, 2805–2813.

Buono, R.J., Lohoff, F.W., Sander, T., Sperling, M.R., O'Connor, M.J., Dlugos, D.J., Ryan, S.G., Golden, G.T., Zhao, H., Scattergood, T.M., et al. (2004). Association between variation in the human KCNJ10 potassium ion channel gene and seizure susceptibility. Epilepsy Res *58*, 175–183.

Butler, T., Zaborszky, L., Wang, X., McDonald, C.R., Blackmon, K., Quinn, B.T., Dubois, J., Carlson, C., Barr, W.B., French, J., et al. (2013). Septal nuclei enlargement in human temporal lobe epilepsy without mesial temporal sclerosis. Neurology.

Camfield, P., and Camfield, C. (2010). Idiopathic generalized epilepsy with generalized tonic-clonic seizures (IGE-GTC): a population-based cohort with >20 year follow up for medical and social outcome. Epilepsy Behav *18*, 61–63.

Carne, R.P., O'Brien, T.J., Kilpatrick, C.J., MacGregor, L.R., Hicks, R.J., Murphy, M.A., Bowden, S.C., Kaye, A.H., and Cook, M.J. (2004). MRI-negative PET-positive temporal lobe epilepsy: a distinct surgically remediable syndrome. Brain *127*, 2276–2285.

Carr, H.Y., and Purcell, E.M. (1954). Effects of Diffusion on Free Precession in Nuclear Magnetic Resonance Experiments. Physical Review *94*, 630–638.

Cavanna, A.E., and Trimble, M.R. (2006). The precuneus: a review of its functional anatomy and behavioural correlates. Brain *129*, 564–583.

Cendes, F., Andermann, F., Gloor, P., Lopes-Cendes, I., Andermann, E., Melanson, D., Jones-Gotman, M., Robitaille, Y., Evans, A., and Peters, T. (1993). Atrophy of mesial structures in patients with temporal lobe epilepsy: cause or consequence of repeated seizures? Ann Neurol *34*, 795–801.

Chenevert, T.L., Brunberg, J.A., and Pipe, J.G. (1990). Anisotropic diffusion in human white matter: demonstration with MR techniques in vivo. Radiology *177*, 401–405.

Ciccarelli, O., Behrens, T.E., Altmann, D.R., Orrell, R.W., Howard, R.S., Johansen-Berg, H., Miller, D.H., Matthews, P.M., and Thompson, a J. (2006). Probabilistic diffusion tractography: a potential tool to assess the rate of disease progression in amyotrophic lateral sclerosis. Brain *129*, 1859–1871.

Ciumas, C., and Savic, I. (2006). Structural changes in patients with primary generalized tonic and clonic seizures. Neurology *67*, 683–686.

Ciumas, C., Wahlin, T.-B.R., Espino, C., and Savic, I. (2010). The dopamine system in idiopathic generalized epilepsies: identification of syndrome-related changes. Neuroimage *51*, 606–615.

Ciumas, C., Wahlin, T.-B.R., Jucaite, A., Lindstrom, P., Halldin, C., and Savic, I. (2008). Reduced dopamine transporter binding in patients with juvenile myoclonic epilepsy. Neurology *71*, 788–794.

Cleveland, G.G., Chang, D.C., Hazlewood, C.F., and Rorschach, H.E. (1976). Nuclear magnetic resonance measurement of skeletal muscle: anisotrophy of the diffusion coefficient of the intracellular water. Biophys J *16*, 1043–1053.

Coan, A.C., Appenzeller, S., Bonilha, L., Li, L.M., and Cendes, F. (2009). Seizure frequency and lateralization affect progression of atrophy in temporal lobe epilepsy. Neurology *73*, 834–842.

Coleman, M.P., and Perry, V.H. (2002). Axon pathology in neurological disease: a neglected therapeutic target. Trends Neurosci *25*, 532–537.

Concha, L., Beaulieu, C., Collins, D.L., and Gross, D.W. (2009). White-matter diffusion abnormalities in temporal-lobe epilepsy with and without mesial temporal sclerosis. J Neurol Neurosurg Psychiatry *80*, 312–319.

Concha, L., Beaulieu, C., and Gross, D.W. (2005a). Bilateral limbic diffusion abnormalities in unilateral temporal lobe epilepsy. Ann Neurol *57*, 188–196.

Concha, L., Beaulieu, C., Wheatley, B.M., and Gross, D.W. (2007). Bilateral white matter diffusion changes persist after epilepsy surgery. Epilepsia *48*, 931–940.

Concha, L., Gross, D.W., and Beaulieu, C. (2005b). Diffusion tensor tractography of the limbic system. AJNR Am J Neuroradiol *26*, 2267–2274.

Concha, L., Gross, D.W., Wheatley, B.M., and Beaulieu, C. (2006). Diffusion tensor imaging of time-dependent axonal and myelin degradation after corpus callosotomy in epilepsy patients. Neuroimage *32*, 1090–1099.

Concha, L., Livy, D.J., Beaulieu, C., Wheatley, B.M., and Gross, D.W. (2010). In vivo diffusion tensor imaging and histopathology of the fimbria-fornix in temporal lobe epilepsy. J Neurosci *30*, 996–1002.

Conturo, T.E., Lori, N.F., Cull, T.S., Akbudak, E., Snyder, A.Z., Shimony, J.S., McKinstry, R.C., Burton, H., and Raichle, M.E. (1999). Tracking neuronal fiber pathways in the living human brain. Proc Natl Acad Sci U S A *96*, 10422–10427.

Corballis, M., and Morgan, M. (1978). On the biological basis of human laterality: I. Evidence for a maturational left-right gradient. Behav Brain Sci *2*, 261–269.

Corcoran, R., and Upton, D. (1993). A role for the hippocampus in card sorting? Cortex *29*, 293–304.

Cormack, F., Gadian, D.G., Vargha-Khadem, F., Cross, J.H., Connelly, A., and Baldeweg, T. (2005). Extra-hippocampal grey matter density abnormalities in paediatric mesial temporal sclerosis. Neuroimage *27*, 635–643.

Cossette, P., Liu, L., Brisebois, K., Dong, H., Lortie, A., Vanasse, M., Saint-Hilaire, J.M., Carmant, L., Verner, A., Lu, W.Y., et al. (2002). Mutation of GABRA1 in an autosomal dominant form of juvenile myoclonic epilepsy. Nat Genet *31*, 184–189.

Coste, S., Ryvlin, P., Hermier, M., Ostrowsky, K., Adeleine, P., Froment, J.C., and Mauguière, F. (2002). Temporopolar changes in temporal lobe epilepsy: a quantitative MRI-based study. Neurology *59*, 855–861.

Coulter, D.A., and Lee, C.J. (1993). Thalamocortical rhythm generation in vitro: extra- and intracellular recordings in mouse thalamocortical slices perfused with low Mg2+ medium. Brain Res *631*, 137–142.

D'Agostino, D., Bertelli, M., Gallo, S., Cecchin, S., Albiero, E., Garofalo, P.G., Gambardella, A., St Hilaire, J.-M., Kwiecinski, H., Andermann, E., et al. (2004). Mutations and polymorphisms of the CLCN2 gene in idiopathic epilepsy. Neurology *63*, 1500–1502.

Das, S.R., Mechanic-Hamilton, D., Korczykowski, M., Pluta, J., Glynn, S., Avants, B.B., Detre, J.A., and Yushkevich, P.A. (2009). Structure specific analysis of the hippocampus in temporal lobe epilepsy. Hippocampus *19*, 517–525.

Davis, T.L., Wedeen, V.J., Weisskof, R.M., and Rosen, B.R. (1993). White matter tract visualization by echo-planar MRI. In Society of Magnetic Resonance in Medicine, 12th Annual Meeting, (New York),.

DeCarli, C., Hatta, J., Fazilat, S., Gaillard, W.D., and Theodore, W.H. (1998). Extratemporal atrophy in patients with complex partial seizures of left temporal origin. Ann Neurol *43*, 41–45.

Deppe, M., Kellinghaus, C., Duning, T., Moddel, G., Mohammadi, S., Deppe, K., Schiffbauer, H., Kugel, H., Keller, S.S., Ringelstein, E.B., et al. (2008). Nerve fiber impairment of anterior thalamocortical circuitry in juvenile myoclonic epilepsy. Neurology *71*, 1981–1985.

Devinsky, O., Gershengorn, J., Brown, E., Perrine, K., Vazquez, B., and Luciano, D. (1997). Frontal functions in juvenile myoclonic epilepsy. Neuropsychiatry Neuropsychol Behav Neurol *10*, 243–246.

Devous, M.D., Thisted, R.A., Morgan, G.F., Leroy, R.F., and Rowe, C.C. (1998). SPECT brain imaging in epilepsy: a meta-analysis. J Nucl Med *39*, 285–293.

Dibbens, L.M., Feng, H.-J., Richards, M.C., Harkin, L.A., Hodgson, B.L., Scott, D., Jenkins, M., Petrou, S., Sutherland, G.R., Scheffer, I.E., et al. (2004). GABRD encoding a protein for extra- or peri-synaptic GABAA receptors is a susceptibility locus for generalized epilepsies. Hum Mol Genet *13*, 1315–1319.

Didelot, A., Ryvlin, P., Lothe, A., Merlet, I., Hammers, A., and Mauguière, F. (2008). PET imaging of brain 5-HT1A receptors in the preoperative evaluation of temporal lobe epilepsy. Brain *131*, 2751–2764.

Diehl, B., Busch, R.M., Duncan, J.S., Piao, Z., Tkach, J., and Luders, H.O. (2008a). Abnormalities in diffusion tensor imaging of the uncinate fasciculus relate to reduced memory in temporal lobe epilepsy. Epilepsia *49*, 1409–1418.

Diehl, B., Busch, R.M., Duncan, J.S., Piao, Z., Tkach, J., and Lüders, H.O. (2008b). Abnormalities in diffusion tensor imaging of the uncinate fasciculus relate to reduced memory in temporal lobe epilepsy. Epilepsia *49*, 1409–1418.

Doelken, M.T., Mennecke, A., Stadlbauer, A., Kecskemeti, L., Kasper, B.S., Struffert, T., Doerfler, A., Stefan, H., and Hammen, T. (2010). Multi-voxel magnetic resonance spectroscopy at 3T in patients with idiopathic generalised epilepsy. Seizure.

Mac Donald, C.L., Dikranian, K., Bayly, P., Holtzman, D., and Brody, D. (2007a). Diffusion tensor imaging reliably detects experimental traumatic axonal injury and indicates approximate time of injury. J Neurosci *27*, 11869–11876.

Mac Donald, C.L., Dikranian, K., Song, S.K., Bayly, P. V, Holtzman, D.M., and Brody, D.L. (2007b). Detection of traumatic axonal injury with diffusion tensor imaging in a mouse model of traumatic brain injury. Exp Neurol *205*, 116–131.

Doran, M., Hajnal, J. V, Van Bruggen, N., King, M.D., Young, I.R., and Bydder, G.M. Normal and abnormal white matter tracts shown by MR imaging using directional diffusion weighted sequences. J Comput Assist Tomogr *14*, 865–873.

Dreifuss, S., Vingerhoets, F.J., Lazeyras, F., Andino, S.G., Spinelli, L., Delavelle, J., and Seeck, M. (2001). Volumetric measurements of subcortical nuclei in patients with temporal lobe epilepsy. Neurology *57*, 1636–1641.

Drew, M. a, Starkey, N.J., and Isler, R.B. (2009). Examining the link between information processing speed and executive functioning in multiple sclerosis. Arch Clin Neuropsychol *24*, 47–58.

Drobyshevsky, A., Song, S.-K., Gamkrelidze, G., Wyrwicz, A.M., Derrick, M., Meng, F., Li, L., Ji, X., Trommer, B., Beardsley, D.J., et al. (2005). Developmental changes in diffusion anisotropy coincide with immature oligodendrocyte progression and maturation of compound action potential. J Neurosci *25*, 5988–5997.

Du, H., Zhang, Y., Xie, B., Wu, N., Wu, G., Wang, J., Jiang, T., and Feng, H. (2011). Regional atrophy of the basal ganglia and thalamus in idiopathic generalized epilepsy. J Magn Reson Imaging *33*, 817–821.

Dudek, F.E., Obenaus, A., Schweitzer, J.S., and Wuarin, J.P. (1994). Functional significance of hippocampal plasticity in epileptic brain: electrophysiological changes of the dentate granule cells associated with mossy fiber sprouting. Hippocampus *4*, 259–265.

Dupont, S., Van de Moortele, P.F., Samson, S., Hasboun, D., Poline, J.B., Adam, C., Lehéricy, S., Le Bihan, D., Samson, Y., and Baulac, M. (2000). Episodic memory in left temporal lobe epilepsy: a functional MRI study. Brain *123 (Pt 8*, 1722–1732.

Dyrby, T.B., Søgaard, L. V, Parker, G.J., Alexander, D.C., Lind, N.M., Baaré, W.F.C., Hay-Schmidt, A., Eriksen, N., Pakkenberg, B., Paulson, O.B., et al. (2007). Validation of in vitro probabilistic tractography. Neuroimage *37*, 1267–1277.

Einstein, A. (1905). Über die von der molekularkinetischen Theorie der Wärme geforderte Bewegung von in ruhenden Flüssigkeiten suspendierten Teilchen. Ann Phys *322*, 549–560.

Engel Jr., J. (2001). A proposed diagnostic scheme for people with epileptic seizures and with epilepsy: report of the ILAE Task Force on Classification and Terminology. Epilepsia *42*, 796–803.

Faber, J., Schoene-Bake, J.-C., Trautner, P., Von Lehe, M., Elger, C.E., and Weber, B. (2013). Progressive fiber tract affections after temporal lobe surgery. Epilepsia 1–5.

Falconer, M.A. (1974). Mesial temporal (Ammon's horn) sclerosis as a common cause of epilepsy. Aetiology, treatment, and prevention. Lancet *2*, 767–770.

Filho, G.M.D.A., Jackowski, A.P., Lin, K., Silva, I., S B Guaranha, M., Guilhoto, L.M.F.F., Júnior, H.C., Yacubian, E.M.T., and Bressan, R.A. (2010). The integrity of corpus callosum and cluster B personality disorders: a quantitative MRI study in juvenile myoclonic epilepsy. Prog Neuropsychopharmacol Biol Psychiatry *34*, 516–521.

Fischl, B., Salat, D.H., Busa, E., Albert, M., Dieterich, M., Haselgrove, C., Van der Kouwe, A., Killiany, R., Kennedy, D., Klaveness, S., et al. (2002). Whole brain segmentation: automated labeling of neuroanatomical structures in the human brain. Neuron *33*, 341–355.

Fischl, B., Salat, D.H., Van der Kouwe, A.J.W., Makris, N., Ségonne, F., Quinn, B.T., and Dale, A.M. (2004). Sequence-independent segmentation of magnetic resonance images. Neuroimage *23 Suppl 1*, S69–84.

Fisher, R.S., Van Emde Boas, W., Blume, W., Elger, C., Genton, P., Lee, P., and Engel, J. (2005). Epileptic seizures and epilepsy: definitions proposed by the International League Against Epilepsy (ILAE) and the International Bureau for Epilepsy (IBE). Epilepsia *46*, 470–472.

Focke, N.K., Yogarajah, M., Bonelli, S.B., Bartlett, P.A., Symms, M.R., and Duncan, J.S. (2008). Voxel-based diffusion tensor imaging in patients with mesial temporal lobe epilepsy and hippocampal sclerosis. Neuroimage *40*, 728–737.

Ford, J.C., Hackney, D.B., Alsop, D.C., Jara, H., Joseph, P.M., Hand, C.M., and Black, P. (1994). MRI characterization of diffusion coefficients in a rat spinal cord injury model. Magn Reson Med *31*, 488–494.

French, J.A., Williamson, P.D., Thadani, V.M., Darcey, T.M., Mattson, R.H., Spencer, S.S., and Spencer, D.D. (1993). Characteristics of medial temporal lobe epilepsy: I. Results of history and physical examination. Ann Neurol *34*, 774–780.

Fuerst, D., Shah, J., Shah, A., and Watson, C. (2003). Hippocampal sclerosis is a progressive disorder: a longitudinal volumetric MRI study. Ann Neurol *53*, 413–416.

Gardiner, M. (2005). Genetics of Idiopathic Generalized Epilepsies. Epilepsia *46*, 15–20.

Genovese, C.R., Lazar, N.A., and Nichols, T. (2002). Thresholding of statistical maps in functional neuroimaging using the false discovery rate. Neuroimage *15*, 870–878.

George, E.B., Glass, J.D., and Griffin, J.W. (1995). Axotomy-induced axonal degeneration is mediated by calcium influx through ion-specific channels. J Neurosci *15*, 6445–6452.

George, R., and Griffin, J.W. (1994). Delayed macrophage responses and myelin clearance during Wallerian degeneration in the central nervous system: the dorsal radiculotomy model. Exp Neurol *129*, 225–236.

Giannelli, M., Cosottini, M., Michelassi, M.C., Lazzarotti, G., Belmonte, G., Bartolozzi, C., and Lazzeri, M. (2009). Dependence of brain DTI maps of fractional anisotropy and mean diffusivity on the number of diffusion weighting directions. J Appl Clin Med Phys *11*, 2927.

Giovagnoli, A.R., Franceschetti, S., Reati, F., Parente, A., Maccagnano, C., Villani, F., and Spreafico, R. (2011). Theory of mind in frontal and temporal lobe epilepsy: cognitive and neural aspects. Epilepsia *52*, 1995–2002.

Gloor, P. (1979). Generalized epilepsy with spike-and-wave discharge: a reinterpretation of its electrographic and clinical manifestations. The 1977 William G. Lennox Lecture, American Epilepsy Society. Epilepsia *20*, 571–588.

Gloor, P., and Fariello, R.G. (1988). Generalized epilepsy: some of its cellular mechanisms differ from those of focal epilepsy. Trends Neurosci *11*, 63–68.

Goldman-Rakic, P.S. (1987). Development of cortical circuitry and cognitive function. Child Dev *58*, 601–622.

Gong, G., Concha, L., Beaulieu, C., and Gross, D.W. (2008a). Thalamic diffusion and volumetry in temporal lobe epilepsy with and without mesial temporal sclerosis. Epilepsy Res *80*, 184–193.

Gong, G., He, Y., Concha, L., Lebel, C., Gross, D.W., Evans, A.C., and Beaulieu, C. (2008b). Mapping Anatomical Connectivity Patterns of Human Cerebral Cortex Using In Vivo Diffusion Tensor Imaging Tractography. Cereb Cortex.

Gong, G., Rosa-Neto, P., Carbonell, F., Chen, Z.J., He, Y., and Evans, A.C. (2009). Age- and gender-related differences in the cortical anatomical network. J Neurosci *29*, 15684–15693.

Govindan, R.M., Makki, M.I., Sundaram, S.K., Juhász, C., and Chugani, H.T. (2008). Diffusion tensor analysis of temporal and extra-temporal lobe tracts in temporal lobe epilepsy. Epilepsy Res *80*, 30–41.

Greenberg, D.A., Cayanis, E., Strug, L., Marathe, S., Durner, M., Pal, D.K., Alvin, G.B., Klotz, I., Dicker, E., Shinnar, S., et al. (2005). Malic enzyme 2 may underlie susceptibility to adolescent-onset idiopathic generalized epilepsy. Am J Hum Genet *76*, 139–146.

Gross, D.W., Concha, L., and Beaulieu, C. (2006). Extratemporal white matter abnormalities in mesial temporal lobe epilepsy demonstrated with diffusion tensor imaging. Epilepsia *47*, 1360–1363.

Hahn, E.L. (1950). SPIN ECHOES. Physical Review *80*, 580–594.

Haki, C., Gumustas, O.G., Bora, I., Gumustas, A.U., and Parlak, M. (2007). Proton magnetic resonance spectroscopy study of bilateral thalamus in juvenile myoclonic epilepsy. Seizure *16*, 287–295.

Hansen, J.R. (1971). Pulsed NMR study of water mobility in muscle and brain tissue. Biochim Biophys Acta *230*, 482–486.

Haug, K., Warnstedt, M., Alekov, A.K., Sander, T., Ramírez, A., Poser, B., Maljevic, S., Hebeisen, S., Kubisch, C., Rebstock, J., et al. (2003). Mutations in CLCN2 encoding a voltage-gated chloride channel are associated with idiopathic generalized epilepsies. Nat Genet *33*, 527–532.

He, Y., Chen, Z.J., and Evans, A.C. (2007). Small-world anatomical networks in the human brain revealed by cortical thickness from MRI. Cereb Cortex *17*, 2407–2419.

Helms, G., Ciumas, C., Kyaga, S., and Savic, I. (2006). Increased thalamus levels of glutamate and glutamine (Glx) in patients with idiopathic generalised epilepsy. J Neurol Neurosurg Psychiatry *77*, 489–494.

Helmstaedter, C., and Elger, C.E. (2009). Chronic temporal lobe epilepsy: a neurodevelopmental or progressively dementing disease? Brain *132*, 2822–2830.

Helmstaedter, C., Kurthen, M., Lux, S., Reuber, M., and Elger, C.E. (2003). Chronic epilepsy and cognition: a longitudinal study in temporal lobe epilepsy. Ann Neurol *54*, 425–432.

Helmstaedter, C., Petzold, I., and Bien, C.G. (2011). The cognitive consequence of resecting nonlesional tissues in epilepsy surgery--results from MRI- and histopathology-negative patients with temporal lobe epilepsy. Epilepsia *52*, 1402–1408.

Hermann, B., Seidenberg, M., Bell, B., Rutecki, P., Sheth, R., Ruggles, K., Wendt, G., O'Leary, D., and Magnotta, V. (2002). The neurodevelopmental impact of childhood-onset temporal lobe epilepsy on brain structure and function. Epilepsia *43*, 1062–1071.

Hermann, B., Seidenberg, M., Bell, B., Rutecki, P., Sheth, R.D., Wendt, G., O'Leary, D., and Magnotta, V. (2003). Extratemporal quantitative MR volumetrics and neuropsychological status in temporal lobe epilepsy. J Int Neuropsychol Soc *9*, 353–362.

Hermann, B.P., Seidenberg, M., Dow, C., Jones, J., Rutecki, P., Bhattacharya, A., and Bell, B. (2006). Cognitive prognosis in chronic temporal lobe epilepsy. Ann Neurol *60*, 80–87.

Hesdorffer, D.C., Logroscino, G., Benn, E.K.T., Katri, N., Cascino, G., and Hauser, W.A. (2011). Estimating risk for developing epilepsy: a population-based study in Rochester, Minnesota. Neurology *76*, 23–27.

Van den Heuvel, M.P., Stam, C.J., Kahn, R.S., and Hulshoff Pol, H.E. (2009). Efficiency of functional brain networks and intellectual performance. J Neurosci *29*, 7619–7624.

Hogan, R.E., Bucholz, R.D., and Joshi, S. (2003). Hippocampal deformation-based shape analysis in epilepsy and unilateral mesial temporal sclerosis. Epilepsia *44*, 800–806.

Hogan, R.E., Wang, L., Bertrand, M.E., Willmore, L.J., Bucholz, R.D., Nassif, A.S., and Csernansky, J.G. (2004). MRI-based high-dimensional hippocampal mapping in mesial temporal lobe epilepsy. Brain *127*, 1731–1740.

Holmes, M.D., Quiring, J., and Tucker, D.M. (2010). Evidence that juvenile myoclonic epilepsy is a disorder of frontotemporal corticothalamic networks. Neuroimage *49*, 80–93.

Horstmann, M.-T., Bialonski, S., Noennig, N., Mai, H., Prusseit, J., Wellmer, J., Hinrichs, H., and Lehnertz, K. (2010). State dependent properties of epileptic brain networks: comparative graph-theoretical analyses of simultaneously recorded EEG and MEG. Clin Neurophysiol *121*, 172–185.

Humphries, M.D., Gurney, K., and Prescott, T.J. (2006). The brainstem reticular formation is a small-world, not scale-free, network. Proc Biol Sci *273*, 503–511.

ILAE (1989). Proposal for revised classification of epilepsies and epileptic syndromes. Commission on Classification and Terminology of the International League Against Epilepsy. Epilepsia *30*, 389–399.

Iqbal, N., Caswell, H.L., Hare, D.J., Pilkington, O., Mercer, S., and Duncan, S. (2009). Neuropsychological profiles of patients with juvenile myoclonic epilepsy and their siblings: a preliminary controlled experimental video-EEG case series. Epilepsy Behav *14*, 516–521.

Iturria-Medina, Y., Sotero, R.C., Canales-Rodríguez, E.J., Alemán-Gómez, Y., and Melie-García, L. (2008). Studying the human brain anatomical network via diffusion-weighted MRI and Graph Theory. Neuroimage *40*, 1064–1076.

Jack, C.R., Sharbrough, F.W., Cascino, G.D., Hirschorn, K.A., O'Brien, P.C., and Marsh, W.R. (1992). Magnetic resonance image-based hippocampal volumetry: correlation with outcome after temporal lobectomy. Ann Neurol *31*, 138–146.

Janz, D. (1985). Epilepsy with impulsive petit mal (juvenile myoclonic epilepsy). Acta Neurol Scand *72*, 449–459.

Jara-Prado, A., Martínez-Juárez, I.E., Ochoa, A., González, V.M., Fernández-González-Aragón, M.D.C., López-Ruiz, M., Medina, M.T., Bailey, J.N., Delgado-Escueta, A. V, and Alonso, M.E. (2012). Novel Myoclonin1/EFHC1 mutations in Mexican patients with juvenile myoclonic epilepsy. Seizure *21*, 550–554.

Jeffrey, D.R., David, L.F., Vicky, C., Ronald, C.K., Devin, K.B., Steven, C.C., Jack, J.L., Riley, J.D., Franklin, D.L., Choi, V., et al. (2010). Altered white matter integrity in temporal lobe epilepsy: Association with cognitive and clinical profiles. Epilepsia *51*, 536–545.

Jerome Engel, J. (2013). Seizures and Epilepsy (Oxford University Press).

Jinde, S., Zsiros, V., and Nakazawa, K. (2013). Hilar mossy cell circuitry controlling dentate granule cell excitability. Front Neural Circuits *7*, 14.

Jones, D.K. (2003). Determining and visualizing uncertainty in estimates of fiber orientation from diffusion tensor MRI. Magn Reson Med *49*, 7–12.

Jones, D.K. (2004). The effect of gradient sampling schemes on measures derived from diffusion tensor MRI: a Monte Carlo study. Magn Reson Med *51*, 807–815.

Jones, D.K. (2008). Tractography gone wild: probabilistic fibre tracking using the wild bootstrap with diffusion tensor MRI. IEEE Trans Med Imaging *27*, 1268–1274.

Jones, D.K., Simmons, A., Williams, S.C., and Horsfield, M.A. (1999). Non-invasive assessment of axonal fiber connectivity in the human brain via diffusion tensor MRI. Magn Reson Med *42*, 37–41.

Jutila, L., Ylinen, A., Partanen, K., Alafuzoff, I., Mervaala, E., Partanen, J., Vapalahti, M., Vainio, P., and Pitkänen, A. (2001). MR volumetry of the entorhinal, perirhinal, and temporopolar cortices in drug-refractory temporal lobe epilepsy. AJNR Am J Neuroradiol *22*, 1490–1501.

Kaaden, S., Quesada, C.M., Urbach, H., Koenig, R., Weber, B., Schramm, J., Rudinger, G., and Helmstaedter, C. (2011). Neurodevelopmental disruption in early-onset temporal lobe epilepsy: evidence from a voxel-based morphometry study. Epilepsy Behav *20*, 694–699.

Kälviäinen, R., Salmenperä, T., Partanen, K., Vainio, P., Riekkinen, P., and Pitkänen, a (1998). Recurrent seizures may cause hippocampal damage in temporal lobe epilepsy. Neurology *50*, 1377–1382.

Keller, S.S., Ahrens, T., Mohammadi, S., Gerdes, J.S., Möddel, G., Kellinghaus, C., Kugel, H., Weber, B., Ringelstein, E.B., and Deppe, M. (2011a). Voxel-Based Statistical Analysis of Fractional Anisotropy and Mean Diffusivity in Patients with Unilateral Temporal Lobe Epilepsy of Unknown Cause. J Neuroimaging 1–8.

Keller, S.S., Ahrens, T., Mohammadi, S., Moddel, G., Kugel, H., Bernd Ringelstein, E., and Deppe, M. (2011b). Microstructural and volumetric abnormalities of the putamen in juvenile myoclonic epilepsy. Epilepsia.

Keller, S.S., Baker, G., Downes, J.J., and Roberts, N. (2009). Quantitative MRI of the prefrontal cortex and executive function in patients with temporal lobe epilepsy. Epilepsy Behav *15*, 186–195.

Keller, S.S., Mackay, C.E., Barrick, T.R., Wieshmann, U.C., Howard, M.A., and Roberts, N. (2002a). Voxel-based morphometric comparison of hippocampal and

extrahippocampal abnormalities in patients with left and right hippocampal atrophy. Neuroimage *16*, 23–31.

Keller, S.S., and Roberts, N. (2008). Voxel-based morphometry of temporal lobe epilepsy: an introduction and review of the literature. Epilepsia *49*, 741–757.

Keller, S.S., Schoene-Bake, J.-C., Gerdes, J.S., Weber, B., and Deppe, M. (2012). Concomitant fractional anisotropy and volumetric abnormalities in temporal lobe epilepsy: cross-sectional evidence for progressive neurologic injury. PLoS One *7*, e46791.

Keller, S.S., Wieshmann, U.C., Mackay, C.E., Denby, C.E., Webb, J., and Roberts, N. (2002b). Voxel based morphometry of grey matter abnormalities in patients with medically intractable temporal lobe epilepsy: effects of side of seizure onset and epilepsy duration. Journal of Neurology, Neurosurgery & Psychiatry *73*, 648–655.

Kemmotsu, N., Girard, H.M., Bernhardt, B.C., Bonilha, L., Lin, J.J., Tecoma, E.S., Iragui, V.J., Hagler, D.J., Halgren, E., and McDonald, C.R. (2011). MRI analysis in temporal lobe epilepsy: Cortical thinning and white matter disruptions are related to side of seizure onset. Epilepsia 1–10.

Kerschensteiner, M., Schwab, M.E., Lichtman, J.W., and Misgeld, T. (2005). In vivo imaging of axonal degeneration and regeneration in the injured spinal cord. Nat Med *11*, 572–577.

Kim, C.H., Chung, C.K., Koo, B.-B., Lee, J.-M., Kim, J.S., and Lee, S.K. (2011). Changes in language pathways in patients with temporal lobe epilepsy: diffusion tensor imaging analysis of the uncinate and arcuate fasciculi. World Neurosurg *75*, 509–516.

Kim, H., Piao, Z., Liu, P., Bingaman, W., and Diehl, B. (2008). Secondary white matter degeneration of the corpus callosum in patients with intractable temporal lobe epilepsy: A diffusion tensor imaging study. Epilepsy Res *81*, 136–142.

Kim, J.H., Im, K.C., Kim, J.S., Lee, S.-A., and Kang, J.K. (2005). Correlation of interictal spike-wave with thalamic glucose metabolism in juvenile myoclonic epilepsy. Neuroreport *16*, 1151–1155.

Kim, J.H., Lee, J.K., Koh, S.-B., Lee, S.-A., Lee, J.-M., Kim, S.I., and Kang, J.K. (2007a). Regional grey matter abnormalities in juvenile myoclonic epilepsy: A voxel-based morphometry study. Neuroimage *37*, 1132–1137.

Kim, J.H., Loy, D.N., Liang, H.F., Trinkaus, K., Schmidt, R.E., and Song, S.K. (2007b). Noninvasive diffusion tensor imaging of evolving white matter pathology in a mouse model of acute spinal cord injury. Magn Reson Med *58*, 253–260.

Kim, J.H., Suh, S.-I., Park, S.-Y., Seo, W.-K., Koh, I., Koh, S.-B., and Seol, H.Y. (2012). Microstructural white matter abnormality and frontal cognitive dysfunctions in juvenile myoclonic epilepsy. Epilepsia *53*, 1371–1378.

Kleefuss-Lie, A., Friedl, W., Cichon, S., Haug, K., Warnstedt, M., Alekov, A., Sander, T., Ramirez, A., Poser, B., Maljevic, S., et al. (2009). CLCN2 variants in idiopathic generalized epilepsy. Nat Genet *41*, 954–955.

Knake, S., Salat, D.H., Halgren, E., Halko, M.A., Greve, D.N., and Grant, P.E. (2009). Changes in white matter microstructure in patients with TLE and hippocampal sclerosis. Epileptic Disord *11*, 244–250.

Kobayashi, E., Zifkin, B., Andermann, F., and Andermann, E. (2008). Juvenile Myoclonic Epilepsy. In Epilepsy: A Comprehensive Textbook, J. Engel, and T. Pedley, eds. (Philidelphia: Lippincott Williams & Wilkins), pp. 2455–2460.

Koch, M.A., Norris, D.G., and Hund-Georgiadis, M. (2002). An investigation of functional and anatomical connectivity using magnetic resonance imaging. Neuroimage *16*, 241–250.

Koepp, M.J. (2005). Juvenile myoclonic epilepsy--a generalized epilepsy syndrome? Acta Neurol Scand Suppl *181*, 57–62.

Koepp, M.J., Hammers, A., Labbé, C., Woermann, F.G., Brooks, D.J., and Duncan, J.S. (2000). 11C-flumazenil PET in patients with refractory temporal lobe epilepsy and normal MRI. Neurology *54*, 332–339.

Koepp, M.J., Labbé, C., Richardson, M.P., Brooks, D.J., Van Paesschen, W., Cunningham, V.J., and Duncan, J.S. (1997). Regional hippocampal [11C]flumazenil PET in temporal lobe epilepsy with unilateral and bilateral hippocampal sclerosis. Brain *120 (Pt 1*, 1865–1876.

Koutroumanidis, M., and Smith, S. (2005). Use and Abuse of EEG in the Diagnosis of Idiopathic Generalized Epilepsies. Epilepsia *46*, 96–107.

Kozlowski, P., Raj, D., Liu, J., Lam, C., Yung, A.C., and Tetzlaff, W. (2008). Characterizing white matter damage in rat spinal cord with quantitative MRI and histology. J Neurotrauma *25*, 653–676.

Kramer, M. a, Kolaczyk, E.D., and Kirsch, H.E. (2008). Emergent network topology at seizure onset in humans. Epilepsy Res *79*, 173–186.

Krampfl, K., Maljevic, S., Cossette, P., Ziegler, E., Rouleau, G.A., Lerche, H., and Bufler, J. (2005). Molecular analysis of the A322D mutation in the GABA receptor alpha-subunit causing juvenile myoclonic epilepsy. Eur J Neurosci *22*, 10–20.

Von Krosigk, M., Bal, T., and McCormick, D.A. (1993). Cellular mechanisms of a synchronized oscillation in the thalamus. Science (80-) *261*, 361–364.

Kwan, P., and Brodie, M. (2000). Early identification of refractory epilepsy. New England Journal of Medicine.

Labate, a, Cerasa, a, Gambardella, a, Aguglia, U., and Quattrone, a (2008). Hippocampal and thalamic atrophy in mild temporal lobe epilepsy: a VBM study. Neurology *71*, 1094–1101.

Labate, A., Cerasa, A., Aguglia, U., Mumoli, L., Quattrone, A., and Gambardella, A. (2011). Neocortical thinning in "benign" mesial temporal lobe epilepsy. Epilepsia *52*, 712–717.

Lambert, M. V, Brierley, B., Al-Sarraj, S., Shaw, P., Polkey, C.E., Chandler, C., Toone, B.K., and David, A.S. (2003). Quantitative magnetic resonance imaging of the amygdala in temporal lobe epilepsy-clinico-pathological correlations (a pilot study). Epilepsy Res *53*, 39–46.

Landman, B.A., Farrell, J.A., Jones, C.K., Smith, S.A., Prince, J.L., and Mori, S. (2007). Effects of diffusion weighting schemes on the reproducibility of DTI-derived fractional anisotropy, mean diffusivity, and principal eigenvector measurements at 1.5T. Neuroimage *36*, 1123–1138.

Landvogt, C., Buchholz, H.-G., Bernedo, V., Schreckenberger, M., and Werhahn, K.J. (2010). Alteration of dopamine D2/D3 receptor binding in patients with juvenile myoclonic epilepsy. Epilepsia *51*, 1699–1706.

Latora, V., and Marchiori, M. (2003). Economic small-world behavior in weighted networks. The European Physical Journal B-Condensed … 17.

Lawes, I.N., Barrick, T.R., Murugam, V., Spierings, N., Evans, D.R., Song, M., and Clark, C.A. (2008). Atlas-based segmentation of white matter tracts of the human brain using diffusion tensor tractography and comparison with classical dissection. Neuroimage *39*, 62–79.

Lazar, M., and Alexander, A.L. (2003). An error analysis of white matter tractography methods: synthetic diffusion tensor field simulations. Neuroimage *20*, 1140–1153.

Lebel, C., Benner, T., and Beaulieu, C. (2012). Six is enough? Comparison of diffusion parameters measured using six or more diffusion-encoding gradient directions with deterministic tractography. Magn Reson Med *68*, 474–483.

Lebel, C., Walker, L., Leemans, A., Phillips, L., and Beaulieu, C. (2008). Microstructural maturation of the human brain from childhood to adulthood. Neuroimage *40*, 1044–1055.

Lee, J.W., Andermann, F., Dubeau, F., Bernasconi, a, MacDonald, D., Evans, A., and Reutens, D.C. (1998). Morphometric analysis of the temporal lobe in temporal lobe epilepsy. Epilepsia *39*, 727–736.

Lee, J.W., Reutens, D.C., Dubeau, F., Evans, A., and Andermann, F. (1995). Morphometry in temporal lobe epilepsy. Magn Reson Imaging *13*, 1073–1080.

Leemans, A., Jeurissen, B., Sijbers, J., and Jones, D. (2009). ExploreDTI : a graphical toolbox for processing , analyzing , and visualizing diffusion MR data. In 17th Annual Meeting of Intl Soc Mag Reson Med, Hawaii, USA, p. 3537.

Li, Y., Du, H., Xie, B., Wu, N., Wang, J., Wu, G., Feng, H., and Jiang, T. (2011). Cerebellum abnormalities in idiopathic generalized epilepsy with generalized tonic-clonic seizures revealed by diffusion tensor imaging. PLoS One *5*, e15219.

Liacu, D., Idy-Peretti, I., Ducreux, D., Bouilleret, V., and De Marco, G. (2012). Diffusion tensor imaging tractography parameters of limbic system bundles in temporal lobe epilepsy patients. J Magn Reson Imaging *000*, 1–8.

Liao, W., Zhang, Z., Pan, Z., Mantini, D., Ding, J., Duan, X., Luo, C., Lu, G., and Chen, H. (2010). Altered functional connectivity and small-world in mesial temporal lobe epilepsy. PLoS One *5*, e8525.

Liao, W., Zhang, Z., Pan, Z., Mantini, D., Ding, J., Duan, X., Luo, C., Wang, Z., Tan, Q., Lu, G., et al. (2011). Default mode network abnormalities in mesial temporal lobe epilepsy: a study combining fMRI and DTI. Hum Brain Mapp *32*, 883–895.

Liew, C.J., Lim, Y.-M., Bonwetsch, R., Shamim, S., Sato, S., Reeves-Tyer, P., Herscovitch, P., Dustin, I., Bagic, A., Giovacchini, G., et al. (2009). 18F-FCWAY and 18F-FDG PET in MRI-negative temporal lobe epilepsy. Epilepsia *50*, 234–239.

Lin, J.J., Riley, J.D., Juranek, J., and Cramer, S.C. (2008). Vulnerability of the frontal-temporal connections in temporal lobe epilepsy. Epilepsy Res *82*, 162–170.

Lin, J.J., Salamon, N., Lee, A.D., Dutton, R.A., Geaga, J.A., Hayashi, K.M., Luders, E., Toga, A.W., Engel Jr., J., Thompson, P.M., et al. (2007). Reduced neocortical thickness and complexity mapped in mesial temporal lobe epilepsy with hippocampal sclerosis. Cereb Cortex *17*, 2007–2018.

Lin, K., Carrete Jr., H., Lin, J., Peruchi, M.M., De Araujo Filho, G.M., Guaranha, M.S., Guilhoto, L.M., Sakamoto, A.C., and Yacubian, E.M. (2009). Magnetic resonance spectroscopy reveals an epileptic network in juvenile myoclonic epilepsy. Epilepsia *50*, 1191–1200.

Liu, M., Concha, L., Lebel, C., Beaulieu, C., and Gross, D.W. (2012). Mesial temporal sclerosis is linked with more widespread white matter changes in temporal lobe epilepsy. NeuroImage: Clinical *1*, 99–105.

Liu, R.S., Lemieux, L., Bell, G.S., Sisodiya, S.M., Bartlett, P.A., Shorvon, S.D., Sander, J.W., and Duncan, J.S. (2005). Cerebral damage in epilepsy: a population-based longitudinal quantitative MRI study. Epilepsia *46*, 1482–1494.

Liu, R.S.., Lemieux, L., Bell, G.., Sisodiya, S.., Shorvon, S.., Sander, J.W. a. ., and Duncan, J.. (2003a). A longitudinal study of brain morphometrics using quantitative magnetic resonance imaging and difference image analysis. Neuroimage *20*, 22–33.

Liu, R.S.N., Lemieux, L., Bell, G.S., Hammers, A., Sisodiya, S.M., Bartlett, P.A., Shorvon, S.D., Sander, J.W.A.S., and Duncan, J.S. (2003b). Progressive neocortical damage in epilepsy. Ann Neurol *53*, 312–324.

Lo, C.-Y., Wang, P.-N., Chou, K.-H., Wang, J., He, Y., and Lin, C.-P. (2010). Diffusion tensor tractography reveals abnormal topological organization in structural cortical networks in Alzheimer's disease. J Neurosci *30*, 16876–16885.

Luciano, A.L., and Shorvon, S.D. (2007). Results of treatment changes in patients with apparently drug-resistant chronic epilepsy. Ann Neurol *62*, 375–381.

Lythgoe, M.F., Busza, A.L., Calamante, F., Sotak, C.H., King, M.D., Bingham, A.C., Williams, S.R., and Gadian, D.G. (1997). Effects of diffusion anisotropy on lesion delineation in a rat model of cerebral ischemia. Magn Reson Med *38*, 662–668.

Macdonald, R.L., Gallagher, M.J., Feng, H.-J., and Kang, J. (2004). GABA(A) receptor epilepsy mutations. Biochem Pharmacol *68*, 1497–1506.

Maljevic, S., Krampfl, K., Cobilanschi, J., Tilgen, N., Beyer, S., Weber, Y.G., Schlesinger, F., Ursu, D., Melzer, W., Cossette, P., et al. (2006). A mutation in the GABA(A) receptor alpha(1)-subunit is associated with absence epilepsy. Ann Neurol *59*, 983–987.

Malykhin, N., Concha, L., Seres, P., Beaulieu, C., and Coupland, N.J. (2008). Diffusion tensor imaging tractography and reliability analysis for limbic and paralimbic white matter tracts. Psychiatry Res *164*, 132–142.

Marsh, L., Morrell, M.J., Shear, P.K., Sullivan, E. V, Freeman, H., Marie, a, Lim, K.O., and Pfefferbaum, a (1997). Cortical and hippocampal volume deficits in temporal lobe epilepsy. Epilepsia *38*, 576–587.

McDonald, C.R., Ahmadi, M.E., Hagler, D.J., Tecoma, E.S., Iragui, V.J., Gharapetian, L., Dale, a M., and Halgren, E. (2008a). Diffusion tensor imaging correlates of memory and language impairments in temporal lobe epilepsy. Neurology *71*, 1869–1876.

McDonald, C.R., Hagler Jr., D.J., Ahmadi, M.E., Tecoma, E., Iragui, V., Dale, A.M., and Halgren, E. (2008b). Subcortical and cerebellar atrophy in mesial temporal lobe epilepsy revealed by automatic segmentation. Epilepsy Res *79*, 130–138.

McDonald, C.R., Hagler Jr., D.J., Ahmadi, M.E., Tecoma, E., Iragui, V., Gharapetian, L., Dale, A.M., and Halgren, E. (2008c). Regional neocortical thinning in mesial temporal lobe epilepsy. Epilepsia *49*, 794–803.

McDonald, C.R., Hagler Jr., D.J., Girard, H.M., Pung, C., Ahmadi, M.E., Holland, D., Patel, R.H., Barba, D., Tecoma, E.S., Iragui, V.J., et al. (2010). Changes in fiber tract integrity and visual fields after anterior temporal lobectomy. Neurology *75*, 1631–1638.

McDonald, C.R., Swartz, B.E., Halgren, E., Patell, A., Daimes, R., and Mandelkern, M. (2006). The relationship of regional frontal hypometabolism to executive function: a resting fluorodeoxyglucose PET study of patients with epilepsy and healthy controls. Epilepsy Behav *9*, 58–67.

McMillan, A.B., Hermann, B.P., Johnson, S.C., Hansen, R.R., Seidenberg, M., and Meyerand, M.E. (2004). Voxel-based morphometry of unilateral temporal lobe epilepsy reveals abnormalities in cerebral white matter. Neuroimage *23*, 167–174.

Medina, M.T., Suzuki, T., Alonso, M.E., Durón, R.M., Martínez-Juárez, I.E., Bailey, J.N., Bai, D., Inoue, Y., Yoshimura, I., Kaneko, S., et al. (2008). Novel mutations in Myoclonin1/EFHC1 in sporadic and familial juvenile myoclonic epilepsy. Neurology *70*, 2137–2144.

Meldrum, B.S. (1993). Excitotoxicity and selective neuronal loss in epilepsy. Brain Pathol *3*, 405–412.

Meng, L., Xiang, J., Kotecha, R., Rose, D., Zhao, H., Zhao, D., Yang, J., and Degrauw, T. (2010). White matter abnormalities in children and adolescents with temporal lobe epilepsy. Magn Reson Imaging *28*, 1290–1298.

Meschaks, A., Lindstrom, P., Halldin, C., Farde, L., and Savic, I. (2005). Regional reductions in serotonin 1A receptor binding in juvenile myoclonic epilepsy. Arch Neurol *62*, 946–950.

Mesulam, M.M. (1998). From sensation to cognition. Brain *121 (Pt 6*, 1013–1052.

Montalenti, E., Imperiale, D., Rovera, A., Bergamasco, B., and Benna, P. (2001). Clinical features, EEG findings and diagnostic pitfalls in juvenile myoclonic epilepsy: a series of 63 patients. J Neurol Sci *184*, 65–70.

Moran, N.F., Lemieux, L., Kitchen, N.D., Fish, D.R., and Shorvon, S.D. (2001). Extrahippocampal temporal lobe atrophy in temporal lobe epilepsy and mesial temporal sclerosis. Brain *124*, 167–175.

Mori, S., Crain, B.J., Chacko, V.P., and Van Zijl, P.C. (1999). Three-dimensional tracking of axonal projections in the brain by magnetic resonance imaging. Ann Neurol *45*, 265–269.

Mori, S., Oishi, K., and Faria, A. V (2009). White matter atlases based on diffusion tensor imaging. Curr Opin Neurol *22*, 362–369.

Mory, S.B., Betting, L.E., Fernandes, P.T., Lopes-Cendes, I., Guerreiro, M.M., Guerreiro, C. a M., Cendes, F., and Li, L.M. (2011). Structural abnormalities of the thalamus in juvenile myoclonic epilepsy. Epilepsy Behav *21*, 407–411.

Mory, S.B., Li, L.M., Guerreiro, C.A., and Cendes, F. (2003). Thalamic dysfunction in juvenile myoclonic epilepsy: a proton MRS study. Epilepsia *44*, 1402–1405.

Moseley, M.E., Cohen, Y., Kucharczyk, J., Mintorovitch, J., Asgari, H.S., Wendland, M.F., Tsuruda, J., and Norman, D. (1990). Diffusion-weighted MR imaging of anisotropic water diffusion in cat central nervous system. Radiology *176*, 439–445.

Mottershead, J.P., Schmierer, K., Clemence, M., Thornton, J.S., Scaravilli, F., Barker, G.J., Tofts, P.S., Newcombe, J., Cuzner, M.L., Ordidge, R.J., et al. (2003). High field MRI correlates of myelin content and axonal density in multiple sclerosis--a post-mortem study of the spinal cord. J Neurol *250*, 1293–1301.

Mueller, S.G., Laxer, K.D., Barakos, J., Cheong, I., Finlay, D., Garcia, P., Cardenas-Nicolson, V., and Weiner, M.W. (2010). Involvement of the thalamocortical network in TLE with and without mesiotemporal sclerosis. Epilepsia *51*, 1436–1445.

Mueller, S.G., Laxer, K.D., Barakos, J., Cheong, I., Garcia, P., and Weiner, M.W. (2009). Subfield atrophy pattern in temporal lobe epilepsy with and without mesial sclerosis detected by high-resolution MRI at 4 Tesla: preliminary results. Epilepsia *50*, 1474–1483.

Mueller, S.G., Laxer, K.D., Cashdollar, N., Buckley, S., Paul, C., and Weiner, M.W. (2006). Voxel-based optimized morphometry (VBM) of gray and white matter in temporal lobe epilepsy (TLE) with and without mesial temporal sclerosis. Epilepsia *47*, 900–907.

Mueller, S.G., Laxer, K.D., Cashdollar, N., Flenniken, D.L., Matson, G.B., and Weiner, M.W. (2004). Identification of abnormal neuronal metabolism outside the seizure focus in temporal lobe epilepsy. Epilepsia *45*, 355–366.

Mueller, S.G., Laxer, K.D., Scanlon, C., Garcia, P., McMullen, W.J., Loring, D.W., Meador, K.J., and Weiner, M.W. (2012). Different structural correlates for verbal memory impairment in temporal lobe epilepsy with and without mesial temporal lobe sclerosis. Hum Brain Mapp *33*, 489–499.

Murray, C.J.L., and Lopez, A.D. (1994). Global comparative assessment in the health sector; disease burden, expenditures, and intervention packages. (Geneva: World Health Organization).

Nadler, J.V. (2003). The recurrent mossy fiber pathway of the epileptic brain. Neurochem Res *28*, 1649–1658.

Natsume, J., Bernasconi, N., Andermann, F., and Bernasconi, A. (2003). MRI volumetry of the thalamus in temporal, extratemporal, and idiopathic generalized epilepsy. Neurology *60*, 1296–1300.

Neligan, A., Bell, G.S., Giavasi, C., Johnson, A.L., Goodridge, D.M., Shorvon, S.D., and Sander, J.W. (2012). Long-term risk of developing epilepsy after febrile seizures: a prospective cohort study. Neurology *78*, 1166–1170.

Newman, M. (2003). The structure and function of complex networks. SIAM Review *45*, 167–256.

Nguyen, D., Vargas, M.I., Khaw, N., Seeck, M., Delavelle, J., Lovblad, K.O., and Haller, S. (2011). Diffusion tensor imaging analysis with tract-based spatial statistics of the white matter abnormalities after epilepsy surgery. Epilepsy Res *94*, 189–197.

Ni, H., Kavcic, V., Zhu, T., Ekholm, S., and Zhong, J. (2006). Effects of number of diffusion gradient directions on derived diffusion tensor imaging indices in human brain. AJNR Am J Neuroradiol *27*, 1776–1781.

Niemeyer, M.I., Cid, L.P., Sepúlveda, F. V, Blanz, J., Auberson, M., and Jentsch, T.J. (2010). No evidence for a role of CLCN2 variants in idiopathic generalized epilepsy. Nat Genet *42*, 3.

O'Muircheartaigh, J., Vollmar, C., Barker, G.J., Kumari, V., Symms, M.R., Thompson, P., Duncan, J.S., Koepp, M.J., and Richardson, M.P. (2011). Focal structural changes and cognitive dysfunction in juvenile myoclonic epilepsy. Neurology *76*, 34–40.

O'Muircheartaigh, J., Vollmar, C., Barker, G.J., Kumari, V., Symms, M.R., Thompson, P., Duncan, J.S., Koepp, M.J., and Richardson, M.P. (2012). Abnormal thalamocortical structural and functional connectivity in juvenile myoclonic epilepsy. Brain *135*, 3635–3644.

Odano, I., Varrone, A., Savic, I., Ciumas, C., Karlsson, P., Jucaite, A., Halldin, C., and Farde, L. (2012). Quantitative PET analyses of regional [11C]PE2I binding to the dopamine transporter--application to juvenile myoclonic epilepsy. Neuroimage *59*, 3582–3593.

Oguz, K.K., Tezer, I., Sanverdi, E., Has, a C., Bilginer, B., Dolgun, a, and Saygi, S. (2012). Effect of Patient Sex on White Matter Alterations in Unilateral Medial Temporal Lobe Epilepsy with Hippocampal Sclerosis Assessed by Diffusion Tensor Imaging. AJNR Am J Neuroradiol.

De Oliveira, M.S., Betting, L.E., Mory, S.B., Cendes, F., and Castellano, G. (2013). Texture analysis of magnetic resonance images of patients with juvenile myoclonic epilepsy. Epilepsy Behav *27*, 22–28.

Ono, J., Harada, K., Takahashi, M., Maeda, M., Ikenaka, K., Sakurai, K., Sakai, N., Kagawa, T., Fritz-Zieroth, B., and Nagai, T. (1995). Differentiation between dysmyelination and demyelination using magnetic resonance diffusional anisotropy. Brain Res *671*, 141–148.

Otte, W.M., Van Eijsden, P., Sander, J.W., Duncan, J.S., Dijkhuizen, R.M., and Braun, K.P.J. (2012). A meta-analysis of white matter changes in temporal lobe epilepsy as studied with diffusion tensor imaging. Epilepsia *53*, 659–667.

Oyegbile, T.O., Bayless, K., Dabbs, K., Jones, J., Rutecki, P., Pierson, R., Seidenberg, M., and Hermann, B. (2011). The nature and extent of cerebellar atrophy in chronic temporal lobe epilepsy. Epilepsia *52*, 698–706.

Oyegbile, T.O., Dow, C., Jones, J., Bell, B., Rutecki, P., Sheth, R., Seidenberg, M., and Hermann, B.P. (2004). The nature and course of neuropsychological morbidity in chronic temporal lobe epilepsy. Neurology *62*, 1736–1742.

Van Paesschen, W., Connelly, a, King, M.D., Jackson, G.D., and Duncan, J.S. (1997). The spectrum of hippocampal sclerosis: a quantitative magnetic resonance imaging study. Ann Neurol *41*, 41–51.

Pail, M., Brázdil, M., Marecek, R., and Mikl, M. (2010). An optimized voxel-based morphometric study of gray matter changes in patients with left-sided and right-sided mesial temporal lobe epilepsy and hippocampal sclerosis (MTLE/HS). Epilepsia *51*, 511–518.

Pal, D.K., Evgrafov, O. V, Tabares, P., Zhang, F., Durner, M., and Greenberg, D.A. (2003). BRD2 (RING3) is a probable major susceptibility gene for common juvenile myoclonic epilepsy. Am J Hum Genet *73*, 261–270.

Papadakis, N.G., Martin, K.M., Mustafa, M.H., Wilkinson, I.D., Griffiths, P.D., Huang, C.L., and Woodruff, P.W. (2002). Study of the effect of CSF suppression on white matter diffusion anisotropy mapping of healthy human brain. Magn Reson Med *48*, 394–398.

Parker, G.J.M., Wheeler-Kingshott, C.A.M., and Barker, G.J. (2002). Estimating distributed anatomical connectivity using fast marching methods and diffusion tensor imaging. IEEE Trans Med Imaging *21*, 505–512.

Partridge, S.C., Mukherjee, P., Henry, R.G., Miller, S.P., Berman, J.I., Jin, H., Lu, Y., Glenn, O.A., Ferriero, D.M., Barkovich, A.J., et al. (2004). Diffusion tensor imaging: serial quantitation of white matter tract maturity in premature newborns. Neuroimage *22*, 1302–1314.

Pascalicchio, T.F., De Araujo Filho, G.M., Da Silva Noffs, M.H., Lin, K., Caboclo, L.O., Vidal-Dourado, M., Ferreira Guilhoto, L.M., and Yacubian, E.M. (2007). Neuropsychological profile of patients with juvenile myoclonic epilepsy: a controlled study of 50 patients. Epilepsy Behav *10*, 263–267.

Pell, G.S., Briellmann, R.S., Pardoe, H., Abbott, D.F., and Jackson, G.D. (2008). Composite voxel-based analysis of volume and T2 relaxometry in temporal lobe epilepsy. Neuroimage *39*, 1151–1161.

Pierpaoli, C., Barnett, A., Pajevic, S., Chen, R., Penix, L.R., Virta, A., and Basser, P. (2001). Water diffusion changes in Wallerian degeneration and their dependence on white matter architecture. Neuroimage *13*, 1174–1185.

Pierpaoli, C., and Basser, P.J. (1996). Toward a quantitative assessment of diffusion anisotropy. Magn Reson Med *36*, 893–906.

Pierpaoli, C., Jezzard, P., Basser, P.J., Barnett, A., and Di Chiro, G. (1996). Diffusion tensor MR imaging of the human brain. Radiology *201*, 637–648.

Pitkänen, A., Nissinen, J., Nairismägi, J., Lukasiuk, K., Gröhn, O.H.J., Miettinen, R., and Kauppinen, R. (2002). Progression of neuronal damage after status epilepticus and during spontaneous seizures in a rat model of temporal lobe epilepsy. Prog Brain Res *135*, 67–83.

Pittau, F., Grova, C., Moeller, F., Dubeau, F., and Gotman, J. (2012). Patterns of altered functional connectivity in mesial temporal lobe epilepsy. Epilepsia *53*, 1013–1023.

Pollen, D.A. (1964). INTRACELLULAR STUDIES OF CORTICAL NEURONS DURING THALAMIC INDUCED WAVE AND SPIKE. Electroencephalogr Clin Neurophysiol *17*, 398–404.

Ponten, S.C., Bartolomei, F., and Stam, C.J. (2007). Small-world networks and epilepsy: graph theoretical analysis of intracerebrally recorded mesial temporal lobe seizures. Clin Neurophysiol *118*, 918–927.

Ponten, S.C., Douw, L., Bartolomei, F., Reijneveld, J.C., and Stam, C.J. (2009). Indications for network regularization during absence seizures: weighted and unweighted graph theoretical analyses. Exp Neurol *217*, 197–204.

Poonawalla, A.H., and Zhou, X.J. (2004). Analytical error propagation in diffusion anisotropy calculations. J Magn Reson Imaging *19*, 489–498.

Powell, H.W.R., Richardson, M.P., Symms, M.R., Boulby, P. a, Thompson, P.J., Duncan, J.S., and Koepp, M.J. (2007). Reorganization of verbal and nonverbal memory in temporal lobe epilepsy due to unilateral hippocampal sclerosis. Epilepsia *48*, 1512–1525.

Pulsipher, D.T., Seidenberg, M., Guidotti, L., Tuchscherer, V.N., Morton, J., Sheth, R.D., and Hermann, B. (2009). Thalamofrontal circuitry and executive dysfunction in recent-onset juvenile myoclonic epilepsy. Epilepsia *50*, 1210–1219.

Raff, M.C., Whitmore, A. V, and Finn, J.T. (2002). Axonal self-destruction and neurodegeneration. Science *296*, 868–871.

Ratzliff, A. d H., Howard, A.L., Santhakumar, V., Osapay, I., and Soltesz, I. (2004). Rapid deletion of mossy cells does not result in a hyperexcitable dentate gyrus: implications for epileptogenesis. J Neurosci *24*, 2259–2269.

Ratzliff, A. d H., Santhakumar, V., Howard, A., and Soltesz, I. (2002). Mossy cells in epilepsy: rigor mortis or vigor mortis? Trends Neurosci *25*, 140–144.

Reese, T.G., Heid, O., Weisskoff, R.M., and Wedeen, V.J. (2003). Reduction of eddy-current-induced distortion in diffusion MRI using a twice-refocused spin echo. Magn Reson Med *49*, 177–182.

Riederer, F., Lanzenberger, R., Kaya, M., Prayer, D., Serles, W., and Baumgartner, C. (2008). Network atrophy in temporal lobe epilepsy: a voxel-based morphometry study. Neurology *71*, 419–425.

Ristić, A.J., Ostojić, J., Kozić, D., Vojvodić, N.M., Popović, L.M., Janković, S., Baščarević, V., and Sokić, D. V (2011). Hippocampal metabolic dysfunction in juvenile myoclonic epilepsy: 3D multivoxel spectroscopy study. J Neurol Sci *305*, 139–142.

Rodrigo, S., Oppenheim, C., Chassoux, F., Golestani, N., Cointepas, Y., Poupon, C., Semah, F., Mangin, J.F., Le Bihan, D., and Meder, J.F. (2007). Uncinate fasciculus fiber tracking in mesial temporal lobe epilepsy. Initial findings. Eur Radiol *17*, 1663–1668.

Roebling, R., Scheerer, N., Uttner, I., Gruber, O., Kraft, E., and Lerche, H. (2009). Evaluation of cognition, structural, and functional MRI in juvenile myoclonic epilepsy. Epilepsia *50*, 2456–2465.

Ronan, L., Alhusaini, S., Scanlon, C., Doherty, C.P., Delanty, N., and Fitzsimons, M. (2012). Widespread cortical morphologic changes in juvenile myoclonic epilepsy: evidence from structural MRI. Epilepsia *53*, 651–658.

Ronan, L., Scanlon, C., Murphy, K., Maguire, S., Delanty, N., Doherty, C.P., and Fitzsimons, M. (2011). Cortical curvature analysis in MRI-negative temporal lobe epilepsy: a surrogate marker for malformations of cortical development. Epilepsia *52*, 28–34.

Rubinov, M., and Sporns, O. (2010). Complex network measures of brain connectivity: uses and interpretations. Neuroimage *52*, 1059–1069.

Saini, J., Sinha, S., Bagepally, B.S., Ramchandraiah, C.T., Thennarasu, K., Prasad, C., Taly, a B., and Satishchandra, P. (2013). Subcortical structural abnormalities in juvenile myoclonic epilepsy (JME): MR volumetry and vertex based analysis. Seizure *22*, 230–235.

Salmenperä, T., Kälviäinen, R., Partanen, K., and Pitkänen, A. (2001). Hippocampal and amygdaloid damage in partial epilepsy: a cross-sectional MRI study of 241 patients. Epilepsy Res *46*, 69–82.

Salvador, R., Suckling, J., Coleman, M.R., Pickard, J.D., Menon, D., and Bullmore, E. (2005). Neurophysiological architecture of functional magnetic resonance images of human brain. Cereb Cortex *15*, 1332–1342.

Sandok, E.K., O'Brien, T.J., Jack, C.R., and So, E.L. (2000). Significance of cerebellar atrophy in intractable temporal lobe epilepsy: a quantitative MRI study. Epilepsia *41*, 1315–1320.

Santhakumar, V., Bender, R., Frotscher, M., Ross, S.T., Hollrigel, G.S., Toth, Z., and Soltesz, I. (2000). Granule cell hyperexcitability in the early post-traumatic rat dentate gyrus: the "irritable mossy cell" hypothesis. J Physiol *524 Pt 1*, 117–134.

Savic, I., Lekvall, A., Greitz, D., and Helms, G. (2000). MR spectroscopy shows reduced frontal lobe concentrations of N-acetyl aspartate in patients with juvenile myoclonic epilepsy. Epilepsia *41*, 290–296.

Savic, I., Osterman, Y., and Helms, G. (2004). MRS shows syndrome differentiated metabolite changes in human-generalized epilepsies. Neuroimage *21*, 163–172.

Schindler, K. a, Bialonski, S., Horstmann, M.-T., Elger, C.E., and Lehnertz, K. (2008). Evolving functional network properties and synchronizability during human epileptic seizures. Chaos *18*, 033119.

Schmierer, K., Wheeler-Kingshott, C.A., Boulby, P.A., Scaravilli, F., Altmann, D.R., Barker, G.J., Tofts, P.S., and Miller, D.H. (2007). Diffusion tensor imaging of post mortem multiple sclerosis brain. Neuroimage *35*, 467–477.

Schoene-Bake, J.C., Faber, J., Trautner, P., Kaaden, S., Tittgemeyer, M., Elger, C.E., and Weber, B. (2009). Widespread affections of large fiber tracts in postoperative temporal lobe epilepsy. Neuroimage *46*, 569–576.

Seeck, M., Dreifuss, S., Lantz, G., Jallon, P., Foletti, G., Despland, P.A., Delavelle, J., and Lazeyras, F. (2005). Subcortical nuclei volumetry in idiopathic generalized epilepsy. Epilepsia *46*, 1642–1645.

Seidenberg, M., Kelly, K.G., Parrish, J., Geary, E., Dow, C., Rutecki, P., and Hermann, B. (2005). Ipsilateral and contralateral MRI volumetric abnormalities in chronic unilateral temporal lobe epilepsy and their clinical correlates. Epilepsia *46*, 420–430.

Semah, F., Picot, M.C., Adam, C., Broglin, D., Arzimanoglou, a, Bazin, B., Cavalcanti, D., and Baulac, M. (1998). Is the underlying cause of epilepsy a major prognostic factor for recurrence? Neurology *51*, 1256–1262.

Seo, Y., Shinar, H., Morita, Y., and Navon, G. (1999). Anisotropic and restricted diffusion of water in the sciatic nerve: A (2)H double-quantum-filtered NMR study. Magn Reson Med *42*, 461–466.

Sequeira, K.M., Tabesh, A., Sainju, R.K., Desantis, S.M., Naselaris, T., Joseph, J.E., Ahlman, M. a., Spicer, K.M., Glazier, S.S., Edwards, J.C., et al. (2013). Perfusion Network Shift during Seizures in Medial Temporal Lobe Epilepsy. PLoS One *8*, e53204.

Shon, Y.M., Kim, Y.I., Koo, B.B., Lee, J.M., Kim, H.J., Kim, W.J., Ahn, K.J., and Yang, D.W. (2010). Group-specific regional white matter abnormality revealed in diffusion tensor imaging of medial temporal lobe epilepsy without hippocampal sclerosis. Epilepsia *51*, 529–535.

Shorvon, S.D. (2011). The etiologic classification of epilepsy. Epilepsia *52*, 1052–1057.

Shu, N., Liu, Y., Li, K., Duan, Y., Wang, J., Yu, C., Dong, H., Ye, J., and He, Y. (2011). Diffusion tensor tractography reveals disrupted topological efficiency in white matter structural networks in multiple sclerosis. Cereb Cortex *21*, 2565–2577.

Sievers, C., Platt, N., Perry, V.H., Coleman, M.P., and Conforti, L. (2003). Neurites undergoing Wallerian degeneration show an apoptotic-like process with Annexin V

positive staining and loss of mitochondrial membrane potential. Neurosci Res *46*, 161–169.

Sisodiya, S.M., Moran, N., Free, S.L., Kitchen, N.D., Stevens, J.M., Harkness, W.F., Fish, D.R., and Shorvon, S.D. (1997). Correlation of widespread preoperative magnetic resonance imaging changes with unsuccessful surgery for hippocampal sclerosis. Ann Neurol *41*, 490–496.

Sloviter, R.S. (1991). Permanently altered hippocampal structure, excitability, and inhibition after experimental status epilepticus in the rat: the "dormant basket cell" hypothesis and its possible relevance to temporal lobe epilepsy. Hippocampus *1*, 41–66.

Sloviter, R.S. (1994). The functional organization of the hippocampal dentate gyrus and its relevance to the pathogenesis of temporal lobe epilepsy. Ann Neurol *35*, 640–654.

Sloviter, R.S., Zappone, C.A., Harvey, B.D., Bumanglag, A. V, Bender, R.A., and Frotscher, M. (2003). "Dormant basket cell" hypothesis revisited: relative vulnerabilities of dentate gyrus mossy cells and inhibitory interneurons after hippocampal status epilepticus in the rat. J Comp Neurol *459*, 44–76.

Song, S.K., Sun, S.W., Ju, W.K., Lin, S.J., Cross, A.H., and Neufeld, A.H. (2003). Diffusion tensor imaging detects and differentiates axon and myelin degeneration in mouse optic nerve after retinal ischemia. Neuroimage *20*, 1714–1722.

Song, S.K., Sun, S.W., Ramsbottom, M.J., Chang, C., Russell, J., and Cross, A.H. (2002). Dysmyelination revealed through MRI as increased radial (but unchanged axial) diffusion of water. Neuroimage *17*, 1429–1436.

Song, S.K., Yoshino, J., Le, T.Q., Lin, S.J., Sun, S.W., Cross, A.H., and Armstrong, R.C. (2005). Demyelination increases radial diffusivity in corpus callosum of mouse brain. Neuroimage *26*, 132–140.

Sonmez, F., Atakli, D., Sari, H., Atay, T., and Arpaci, B. (2004). Cognitive function in juvenile myoclonic epilepsy. Epilepsy Behav *5*, 329–336.

Sowell, E.R., Peterson, B.S., Kan, E., Woods, R.P., Yoshii, J., Bansal, R., Xu, D., Zhu, H., Thompson, P.M., and Toga, A.W. (2007). Sex differences in cortical thickness mapped in 176 healthy individuals between 7 and 87 years of age. Cereb Cortex *17*, 1550–1560.

Spanaki, M. V, Spencer, S.S., Corsi, M., MacMullan, J., Seibyl, J., and Zubal, I.G. (1999). Sensitivity and specificity of quantitative difference SPECT analysis in seizure localization. J Nucl Med *40*, 730–736.

Spencer, S.S. (2002). Neural networks in human epilepsy: evidence of and implications for treatment. Epilepsia *43*, 219–227.

Sporns, O., Tononi, G., and Kötter, R. (2005). The human connectome: A structural description of the human brain. PLoS Comput Biol *1*, e42.

Sporns, O., and Zwi, J.D. (2004). The small world of the cerebral cortex. Neuroinformatics *2*, 145–162.

Staempfli, P., Reischauer, C., Jaermann, T., Valavanis, A., Kollias, S., and Boesiger, P. (2008). Combining fMRI and DTI: a framework for exploring the limits of fMRI-guided DTI fiber tracking and for verifying DTI-based fiber tractography results. Neuroimage *39*, 119–126.

Stanisz, G.J., Szafer, A., Wright, G.A., and Henkelman, R.M. (1997). An analytical model of restricted diffusion in bovine optic nerve. Magn Reson Med *37*, 103–111.

Stejskal, E.O., and Tanner, J.E. (1965). Spin Diffusion Measurements: Spin Echoes in the Presence of a Time-Dependent Field Gradient. The Journal of Chemical Physics *42*, 288.

Steriade, M., and Contreras, D. (1995). Relations between cortical and thalamic cellular events during transition from sleep patterns to paroxysmal activity. J Neurosci *15*, 623–642.

Stichel, C.C., and Müller, H.W. (1994). Extensive and long-lasting changes of glial cells following transection of the postcommissural fornix in the adult rat. Glia *10*, 89–100.

Sun, S.W., Liang, H.F., Cross, A.H., and Song, S.K. (2008). Evolving Wallerian degeneration after transient retinal ischemia in mice characterized by diffusion tensor imaging. Neuroimage *40*, 1–10.

Sun, S.-W., Liang, H.-F., Trinkaus, K., Cross, A.H., Armstrong, R.C., and Song, S.-K. (2006). Noninvasive detection of cuprizone induced axonal damage and demyelination in the mouse corpus callosum. Magn Reson Med *55*, 302–308.

Sutula, T.P., Golarai, G., and Cavazos, J. (1992). Assessing the functional significance of mossy fiber sprouting. Epilepsy Res Suppl *7*, 251–259.

Suzuki, T., Delgado-Escueta, A. V, Aguan, K., Alonso, M.E., Shi, J., Hara, Y., Nishida, M., Numata, T., Medina, M.T., Takeuchi, T., et al. (2004). Mutations in EFHC1 cause juvenile myoclonic epilepsy. Nat Genet *36*, 842–849.

Suzuki, T., Miyamoto, H., Nakahari, T., Inoue, I., Suemoto, T., Jiang, B., Hirota, Y., Itohara, S., Saido, T.C., Tsumoto, T., et al. (2009). Efhc1 deficiency causes spontaneous myoclonus and increased seizure susceptibility. Hum Mol Genet *18*, 1099–1109.

Swartz, B.., Halgren, E., Simpkins, F., and Syndulko, K. (1994). Primary memory in patients with frontal and primary generalized epilepsy. Journal of Epilepsy *7*, 232–241.

Swartz, B.E., Simpkins, F., Halgren, E., Mandelkern, M., Brown, C., Krisdakumtorn, T., and Gee, M. (1996). Visual working memory in primary generalized epilepsy: an 18FDG-PET study. Neurology *47*, 1203–1212.

Tae, W., Hong, S., Joo, E., Han, S., Cho, J., Seo, D., Lee, J., Kim, I., Byun, H., and Kim, S. (2006). Structural brain abnormalities in juvenile myoclonic epilepsy patients: volumetry and voxel-based morphometry. Korean J Radiol *7*, 162–172.

Tae, W.S., Joo, E.Y., Han, S.J., Lee, K.-H., and Hong, S.B. (2007). CBF changes in drug naive juvenile myoclonic epilepsy patients. J Neurol *254*, 1073–1080.

Tae, W.S., Joo, E.Y., Kim, J.H., Han, S.J., Suh, Y.-L., Kim, B.T., Hong, S.C., and Hong, S.B. (2005). Cerebral perfusion changes in mesial temporal lobe epilepsy: SPM analysis of ictal and interictal SPECT. Neuroimage *24*, 101–110.

Tae, W.S., Kim, S.H., Joo, E.Y., Han, S.J., Kim, I.Y., Kim, S.I., Lee, J.M., and Hong, S.B. (2008). Cortical thickness abnormality in juvenile myoclonic epilepsy. J Neurol *255*, 561–566.

Takahashi, M., Hackney, D.B., Zhang, G., Wehrli, S.L., Wright, A.C., O'Brien, W.T., Uematsu, H., Wehrli, F.W., and Selzer, M.E. (2002). Magnetic resonance microimaging of intraaxonal water diffusion in live excised lamprey spinal cord. Proc Natl Acad Sci U S A *99*, 16192–16196.

Taoka, T., Sakamoto, M., Iwasaki, S., Nakagawa, H., Fukusumi, A., Hirohashi, S., Taoka, K., Kichikawa, K., Hoshida, T., and Sakaki, T. (2005). Diffusion tensor imaging in cases with visual field defect after anterior temporal lobectomy. AJNR Am J Neuroradiol *26*, 797–803.

Tasch, E., Cendes, F., Li, L.M., Dubeau, F., Andermann, F., and Arnold, D.L. (1999). Neuroimaging evidence of progressive neuronal loss and dysfunction in temporal lobe epilepsy. Ann Neurol *45*, 568–576.

Tauck, D.L., and Nadler, J. V (1985). Evidence of functional mossy fiber sprouting in hippocampal formation of kainic acid-treated rats. J Neurosci *5*, 1016–1022.

Thivard, L., Lehericy, S., Krainik, A., Adam, C., Dormont, D., Chiras, J., Baulac, M., and Dupont, S. (2005). Diffusion tensor imaging in medial temporal lobe epilepsy with hippocampal sclerosis. Neuroimage *28*, 682–690.

De Tisi, J., Bell, G.S., Peacock, J.L., McEvoy, A.W., Harkness, W.F.J., Sander, J.W., and Duncan, J.S. (2011). The long-term outcome of adult epilepsy surgery, patterns of seizure remission, and relapse: a cohort study. Lancet *378*, 1388–1395.

Tuch, D.S., Reese, T.G., Wiegell, M.R., Makris, N., Belliveau, J.W., and Wedeen, V.J. (2002). High angular resolution diffusion imaging reveals intravoxel white matter fiber heterogeneity. Magn Reson Med *48*, 577–582.

Tuch, D.S., Wisco, J.J., Khachaturian, M.H., Ekstrom, L.B., Kotter, R., and Vanduffel, W. (2005). Q-ball imaging of macaque white matter architecture. Philosophical Transactions of the Royal Society B: Biological Sciences *360*, 869–879.

Tzourio-Mazoyer, N., Landeau, B., Papathanassiou, D., Crivello, F., Etard, O., Delcroix, N., Mazoyer, B., and Joliot, M. (2002). Automated anatomical labeling of activations in SPM using a macroscopic anatomical parcellation of the MNI MRI single-subject brain. Neuroimage *15*, 273–289.

Vargas, M.E., and Barres, B. a (2007). Why is Wallerian degeneration in the CNS so slow? Annu Rev Neurosci *30*, 153–179.

Velísek, L., and Moshé, S.L. (2003). Temporal lobe epileptogenesis and epilepsy in the developing brain: bridging the gap between the laboratory and the clinic. Progression, but in what direction? Epilepsia *44 Suppl 1*, 51–59.

Velíšek, L., Shang, E., Velíšková, J., Chachua, T., Macchiarulo, S., Maglakelidze, G., Wolgemuth, D.J., and Greenberg, D.A. (2011). GABAergic neuron deficit as an idiopathic generalized epilepsy mechanism: the role of BRD2 haploinsufficiency in juvenile myoclonic epilepsy. PLoS One *6*, e23656.

Vercauteren, T., Pennec, X., Perchant, A., and Ayache, N. (2009). Diffeomorphic demons: efficient non-parametric image registration. Neuroimage *45*, S61–72.

Vijai, J., Kapoor, A., Ravishankar, H.M., Cherian, P.J., Girija, A.S., Rajendran, B., Rangan, G., Jayalakshmi, S., Mohandas, S., Radhakrishnan, K., et al. (2003). Genetic association analysis of KCNQ3 and juvenile myoclonic epilepsy in a South Indian population. Hum Genet *113*, 461–463.

Vollmar, C., O'Muircheartaigh, J., Symms, M.R., Barker, G.J., Thompson, P., Kumari, V., Stretton, J., Duncan, J.S., Richardson, M.P., and Koepp, M.J. (2012). Altered microstructural connectivity in juvenile myoclonic epilepsy: the missing link. Neurology *78*, 1555–1559.

Vulliemoz, S., Vollmar, C., Koepp, M.J., Yogarajah, M., O'Muircheartaigh, J., Carmichael, D.W., Stretton, J., Richardson, M.P., Symms, M.R., and Duncan, J.S. (2011). Connectivity of the supplementary motor area in juvenile myoclonic epilepsy and frontal lobe epilepsy. Epilepsia.

Waites, A.B., Briellmann, R.S., Saling, M.M., Abbott, D.F., and Jackson, G.D. (2006). Functional connectivity networks are disrupted in left temporal lobe epilepsy. Ann Neurol *59*, 335–343.

Wakana, S., Caprihan, A., Panzenboeck, M.M., Fallon, J.H., Perry, M., Gollub, R.L., Hua, K., Zhang, J., Jiang, H., Dubey, P., et al. (2007). Reproducibility of quantitative tractography methods applied to cerebral white matter. Neuroimage *36*, 630–644.

Wakana, S., Jiang, H., Nagae-Poetscher, L.M., Van Zijl, P.C.M., and Mori, S. (2004). Fiber tract-based atlas of human white matter anatomy. Radiology *230*, 77–87.

Wandschneider, B., Kopp, U.A., Kliegel, M., Stephani, U., Kurlemann, G., Janz, D., and Schmitz, B. (2010). Prospective memory in patients with juvenile myoclonic epilepsy and their healthy siblings. Neurology *75*, 2161–2167.

Wang, Y., Gupta, A., Liu, Z., Zhang, H., Escolar, M.L., Gilmore, J.H., Gouttard, S., Fillard, P., Maltbie, E., Gerig, G., et al. (2011). DTI registration in atlas based fiber analysis of infantile Krabbe disease. Neuroimage *55*, 1577–1586.

Watts, D.J., and Strogatz, S.H. (1998). Collective dynamics of "small-world" networks. Nature *393*, 440–442.

Weil, S., Noachtar, S., Arnold, S., Yousry, T.A., Winkler, P.A., and Tatsch, K. (2001). Ictal ECD-SPECT differentiates between temporal and extratemporal epilepsy: confirmation by excellent postoperative seizure control. Nucl Med Commun *22*, 233–237.

Werhahn, K.J., Landvogt, C., Klimpe, S., Buchholz, H.-G., Yakushev, I., Siessmeier, T., Müller-Forell, W., Piel, M., Rösch, F., Glaser, M., et al. (2006). Decreased dopamine D2/D3-receptor binding in temporal lobe epilepsy: an [18F]fallypride PET study. Epilepsia *47*, 1392–1396.

Wheatley, B.M. (2008). Selective amygdalohippocampectomy: the trans-middle temporal gyrus approach. Neurosurg Focus *25*, E4.

Whitcher, B., Tuch, D.S., Wisco, J.J., Sorensen, A.G., and Wang, L. (2008). Using the wild bootstrap to quantify uncertainty in diffusion tensor imaging. Hum Brain Mapp *29*, 346–362.

Wieser, H.-G. (2004). ILAE Commission Report. Mesial temporal lobe epilepsy with hippocampal sclerosis. Epilepsia *45*, 695–714.

Wieshmann, U.C., Symms, M.R., Clark, C. a, Lemieux, L., Franconi, F., Parker, G.J., Barker, G.J., and Shorvon, S.D. (1999). Wallerian degeneration in the optic radiation after temporal lobectomy demonstrated in vivo with diffusion tensor imaging. Epilepsia *40*, 1155–1158.

Wilke, C., Worrell, G., and He, B. (2011). Graph analysis of epileptogenic networks in human partial epilepsy. Epilepsia *52*, 84–93.

Woermann, F., Free, S., Koepp, M., Ashburner, J., and Duncan, J. (1999a). Voxel-by-voxel comparison of automatically segmented cerebral gray matter--A rater-independent comparison of structural MRI in patients with epilepsy. Neuroimage *10*, 373–384.

Woermann, F., Free, S., Koepp, M., Sisodiya, S., and Duncan, J. (1999b). Abnormal cerebral structure in juvenile myoclonic epilepsy demonstrated with voxel-based analysis of MRI. Brain *122 (Pt 1*, 2101–2108.

Woermann, F.G., Van Elst, L.T., Koepp, M.J., Free, S.L., Thompson, P.J., Trimble, M.R., and Duncan, J.S. (2000). Reduction of frontal neocortical grey matter associated with affective aggression in patients with temporal lobe epilepsy: an objective voxel by voxel analysis of automatically segmented MRI. J Neurol Neurosurg Psychiatry *68*, 162–169.

Woermann, F.G., Sisodiya, S.M., Free, S.L., and Duncan, J.S. (1998). Quantitative MRI in patients with idiopathic generalized epilepsy. Evidence of widespread cerebral structural changes. Brain *121 (Pt 9*, 1661–1667.

Wolf, P., and Goosses, R. (1986). Relation of photosensitivity to epileptic syndromes. J Neurol Neurosurg Psychiatry *49*, 1386–1391.

Won, H.J., Chang, K.H., Cheon, J.E., Kim, H.D., Lee, D.S., Han, M.H., Kim, I.O., Lee, S.K., and Chung, C.K. (1999). Comparison of MR imaging with PET and ictal SPECT in 118 patients with intractable epilepsy. AJNR Am J Neuroradiol *20*, 593–599.

Wu, Q., Butzkueven, H., Gresle, M., Kirchhoff, F., Friedhuber, A., Yang, Q., Wang, H., Fang, K., Lei, H., Egan, G.F., et al. (2007). MR diffusion changes correlate with ultra-structurally defined axonal degeneration in murine optic nerve. Neuroimage *37*, 1138–1147.

Xu, J., Sun, S.W., Naismith, R.T., Snyder, A.Z., Cross, A.H., and Song, S.K. (2008). Assessing optic nerve pathology with diffusion MRI: from mouse to human. NMR Biomed *21*, 928–940.

Yan, C., Gong, G., Wang, J., Wang, D., Liu, D., Zhu, C., Chen, Z.J., Evans, A., Zang, Y., and He, Y. (2011). Sex- and brain size-related small-world structural cortical networks in young adults: a DTI tractography study. Cereb Cortex *21*, 449–458.

Yogarajah, M., Focke, N.K., Bonelli, S., Cercignani, M., Acheson, J., Parker, G.J.M., Alexander, D.C., McEvoy, A.W., Symms, M.R., Koepp, M.J., et al. (2009). Defining Meyer's loop-temporal lobe resections, visual field deficits and diffusion tensor tractography. Brain *132*, 1656–1668.

Yogarajah, M., Focke, N.K., Bonelli, S.B., Thompson, P., Vollmar, C., McEvoy, A.W., Alexander, D.C., Symms, M.R., Koepp, M.J., and Duncan, J.S. (2010). The structural plasticity of white matter networks following anterior temporal lobe resection. Brain *133*, 2348–2364.

Yogarajah, M., Powell, H.W.R., Parker, G.J.M., Alexander, D.C., Thompson, P.J., Symms, M.R., Boulby, P., Wheeler-Kingshott, C.A., Barker, G.J., Koepp, M.J., et al. (2008). Tractography of the parahippocampal gyrus and material specific memory impairment in unilateral temporal lobe epilepsy. Neuroimage *40*, 1755–1764.

Zaknun, J.J., Bal, C., Maes, A., Tepmongkol, S., Vazquez, S., Dupont, P., and Dondi, M. (2008). Comparative analysis of MR imaging, ictal SPECT and EEG in temporal lobe epilepsy: a prospective IAEA multi-center study. Eur J Nucl Med Mol Imaging *35*, 107–115.

Zappone, C.A., and Sloviter, R.S. (2004). Translamellar disinhibition in the rat hippocampal dentate gyrus after seizure-induced degeneration of vulnerable hilar neurons. J Neurosci *24*, 853–864.

Zaveri, H.P., Duckrow, R.B., De Lanerolle, N.C., and Spencer, S.S. (2001). Distinguishing subtypes of temporal lobe epilepsy with background hippocampal activity. Epilepsia *42*, 725–730.

Zeisel, A., Zuk, O., and Domany, E. (2011). FDR control with adaptive procedures and FDR monotonicity. The Annals of Applied Statistics *5*, 943–968.

Zhai, Q., Wang, J., Kim, A., Liu, Q., Watts, R., Hoopfer, E., Mitchison, T., Luo, L., and He, Z. (2003). Involvement of the ubiquitin-proteasome system in the early stages of wallerian degeneration. Neuron *39*, 217–225.

Zhang, H., Avants, B.B., Yushkevich, P. a, Woo, J.H., Wang, S., McCluskey, L.F., Elman, L.B., Melhem, E.R., and Gee, J.C. (2007). High-dimensional spatial normalization of diffusion tensor images improves the detection of white matter differences: an example study using amyotrophic lateral sclerosis. IEEE Trans Med Imaging *26*, 1585–1597.

Zhang, J., Jones, M., DeBoy, C.A., Reich, D.S., Farrell, J.A., Hoffman, P.N., Griffin, J.W., Sheikh, K.A., Miller, M.I., Mori, S., et al. (2009). Diffusion tensor magnetic resonance imaging of Wallerian degeneration in rat spinal cord after dorsal root axotomy. J Neurosci *29*, 3160–3171.

Zifkin, B., Andermann, E., and Andermann, F. (2005). Mechanisms, genetics, and pathogenesis of juvenile myoclonic epilepsy. Curr Opin Neurol *18*, 147–153.

Appendix

Impact of number of diffusion weighting direction and number of repetitions on DTI measurements of the fornix

Introduction

Recent simulation studies have suggested using more than six directions to provide better estimates for DTI measurement with less error (Jones, 2004; Poonawalla and Zhou, 2004). Our group has previously addressed the issue for standard DTI by comparing the FA and MD of ten major white matter tracts between six-direction diffusion tensor imaging data to 30- or 60-direction data (Lebel et al., 2012). The results showed similar and robust diffusion measurements when using six-direction DTI. However, question remains for the smaller white matter tract fornix which borders CSF and suffers from partial volume effect when using standard DTI. The effect of using six or more direction on measuring the fornix is of particular interest in this thesis since limbic tract is heavily involved in TLE. To address the concerns, the diffusion measurements of the fornix using six-direction FLAIR DTI were compared to 30-direction FLAIR DTI.

Methods

Seven healthy volunteers were recruited in the supplementary study (Mean age $\pm$ SD: 25 $\pm$ 5 years, 4 F/3 M). FLAIR DTI with six directions and 30 directions were performed on the same 1.5T Siemens Sonata scanner (Erlangen, Germany) sequentially. They used the same dual spin-echo, single shot echo planar imaging (EPI) sequence and shared major imaging parameters (2 mm thick slices with no inter-slice gap; TR = 8 s, TE = 97 ms, TI = 2200 ms, FOV = 224 mm $\times$ 224 mm, acquisition matrix = 112 $\times$ 112 with 75% phase partial Fourier (interpolated to 224 $\times$ 224), voxel dimension $2 \times 2 \times 2$ mm^3 (interpolated to $1 \times 1 \times 2$ mm^3), 22 axial slices with coverage of fornices, b = 1000 s/mm^2) except the sampling scheme of diffusion weighting directions (six noncollinear directions following dual gradient scheme versus 30 noncollinear directions). The six direction DTI with one b0 image was repeated five times (6D x 5) to match one acquisition of the 30 direction

DTI with five b0 images (30D x 1), yielding the same number of diffusion weighted images (n = 30) and b0 images (n = 5) for the two protocols. The scan time was 4:50 mins for both. These protocols were repeated twice, generating two 6D x 5 and two 30D x 1 datasets. Before tensor calculation, all images from the four datasets were coregistered to the b0 image of the first 6D x 5 dataset to minimize eddy current distortion and motion artifacts during and between scans using AIR 5.0 (http://bishopw.loni.ucla.edu/AIR5). The two 6D x 5 and two 30D x 1 datasets were averaged to produce two additional datasets, six direction DTI with ten repetitions (6D x 10) and 30 direction DTI with two repetitions (30D x 2), both yielding 60 diffusion weighted images and 10 b0 images. Bilateral fornices were depicted by manual tractography using the same ROIs defined on the 6D x 5 dataset and then copying onto 6D x 10, 30D x1 and 30D x 2 datasets for consistency. The volume of fornices and the four diffusion parameters, i.e. FA, MD, $\lambda_\parallel$ and $\lambda\perp$, of bilateral fornices were calculated for each of the four datasets. With the primary interest of the effects of the number of diffusion weighting directions, paired t-tests were performed on the five parameters for two comparing pairs, 6D x 5 versus 30D x1 and 6D x 10 versus 30D x 2. We were also interested in the effects of the number of repetitions. Thus paired t-tests were applied between 6D x 5 and 6D x 10, and between 30D x 1 and 30D x 2 separately. False discovery rate at $p = 0.05$ was used for multiple comparison correction within each comparison.

Results

The fornix trajectory based on six or 30 direction DTI was similar (Appendix Figure A.1). There is no tract volume difference among the four datasets. Paired t-test revealed significant difference of FA/MD/$\lambda_\parallel$/$\lambda\perp$ between 6D x 5 and 30D x1 as well as 6D x 10 and 30D x 2 with 30D datasets consistently showing higher values (Appendix Figure A.2, Appendix Table A.1). 6D x 10 showed lower FA and $\lambda_\parallel$ compared to 6D x 5 while MD and $\lambda\perp$ were similar for the two. 30D x 2 showed lower FA compared to 30D x 1 while the three diffusivities were similar for the two.
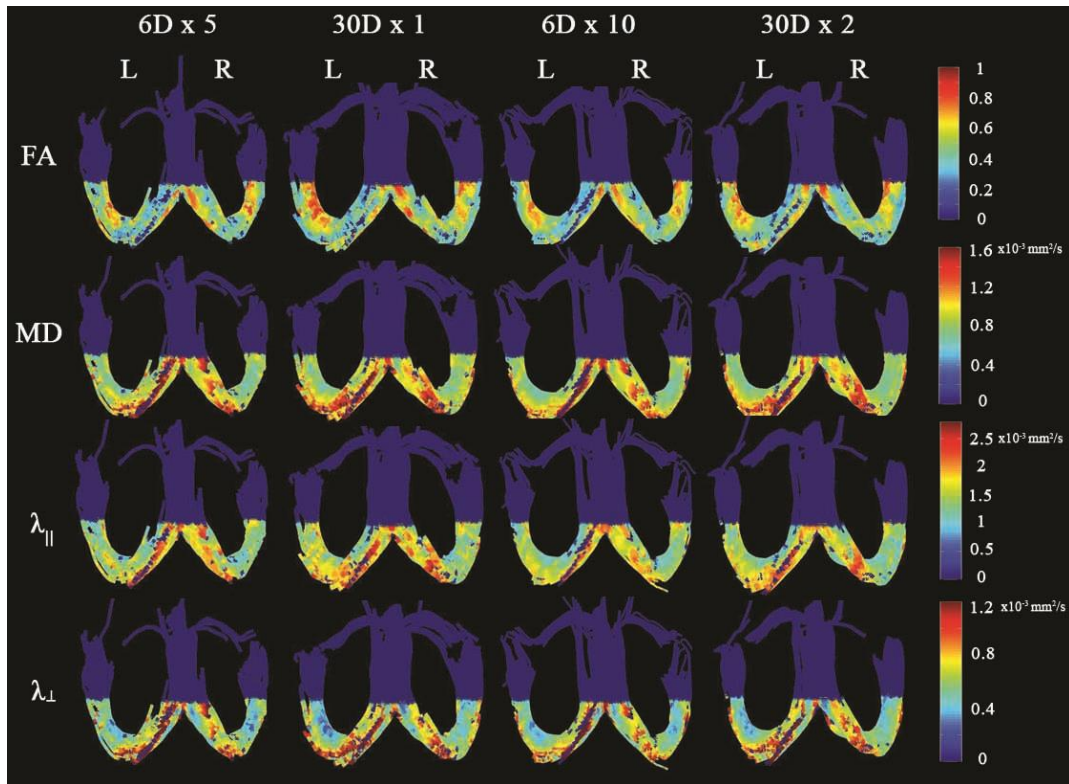
Appendix Figure A.1 Bilateral 3D visualization of fornices (viewed from above) in a 25 year old healthy volunteer where FA, MD, $\lambda_{\parallel}$ and $\lambda_{\perp}$ index values are color-coded for each measured voxel. No trajectory difference was observed from the tractography results using six or 30 direction DTI. L, left; R, right.
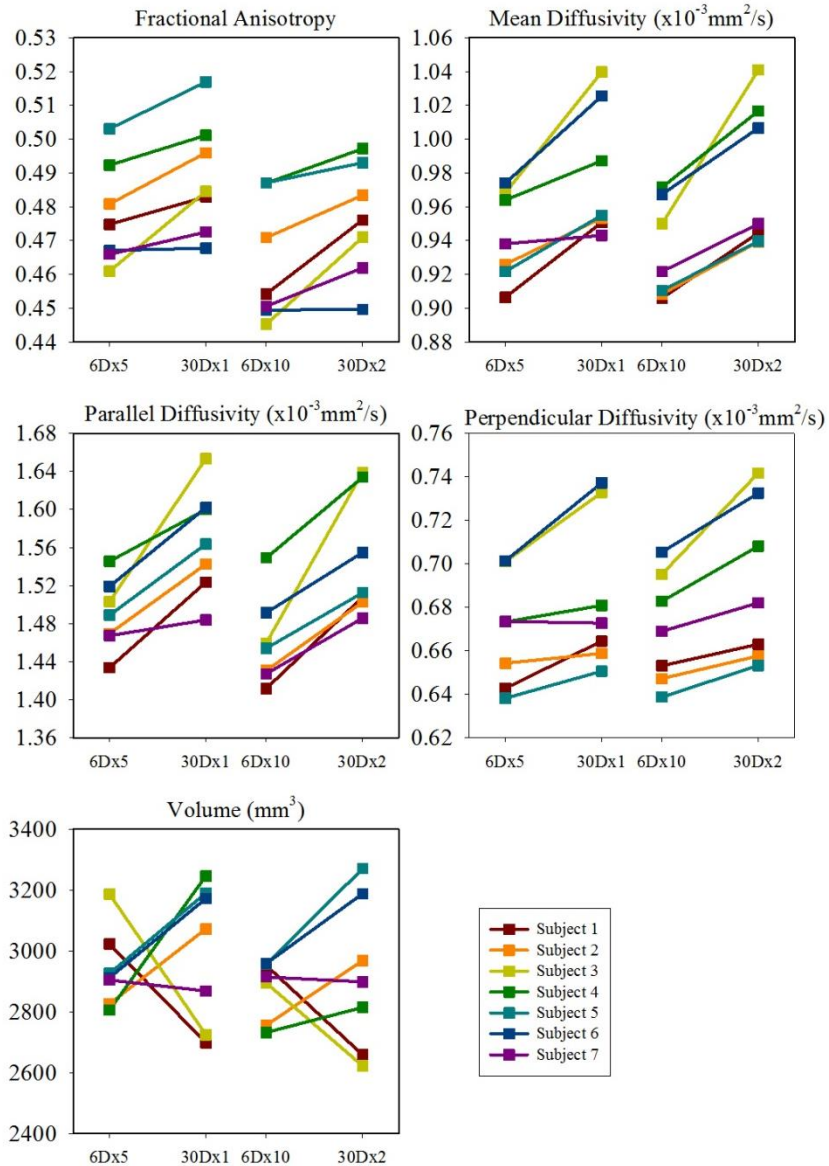
Appendix Figure A.2 FA, MD, $\lambda_{\parallel}$, $\lambda_{\perp}$ and tract volume for each subject derived from four different diffusion weighting schemes, that is, six direction DTI with five repetitions (6D x 5), six direction DTI with ten repetitions (6D x 10), 30 direction DTI with one acquisition (30D x 1), and 30 direction DTI with two repetitions (30D x 2).

Appendix Table A.1 The false discovery rate corrected *p* values from paired t-tests of the diffusion parameters (fractional anisotropy and mean, parallel and perpendicular diffusivities) derived from different diffusion weighting schemes, that is, six direction DTI with five repetitions (6D x 5), six direction DTI with ten repetitions (6D x 10), 30 direction DTI with one acquisition (30D x 1), and 30 direction DTI with two repetitions (30D x 2). Significant *p* values are marked with asterisks.

	6Dx5 vs. 30Dx1	6Dx10 vs. 30Dx2	6Dx5 vs. 6Dx10	30Dx1 vs. 30Dx2
FA	0.012*	0.011*	0.002*	0.010*
Mean Diffusivity	0.010*	0.010*	0.085	0.716
Parallel Diffusivity	0.010*	0.005*	0.008*	0.375
Perpendicular Diffusivity	0.028*	0.005*	0.713	0.340
Volume	0.680	0.704	0.268	0.333

Discussion

This study demonstrated that the six direction scheme yielded a similar tractography outcome (trajectory and volume, Appendix Figure A.1), however, systematically lower FA and diffusivities of fornices with respect to the 30 direction scheme when the only difference of the two FLAIR DTI protocols were the number of diffusion gradient directions on our scanner. It can be observed that the elevation of FA index derived from the 30 direction scheme is a consequence of a larger increase of the estimation of $\lambda_{\parallel}$ than $\lambda_{\perp}$ prominently at the level of fusion of the two fornix crura which are adjacent to lateral ventricles (Appendix Figure A.1). It is possible that the more variable eddy current with 30 direction DTI slightly varies the tenor estimation of the fornix that leads to the difference. It is also possible that although the inversion recovery technique used in FLAIR DTI was able to suppress the signal from cerebrospinal fluid (CSF), the incomplete suppression due to the variable T1 value in different subjects as well as a relative large voxel size (2 x 2 x 2 mm^3) used in EPI sequence still leave the partial volume effect outstanding and spoil the tensor estimation in the fornices. It is unclear whether higher number of repetitions or higher number of diffusion weighted gradients can better reduce the effect of the CSF contamination. Our observation was that 30 direction scheme yielded overall higher diffusivities than the six direction scheme in dealing with this issue. The noise may also introduce error in tensor estimation. However,

it is hardly to be a major factor since the numeric discrepancy between six direction scheme and 30 direction scheme persists after the number of repetitions doubled in both protocols, i.e. FA and diffusivities were higher in 30D x 1 than 6D x 5 and higher in 30D x 2 than 6D x 10. As these shifts were consistent across subjects for each DTI parameter (Appendix Figure A.2), it can be concluded that adding more diffusion weighting direction (> 6) will not change the results from cross sectional analysis, e.g. comparison between patients and controls, for our specific scanner and FLAIR DTI protocols. A couple of previous in vivo experiments probing the relationship between the number of repetitions and number of gradient directions had observations and conclusions distinct from each other (Ni et al., 2006; Giannelli et al., 2009). One study showed that FA was strongly dependent on the number of diffusion gradient used (Giannelli et al., 2009) while the other concluded that FA was independent of the number of diffusion gradient used (Ni et al., 2006). The discrepancy may lie in the fact that the hardware and software conditions in these studies and ours were different and subtle change would affect the final results. Therefore we remain cautious on generalizing our results to a larger scale but hold this conclusion specific to our scanner and protocols.

The other observation in our study was that the FA decreased as the number of repetitions increased from five to ten in six direction DTI and from one to two in 30 direction DTI. This is in accordance with previous Monte Carlo analysis in that noise elicits overestimation of FA and the increase of SNR can partly mitigate the problem (Pierpaoli and Basser, 1996). The parallel diffusivity decreased in 6D x 10 as to 6D x 5 datasets but not in 30D datasets. It can be seen that the mildly decreased $\lambda_\parallel$ and increased $\lambda\perp$ in the high repetition datasets relative to the low repetition datasets despite of the number of gradients used was the reason for the significantly decreased FA and an unaltered MD in the high repetition datasets. Although increasing SNR facilitates more accurate estimation of the diffusion tensor, long time scan is usually not feasible in clinical settings. It also increases the chance of head motion which would impair the tensor calculation in the following steps.